UNIVERSITY OF CALIFORNIA, SAN DIEGO

A battle with superbugs: New compounds and targets against drug-resistant pathogens

A dissertation submitted in partial satisfaction of the requirements for the degree Doctor of Philosophy

in

Biomedical Sciences

by

Nina M. Haste

Committee in charge:

Professor Victor Nizet, Chair
Professor Laurence Brunton
Professor Pieter Dorrestein
Professor Bradley Moore
Professor Susan S. Taylor

2012

The Dissertation of Nina M. Haste is approved, and it is acceptable in quality and form for publication on microfilm and electronically:

Chair

University of California, San Diego

2012

DEDICATION

For my family

TABLE OF CONTENTS

LIST OF FIGURES

Chapter 1.

Chapter 2.

Chapter 3.

LIST OF TABLES

Chapter 2.

Chapter 3.

Chapter 4.

Chapter 5.

LIST OF COMMON ABBREVIATIONS

AKAP	A-kinase anchoring protein
ATP	adenosine triphosphate
cAMP	Adenosine 3', 5'-cyclic monophosphate
Å	Angstrom
CA-MHB	Calcium $^{2+}$/Magnesium $^{2+}$ (cation)-adjusted Mueller Hinton broth
cfu	colony forming units
Cm	chloramphenicol
CNB	Cyclic nucleotide binding
C-subunit	Catalytic Subunit of cAMP-dependent Protein Kinase A
C-terminus	carboxy-terminus
D/D	Dimerization / Docking domain of Protein Kinase A
DNA	deoxyribonucleic acid
DNase	deoxyribonuclease
DTT	dithiothreitol
E. coli	*Escherichia coli*
EDTA	ethylenediaminetetraacetic acid
EGTA	[ethylenebis(oxyethylenenitrilo)] tetraacetic acid
Em	erythromycin
FBS	fetal bovine serum
GISA	glycopeptide intermediate *Staphylococcus aureus*
Hla	*Staphylococcus aureus* alpha hemolysin
i.p.	intraperitoneal
kDa	kilodaltons
$MgCl_2$	magnesium chloride
MALDI	Matrix-Assisted Laser Desorption/Ionization
MBC	minimum bactericidal concentration
MRSA	methicillin resistant *Staphylococcus aureus*
CA-MRSA	Community-associated MRSA
HA-MRSA	Hospital-associated MRSA
MIC	minimum inhibitory concentration
µg	microgram
µl	microliter
µM	micromoles / liter
mg	milligram
ml	milliliter
mM	millimoles / liter
MES	2-(N-morpholino) ethanesulfonic acid
MOPS	3-(N-morpholino) propanesulfonic acid
MOI	multiplicity of infection
MHB	Mueller Hinton broth
NaCl	sodium chloride
NETs	neutrophil extracellular traps
N-terminus	amino-terminus
PAE	Post-antibiotic effect
PAGE	polyacrylamide gel electrophoresis

PBS	phosphate buffered saline
P.falciparum	*Plasmodium falciparum*
PCR	polymerase chain reaction
PDB	Protein data bank
PKA	Protein Kinase A or cyclic-AMP Dependent Protein Kinase
PKI	Protein kinase A inhibitor
Pf-R	*Plasmodium falciparum* PKA Regulatory Subunit
PMN	polymorphonuclear cells (neutrophils)
R-subunit	Regulatory Subunit of PKA
RT-PCR	Real-Time polymerase chain reaction
RNA	ribonucleic acid
SDS-PAGE	sodium dodecyl sulfate-polyacrylamide gel electrophoresis
TCEP	tris(2-carboxyethyl) phosphine hydrochloride
THA	Todd-Hewitt agar
THB	Todd-Hewitt broth
Tris	tris hydroxymethylaminoethane
VISA	vancomycin intermediate *Staphylococcus aureus*
VRE	vancomycin resistant *Enterococcus faecalis*
VRSA	vancomycin resistant *Staphylococcus aureus*
WT	wild-type

ACKNOWLEDGEMENTS

I am extremely lucky. I came to the University of California, San Diego in 1999 as a first year undergraduate, immediately struck by the size, intensity and opportunities that this university offered. Early on in that first year here, I applied for an administrative job in Susan Taylor's lab. At that time, I had no idea that this was the best decision I could have ever made for my future. Since joining Susan's lab as a first year undergraduate, I have had so many amazing opportunities to work with, learn from and collaborate with countless people in the field of science. I have made friends around the world, met my best friend and worked with so many talented, extraordinary people and been so fortunate to have two amazing and brilliant advisors that I am so grateful for. I am extremely lucky.

My PhD work was conducted in the lab of Victor Nizet. My time in Victor's lab has been filled with unending support, motivation and encouragement. Victor has not only been a wonderful advisor to my PhD work, but also a true mentor for my career. He has gone above and beyond to help guide me through the PharmD/ PhD program, set up meetings with faculty, establish guidelines for achievements and really created a path for the future. As one of the first PharmD/ PhD students, I am so grateful to the many hours and significant efforts he has put forth in further establishing the program. I feel so lucky to fortunate to have a P.I. that cares so much for the people in his laboratory, who goes out of his way to make their goals a success and help them achieve what they want most in their lives as a whole.

When looking back today, I realize that I have known Susan Taylor for over a third of my life. She has seen me grow as a student, a scientist, but more importantly, as a person. I consider her my scientific mother and could never thank her enough

for her continued support and guidance and for bestowing on to me her intense enjoyment in learning and excitement for science. Thank you for everything you have done for me.

I gratefully acknowledge my thesis committee: Victor Nizet, Laurence Brunton, Pieter Dorrestein, Bradley Moore and Susan Taylor. Each of them has made a significant impact on my professional career, provided important insights, words of wisdom and helpful suggestions. I feel extremely lucky that I could walk into any of their offices on a given day and discuss professional, scientific and personal matters. I am eternally grateful for all of their support.

I would also like to thank Dean Palmer Taylor for everything he has done for me. Not only has Dean Taylor been an important mentor to me throughout my time in the PharmD/ PhD program, he has helped build a school that I am so proud to be a part of. His tireless work ethic is inspiring.

It is the people who have made my time at UC San Diego and in the PharmD/ PhD program so memorable and so much fun. I have had the great fortune of working in two amazing laboratories where I have made so many wonderful friends that now live throughout the world and here in San Diego. Each of these people, too numerous to mention here, has made a significant impact on my life. I especially want to thank a group of people that I shared offices and lab space with and now lifelong friendships: Cheryl Okumura, Tina Tran, Maren von Köckritz-Blickwede, Suzan Rooijakkers and Evelien Berrends (my CMG homies). In addition, I had the great fortune of working Mary Hensler on the majority of my thesis projects. I will always remember the awesome scientific discussions as well as the opportunity to sit and chat about life and science. I thank so many people I collaborated with

throughout the lab including my friends Morgan, Jason, Andrew, Samira, Kathryn, David, George and countless others.

To the Skaggs School of Pharmacy and Pharmaceutical Sciences, Class of 2009, I could not have picked a more amazing group of people to spend three years with. I have made lifelong friends with so many of you and am so grateful for your continued support. Specifically, I want to thank Andy Chang, my great friend and co-PharmD/PhD classmate. You have an amazing ability to make people laugh on command; your zest for life is infectious. I could not imagine going through this program with any one else. Thank you for your support and friendship always.

Thank you to my family. You have believed in me every step of the way and given me so much love and support throughout my entire life. To my parents who have always put the needs of me, my sister and my brother before their own. They have given us so much love. I only hope that some day I can give to my own children as much as they have to me. I love you very much. To Amy, my sister, and Matthew, my brother, thank you for being there for me always, for your hugs, and laughter, for challenging me and lifting my spirits and for your friendship and love. To my extended family, thank you for your unending love and support. My life is rich with the love of my family.

To Brandon, you have given me new perspective on life. You have challenged me, taught me how to relax and not worry, listened and cared during my struggles and celebrated with me during success. You are my best friend and I am so grateful every day to have you in my life. Thank you for your love.

*****

*****

This work detailed in this thesis is a combination of works published, submitted or in preparation for publication. Permission was obtained from all co-authors of manuscripts presented herein prior to submission of this thesis.

Chapter 2. of this dissertation a combination of: (1) a published manuscript which I was the primary author, under the supervisors Victor Nizet and Mary Hensler: Haste NM, Hughes CC, Tran DN, Fenical W, Jensen PR, Nizet V, Hensler ME. Pharmacological properties of the marine natural product marinopyrrole A against methicillin-resistant *Staphylococcus aureus*. *Antimicrob Agents Chemother*. (2011), 55:3305-12, PMC3122406 with permission from co-authors **(Chapter 2.3.1.)**; (2) a published manuscript which I was a contributing author, Nicolaou KC, Simmons NL, Chen JS, Haste NM, Nizet V. Total synthesis and biological evaluation of marinopyrrole A and analogues. *Tetrahedron Lett.* (2011) **(Chapter 2.3.2.)**; (3) and two- three manuscripts in preparation with Rongshi Li, PhD from the H. Lee Moffitt Cancer Center in Florida in which I will be the primary and secondary author **(Chapter 2.3.3.)**.

Chapter 3. of this dissertation a combination of: (1) a published manuscript which I was the primary author, under the supervisors Victor Nizet and Mary Hensler**:** Haste NM, Perera VR, Maloney KN, Tran DN, Jensen P, Fenical W, Nizet V,Hensler ME. Activity of the streptogramin antibiotic etamycin against methicillin-resistant *Staphylococcus aureus*. J Antibiot (Tokyo). (2010), 63(5):219-24, PMCID: PMC2889693 **(Chapter 3.3.1.)**; (2) a published manuscript which I was a

contributing author: Sun P, Maloney KN, Nam SJ, Haste NM, Raju R, Aalbersberg W, Jensen PR, Nizet V, Hensler ME, Fenical W. Fijimycins A-C, three antibacterial etamycin-class depsipeptides from a marine-derived *Streptomyces sp*. *Bioorg Med Chem.* (2011), 19:6557-62, PMC3205191 **(Chapter 3.3.1.)**; (3) a published manuscript from which I was the primary author under the supervision of Victor Nizet and Mary Hensler: Haste NM, Farnaes L, Perera VR, Fenical W, Nizet V, Hensler ME.Bactericidal kinetics of marine-derived napyradiomycins against contemporary methicillin-resistant *Staphylococcus aureus*. *Mar Drugs.* (2011);9:680-9,PubMed Central PMC3124980 **(Chapter 3.3.2.);** (4) a manuscript in preparation: Haste N, Thienphrapa W, Sakoulas G, Tran D, Perera V, Loesgen S, Jensen P, Fenical W, Nizet V, Hensler ME. Characterization of Nosiheptide Activity Against Contemporary Methicillin-Resistant *Staphylococcus aureus,* in preparation (2011) **(Chapter 3.3.3.)**.

Chapter 4 of this dissertation is work done in collaboration with Menachem Shoham, PhD from Case Western University. N.M.H. wrote the chapter and Mary Hensler, Morgan Pence, Cheryl Okumura, Josh Olson, Jason Cole, Kathryn Akong, David Gonzalez, Wdee Thienphrapa and Victor Nizet also contributed to work in this chapter.

Chapter 5 of this dissertation involves a collaboration with Gordon Langsley, PhD at INSERM in Paris N.M.H designed and conducted and analyzed most of the experiments. Alex Doo contributed equally and was involved in the design and analysis of many experiments. Ganapathy Sarma, PhD served as a very helpful advisor early on in this project. Mira Sastri, PhD, Manjula Darshi, PhD, Michael Deal,

PhD, Jessica Bruystens helped out immensely on technical advise, experimental design and trouble-shooting. Jian Wu, PhD has contributed substantial work in crystallization trials. N.M.H wrote the paper. Some of this work will appear in modified form in a Special Issue of *Microbes & Infection*.

This work was supported by the National Institutes of Health Training Program in Marine Biotechnology (TPMB) (**T32 GM067550)** and **Ruth L. Kirschstein National Research Service Award (NRSA) from National Institutes of Health Grants (5 F31 GM090658-02).**

VITA

EDUCATION

2005 - present	**Pharm.D. Candidate / Ph.D.** **University of California, San Diego, CA**
2008 – 2012	Ph.D., Biomedical Sciences Graduate Program, UC San Diego
2005 – present	Pharm.D., Skaggs School of Pharmacy & Pharmaceutical Sciences, UC San Diego
1999-2003	**University of California, San Diego, La Jolla, CA.** B.S., Biochemistry / Cell Biology, Muir College / Department of Biology

PUBLICATIONS

Haste NM, Thienphrapa W, Sakoulas G, Tran D, Perera V, Loesgen S, Fenical W, Nizet V, and M. Hensler. Characterization of marine-derived nosiheptide activity against contemporary methicillin-resistant *Staphylococcus aureus. Manuscript in preparation,* (2011).

Haste, N.M., Doo, A., Langsley, G. and S.S. Taylor. Exploring the *Plasmodium falciparum* cyclic-adenosine monophosphate (cAMP)-dependent Protein kinase (PKA) Regulatory Subunit (*Pf*PKA-R) as a therapeutic target. *Manuscript in preparation for Special Issue: Microbes and Infection* (2011).

Haste NM, Doo A, Langsley, G, Taylor SS, et al. An N-terminal localization motif in the *Plasmodium falciparum* cyclic-adenosine monophosphate (cAMP)-dependent Protein kinase (PKA) Regulatory Subunit (*Pf*PKA-R), *In preparation*, (2011).

Haste NM, Liu Y, Thienphrapa W, Nizet, V**.**, Li R, and M. Hensler, et al. Characterization of synthetic marinopyrrole derivatives for their activities against contemporary methicillin-resistant *Staphylococcus aureus. Manuscript in preparation,* (2011).

Liu Y, **Haste NM**, Thienphrapa W, Nizet V, Hensler ME and R. Li. Marinopyrrole Derivatives as Potential Antibiotic Agents against Methicillin-Resistant *Staphylococcus aureus* (I). *Manuscript in preparation for J. Med. Chem*., (2011).

Haste NM, Liu Y, Thienphrapa W, Nizet V, Hensler ME and R Li. Marinopyrrole Derivatives as Potential Antibiotic Agents against Methicillin-Resistant *Staphylococcus aureus* (II). *Manuscript in preparation for J. Med. Chem*., (2011).

Taras, H., **Haste, N.M.,** Tran Berry, A., Tran, J. and R. Singh. Medications at School: Disposing of Pharmaceutical Waste. *Manuscript submitted,* (2011).

Sun P, Maloney KN, Nam SJ, **Haste NM**, Raju R, Aalbersberg W, Jensen PR, Nizet V, Hensler ME, Fenical W. Fijimycins A-C, three antibacterial etamycin-class depsipeptides from a marine-derived *Streptomyces sp. Bioorg Med Chem.* **19**:6557-62 (2011) (PMC3205191).

Haste NM, Farnaes L, Perera VR, Fenical W, Nizet V and ME Hensler. Bactericidal kinetics of marine-derived napyradiomycins against contemporary methicillin-resistant *Staphylococcus aureus. Mar Drugs*. **9**:680-9 (2011) (PMC3124980).

Gonzalez DJ**, Haste NM**, Hollands A, Fleming TC, Hamby M, Pogliano K, Nizet V and PC Dorrestein.. Microbial competition between *Bacillus subtilis* and *Staphylococcus aureus* monitored by imaging mass spectrometry. *Microbiology.* **157**:2485-92 (2011).

Haste NM, Hughes CC, Tran DN, Fenical W, Jensen PR, Nizet V and ME Hensler ME. Pharmacological properties of the marine natural product marinopyrrole A against methicillin-resistant *Staphylococcus aureus*. *Antimicrob Agents Chemother*. **55**:3305-12 (2011) (PMC3122406).

Nicolaou KC, Simmons NL, Chen JS, **Haste NM** and V Nizet. Total synthesis and biological evaluation of marinopyrrole A and analogues. *Tetrahedron Lett.* **52**:2041-2043 (2011) (PMC3077031).

Berends ET, Horswill AR, **Haste NM**, Monestier M, Nizet V and M von Köckritz-Blickwede. Nuclease expression by *Staphylococcus aureus* facilitates escape from neutrophil extracellular traps. *J Innate Immun.* **2**:576-86 (2010) (PMC2982853).

Liu WT, Yang YL, Xu Y, Lamsa A, **Haste NM**, Yang JY, Ng J, Gonzalez D, Ellermeier CD, Straight PD, Pevzner PA, Pogliano J, Nizet V, Pogliano K and PC Dorrestein. Imaging mass spectrometry of intraspecies metabolic exchange revealed the cannibalistic factors of *Bacillus subtilis*. *Proc Natl Acad Sci USA*. **107**:16286-90 (2010) (PMC2941286).

Haste NM, Perera VR, Maloney KN, Tran DN, Jensen P, Fenical W, Nizet V and ME Hensler. Activity of the streptogramin antibiotic etamycin against methicillin-resistant *Staphylococcus aureus*. *J Antibiot* (Tokyo). **63**:219-24 (2010) (PMC2889693).

McGillivray SM, Ebrahimi CM, Fisher N, Sabet M, Zhang DX, Chen Y, **Haste NM**, Aroian RV, Gallo RL, Guiney DG, Friedlander AM, Koehler TM, Nizet V. ClpX contributes to innate defense peptide resistance and virulence phenotypes of *Bacillus anthracis*. *J Innate Immun*. **1**:494-506 (2009) (PMC2920483).

Kannan N , **Haste NM,** Taylor SS and AF Neuwald. The hallmark of AGC kinase functional divergence is its C-terminal tail, a cis-acting regulatory module.

Proc.Natl.Acad.Sci. U S A.**104**:1272-7(2007) (PMC1783090).

Kornev AP, **Haste NM,** Taylor SS and LF Ten Eyck. Surface comparison of active and inactive protein kinases identifies a conserved activation mechanism. *Proc. Natl. Acad. Sci. U S A*. **103**:17783-8 (2006) (PMC1693824).

Niedner RH, Buzko OV, **Haste NM**, Taylor A, Gribskov M, and SS Taylor. The Protein Kinase Resource: an integrated environment for phosphorylation research. *Proteins* **63**:78-86 (2006).

Taylor SS, Kim C, Vigil D, **Haste NM**, Yang J, Wu J and GS Anand. Dynamics of Signaling by PKA. *Biochim Biophys Acta.* **1754**(1-2):25-37 (2005).

Taylor SS, **Haste NM**, and G Ghosh. PKR and eIF2alpha: integration of kinase dimerization, activation, and substrate docking. *Cell* **122**(6):823-5 (2005).

Berman HM, Ten Eyck LF, Goodsell DS, **Haste NM,** Kornev A and SS Taylor. The Cyclic Adenosine Monophosphate Binding Domain: An Ancient Signaling Module. *Proc. Natl. Acad. Sci. U S A*. **102**:45-50 (2005) (PMC544069).

Taylor SS, Yang J, Wu J, **Haste NM**, Radzio-Andzelm E and G Anand. PKA: a portrait of protein kinase dynamics. *Biochim. Biophys. Acta.* **1697**:259-69 (2004).

Buzko O, Niedner H, **Haste N**, Taylor A, Gribskov M and S Taylor. The Protein Kinase Resource. 12th International Conference on Second Messengers and Phosphoproteins Montreal, Canada, August 3-7, 2004. pp.87-92 ©2004, Medimond S.r.l.

Banky P, Roy M, Newlon MG, Morikis D, **Haste NM**, Taylor SS and PA Jennings. Related protein-protein interaction modules present drastically different surface topographies despite a conserved helical platform. *J. Mol. Biol.* **330**:1117-29 (2003).

ABSTRACTS

Haste NM, Thienphrapa W, Sakoulas G, Tran D, Perera V, Loesgen S, Fenical W, Nizet V, and M Hensler. Characterization of Nosiheptide Activity Against Contemporary Methicillin-Resistant *Staphylococcus* **Poster #36,** 2011 Pediatric Translational Research Symposium , Rady Children's Hospital, San Diego, October 25, 2011.

Haste NM, Hughes CC, Tran DN, Fenical W, Jensen PR, Nizet V and ME Hensler ME. Pharmacological properties of the marine natural product marinopyrrole A against methicillin-resistant *Staphylococcus aureus*. 49th Interscience Conference on Antimicrobial Agents and Chemotherapy (ICAAC), 2009 (Abstract # F1-1501)

Haste NM, Tran-Berry A, Tran JM, Singh RF and H Taras. Centralized Medication Disposal Partnership Between a School District and a Healthcare System. ASHP-

Midyear, Orlando Florida, December 2008.

Haste NM, Tran D, Jensen PR, Fenical W, Hensler ME and V Nizet. The Discovery of New Antibiotics from Deep Sea Actinomycete Bacteria. L.S. Skaggs Biomedical Research Symposium, Salt Lake City, Utah. (November 10-11, 2008).

McGillivray SM, Ebrahimi CM, Sabet M, **Haste NM**, Arojan R, Gallo RL, Guiney DG and V Nizet. ClpX protease contributes to *B. anthracis* hemolysis, cathelicidin antimicrobial peptide resistance and systemic virulence. American Society for Microbiology, 2008. *(Did not attend conference)*

Pancoast P, **Haste N**, and JD Hirsch. A Detailed Observational Study on the Practice of Community Pharmacy in Four European Countries: Comparing and Evaluating the Role of the Community Pharmacist in Europe and the United States. American Pharmacists Association (APhA) Annual Meeting and Exposition. San Diego, CA, March 14-17, 2008. *(Attended conference)*

Buzko O, Niedner H, **Haste N**, Taylor A, Gribskov M and S Taylor. Protein Kinase Resource. *Contributed poster.* 3rd International Protein Phosphorylation Drug Discovery Summit. La Jolla, CA, March 2005. *(Did not attend this conference)*

Buzko O, Niedner H, **Haste N**, Taylor A, Gribskov M and S Taylor.. Protein Kinase Resource. *Contributed Poster.* 3rd International Conference on Structural Biology and Functional Genomics. Singapore, December 2004. *(Did not attend conference)*

Buzko O, Niedner H, **Haste N**, Taylor A, Gribskov M and S Taylor. Protein Kinase Resource: An online environment for phosphorylation research. 12th International Conference on Second Messangers and Phosphoproteins, Montreal, Canada, August 3-7th, 2004. *(Attended conference)*

Buzko O, Niedner H, **Haste N,** Ostrem J, Gribskov M and S Taylor. Protein Kinase Resource: An online environment for phosphorylation research. *Contributed poster*. Gordon Research Conference on Growth Factor Signaling. Oxford, UK, July 2004. *(Did not attend conference)*

The Protein Kinase Resource (Poster #111). Salk/EMBL Oncogenes and Growth Control Meeting. The Salk Institute La Jolla, California, August 15-19, 2003. *(Attended Conference)*

INVITED PRESENTATIONS

Haste NM, Pancoast P, Hirsch JD. A Survey of Community Pharmacy Practice in Europe. California Pharmacists Association Outlook Conference. Sacramento, CA. February, 2008.

Haste NM, Pancoast P, Hirsch JD. A Survey of Community Pharmacy Practice in Europe. Course Lecture: SSPPS 217- Health Systems by J.D. Hirsch. October 18, 2007.

ACADEMIC AND PROFESSIONAL HONORS

03/2010 – 12/2011	Ruth L. Kirschstein National Research Service Award (NRSA) from National Institutes of Health Grants (5 F31 GM090658-02
09/2008 – 06/2009	Graduate Student Fellowship, Training Program in Marine Biotechnology (TPMB) T32 GM067550, Scripps Institution of Oceanography, UC San Diego
04/2008 – 11/2009	Student Pharmacist Manager, UC San Diego Student Run Free Clinic. Pacific Beach Center.
09/2007 – 06/2008	VP Communications, American Pharmacists Association, UC San Diego Student Chapter
09/2006 – 06/2008	VP Communications, Skaggs School of Pharmacy & Pharm. Sci. Associated Students
09/2006 – 06/2008	Webmaster, Kappa Psi Professional Pharmaceutical Fraternity, UC San Diego Chapter
09/2005 – 06/2008	Chancellor's Fellowship, Skaggs School of Pharmacy & Pharm. Sci,, UC San Diego
06/2003	Phi Beta Kappa Honor Society, UC San Diego
06/2003	Cum Laude, UC San Diego

ABSTRACT OF THE DISSERTATION

A battle with superbugs:
New compounds and targets against drug-resistant pathogens

by

Nina M. Haste

Doctor of Philosophy in Biomedical Sciences
University of California, San Diego, 2012

Victor Nizet, Chair

Drug-resistant pathogens throughout the world, in first and third world countries, create a continual burden on public health. With global emergence of multiply-drug resistant pathogens such as methicillin-resistant *Staphylococcus aureus* (MRSA) and parasites like *Plasmodium falciparum*, there is a distinct need for the development of novel anti-infectives to target these infections. Our data encompasses interdisciplinary links between pharmacology, natural product chemistry, infectious disease pathogenesis and innate immunity. We have (I) characterized novel antibiotics as new classical-type antibiotics, (II) identified a significant virulence factor, alpha-toxin, in MRSA and characterized its potential as a therapeutic target and (III) investigated a pathogen-specific cAMP-dependent protein kinase (PKA) regulatory subunit as a possible therapeutic target in the treatment of *P.*

falciparum.

From this multi-dimensional approach, we have identified potent antibacterial therapies. Our data highlights the ocean as an extremely rich resource of chemically diverse scaffolds. Here, we comprehensively characterize four marine-derived chemical scaffolds, marinopyrrole, napyradiomycin, etamycin and nosiheptide for their potent antibacterial activities against contemporary strains of multi-drug resistant MRSA. Further, in this work, we identify a potential MRSA virulence factor inhibitor. Diflunisal, a known and commonly used non-steroidal anti-inflammatory agent, was predicted via virtual screening to inhibit the production of a pore-forming *S. aureus* toxin. Our data emphasizes the potent anti-virulence properties of diflunisal and identifies a wide range of supplementary anti-bacterial and anti-virulence properties that could prove extremely useful in treating virulent and pathogenic MRSA infections. Finally, we investigate the PKA regulatory subunit of *P. falciparum* to identify pathogen-specific features that may be implicated in its roles in malarial parasite development, host invasion and pathogenesis. We conclude it to be a valid therapeutic target by identifying species-specific differences parasitic and mammalian isoforms that may prove useful in the development and engineering of therapeutic inhibitors.

This work highlights three novel approaches to anti-pathogen research where we pinpoint valid therapeutic targets and potential therapies in the ongoing battle against emerging superbugs.

CHAPTER 1.

Introduction

1.1. INTRODUCTION

With the global emergence of drug-resistance, there is an urgent need for new therapies to treat infections caused by multiple-drug resistant pathogens. Theoretically, there are three ways that new targets and therapies can be identified and characterized. Only one of these methods has yielded the currently used antibiotics we employ today. Since the advent of antibiotic research with Alexander Flemming's discovery of Penicillin in the 1920s, the scientific community has focused primarily on finding classical antibiotics that target bacterial vitality. This method of discovery has yielded hundreds of antibiotics in a variety of classes to combat gram-positive and gram-negative pathogens. More recently, a main focus of antibiotic discovery is the derivatization of known active molecules, with hopes to engineer out resistance and cytotoxicity and enhance therapeutic potential. Novel approaches are warranted in the battle against superbugs.

1.1.1. A three-pronged approach to anti-pathogen drug discovery: Three approaches can theoretically be used to find new therapies for the treatment of infections **(FIGURE 1.1.)**. First, novel structures of classical antibiotics have the potential for great use in the clinic. To discover novel structures, we can probe an untapped resource for these antibiotics. The world's oceans are an extremely diverse, chemically rich source of natural products (Fenical and Jensen, 2006; Gontag, 2006).

Because the majority of antibiotics scaffolds used in the market today are natural-product derived, it is feasible to discern that novel scaffolds for potential classical-type antibiotics will come from mining this largely untapped resource.

Secondly, in targeting the pathogen, therapies specifically engineered to inhibit the virulence properties of a particular organism can greatly decrease its ability to cause disease. *Staphylococcus aureus* encodes for numerous factors that allow it to circumvent the host response, prevent recognition by immune cells and utilize nutrients for its own survival. The effects of virulence factors can have wide-ranging destructive and inflammatory consequences to the host. Theoretically, by inhibiting a necessary virulence factor **(FIGURE 1.1.)**, a drug can effectively remove a pathogen's weapons, destroy its protective shield and render it susceptible to antibiotic therapies or host immune response.

The third mechanism for anti-pathogen drug discovery lies not within the pathogen, but instead the host. Theoretically, a therapy has great potential if it can enhance the immune system's ability to recognize an invading pathogen, neutralize the infection and kill the treat.

Despite their theoretical benefits, no therapies currently exist on the market that are engineered specifically as virulence factor inhibitors or immune-boosting agents. However, contemporary research has shown some commonly used therapies to have repurposed off-target effects that yield anti-virulence or immune-boosting effects.

This work focuses on targeting the pathogen, through the characterization of novel marine-derived antibiotics as potential anti-MRSA agents and targeting pathogen-specific virulence factors with the hope to render the organism non-pathogenic and susceptible to host or antibiotic / antiparastic chemotherapies.

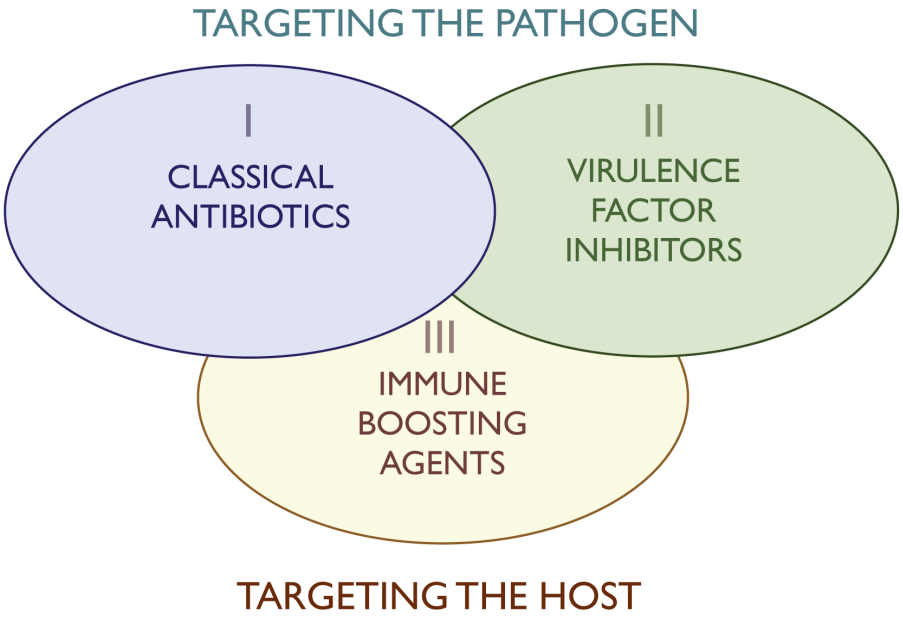

FIGURE 1.1. Three approaches to anti-pathogen drug discovery.

1.2. ANTIBIOTIC DRUG DISCOVERY

1.2.1. The need for new and novel antibiotics to treat drug-resistant pathogens: The twentieth century became the "golden age" of antibiotics with the discovery of a penicillin-producing fungus by Alexander Fleming in 1928 (Fenical and Jensen, 2006; Newman et al., 2002). The introduction of sulfonamides in the 1930s and penicillin in the 1940s revolutionized the practice of medicine and the treatment of infectious diseases **(FIGURE 1.2.)**. In the three decades that followed, many of today's antibiotics were discovered. However, with the exception of the oxazolidinone core of linezolid in 2000 and the lipopeptide daptomycin in 2003, no new scaffolds for antibiotics have emerged in the past 30 years **(FIGURE 1.2.)**.

The widespread and common use of antibiotics to treat many infectious diseases has allowed for the selection and continual emergence of multiple drug-resistant pathogens. The medical community now faces the great challenge of combating these microorganisms, defining an urgent need for new drugs, especially those that that might possess novel mechanisms of action. According to the Antimicrobial Availability Task Force of the Infectious Disease Society of America, roughly two million people become infected with microbial pathogens in U.S. hospitals every year. Of these people, 90,000 die and roughly 70% of the bacteria causing infections are resistant to at least one drug (Spellberg et al., 2008; Talbot et al., 2006). Resistance has been acquired in every antibiotic used in clinical practice and these resistant pathogens have led to increasing health care costs, requiring durations of therapy, more expensive medications and extended hospital stays (Payne et al., 2007). Resistance to antimicrobial drugs arises through a variety of mechanisms including: (1) alteration in the antibiotic target (eg, penicillin binding proteins), (2) reduction in the amount of drug accumulating in the bacteria (eg, efflux pumps,

changes in permeability), (3) acquisition of a gene encoding an enzyme for drug inactivation (eg, beta-lactamase), (4) production of metabolic "bypass" pathways (Tenover, 2006).

The decline of new antimicrobial discoveries over the last-half century has led to an urgent need for new classes of antibiotics **(FIGURE 1.2.)** with novel mechanisms of action **(FIGURE 1.3.)**. Since the majority of effective antibiotics are derived from secondary metabolites of actinomycete bacteria, it can be argued that by further studying this great source of chemical diversity and biological potency, we can predict that new antibiotics with novel mechanisms of action can be discovered.

***1.2.2. Natural Products: providing the scaffolds for current and future antibiotics*:** Actinomycetes are Gram-positive, high G-C content filamentous bacteria. They produce a great number of chemically diverse, biologically potent secondary metabolites (Fenical and Jensen, 2006). It was first thought that bacteria in the actinomycetales order were exclusively soil inhabitants. However in the 1960s they were discovered to exist in sea water and adapt to their marine environments (Mincer et al., 2002). Oceans cover over 70% of the Earth's surface. Because roughly 10^9 bacteria reside within 1 mm^3 of ocean-floor sediment (Fenical and Jensen, 2006), the oceans are a source of rich phylogenetic diversity (Gontag et al., 2006; Jensen et al., 1991; Jensen and Fenical, 1996; Jensen et al., 2005a; Jensen et al., 2005b; Mincer et al., 2002; Woese, 2000). Worldwide expeditions by the Fenical lab and others working on the biosyntheses (B. Moore, P. Dorrestein (UCSD)), chemical syntheses (K.C. Nicholaou (TSRI), and Rongshi Li, (H. Lee Moffitt Cancer Center)) provide a vast resource for new scaffolds. In the first two chapters, we characterize four marine-derived natural products: marinopyrrole, napyradiomycin, etamycin and nosiheptide.

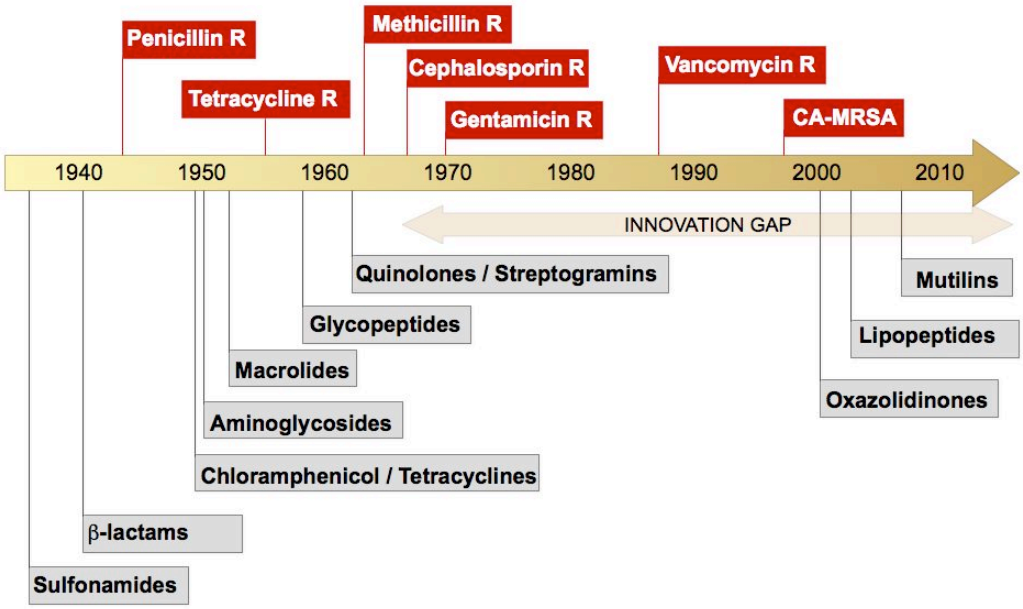

FIGURE 1.2. The development of antibiotics and the emergence of resistance: a timeline. The introduction of new antibiotic classes to the therapeutic use (grey) and the rapid emergence of antibiotic resistance shortly after most chemical scaffolds were introduced (red). The innovation gap, indicated by a tan double arrow, indicates a period in which only three new chemical scaffolds were brought to market. (Figure was partially modeled after Fischbach and Walsh 2009, Figure 2).

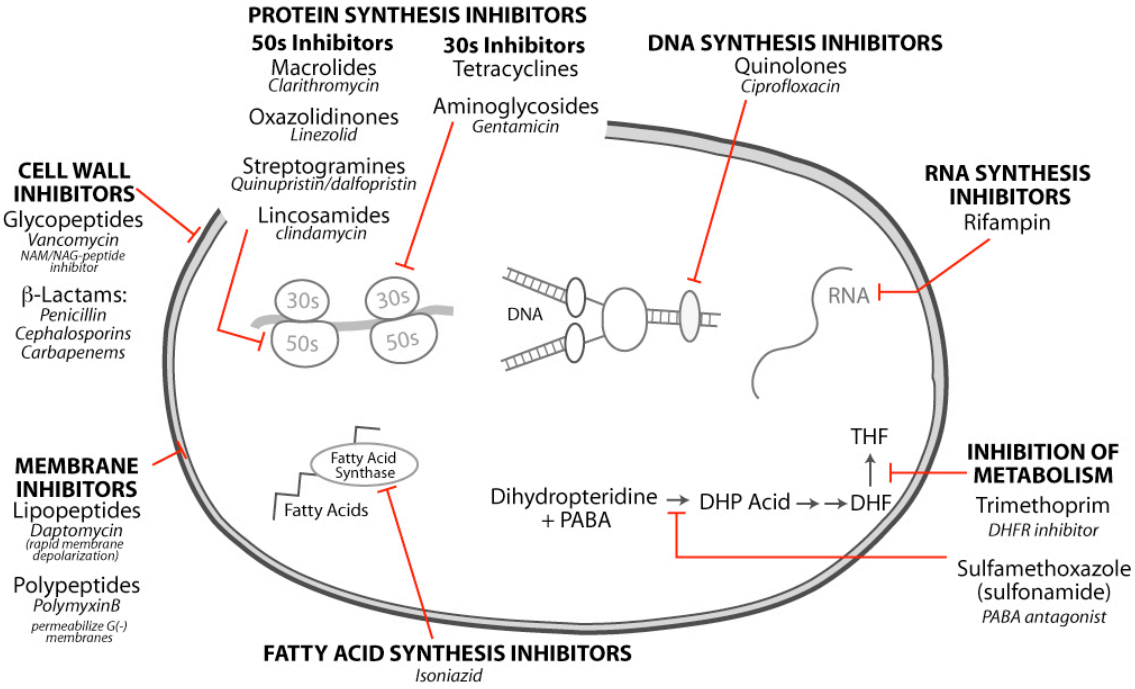

FIGURE 1.3. Current antibiotics and their mechanisms of action. The main classes of antibiotics are shown according to their mechanisms of action in the bacterial cell. These classes can be generally subdivided into four major classes: (1) interference with cell wall synthesis, (2) inhibition of protein synthesis, (3) inhibition of nucleic acid synthesis and (4) inhibition of a metabolic pathway.

1.2.3. Four marine-derived antibiotic scaffolds: **Marinopyrrole A**, a bactericidal anti-MRSA compound, was isolated from CNQ-418, a strain collected at a depth of 51m off the La Jolla, CA coast (Hughes et al., 2008). Initially shown to have strong *in vitro* activities against gram-positive organisms (MIC <2ug/ml), MPA represented a possible new antibiotic scaffold. The novel structure of marinopyrrole A represents the first examples of a natural product with a *N,C*2-linked bispyrrole structure (Hughes et al., 2008). **Etamycin,** a bacteriostatic marine-derived streptogramin B was isolated from CNS-575, a strain collected from the Fiji coastline. This classical depsipeptide antibiotic was discovered more than 5 decades ago from the terrestrial *S. griseoviridus*. We reported the first purification of etamycin from a marine species. Streptogramin antibiotics exist in two forms, streptogramin A (quinupristin-like) and B (dalfopristin-like), which act synergistically on the 50S ribosome to inhibit protein synthesis. Our results highlight the potent antibiotic activities of etamycin and suggest that it should be re-evaluated as an anti-MRSA antibiotic candidate. **Napyradiomycin**, CNQ-525, was isolated from ocean sediments off La Jolla, CA. This actinomycete produces chlorine-containing terpenoid dihydroquinone compounds. Some compounds from this structural class, the napyradiomycins, have been previously isolated from collections of terrestrial derived *Streptomyces* strains (Fukuda et al., 1990). The discovery of CNQ-525 yielded novel napyradiomycin derivatives with new chemical properties. Initial *in vitro* screens by the Fenical – Jensen Group showed that these compounds possess significant cytotoxic and antibacterial activities (Soria-Mercado et al., 2005). Our analyses highlight the potent bactericidal kinetics of napyradiomycins against MRSA. **Nosiheptide** was recently discovered from a marine actinomycete. We discovered its potent anti-MRSA

activities in both the presence and absence of serum. This compound shows potent *in vivo* activities despite its poor solubility.

Promising marine-derived natural products such as the marinopyrroles, etamycin, nosiheptide and the napyradiomycins have potent antibacterial properties against MRSA. These chemical scaffolds not only show promise in future therapeutic discovery and characterization, but they also provide important contributions of structure activity relationship data in intelligently developing new antibiotic therapies.

1.3. A NOVEL INHIBITOR OF MRSA ALPH-TOXIN EXPRESSION

1.3.1. Virulence factors as targets for antimicrobial therapy: *S. aureus* can subvert host immune responses and protect itself from phagocytosis, antimicrobial peptides and oxidative burst. In addition, it can secrete additional factors that allow for it to establish and maintain infection in a host niche. Therapies that neutralize specific virulence factors are one theoretical approach that could potentially prove useful in the treatment of bacterial pathogens.

1.3.2. Diflunisal is a potent inhibitor of alpha-toxin: Through a virtual screening approach we identified diflunisal as a potential inhibitor of AgrA, a transcription factor upstream of alpha-toxin production. AgrA is part of the quorum-sensing accessory gene regulation operon which controls the production of numerous virulence factors and toxins. By inhibiting AgrA, one could theoretically decrease the transcription and production of alpha toxin.

Virtual screening identified diflunisal as a potential AgrA inhibitor. We show through in vitro assays that diflunisal is inhibiting MRSA hemolysis and reducing the overall

expression of alpha-toxin. In addition, we observe that the effects of diflunisal are much more diverse and complex than just at the site of AgrA inhibition. Our work summarizes the effect of diflunisal on MRSA virulence for the first time.

1.4. A DRUG TARGET IN *PLASMODIUM FALCIPARUM*

1.4.1. Exploring the Plasmodium falciparum PKA R-subunit (PfR) as a drug target: Malaria is abundant throughout the third-world. Caused by the parasite species *plasmodium*, nearly 3 million people die each year from malaria (Wells, 2010; Winzeler, 2008). With 515 million cases each year and widespread resistance, there is undoubtedly a need for new therapeutics and therapeutic targets to treat malaria. The majority of cases are caused by *Plasmodium falciparum* (*Pf*), a mosquito parasite abundant in Africa. *Pf*-malaria is characterized by anemia, fever, metabolic acidosis, neurological symptoms (Winzeler, 2008). These symptoms arise during parasite development in the red blood cell (RBC). Briefly, the intracellular parasite establishes anion channels and "new permeation pathways" (NPPs) in the RBC membrane to pass nutrients like sugars, peptides, amino acids, nucleotides and anions/ cations into the RBC (Martin et al., 2009; Merckx et al., 2008). Malarial symptoms are further induced by parasitic degradation of RBC hemoglobin for nutrient extraction. Malarial pathogenesis depends largely on intracellular molecular signaling pathways, specifically mediated by phosphoinositide, Ca^{2+} -dependent mechanisms and cyclic-adenosine monophosphate (cAMP).

1.4.2. The role of PKA in malarial pathogenesis: Recently, the gene encoding the cAMP-dependent Protein Kinase A (PKA) catalytic subunit (C-subunit) was identified on the *P. falciparum* genome. In fact, it is now known that many

parasites have acquired kinases that are known to be fundamental to mammalian survival (PKA, PKG, PKC, MAPK) (Doerig, 2004; Doerig et al., 2009; Doerig et al., 2005; Doerig and Meijer, 2007; Doerig and Tobin, 2010). It seems that parasites may use their own versions of these proteins to help them survive in the host. For example, importance of phospho-signaling has been demonstrated in malarial development and pathogenesis (Merckx et al., 2008). NPP channels can be activated via phosphorylation and as described above, are crucial for parasite survival. Further, the interplay between the host and parasitic PKA and PKC, both endogenously expressed in RBC, provides an intriguing platform for studying host-pathogen interactions.

Previous results have shown that a number of factors involving the *Pf*-PKA inhibit parasite proliferation. These include the over-expression of *Pf*R and the addition of H89, a PKA C-subunit inhibitor (Syin et al., 2001). Further, it has been shown that the kinase inhibitor staurosporine prevents malarial invasion of erythrocytes. These data highlight the importance of the PKA-regulatory subunit in the study of malarial pathogenesis. The defined role for PKA in *plasmodia* signaling and development establish a key platform for investigating *Pf*R specific features and considering it a valid therapeutic target.

1.5. SUMMARY

The three-pronged approach to anti-pathogen drug discovery provides numerous targets for further research and study. Because only one of these approaches has yielded currently-marketed therapeutics, the other two, virulence factor inhibitors and immune-boosting agents, could potentially impact the global battle against superbugs. Theoretically, with these therapies, we can help tip the balance in the battle against multi-drug resistant pathogens back in favor of the host.

1.6. REFERENCES

Doerig, C. (2004). Protein kinases as targets for anti-parasitic chemotherapy. Biochim Biophys Acta *1697*, 155-168.

Doerig, C., Abdi, A., Bland, N., Eschenlauer, S., Dorin-Semblat, D., Fennell, C., Halbert, J., Holland, Z., Nivez, M.P., Semblat, J.P.*, et al.* (2009). Malaria: targeting parasite and host cell kinomes. Biochim Biophys Acta *1804*, 604-612.

Doerig, C., Billker, O., Pratt, D., and Endicott, J. (2005). Protein kinases as targets for antimalarial intervention: Kinomics, structure-based design, transmission-blockade, and targeting host cell enzymes. Biochim Biophys Acta *1754*, 132-150.

Doerig, C., and Meijer, L. (2007). Antimalarial drug discovery: targeting protein kinases. Expert Opin Ther Targets *11*, 279-290.

Doerig, C., and Tobin, A.B. (2010). Parasite protein kinases: at home and abroad. Cell Host Microbe *8*, 305-307.

Fenical, W., and Jensen, P.R. (2006). Developing a new resource for drug discovery: marine actinomycete bacteria. Nat Chem Biol *2*, 666-673.

Fukuda, D.S., Mynderse, J.S., Baker, P.J., Berry, D.M., Boeck, L.D., Yao, R.C., Mertz, F.P., Nakatsukasa, W.M., Mabe, J., Ott, J.*, et al.* (1990). A80915, a new antibiotic complex produced by Streptomyces aculeolatus. Discovery, taxonomy, fermentation, isolation, characterization, and antibacterial evaluation. J Antibiot (Tokyo) *43*, 623-633.

Gontag, E., Fenical, W., and Jensen, P.R. (2006). Genetic diversity of gram-positive bacteria cultured from marine sediments. Appl Env Micro *73*, 3272-3282.

Gontag, E., Fenical, W. and P.R. Jensen. (2006). Genetic diversity of gram-positive bacteria cultured from marine sediments. Appl Env Micro *73*, 3272-3282.

Hughes, C.C., Prieto-Davo, A., Jensen, P.R., and Fenical, W. (2008). The marinopyrroles, antibiotics of an unprecedented structure class from a marine Streptomyces sp. Org Lett *10*, 629-631.

Jensen, P.R., Dwight, R., and Fenical, W. (1991). Distribution of actinomycetes in near-shore tropical marine sediments. Appl Environ Microbiol *57*, 1102-1108.

Jensen, P.R., and Fenical, W. (1996). Marine bacterial diversity as a novel resource for microbial products. J Indust Microbiol *17*, 346-351.

Jensen, P.R., Gontang, E., Mafnas, C., Mincer, T.J., and Fenical, W. (2005a). Culturable marine actinomycete diversity from tropical Pacific Ocean sediments. Environ Microbiol *7*, 1039-1048.

Jensen, P.R., Mincer, T.J., Williams, P.G., and Fenical, W. (2005b). Marine actinomycete diversity and natural product discovery. Antonie Van Leeuwenhoek *87*, 43-48.

Martin, R.E., Ginsburg, H., and Kirk, K. (2009). Membrane transport proteins of the malaria parasite. Mol Microbiol *74*, 519-528.

Merckx, A., Nivez, M.P., Bouyer, G., Alano, P., Langsley, G., Deitsch, K., Thomas, S., Doerig, C., and Egee, S. (2008). Plasmodium falciparum regulatory subunit of cAMP-dependent PKA and anion channel conductance. PLoS Pathog *4*, e19.

Mincer, T.J., Jensen, P.R., Kauffman, C.A., and Fenical, W. (2002). Widespread and persistent populations of a major new marine actinomycete taxon in ocean sediments. Appl Environ Microbiol *68*, 5005-5011.

Newman, D.J., Cragg, G.M., Holbeck, S., and Sausville, E.A. (2002). Natural products and derivatives as leads to cell cycle pathway targets in cancer chemotherapy. Curr Cancer Drug Targets *2*, 279-308.

Payne, D.J., Gwynn, M.N., Holmes, D.J., and Pompliano, D.L. (2007). Drugs for bad bugs: confronting the challenges of antibacterial discovery. Nat Rev Drug Discov *6*, 29-40.

Soria-Mercado, I.E., Prieto-Davo, A., Jensen, P.R., and Fenical, W. (2005). Antibiotic terpenoid chloro-dihydroquinones from a new marine actinomycete. J Nat Prod *68*, 904-910.

Spellberg, B., Guidos, R., Gilbert, D., Bradley, J., Boucher, H.W., Scheld, W.M., Bartlett, J.G., and Edwards, J., Jr. (2008). The epidemic of antibiotic-resistant infections: a call to action for the medical community from the Infectious Diseases Society of America. Clin Infect Dis *46*, 155-164.

Syin, C., Parzy, D., Traincard, F., Boccaccio, I., Joshi, M.B., Lin, D.T., Yang, X.M., Assemat, K., Doerig, C., and Langsley, G. (2001). The H89 cAMP-dependent protein kinase inhibitor blocks Plasmodium falciparum development in infected erythrocytes. Eur J Biochem *268*, 4842-4849.

Talbot, G.H., Bradley, J., Edwards, J.E., Jr., Gilbert, D., Scheld, M., and Bartlett, J.G. (2006). Bad bugs need drugs: an update on the development pipeline from the Antimicrobial Availability Task Force of the Infectious Diseases Society of America. Clin Infect Dis *42*, 657-668.

Tenover, F.C. (2006). Mechanisms of antimicrobial resistance in bacteria. Am J Med *119*, S3-10; discussion S62-70.

Wells, T.N. (2010). Microbiology. Is the tide turning for new malaria medicines? Science *329*, 1153-1154.

Winzeler, E.A. (2008). Malaria research in the post-genomic era. Nature *455*, 751-756.

Woese, C.R. (2000). Interpreting the universal phylogenetic tree. Proc Natl Acad Sci U S A *97*, 8392-8396.

CHAPTER 2.

Pharmacological properties of the marine natural product marinopyrrole A against methicillin-resistant *Staphylococcus aureus*

2.1. ABSTRACT

The ongoing spread of methicillin-resistant *Staphylococcus aureus* (MRSA) strains in hospital and community settings presents a great challenge to public health and demonstrates the urgency for new antibiotics. Marinopyrrole A is a member of a structurally novel class of compounds identified from marine-derived *streptomycetes* with evidence of anti-staphylococcal activity. We show that marinoyrrole A has potent concentration-dependent bactericidal activity against clinically-relevant hospital- and community-acquired MRSA strains, prolonged post-antibiotic effects superior to the first-line current agents vancomycin and linezolid, and a favorable resistance profile. Marinopyrrole A showed limited toxicity to mammalian cell lines (at > 20X MIC). However, its antibiotic activity was effectively neutralized by 20% human serum. A variety of marinopyrrole analogs were isolated from culture or synthetically produced with to try to overcome the inhibitory effect of serum. The majority of analogs retained potent bactericidal effects against MRSA, yet most were still inhibited by serum. The activity of one novel synthetic derivative (YL10124) is not completely abolished in serum. Further derivatization of this structurally novel class of compounds may yield analogs with great potential for anti-MRSA therapeutic utility.

2.2 INTRODUCTION

Methicillin-resistant *Staphylococcus aureus* (MRSA) infections have reached epidemic proportions in many countries (Grundmann et al., 2006) and now represent the most common cause of skin and soft tissue infections in the United States (Como-Sabetti et al., 2009). Both hospital-associated (HA) and community-associated (CA) MRSA can exhibit broader resistance to multiple classes of antibiotics (Chambers and Deleo, 2009; Grundmann et al., 2006). Notwithstanding the oxazolidinone linezolid in 2000 and the lipopeptide daptomycin in 2003, the low number of new antibiotics discovered over the last half-century has defined an urgent need for novel agents to treat MRSA infections (Butler and Buss, 2006).

Beginning with the introduction of penicillin, natural products have provided diverse chemical scaffolds leading to nine of the 12 classes of antibiotics currently used in the clinic (Butler and Buss, 2006; Fenical and Jensen, 2006; Hughes, 2010b). The majority of these bioactive secondary metabolites are derived from terrestrial actinomycete bacteria. Although much less explored than terrestrial environments, the ocean has been shown to be a bountiful resource of biological and genetic diversity (Gontag, 2006) which leads to chemically-novel natural products (Fenical and Jensen, 2006; Hughes, 2010b).

We recently isolated a novel chemical scaffold from a previously uncharacterized marine actinomycete, designated CNQ-418 (Hughes, 2010a; Hughes et al., 2008). This natural product, marinopyrrole A, was found to contain an uncommon 1,3'-bipyrrole pharmacophore, and initial screening revealed potent anti-staphylococcal activity (Hughes, 2010a; Hughes et al., 2008).

Here, we characterize the *in vitro* activities of marinopyrrole A against a variety of clinically important MRSA strains. Key pharmacological properties of marinopyrrole A that are relevant to anti-MRSA activity, including time-kill kinetics, post-antibiotic effect, tendency to develop resistance in serial passage, cytotoxicity, serum inactivation, and plastic binding were assessed. Additionally, several derivatives of the novel marinopyrrole A scaffold were evaluated for assessment of structure-activity relationships targeting contemporary strains of MRSA. Our data show that marinopyrrole A exhibits a number of favorable anti-MRSA activities, including rapid killing kinetics, a prolonged post-antibiotic effect and limited eukaryotic cell cytotoxicity.

2.3. RESULTS AND DISCUSSION

2.3.1. Pharmacological Properties of Marinopyrrole A against MRSA

2.3.1.1. In vitro antimicrobial activity: Marinopyrrole A showed activity against all tested *S. aureus* strains, including glycopeptide-intermediate and vancomycin-resistant MRSA, and had potent activities against other gram-positive organisms. In addition marinopyrrole A was active against *H. influenzae,* but was inactive against other tested gram-negative strains **(TABLE 2.1.)**. The MICs of marinopyrrole A against the panel of HA- and CA-MRSA strains (0.188-0.750 μg/ml) were generally lower than those measured for vancomycin or linezolid, and the measured MICs against VRE (1 μg/ml) and *H. influenzae* (2 μg/ml) were also favorably potent.

2.3.1.2. Concentration–dependent bactericidal killing: *In vitro* time-kill studies were used to further characterize marinopyrrole A activity against MRSA. Marinopyrrole A displayed substantial concentration-dependent killing against MRSA strain TCH1516 **(FIGURE 2.1A.)** and was far more rapid in its antibiotic action than either vancomycin **(FIGURE 2.1B. and 2.1C.)** or linezolid **(FIGURE 2.1B. and 2.1D.)**. For example, marinopyrrole A at 10 X MIC (3.75 μg/ml) showed a 2-log kill of MRSA TCH1516 within 9 h, while the activity of vancomycin at 10X MIC (20 μg/ml) was much slower, reducing the initial inoculum by only about 10-fold. Treatment with 20X MIC (7.5 μg/ml) marinopyrrole A reduced the initial inoculum by nearly a 6 log-fold within 9 h.

TABLE 2.1. *In vitro* activities [MIC (μg/ml)] of marinopyrrole A compared to commonly used antibiotics against selected clinical drug-resistant strains.

MRSA	Classification	Marinopyrrole A	Vancomycin	Linezolid
S.aureus ATCC 29213	MSSA	0.5 – 1	1 – 2	n/a
UAMS1 (USA200)	MSSA	0.75	1.5	n/a
TCH1516 (USA300)	CA-MRSA	0.188 – 0.375	2	3
UAMS1182 (USA300)	CA-MRSA	0.188 – 0.375	1.56	3
NRS386 (USA700)	CA/HA-MRSA	0.375	2 – 4	3
Sanger 252	HA-MRSA	0.375	1 – 2	3
MRSA ATCC 33591	HA-MRSA	0.188 – 0.375	1.56	n/a
VRSA (Michigan)	VRSA	0.375 – 1.5	>256	n/a
VRSA (Pennsylvania)	VRSA	0.375 – 1	>256	n/a
A5940 *	Hetero-GISA	0.25 – 0.5	4	n/a
PC-3 (New York) *	VISA	0.25 – 0.5	8	n/a
HIP5836 (New Jersey) *	VISA	0.25 – 0.5	4 – 8	n/a

* (Sakoulas et al., 2002)

Other	Classification	Marinopyrrole A
E. faecalis	vanB	1
S. pyogenes	GAS (MI-5548)	1
S. pyogenes	GAS (M49-NZ131)	1
S. agalactiae	GBS (COHI)	2
S. epidermidis	ATCC 112228	0.25 – 1
B. anthracis	Sterne strain	1 – 2
B. subtilis	Strain 3610	0.94 – 1.87
H. influenzae	ATCC 1021	2
K. pneumoniae	ATCC 700603	>16
P. aeruginosa	ATCC 27853	>96
E. coli	ATCC 25922	>120

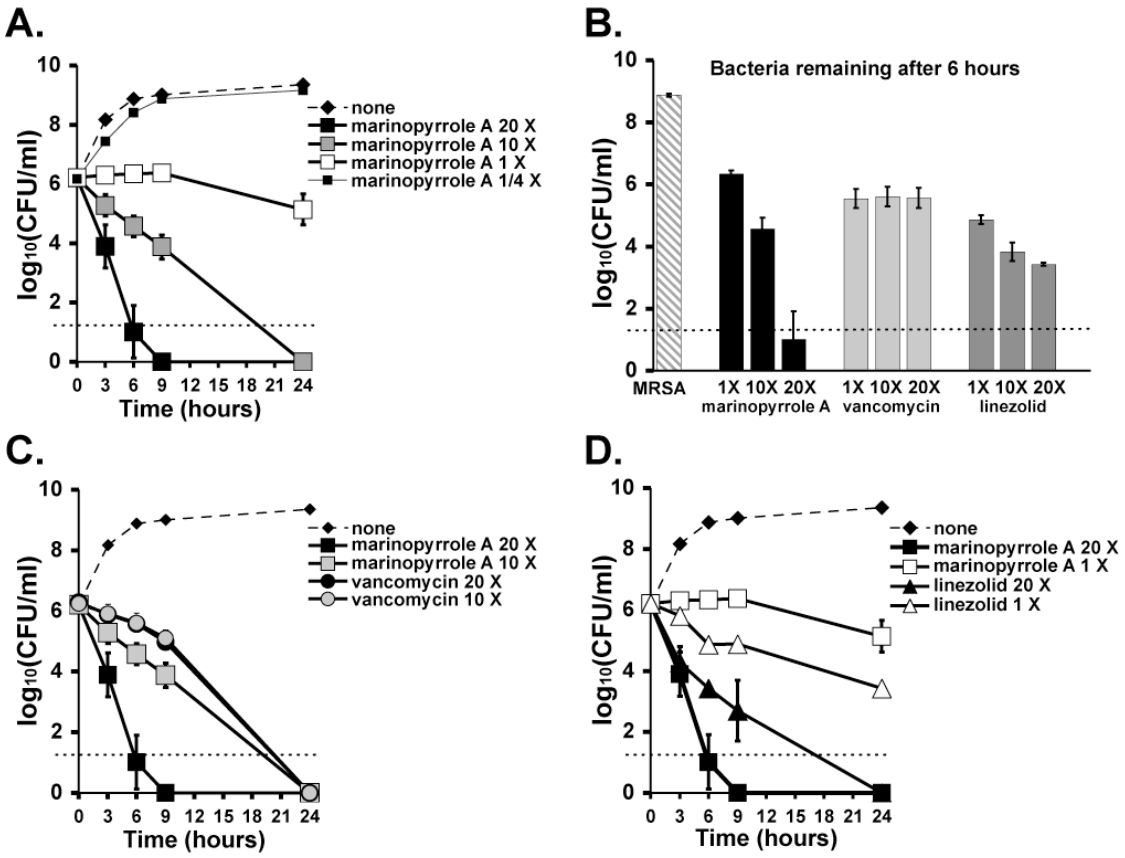

FIGURE 2.1. *In* vitro time-kill kinetic analysis of marinopyrrole A compared with linezolid and vancomycin. Time-kill kinetics of marinopyrrole A, vancomycin and linezolid against MRSA (USA300 strain TCH1516) at multiples of their MICs (0.375 μg/ml, 2 μg/ml and 3 μg/ml, respectively). **(A)** Concentration-dependent effects of marinopyrrole at multiples above and below the MIC. **(B)** Quantitative-cultures of surviving MRSA after 6-h incubation with 20X, 10X or 1X MIC of each compound, highlighting concentration-dependent killing of marinopyrrole A in comparison to equal ratios of linezolid and vancomycin. **(C)** Marinopyrrole A and vancomycin kinetics and 20X and 10X MIC. **(D)** Marinopyrrole A and linezolid kinetics at 10X and 1X MIC.

2.3.1.3. Prolonged post-antibiotic effect: Given its rapid and concentration-dependent activity, we investigated the potential post-antibiotic effect (PAE) of marinopyrrole A against MRSA. As shown in **FIGURE 2.2A.**, marinopyrrole at 1, 10, or 20X MIC exhibited a concentration-dependent PAE against MRSA strain TCH1516. Comparing vancomycin, linezolid and marinopyrrole A, each at 20X MIC **(FIGURE 2.2B.)**, a significantly longer recovery of the culture treated with marinopyrrole A was evident, with a calculated PAE = T – C of between 4 – 6 h. Evidence of this prolonged recovery is also seen at 10X MIC of marinopyrrole A in comparison to the other tested antibiotics **(FIGURE 2.2C.)**. Rapid concentration-dependent killing and a prolonged PAE against MRSA are highly favorable and distinguish the pharmacological activity of marinopyrrole A from that of vancomycin and linezolid.

2.3.1.4. Resistance studies by serial-passage mutagenesis: To assess the propensity of MRSA to develop resistance to marinopyrrole A, we tested two MRSA strains, CA-MRSA USA 300 TCH1516 and HA-MRSA Sanger 252, in a serial-passage experiment (Silverman et al., 2001). We found that the MIC remained unchanged (MIC = 0.375 μg/ml) during 10 passages **(FIGURE 2.3.)**. The MIC of the multi-drug resistant hospital-associated strain Sanger 252 increased by one-fold to 0.75 mg/ml during 10 passages. Thus, marinopyrrole A favorably exhibited sustained potent inhibitory activities despite repeated bacterial passage in sub-MIC doses of the compound.

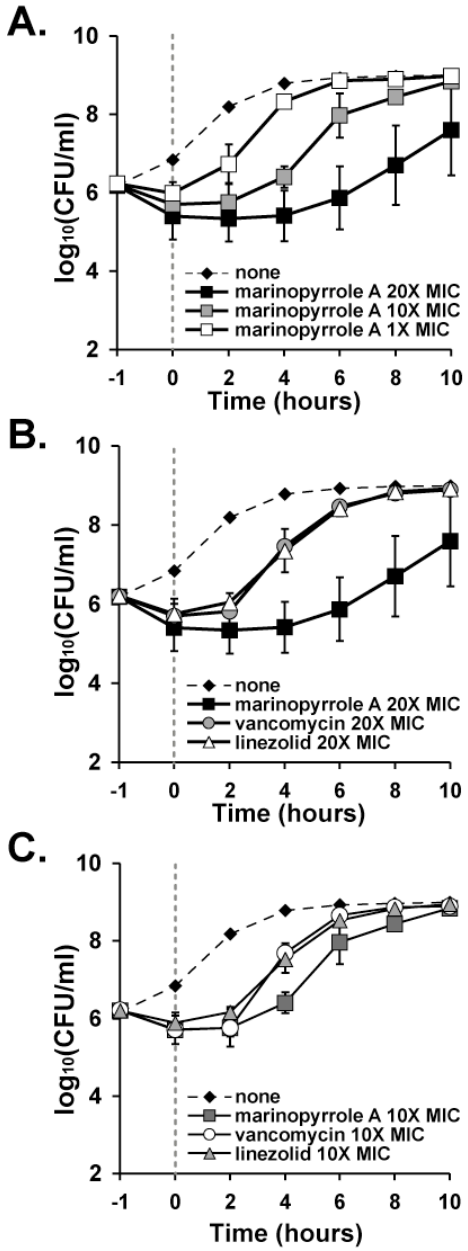

FIGURE 2.2. Post-antibiotic effects (PAE) of marinopyrrole A and reference compounds. TCH1516 was incubated for 1 hour with tested compounds at multiples of 20X, 10X and 1X their respective MICs of 0.375 μg/ml (marinopyrrole A), 2 μg/ml (vancomycin) and 3 μg/ml (linezolid). Antibiotics were subsequently removed; bacteria were washed (time 0) and allowed to recover in antibiotic free media. Curves show the rate of growth recovery for bacteria against tested compounds. **(A**) Concentration-dependent PAEs for marinopyrrole A at 20X, 10X and 1X MIC and comparisons of marinopyrrole A, vancomycin and linezolid **(B)** at 20X MIC and **(C)** 10X MIC.

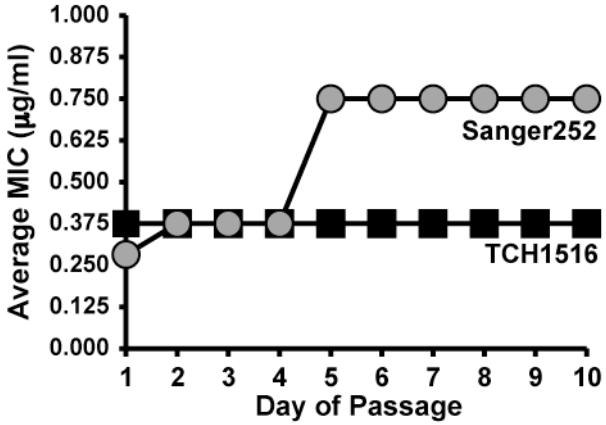

FIGURE 2.3. Serial passage of MRSA strains in sub-MIC concentrations of marinopyrrole A. The tendency for two strains, HA-MRSA Sanger 252 (grey circles) and CA-MRSA TCH1516 (black squares), to develop resistance to marinopyrrole A was evaluated over the course of ten days. Average MIC of Sanger 252 increased two-fold while that of TCH1516 did not change during serial passage.

2.3.1.5. Cytotoxicity profile: *To* estimate a therapeutic index for marinopyrrole A, we tested it for cytotoxicity against two mammalian cell lines. Marinopyrrole A exhibited a favorable therapeutic index, with IC_{50} values in excess of 20X above the MIC in each case: 32 – 64 μg/ml against HeLa cells and 8 – 32 μg/ml against L929 cells.

2.3.1.6. Activity in the presence of human serum: In order to determine the potential for marinopyrrole A as a systemic therapeutic, we investigated the MIC in the presence of normal human serum. The MIC of marinopyrrole A in the presence of 20% serum was ~ 96 μg/ml, approximately 256-fold higher than the MIC in the absence of serum. This property, presumably reflecting a high degree of protein binding, greatly reduces the activity of marinopyrrole and compromises its prospects as a therapeutic to treat systemic bacterial infections.

2.3.1.7. Activities of marinopyrrole derivatives: Following the discovery that the potent anti-MRSA activity of marinopyrrole A was effectively abolished in serum, derivatives of the marinopyrrole A scaffold were tested for their ability to bypass this inherent pharmacologic limitation. A set of 16 derivatives of marinopyrrole A, whose preparation is described in detail elsewhere (Hughes, 2010a) were analyzed. These derivatives include semisynthetic and synthetic analogs in addition to a range of minor metabolites produced by streptomycete strain CNQ-418. Two distinct chemical scaffolds were herein explored. The first group consists of derivatives that contain the 2,2'-salicyloyl-1,3'-bipyrrole structure of the parent compound **(FIGURE 2.4., MPA)**, produced semisynthetically or isolated from culture

(FIGURE 2.4., D1 – D8). The second group of derivatives were completely synthetic and include pyoluteorin-like compounds **(FIGURE 2.5., M1 – M6)** as well as two 1,3'-bipyrroles lacking salicyloyl substituents **(FIGURE 2.5., 15 - 16)**.

The 16 marinopyrrole A derivatives **(FIGURE 2.4., D1 – D8 and FIGURE 2.5., M1 – M6, 15 and 16)** were tested for activity against CA-MRSA TCH1516, HA-MRSA Sanger 252, and vancomycin-resistant *E. faecalis*. Many of these structural analogs retained potent activities against the three bacterial strains tested in the low μg/ml range. However, the marked inhibitory effect of 20% human serum on the activity of marinopyrrole A could not be overcome with any of the structural modifications **(FIGURE 2.4. and 2.5.)**.

Similar to marinopyrrole A, the majority of the semisynthetic bipyrrole-containing analogs in **FIGURE 2.4. (MPA, D1, D6, D8)** showed concentration-dependent killing **(FIGURE 2.6A.)**. For two pyrrole derivatives, the bromo-monodeoxypyoluteorin **(FIGURE 2.5., M2)** and iodo-monodeoxypyoluteorin **(FIGURE 2.5., M3)**, a noticeable phenomenon of time-dependent killing was observed. For these compounds, treatment of MRSA at 10X and 1X MIC initially inhibited its growth without significant bactericidal activity **(FIGURE 2.6B.)**.

Within 24 h, however, these compounds displayed significant bactericidal activity at 10X MIC. An interesting time-kill kinetic was shared by *O,O'*- diacetyl marinopyrrole A **(FIGURE 2.4., D3)** and *O*-acetyl bromo-monodeoxypyoluteorin **(FIGURE 2.5., M5)**. Both *O*-acetylated derivatives allowed for an initial increase in bacterial growth in the *in vitro* assay but ultimately inhibited further bacterial growth **(FIGURE 2.6C.)**. This effect can likely be attributed to the gradual hydrolysis of the phenolic esters to their free phenolic counterparts, which are bactericidal.

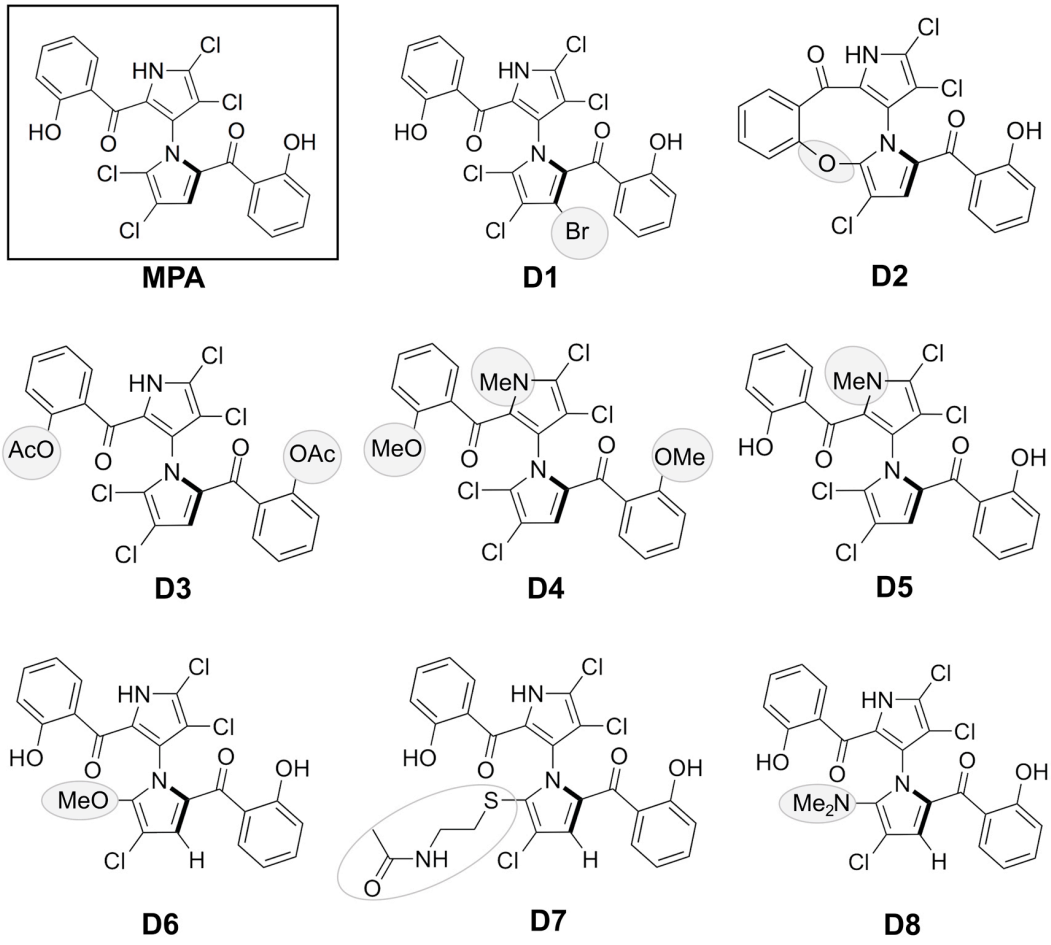

***In vitro* MICs (μg/ml) of 1,3'-bipyrrole biosynthetic derivatives.**

#	Identification	Description	TCH 1516 0% serum	TCH 1516 20% serum	Sanger 252	VRE
MPA	CNQ-418.508A	marinopyrrole A	0.188 - 0.375	≥96	0.375	1
D1	CNQ-418.586A	marinopyrrole B	0.188 - 0.375	≥96	0.188	1.5 - 3
D2	CNQ-418.472	marinopyrrole F	1.5 - 3	>96	>96	48
D3	CNQ-418.508(592)	diacetylated mar. A	1.5	≥96	3	12
D4	CNQ-418.508(550)	trimethylated mar. A	>96	>96	>96	>96
D5	CNQ-418.508(522)	*N*-methylated mar. A	>96	>96	>96	>96
D6	CNQ-418.508(504)	methoxide adduct	1.5 – 3	≥96	3	6
D7	CNQ-418.508(591)	cysteamine adduct	12	>96	12	>96
D8	CNQ-418.508(517)	dimethylamine adduct	1.5	≥96	1.5	3 - 6

FIGURE 2.4. 1,3'-Bipyrrole derivatives of marinopyrrole. The in vitro MICs of the 1,3' bipyrrole biosynthetic derivatives.

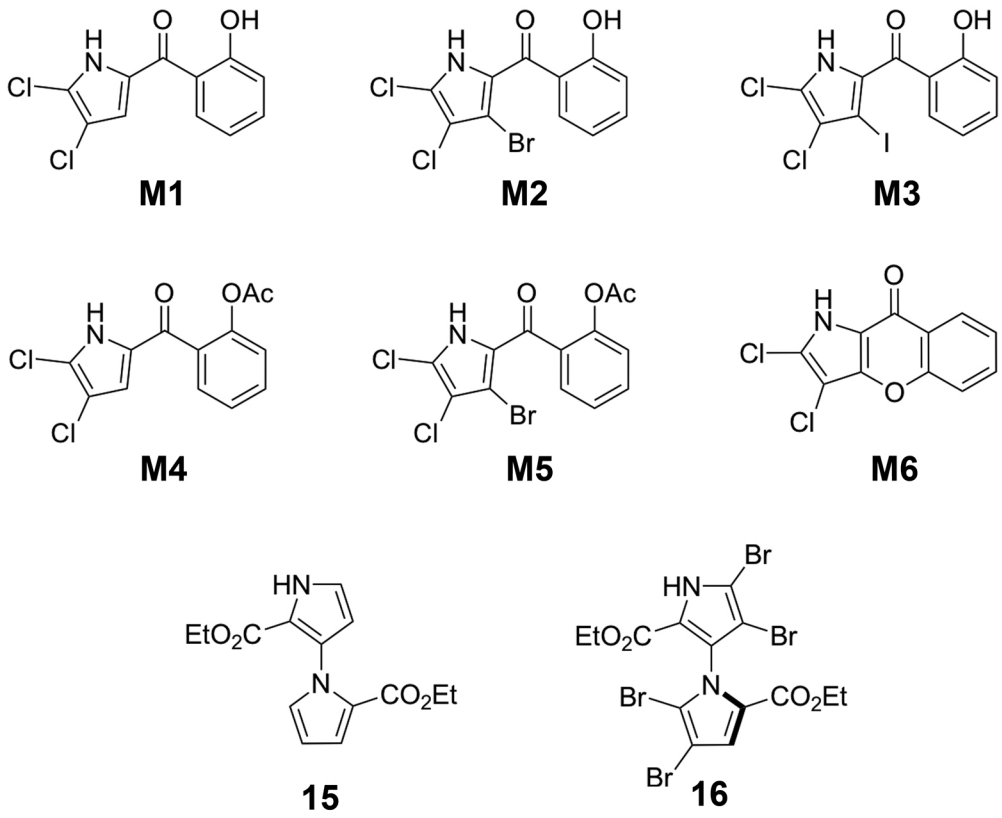

***In vitro* MICs (μg/ml) of pyoluteorin derivatives and bipyrrole derivatives.**

#	Identification	Description	TCH 1516 0% serum	TCH 1516 20% serum	Sanger 252	VRE
M1	CNQ-418.255	monodeoxypyoluteorin	>96	≥96	>96	12
M2	CNQ-418.255(333)	bromo-monodeoxypyolutoerin	1.5	≥48	1.5	24
M3	CNQ-418.255(381)	iodo-monodeoxypyolutoerin	1.5	≥48	1.5	24
M4	CNQ-418.255(297)	*O*-acetyl monodeoxypyoluteorin	12	48	12 - 48	>96
M5	CNQ-418.255(375)	*O*-acetyl, bromo-monodeoxypyoluteorin	3	≥48	48	48
M6	CNQ-418.255(253)	chromeneone	>96	>96	>96	>96
15	CNQ-418.276(S)	bipyrrole ester	>96	>96	>96	>96
16	CNQ-418.588(S)	tetrabrominated bipyrrole ester	6	>96	6 - 24	>96

FIGURE 2.5. Pyoluteorin derivatives and synthetic 1,3'-bipyrrole derivatives of marinopyrrole.

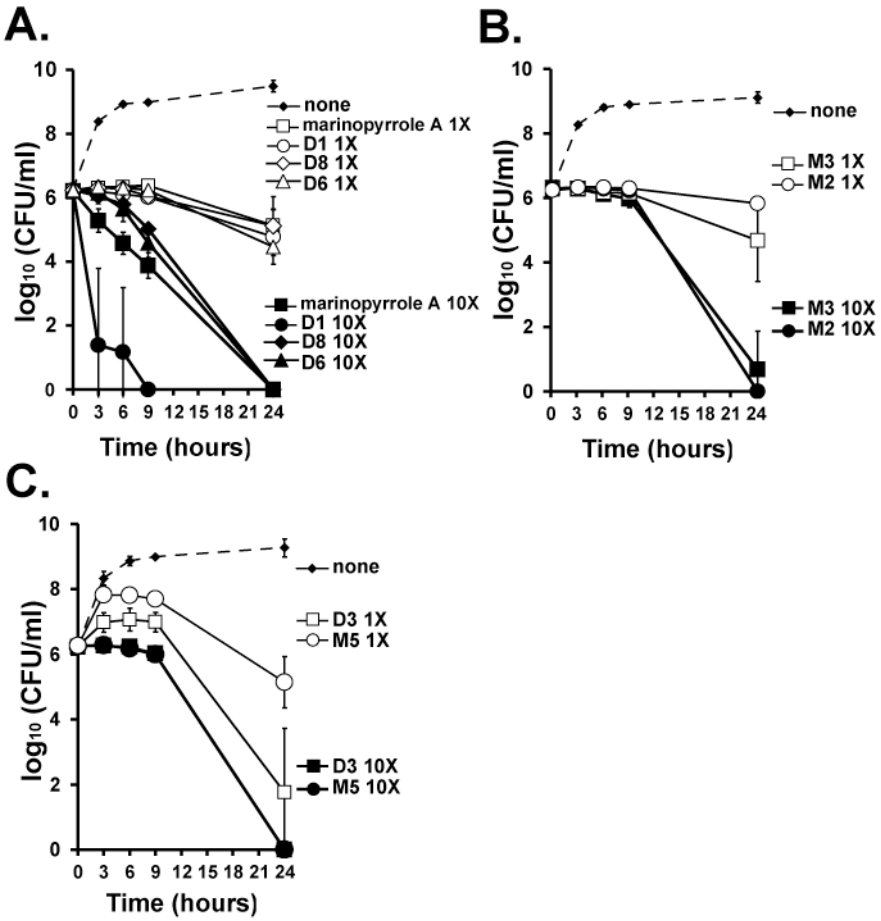

FIGURE 2.6. ***In vitro*** **kinetics of the marinopyrrole analogs against MRSA (TCH1516). (A)** Concentration-dependent kinetics of marinopyrrole analogs (refer to **FIGURE 2.4.**). **(B)** Kinetics of pyoluteorin analogs (refer to **FIGURE 2.5.**). **(C)** Kinetics of two acetylated marinopyrrole A derivatives (refer to compounds in **FIGURE 2.4. and 2.5.**).

2.3.1.8. Marinopyrrole A adsorption to plastic: Our initial studies of marinopyrrole A in the macrodilution assay (as described above) showed the MIC was two to four-fold lower in glass test tubes than in polystyrene tubes (e.g. 0.094 μg/ml for TCH1516 with glass tubes). We hypothesized that marinopyrrole A in solution was partially binding to plastic, a phenomenon described for other antibiotics including doxycycline and minocycline (Ciarlone, 1990). The event, called sorption, can occur when a drug is initially adsorbed and subsequently absorbed by its plastic container (Ciarlone, 1990; Illum, 1982), which may be ascribed to the very hydrophobic and slightly acidic nature of marinopyrrole A. To examine this possibility, the loss of marinopyrrole A to the walls of polystyrene vs. glass tubes was measured by methanol extraction of adsorbed drug and UV spectrometric quantification at A_{324nm}. Our results **(FIGURE 2.7A.)** showed that the amount of marinopyrrole A that adsorbed to plastic increased in a linear fashion as the tested concentration increased from 1, 2, 5 and 10 times the MIC, from 0.0046 ± 0.0010 (1X MIC) to 0.0316 ± 0.0007 (10X MIC). At the tested concentration greater than 10X MIC, the absorbances seem to plateau, possibly indicating saturation of binding **(FIGURE 2.7A.)**. Conversely, the absorbance results show that the glass tubes did not retain marinopyrrole A at any of the tested concentrations **(FIGURE 2.7A.)**. The resulting amounts (μg) of marinopyrrole A recovered by methanol extraction from plastic tubes were calculated from the measured absorbances **(FIGURE 2.7B)** and similarly showed a linear increase in adsorbed compound with saturation after 10X MIC.

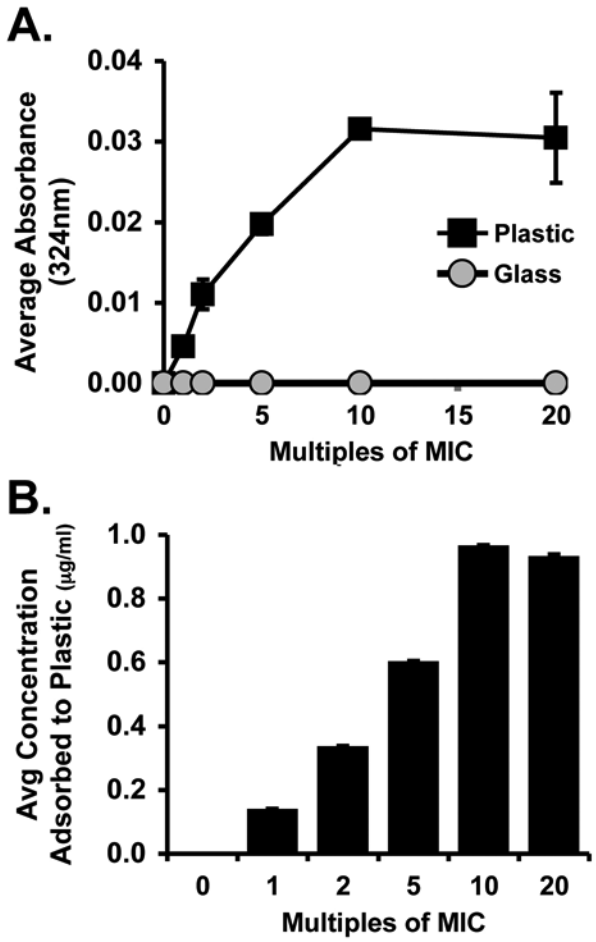

FIGURE 2.7. The tendency for marinopyrrole A to adsorb to plastic. This observation was tested by incubating plastic and glass test tubes for 22 h with increasing concentrations of marinopyrrole A. After incubation, methanol extraction was used to remove any adsorbed marinopyrrole A. **(A)** UV spectrometric quantification. Average absorbances (324 nm) of the resulting plastic and glass tubes at increasing multiples of the MIC. Marinopyrrole A adsorbs to plastic tubes but not glass. **(B)** Average concentration of marinopyrrole A removed from plastic tubes via methanol extraction increases as the compound concentration is increased.

2.3.1.9. Summary of the potent antibacterial activities of the marine-derived marinopyrrole A: We have shown that the recently discovered marine natural product marinopyrrole A **(FIGURE 2.4., (1))** possesses potent *in vitro* antimicrobial activities against both HA- and CA- strains of MRSA and VRE at submicromolar levels. Furthermore, marinopyrrole A maintained similar submicromolar MICs against glycopeptide-intermediate and vancomycin resistant *S.aureus* strains such as VRSA from Pennsylvania and Michigan, VISA strains HIP5836, PC-3 and Hetero-GISA A5940. Marinopyrrole A is also active against *H. influenzae*, but its Gram-negative spectrum does not extend to *P. aeruginosa* or *E.coli*.. When compared to vancomycin and linezolid, marinopyrrole A demonstrated potent concentration-dependent bactericidal kinetics against MRSA, with a 4 $\log_{10}$ increase in bacterial killing at 20X vs. 1X MIC. In contrast, vancomycin showed time-dependent kinetics in which all three concentrations tested (1X, 10X and 20X MIC) yielded equal quantities of surviving MRSA at 6 h. Such delayed killing kinetics of vancomycin against MRSA have been previously described (Lowdin et al., 1998).

Marinopyrrole A also displayed a concentration-dependent PAE profile **(FIGURE 2.2.)**, giving a significantly more favorable PAE (4 - 6 h) than either vancomycin or linezolid at concentrations 10 - 20X their respective MICs. At 10X MIC, the concentration of marinopyrrole A, 3.75 μg/ml, is still ~ 2X less than the IC_{50} against L929 cells (8 – 32 μg/ml) and ~ 8X less than the IC_{50} against HeLa cells (32 – 64 μg/ml). From these results, we can conclude that high doses of marinopyrrole A that may cause minimal mammalian *in vitro* toxicity can retard the regrowth of MRSA for a prolonged period. Furthermore, marinopyrrole A showed sustained and potent

MIC activities in serial-passage experiments **(FIGURE 2.3.)**. Despite repeated serial-passage in sub-MIC concentrations of marinopyrrole A, TCH1516 failed to develop resistance over a 10 day period and the MIC of Sanger 252 only increased by one-fold **(FIGURE 2.3.)**. Beyond these favorable pharmacokinetic parameters, marinopyrrole A displayed the potential for a reasonable therapeutic index, since mammalian cell cytotoxicity was observed only at concentrations in excess of 20X the MIC. Further, marinopyrrole A showed sustained and potent MIC activities in serial passage.

Although the mechanism of action of marinopyrrole A remains undefined, the potent and rapid killing kinetics as well as low but detectable cytotoxicity profile against mammalian cells suggest that this compound may nonspecifically kill target bacteria. Although not detailed in this paper, the results of preliminary metabolic labeling studies indicate that marinopyrrole A acts in a general manner without specifically targeting DNA, RNA, protein, or cell wall syntheses (data not shown). However, it is also possible that marinopyrrole A may specifically target a bacterial process not studied in the metabolic labeling assay (eg, fatty acid biosynthesis), and this possibility is currently under investigation.

However, marinopyrrole A was found to have a critical deficiency in its pharmacological profile that will likely prevent its use as a systemic antibacterial therapy, namely marked inhibition of antibiotic activity by serum. Therefore, we analyzed a series of 16 structural analogs **(FIGURE 2.4. and 2.5.)** of marinopyrrole A, some retaining the 1,3-bipyrrole scaffold and others possessing a single pyrrole resembling the pyoluteorin structure. While many of these derivations retained potent

anti-MRSA and anti-VRE activity, none were able to overcome the inhibitory effect of serum.

From these results, we conceive that marinopyrrole A could be used as a topical agent or in local therapy of device-related Gram-positive bacterial infections that are increasingly common in inpatient settings. In the latter case, e.g. as an antibiotic-lock agent, the affinity of marinopyrrole A for binding to plastic surfaces could prove advantageous, and serum inactivation would limit the potential for systemic toxicity. Further medicinal chemistry analysis of the structure-activity relationships of this potent and rapidly-acting bactericidal marine natural product antibiotic are required to illuminate its potential therapeutic utility.

Further studies involving fully-synthetic marinopyrrole A derivatives has yielded many analogs with potent bactericidal MRSA activities. We embarked on two collaborations in which over thirty marinopyrrole derivatives were tested for comparison to marinopyrrole A. The overall goal of these studies were to discover a structural conformation with less serum inhibition than the parent.

2.3.2. Biological evaluation of synthetic marinopyrrole and analogs

Marinopyrrole A and B **(FIGURE 2.8.)** exhibit promising antibiotic activities against methicillin-resistant *Staphylococcus aureus* (MRSA) (Haste et al., 2011; Hughes, 2010a; Hughes et al., 2008). The novel molecular structure and promising biological activities of marinopyrrole A attract considerable attention. Because of this, a total synthesis of this compound is warranted. The development of biologically active compounds through total synthesis could potentially yield large amounts of the

scaffold structure that could be used for structure analysis and analog design. With synthetic analogs in hand a wide range of structure-activity relationship data could be obtained. In collaboration with Nick Simmons and K.C. Nicolaou at The Scripps Research Institute in La Jolla, a number of synthesized marinopyrrole analogs were prepared through a short and efficient total synthesis **(Figure 2.8.)**.

2.3.2.1. Synthetic analogs yield important structure-activity relationships: A five-step synthesis of marinopyrrole was achieved (Nicolaou et al., 2011). Further derivatization yielded a diverse set of structural analogs for biological testing. These compounds **(FIGURE 2.8., [(±)-1, (+)-1, (–)-1, (±)-10, and 11– 16])** were evaluated for their antibacterial activities against the USA300 CA-MRSA strain TCH1516. The minimum inhibitory concentrations of these derivatives are shown in **FIGURE 2.8**. Synthetic racemic **[(±)-1]** and enantiopure **[(+)-1 and (–)-1]** marinopyrroles (**entries 1–3)** displayed anti-MRSA bactericidal potencies that were comparable to their naturally-derived counterparts **(FIGURE 2.4.)** (Haste et al., 2011). Interestingly, the tetrabrominated relative of marinopyrrole A **(FIGURE 2.8., analog 13 (entry 8))** demonstrated similar effectiveness to marinopyrrole A.

Conversely, the de-halogenated analog 11 **(Figure 2.8., entry 6)** was significantly less active. This result was important in the analysis of structure-activity relationships, indicating the importance of the halogen atoms for antibacterial activity. As shown by three dimethylated analogs **[9, (±)-10, and 12]**, free phenolic groups inherent to the parent marinopyrrole structure were required for biological activity **(FIGURE 2.8., entries 4, 5, and 7, respectively)**. Bis-acetylated marinopyrrole 14 **(FIGURE 2.8, entry 9)** showed similar antibacterial potency to marinopyrrole [(±)-1]

itself, possibly due to *in situ* ester hydrolysis within the cell. Removal of one of the two phenolic rings from the core marinopyrrole structure led to active, but less potent analogs, as demonstrated by compounds **15** and **16 (FIGURE 2.8., entries 10 and 11, respectively)**.

2.3.2.2 Synthetic analogs lack activity in 20% human serum: All twelve synthetic compounds were tested for antibacterial activities against MRSA in the presence of 20% normal pooled human serum. Each compound showed to be inactivated in the presence of serum. This indicated that while many of these compounds maintained potent bactericidal activities against MRSA, the challenge still remains as to how to engineer out the effect of serum on marinopyrrole activity.

2.3.3. Antibiotic activities of new synthetic marinopyrrole derivatives.

A nine-step synthesis pathway was developed by Rongshi Li and colleagues at the H. Lee Moffitt Cancer Center and Research Institute (Tampa/ St. Petersburg, Florida) (Cheng et al., 2010). The nine-step synthetic pathway achieved a marinopyrrole yield of 30%. In this study, compounds were synthesized to compare both their antibiotic and potential anti-cancer utilities. From this nine-step pathway, efficient production of novel derivatives is achieved. In collaboration with Li and colleagues, we have tested twenty new marinopyrrole analogs for their antibacterial effects against the CA-MRSA USA300 strain TCH1516.

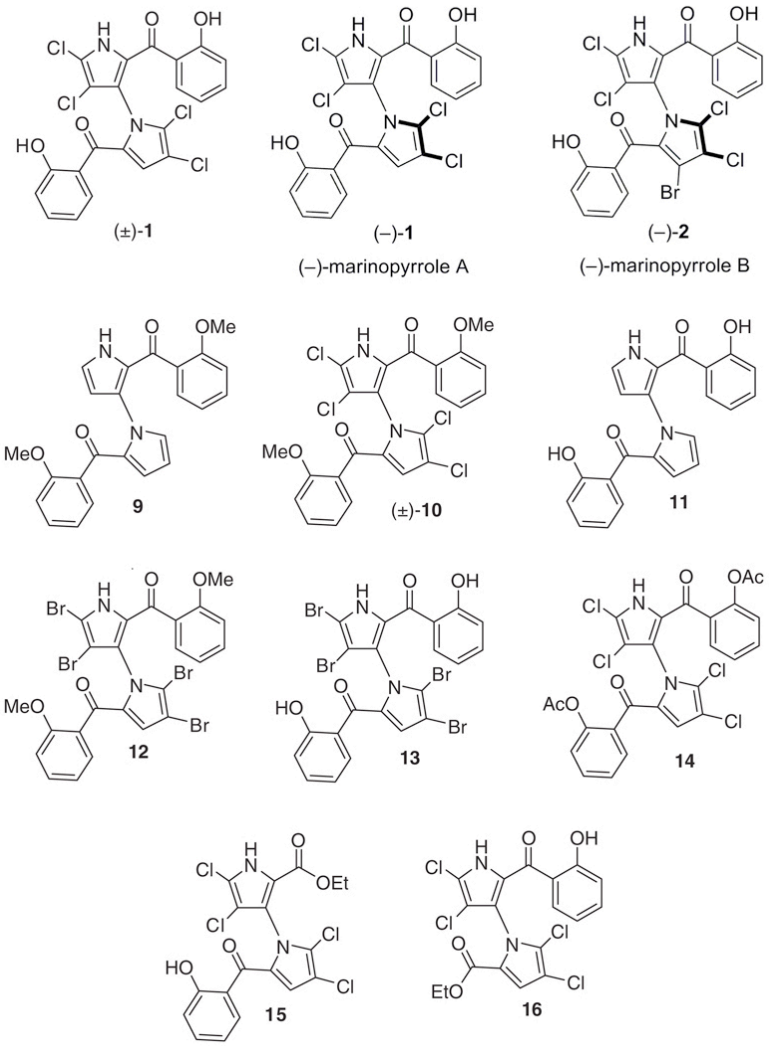

Entry	compound	MIC[a] (μg/mL)	Nizet Lab ID
1	(±)-**1**	0.375–0.750	MPA001
2	(+)-**1**	0.189 – 0.375	MPA (+)
3	(–)-**1**	0.189 – 0.375	MPA (-)
4	**9**	>96	MPA004
5	(±)-**10**	>96	MPA002
6	**11**	≥48	MPA003
7	**12**	>96	MPA006
8	**13**	0.75	MPA005
9	**14**	0.75 - 3	MPA007
10	**15**	>96	MPA008
11	**16**	1.5	MPA009

[a] Tested against TCH1516 (ATCC BAA-1717) a MRSA USA300 isolate.

FIGURE 2.8. Chemically synthesized marinopyrrole derivatives.

2.3.3.1. Seventy-five percent of marinopyrrole synthetic derivatives exhibited potent anti-MRSA activities: Of the twenty tested marinopyrrole derivatives from the nine-step synthetic pathway, fifteen showed potent antibiotic activities against MRSA. These compounds were tested in two batches **(TABLE 2.2.)**. Of the synthetic derivatives tested in the first batch, six of eleven showed anti-MRSA activities. The most potent of these were **YL10124**, **YL10125** and **YL10132**, all with equally potent activities to the parent marinopyrrole **(TABLE 2.2.)**.

With data indicating that three compounds maintained extremely potent activities, new derivatives guided by the structure-activity data were designed for further biological testing **(TABLE 2.2., Batch 2)**. All of these compounds maintained activities against MRSA, however, only one, **YL1143**, had sub-micromolar activities against TCH1516. Further insight can be gained from the structure-activity data to design new potent analogs.

2.3.3.2. Two synthetic derivatives maintain minimal activities in the presence of 20% human serum: Our previous studies showed that marinopryrrole A and semi-synthetic analogs were inactive in the presence of 20% serum. This constitutes a major challenge for a potential therapeutic. Previous studies on synthetic derivatives yielded no new analogs that retained antibacterial activities in the presence of serum (Nicolaou et al., 2011). We tested **Batch 1 (TABLE 2.2.)** derivatives in serum and determined that several compounds maintained some antibiotic activities.

Derivatives **YL10124**, **YL10125**, **YL10132** and **YL10133** all exhibited some

activity against MRSA in the presence of serum. **YL10124**, which had an MIC of 0.19 – 0.78 μM in the absence of serum, experienced a 60 -70 X increase in MIC in the presence of 20% normal human serum. This contrasts greatly from marinopyrrole A, in which the MIC increased over 250 X in the presence of serum **(Table 2.2.).**

2.3.3.3. Synthetic marinopyrrole analogs retain rapid and potent bactericidal activities in time-kill studies. *In vitro* time-kill studies were done to characterize killing kinetics of synthetic derivatives at 20X, 10X and 1X MIC and compare them to marinopyrrole A. **YL10124** and **YL10125** displayed rapid and potent concentration-dependent killing against the USA300 MRSA strain TCH1516 **(FIGURE 2.9A. and B.)**. This activity is much more rapid than vancomycin or linezolid, thus very similar in profile to the parent compound **(FIGURE 2.1.)**. **YL10124** and **YL10125** at 20X the MIC (37.5 μM) had potent effects, showing more than a 4-log kill of TCH1516. The kinetics of **YL10132**, however, significantly differed from those of marinopyrrole A and **YL10124** and **YL10125**. **YL10132** exhibited kinetics more similar to time-dependent antibiotics. For example, at 6 hours, **YL10132** killed equal concentrations of bacteria at all three tested concentrations.

Important insight can be gained from *in vitro* time-kill kinetics. The differences between **YL10124** and **YL10132** kinetics demonstrates that the scaffold could have two independent anti-bacterial effects or mechanisms of action. Further insight must be gained in regards to the structure activity data from these compounds. The kinetics exhibited by **YL10132** is similar to two semi-synthetic pyoluteorin derivatives **(FIGURE 2.4., M2 and M3, FIGURE 2.6B.).**

TABLE 2.2. MIC (μM) of Synthetic Marinopyrrole Analogs

Analog ID	THB (0% Serum) (μM)	20% Serum (THB) (μM)
Marinopyrrole A (rough MW 510)	0.375ug/ml (~ 0.75uM)	48 – 96ug/ml (~94uM – 188uM)
Batch 1		
RL034	> 200	> 200
RL036	6.25 - 25	100 - 200
RL038	25 - 50	>200
RL040	≥ 100	100 - 200
YL10122	≥ 200	>200
YL10123	≥ 200	>200
YL10124	0.19 – 0.78	25 - 50
YL10125	0.19 – 0.39	12.5 - 25
YL10132	0.39 – 0.78	25 - 100
YL10133	0.78 – 3.125	25 - 100
YL10143	≥ 200	>200
Batch 2		
YL1125	6.25	ND
YL1126B	3 – 6	ND
YL1127	1.56	ND
YL1128	6.25	ND
YL1129	3.125	ND
YL1142	1.56	ND
YL1143Na	1.56	ND
YL1143	0.78	ND
YL1144	3.125	ND

ND = not determined

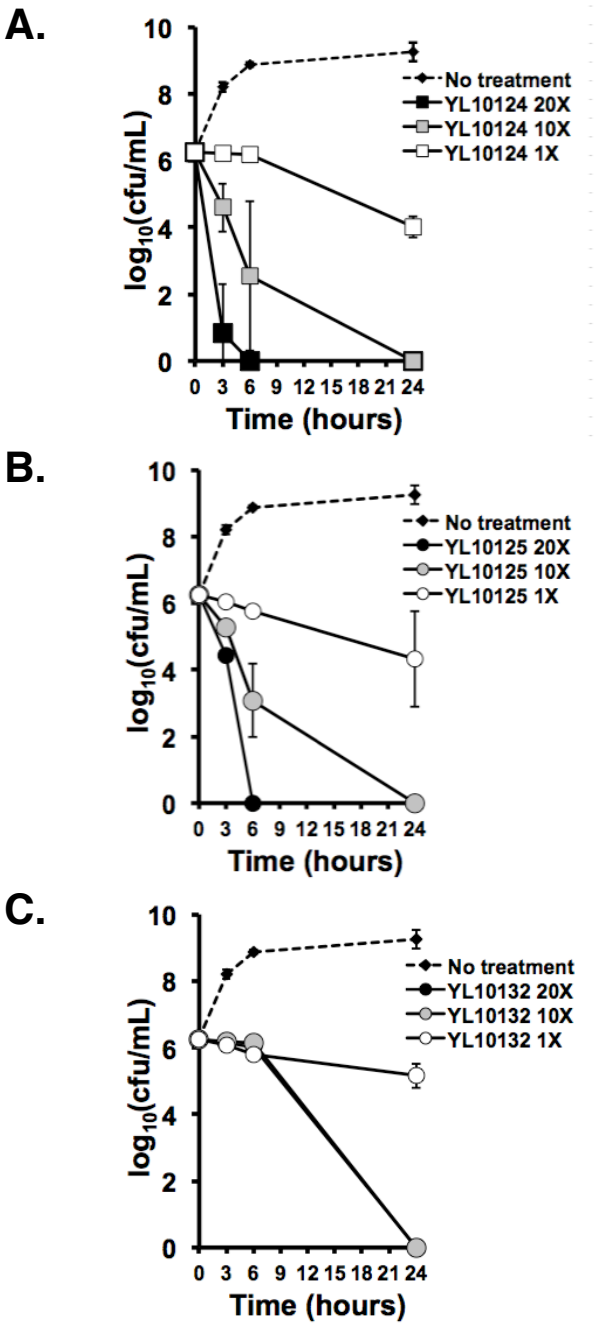

FIGURE 2.9. *In vitro* Time-kill Analysis for Marinopyrrole Analogs (MIC = 0.39 μM) against the USA300 CA-MRSA TCH1516. Tested concentrations are multiples 20X, 10X and 1X the MIC. **(A)** YL10124 and **(B)** Yl10125 showed potent concentration-dependent killing kinetics. **(C)** YL10132 demonstrated more time-kill *in vitro* kinetics.

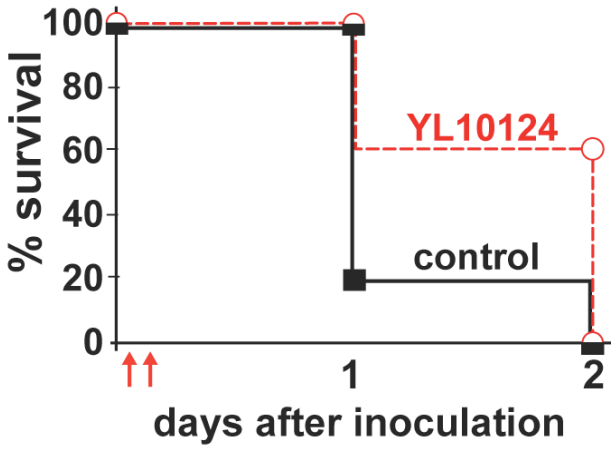

FIGURE 2.10. Preliminary studies of the *In vivo* efficacy of the marinopyrrole analog YL10124 in a murine model of MRSA sepsis. Female CD1 mice (8 week old) were injected intraperitoneally (i.p.) with 10^9 cfu of HA- MRSA strain Sanger 252 in 1% mucin. At 30 m and 4 h after infection (indicated by arrows), the mice were injected i.p. with either 10 mg/kg YL10124 (n = 10) or DMSO vehicle control (n=10). The mice were monitored for signs of sepsis for up to 72h, and mice that became moribund were humanely euthanized.

2.3.3.4. Preliminary results indicate that YL10124 may offer some protection in a systemic murine infection model of HA-MRSA: **YL10124** showed potent MICs in the presence and absence of serum as well as rapid time-kill kinetics. To test the *in* vivo efficacy of the compound, we subjected mice to a 48 h systemic infection of hospital-associated MRSA Sanger252. Female CD1 mice (roughly 8 weeks old) were treated with **YL10124** or vehicle control at a dose of 10 mg/kg at 30 minutes and 4 h following an intraperitoneal (i.p.) inoculation with Sanger 252. The survival and general health of mice were followed for 48 h. There was a marked difference in survival at 24 h where we observed some protection by **YL10124**. At that time point, we observed that mice treated with **YL10124** exhibited 40% mortality compared to the 80% of the control group. It should be noted that the solubility of YL10124 presented a challenge in the dosing in this model and could have played a role in the conferred protection or lack thereof. Further *in vivo* studies with this compound indicated that its cytotoxicity outweigh any protection benefits in this model, and suggested administration of this compound may increase mortality. With limited solubility and high cytotoxicity (*in vitro* at 72 hours), additional work is warranted to obtain a molecule with an enhanced safety profile.

2.3.3.5. Summary of synthetic marinopyrrole derivatives. In summary, concise total syntheses of marinopyrrole A (Cheng et al., 2010; Nicolaou et al., 2011) that allow for large-scale preparation of this novel natural product and its analogs allow for in-depth analyses of structure-activity relationships and educated engineering of future derivatives. The synthesized compounds evaluated for activity against TCH1516, a virulent community-associated MRSA. A great number of

analogs showed antibacterial activities **(FIGURE 2.8., TABLE 2.2.)**. Many suffered complete loss of antibacterial activity in the presence of human serum, suggesting benefit in topical but not systemic formulations. However, a few compounds derived from the nine-step syntheses by Rongshi Li and colleagues exhibited some activity in the presence of serum. The MICs for these compounds were only increased by roughly 65-fold rather than over 250-fold as seen in the parent compound. **YL10124** was one of these potent marinopyrrole analogs. An *in* vivo murine systemic infection model further probed the efficacy of **YL10124** as a therapeutic. In an initial model, some protection was seen against the hospital-associated MRSA infection at 24 h, However, these results were not repetitive and suggested that the compound provided more detrimental then beneficial effects. Further analyses are warranted to improve the *in* vivo effectiveness of future synthetic compounds and to improve the solubility profile of the analogs.

2.3.4. Chapter Summary

We have shown that the recently discovered marine-natural product, marinopyrrole A, is a potent anti-MRSA antibiotic. With submicromolar MICs against multi-drug resistant MRSA strains, marinopyrrole A shows promise as a potential therapeutic. Semi-synthetic derivatives of the core structure, in general, retained the antibiotic activities characteristic of marinopyrrole. Further many of these derivatives exhibited the potent, concentration-dependent time-kill kinetics observed with the marine-derived marinopyrrole. With prolonged postantibiotic effects, marinopyrrole A has exciting therapeutic potential with lasting antibiotic activities. Major challenges exist that would likely prevent its use in systemic therapy. For example, marinopyrrole

A and many of the structural analogs, semi-synthetic and fully synthetic in nature are completely inhibited in the presence of serum. A few synthetic derivatives have recently shown to maintain some activity in the presence of 20% human serum. This exciting result further verifies that additional structure-activity analyses and educated engineering of future derivatives could potentially yield potent new derivatives with enhanced pharmacological profiles. Further structural modifications, including the design of prodrug-like compounds, may be necessary in order to improve activity in serum, enhance solubility, and maintain the potent antibiotic effects of the marinopyrroles.

2.4. MATERIALS AND METHODS

2.4.1. Bacterial strains and media: A panel of multiple resistance Gram-positive and Gram-negative pathogens was used to probe the antimicrobial activity of marinopyrrole A. We tested the methicillin-sensitive reference *S.aureus* strain, ATCC 29213, the MSSA USA200 strain, UAMS-1, the MRSA USA300 strains UAMS-1182 and TCH1516 (ATCC BAA-1717), the CA/HA-MRSA USA700 isolate NRS386, and HA-MRSA strains Sanger 252 and ATCC 33591. To expand the evaluation of marinopyrrole A against multiresistant *S. aureus* strains, we tested a panel of glycopeptide-intermediate (GISA) and two vancomycin-resistant (VRSA) strains, including HIP5836 (GISA, New Jersey), A5940 (Hetero-GISA), PC-3 (GISA, New York), and VRSA (Michigan) and VRSA (Pennsylvania). Further, our analyses included a wider panel of Gram-positive organisms, including *Streptococcus pyogenes* (GAS), strains M1-5548 and M49-NZ131, *Streptococcus agalactiae* (GBS),

strain COHI, *Staphylococcus epidermidis* ATCC 12228, *Bacillus anthracis* (Sterne strain), *Bacillus subtilis* (strain 3610), and a vancomycin-resistant *Enterococcus faecalis* (VRE) isolate (ATCC 51299). In addition we tested marinopyrrole A against four gram-negative strains, a *Pseudomonas aeruginosa* blood isolate (ATCC 27853), *Haemophilus influenzae* (type b, ATCC 1021), *Klebsiella pneumoniae* (ATCC 700603) and *Escherichia coli* (ATCC25922). Strains designated with NRS were obtained through the Network of Antimicrobial Resistance in *S. aureus* (NARSA) program (Chantilly, VA) supported under NIAID/NIH contract # HHSN272200700055C. UAMS-1 and UAMS-1182 isolates were provided by Greg Somerville at the University of Nebraska, Lincoln, and originally obtained from Mark Smeltzer at the University of Arkansas Medical Center. Strains designated ATCC were obtained from the American Type Culture Collection (Manassas, VA). *B. subtilis* (strain 3610) was provided by Pieter Dorrestein, UCSD. Glycopeptide-intermediate and resistant strains were obtained from George Sakoulas, UCSD. For all strains except *H. influenzae*, Todd-Hewitt Broth (THB, Sigma, St. Louis, MO) was used for susceptibility, time-kill kinetic, and post-antibiotic effect studies, with overnight plating on Todd-Hewitt agar (THA) performed for enumeration of colony-forming units (cfu). For *H. influenzae,* brain-heart-infusion media (BHI) was supplemented with hemin (10 μg/ml) and nicotinamide adenine dinucleotide (NAD, Sigma, St. Louis, MO) (10 μg/ml).

2.4.2. Antimicrobial agents: The marine natural product, marinopyrrole A (**Figure 2.4., MPA**), was produced by cultivation of the actinomycete strain CNQ-418; methods describing its extraction, purification and structure elucidation were

published by Hughes, et al. (Hughes et al., 2008). The purified yellow metabolite was solubilized in dimethyl sulfoxide (DMSO, Sigma-Aldrich, St. Louis, MO), stored at -20°C, and thawed immediately prior to each use. Derivatives of marinopyrrole A were prepared similarly or synthesized for susceptibility studies (Hughes et al 2008). Vancomycin (NOVAPLUS Hospira, Inc. Lake Forest, IL) and linezolid (Zyvox Pfizer, Kalamazoo, MI) (2 mg/ml) were obtained from the pharmacy service at UC San Diego Medical Center.

2.4.3. Susceptibility testing: The susceptibility of a bacterial strain to marinopyrrole A was tested by broth macrodilution in duplicate 5 ml polystyrene round-bottom tubes (Falcon, Bedford, MA). Each tube contained a final volume of 4 ml that was first inoculated with 5 x 10^5 cfu/ml and then incubated with shaking at 37°C for 22 - 24 h. After incubation, 0.2 ml of media from each of the duplicate tubes, including the growth and blank media control tubes, was transferred into a sterile 96-well plate for turbidimetric measurement at $OD_{600.}$ Susceptibility testing for the marinopyrrole derivatives (**Figure 2.4., D1 – D8** and **Figure 2.4., M1 – M6, 15 - 16**) and for marinopyrrole A against some bacterial strains (**Table 2.1.**) was accomplished by microbroth dilution in tissue culture-treated 96-well flat-bottom polystyrene plates (Falcon Becton Dickinson, Franklin Lakes, NJ). Cultures were inoculated with 5 x 10^5 cfu/ml and incubated with shaking at 37°C for 22 - 24 h. The minimum inhibitory concentration (MIC) was determined to be the lowest concentration of antibiotic that inhibited visible bacterial growth as measured turbidimetrically at OD_{600}.

2.4.4. Cytotoxicity: Marinopyrrole A cytotoxicity was assessed by seeding 2 x 10^4 HeLa or L929 cells per well in sterile 96-well tissue culture-treated plates (Falcon Becton Dickinson, Franklin Lakes, NJ). After 24 h, the media was replaced with fresh media containing increasing concentrations of marinopyrrole A, and the plates were incubated at 37^{o}C in 5% CO_2 for 24 h. Cytotoxicity was assayed at 24 h by measuring the reduction of MTS, 3-(4,5-dimethylthiazol-2-yl)-5-(3-carboxymethoxyphenyl)-2-(4-sulfophenyl)-2*H*-tetrazolium, using the CellTiter 96® Aqueous non-radioactive cell proliferation assay per manufacturer's instructions (Promega, Madison, WI).

2.4.5. Time-kill analysis: Bactericidal activities of marinopyrrole A, vancomycin and linezolid against the CA-MRSA isolate TCH1516 were assessed by time-kill analysis essentially as described previously (Chin et al., 2007; Credito et al., 2007; Ueda et al., 2005). MRSA was grown overnight in THB at 37 °C with shaking, and then fresh THB was inoculated for growth to mid-logarithmic phase. Bacteria were added at a starting inoculum of ~5 x 10^5 cfu/ml to duplicate 5 ml polystyrene round-bottom tubes (Falcon, Bedford, MA). Marinopyrrole A, vancomycin and linezolid were added to final concentrations equal to 0.25, 1.0, 10 or 20 times their experimentally determined MICs of 0.375 μg/ml, 2 μg/ml and 3 μg/ml, respectively. Bacteria grown in the presence of an equivalent percentage of antibiotic diluent (DMSO) served as the growth control. Cultures were incubated in a 37 ^{o}C shaking incubator, and aliquots were removed from each tube at 0, 3, 6, 9 and 24 h and serially diluted for cfu enumeration on THA plates. To compare rates of antibiotic

killing, the decline of viable bacteria (log_{10} cfu/ml) was evaluated at the measured time points. The limit of detection for this assay was 1.6 (log_{10} CFU/ml).

2.4.6. Post-antibiotic effect: Post-antibiotic effect (PAE) was determined by the viable plate count method (Craig, 1996) using THB. A mid-logarithmic phase culture of the CA-MRSA strain TCH1516 was prepared as described for the time-kill studies. A starting inoculum of ~5 x 10^5 CFU/ml logarithmic phase bacteria in a final volume of 4 ml were exposed to concentrations of either marinopyrrole A, vancomycin or linezolid at 1, 10 or 20 times the respective MIC for 1 h at 37°C with shaking. Each solution was prepared in duplicate in 5 ml polystyrene tubes (Falcon, Bedford, MA) with a growth control included as above. After 1 h, each culture was centrifuged at 4,000 rpm for 10 min. The supernatant was removed, and the bacterial pellet was washed with 4 ml of antibiotic-free THB. The bacterial pellets were then resuspended in fresh THB to a total volume of 4 ml and allowed to recover in a 37°C shaking incubator. Aliquots were removed at -1, 0, 2, 4, 6, 8 and 10 h for CFU enumeration on THA as detailed in the time-kill procedure. PAE was calculated according to the Craig and Gudmundsson formula: $PAE = T - C$ (Craig, 1996), where T refers to the time required for the treated culture to recover by one-log_{10} CFU greater than that observed immediately after drug removal (time 0), and C refers to the corresponding recovery time observed for the untreated control (Craig, 1996).

2.4.7. Resistance studies by serial-passage mutagenesis: Serial passage mutagenesis studies were done according to the assay described by Silverman, et al (Silverman et al., 2001). Briefly, on day 1 duplicate sets of

polystyrene tubes containing THB and marinopyrrole A at either 4X (1.5 μg/ml), 2X (0.75 μg/ml), 1X (0.375μg/ml), 0.5X (0.189 μg/ml), or 0.25X MIC (0.094 μg/ml) or 0 μg/ml were inoculated with a single colony of *S. aureus* strains TCH1516 (USA300 CA-MRSA) or Sanger 252 (HA-MRSA). MRSA cultures were incubated at 37 ºC overnight with shaking. At 16 - 24 h of incubation the culture at the highest concentration of marinopyrrole A that supported bacterial growth was diluted 1:10,000 into sets of fresh media and marinopyrrole A at the same concentrations listed above. This serial passage experiment was continued for 10 days, ending when cultures did not show a change in susceptibility for three successive days (Silverman et al., 2001).

2.4.8. Effect of human serum on antibiotic activity: The MIC of marinopyrrole A compared to vancomycin against CA-MRSA strain TCH1516 was determined in the presence of 20% pooled human serum in THB. Using 96-well tissue culture-treated plates (MICROTEST^{TM} 96, Becton-Dickinson, Franklin Lakes, NJ), MICs in the presence and absence of serum were determined using an adaptation of the standard broth microdilution method (Zurenko et al., 1996). Due to the opacity produced by addition of serum to the assay, the color-change indicator, resazurin (Sigma-Adrich, St. Louis, MO), was used as a surrogate indicator of bacterial growth (Sarker et al., 2007). Oxidoreductases of viable bacteria reduce blue resazurin to pink resorufin (Sarker et al., 2007; Zurenko et al., 1996). For this assay, resazurin sodium salt powder was solubilized in sterile water to a final concentration of 6.75 mg/ml (Sarker et al., 2007), filtered using a Costar #8160 Spin-X® Centrifuge Tube Filter by centrifugation at 10,000 rpm for 10 min, and the filtrate was added to each well of the test plate to a final concentration of 10% (Zurenko et al., 1996). Mid-

logarithmic phase MRSA were added at a starting inoculum of 5 x 10^5 CFU/ml to the test plates containing the serially diluted antibiotics + 10% resazurin solution. Plates were covered in foil and incubated for 24 h with shaking at 37 ºC. After overnight incubation, the plates were evaluated visually for blue-to-pink color change indicative of bacterial growth. The MIC was determined to be the lowest antibiotic concentration that did not induce the blue to pink color change.

2.4.9. Antibiotic adsorption to plastic: Marinopyrrole A adsorption to plastic and glass was compared in similarly sized disposable borosilicate 12 x 75 mm glass test tubes (VWR® Culture Tubes) and 5 ml-polystyrene round-bottom tubes (Falcon, St. Louis, MO). Marinopyrrole A was added to a final volume of 4 ml THB in each tube at 0, 1, 2, 5, 10 or 20 times the MIC for the MRSA strain, TCH1516, 0.375 μg/ml. Each tube was incubated in the absence of bacteria for 22 – 24 h in a 37ºC shaking incubator to mimic the experimental conditions of the time-kill kinetic studies. Following incubation, media containing antibiotic was removed from each tube and the inside walls of the plastic and glass tubes were washed repeatedly five times with 5 ml water. Then, the adsorbed antibiotic was extracted with 4.0 ml methanol. The resulting sample was analyzed in triplicate via UV spectroscopy at 324 nm. The UV data were averaged to quantify the drug adsorbed to the glass and plastic tubes at the tested concentrations.

2.4.10. In vivo MRSA challenge: Female CD1 mice (8 week old) were injected intraperitoneally (i.p.) with 10^9 cfu of HA- MRSA strain Sanger 252 in 1% mucin. At 30 m and 4 h after infection (indicated by arrows), the mice were injected

i.p. with either 10 mg/kg YL10124 (n = 10) or DMSO vehicle control (n=10). The mice were monitored for signs of sepsis for up to 72h, and mice that became moribund were humanely euthanized.

2.5. ACKNOWLEDGEMENTS

This chapter was reproduced with permission from co-authors and modified from three different papers, two published and one in preparation.

Work described in **Chapter 2.3.1.** was modified from: Haste NM, Hughes CC, Tran DN, Fenical W, Jensen PR, Nizet V, Hensler ME. Pharmacological properties of the marine natural product marinopyrrole A against methicillin-resistant *Staphylococcus aureus*. *Antimicrob Agents Chemother*. (2011), 55:3305-12, PMC3122406. This work was supported the National Institutes of Health grant GM084350 (WF and VN) and National Institutes of Health International Cooperative Biodiversity Groups program TW007401 (WF and PRJ). N.M.H was supported by the National Institutes of Health Training Program in Marine Biotechnology (T32 GM067550) and Ruth L. Kirschstein National Research Service Award (NRSA) from National Institutes of Health Grants (5 F31 GM090658-02). A portion of this work was presented previously at the 49th Interscience Conference on Antimicrobial Agents and Chemotherapy (ICAAC), 2009 (Abstract # F1-1501) (Haste, 2009).

Work described in **Chapter 2.3.2.** was modified from: Nicolaou KC, Simmons NL, Chen JS, Haste NM, Nizet V. Total synthesis and biological evaluation of marinopyrrole A and analogues. *Tetrahedron Lett.* (2011) 52(17):2041-2043, PMCID: PMC3077031. Financial support for this work was provided by The Skaggs Institute for Chemical Biology, a National Institutes of Health (U.S.A.) grant and Ruth L. Kirschstein National Research Service Award (NRSA) (to N.M.H.).

Work detailed in **Chapter 2.3.3.** is in preparation for publication and was in collaboration with Rongshi Li, PhD and colleagues at the H. Lee Moffitt Cancer Center and Research Institute (Tampa / St. Petersburg, Florida).

2.6. REFERENCES

Butler, M.S., and Buss, A.D. (2006). Natural products--the future scaffolds for novel antibiotics? Biochem Pharmacol *71*, 919-929.

Chambers, H.F., and Deleo, F.R. (2009). Waves of resistance: Staphylococcus aureus in the antibiotic era. Nat Rev Microbiol *7*, 629-641.

Cheng, C., Pan, L., Chen, Y., Song, H., Qin, Y., and Li, R. (2010). Total synthesis of (+/-)-marinopyrrole A and its library as potential antibiotic and anticancer agents. J Comb Chem *12*, 541-547.

Chin, J.N., Rybak, M.J., Cheung, C.M., and Savage, P.B. (2007). Antimicrobial activities of ceragenins against clinical isolates of resistant Staphylococcus aureus. Antimicrob Agents Chemother *51*, 1268-1273.

Ciarlone, A.E., Fry, B.W. and D.M. Ziemer (1990). Some observations on the adsorption of tetracyclines to glass and plastic labware. Microchemical J *42*, 250-255.

Como-Sabetti, K., Harriman, K.H., Buck, J.M., Glennen, A., Boxrud, D.J., and Lynfield, R. (2009). Community-associated methicillin-resistant Staphylococcus aureus: trends in case and isolate characteristics from six years of prospective surveillance. Public Health Rep *124*, 427-435.

Craig, W.A., and S. Gudmundsson (1996). Postantibiotic effect. In *In* V Lorian (ed), Antibiotics in laboratory medicine, 4th ed (Baltimore, Md., The Williams and Wilkins Co.), pp. 296-329.

Credito, K., Lin, G., and Appelbaum, P.C. (2007). Activity of daptomycin alone and in combination with rifampin and gentamicin against Staphylococcus aureus assessed by time-kill methodology. Antimicrob Agents Chemother *51*, 1504-1507.

Fenical, W., and Jensen, P.R. (2006). Developing a new resource for drug discovery: marine actinomycete bacteria. Nat Chem Biol *2*, 666-673.

Gontag, E., Fenical, W. and P.R. Jensen. (2006). Genetic diversity of gram-positive bacteria cultured from marine sediments. Appl Env Micro *73*, 3272-3282.

Grundmann, H., Aires-de-Sousa, M., Boyce, J., and Tiemersma, E. (2006). Emergence and resurgence of meticillin-resistant Staphylococcus aureus as a public-health threat. Lancet *368*, 874-885.

Haste, N., D. Tran, V. Perera, C. Hughes, P.R. Jensen, W. Fenical, V. Nizet, and M. Hensler (2009). In Vitro Activity of the Novel Marine Natural Product Marinopyrrole A against MRSA, abstr F1-1501. In 49th Intersci Conf Antimicrob Agents Chemother American Society for Microbiology (San Francisco, CA).

Haste, N.M., Hughes, C.C., Tran, D.N., Fenical, W., Jensen, P.R., Nizet, V., and Hensler, M.E. (2011). Pharmacological properties of the marine natural product

marinopyrrole A against methicillin-resistant Staphylococcus aureus. Antimicrobial agents and chemotherapy *55*, 3305-3312.

Hughes, C.C., and Fenical, W. (2010a). Structures, Reactivities, and Antibiotic Properties of the Marinopyrroles A-F. J Org Chem *75*, 3240-3250.

Hughes, C.C., Fenical, W. (2010b). Antibacterials from the sea. Chemistry *16*, 12512-12525.

Hughes, C.C., Prieto-Davo, A., Jensen, P.R., and Fenical, W. (2008). The marinopyrroles, antibiotics of an unprecedented structure class from a marine Streptomyces sp. Org Lett *10*, 629-631.

Illum, L.a.B., H. (1982). Sorption of drugs by plastic infusion bags. Inter J of Pharmaceutics *10*, 339-351.

Lowdin, E., Odenholt, I., and Cars, O. (1998). In vitro studies of pharmacodynamic properties of vancomycin against Staphylococcus aureus and Staphylococcus epidermidis. Antimicrob Agents Chemother *42*, 2739-2744.

Nicolaou, K.C., Simmons, N.L., Chen, J.S., Haste, N.M., and Nizet, V. (2011). Total synthesis and biological evaluation of marinopyrrole A and analogues. Tetrahedron Lett *52*, 2041-2043.

Sakoulas, G., Eliopoulos, G.M., Moellering, R.C., Jr., Wennersten, C., Venkataraman, L., Novick, R.P., and Gold, H.S. (2002). Accessory gene regulator (agr) locus in geographically diverse Staphylococcus aureus isolates with reduced susceptibility to vancomycin. Antimicrob Agents Chemother *46*, 1492-1502.

Sarker, S.D., Nahar, L., and Kumarasamy, Y. (2007). Microtitre plate-based antibacterial assay incorporating resazurin as an indicator of cell growth, and its application in the in vitro antibacterial screening of phytochemicals. Methods *42*, 321-324.

Silverman, J.A., Oliver, N., Andrew, T., and Li, T. (2001). Resistance studies with daptomycin. Antimicrob Agents Chemother *45*, 1799-1802.

Ueda, Y., Kanazawa, K., Eguchi, K., Takemoto, K., Eriguchi, Y., and Sunagawa, M. (2005). In vitro and in vivo antibacterial activities of SM-216601, a new broad-spectrum parenteral carbapenem. Antimicrob Agents Chemother *49*, 4185-4196.

Zurenko, G.E., Yagi, B.H., Schaadt, R.D., Allison, J.W., Kilburn, J.O., Glickman, S.E., Hutchinson, D.K., Barbachyn, M.R., and Brickner, S.J. (1996). In vitro activities of U-100592 and U-100766, novel oxazolidinone antibacterial agents. Antimicrob Agents Chemother *40*, 839-845.

CHAPTER 3.

Forgotten Treasures: Natural product-derived antibiotics for the treatment of contemporary drug-resistant methicillin-resistant *Staphylococcus aureus*

3.1. ABSTRACT

The alarming rise of hospital- and community-associated methicillin-resistant *Staphylococcus aureus* (HA- and CA-MRSA) infections has prompted a desperate search for novel antibiotics. As discussed in Chapter 2, new chemical scaffolds have been discovered throughout the world's ocean floors. It should be noted, however, that the likelihood of finding the cure for a particular disease is very minimal. Roughly, for every 10000 new compounds that enter the research pipeline, only one will be approved for clinical therapy. With the already daunting task of discovering potent chemical scaffolds arrives added difficulty in finding a drug that is safe yet effective, potent yet not toxic, that works *in vivo*, is delivered to the wanted action site and that acts on the target receptor or protein without interacting greatly on "off-target" machinery so as to limit unwanted side effects. This challenge is combined with the knowledge that it takes 10 – 15 years on average to develop one new therapy and that with each successful drug is an associated $1 billion dollars in research and development costs. With the advent of increasing *Staphylococcus aureus* resistance, there is a dire need for drugs to treat these infections. One way to find new therapies is to re-characterize old ones. Many of the previously tested

antibiotics were evaluated on bacteria that were highly susceptible to the “new scaffolds” of their time. It is likely that many of these compounds were essentially thrown out and compounds with slightly better efficacy, toxicity profiles and other were pursued. In this chapter, we focus on three different groups of chemical scaffolds that were previously discovered, the depsipeptides, napyradiomycins and nosiheptide. Here we characterize their potent activities to virulent and highly resistant contemporary MRSA strains.

3.2. INTRODUCTION

The alarming rise of methicillin-resistant *Staphylococcus aureus* (MRSA) infections in several countries worldwide has provided urgency to the search for structurally novel antibiotics that target these organisms (Cornaglia and Rossolini, 2009). Hospital-associated (HA)-MRSA are frequently resistant to multiple antibiotic classes, and rapidly emergent strains of community-associated (CA)-MRSA, which have demonstrated unusually high virulence and ease of transmission, now represent the most common cause of skin and soft tissue infections in the United States (Como-Sabetti, 2009; Patel, 2009). These pathogens pose a great risk to human health. Furthermore, the approval of novel antibiotics for human medicine has not kept pace with the development of resistance by important bacterial pathogens such as MRSA. Just a few drugs with novel scaffolds (linezolid, daptomycin) have been introduced to the antibacterial formulary in the past 11 years, and only three new antibacterial compounds are in advanced stages of clinical development (Boucher, 2009; Spellberg, 2008). Both HA- and CA-MRSA strains have already demonstrated the capacity to evolve resistance to linezolid and daptomycin.

Natural products represent a vast source of potential new chemical structures possessing antimicrobial activity. At least three of every four current antibacterial agents are related in some way to natural products (Demain, 2009) and a majority of these discoveries have come from filamentous bacteria of the order *Actinomycetales* (actinomycetes). This group of filamentous spore-forming bacteria have yielded a great number of today's clinical therapies, including the commonly used antibiotics gentamicin, rifampin and vancomycin (Boucher, 2009; Spellberg, 2008). In fact,

more than 9000 biologically active molecules have been isolated from actinomycetes, yielding 460 pharmaceutical agents used in the medical or agricultural fields (Demain, 2009). Although terrestrial (soil) actinomycetes were the mainstay for antibiotic discovery efforts in the previous five decades, there is evidence that this resource is becoming exhausted. In contrast, the marine environment, covering more than three-fourths of the world's surface, represents a vast and relatively untapped source of novel scaffolds with unique antimicrobial properties (Fenical and Jensen, 2006; Kwon et al., 2006; Mincer et al., 2002; Soria-Mercado et al., 2005a). Recently, structures identified from new marine actinomycete species have been shown to exhibit potent anti-MRSA activity with desirable cross-activity against other bacterial pathogens (Hughes et al., 2008; McArthur, 2008).

3.2.1. Depsipeptides: Etamycin and related Fijimycins: In the course of screening a library of extracts from previously unidentified species of marine-derived actinomycetes for anti-MRSA activity, we followed a hit and purified an active secondary metabolite that we confirmed by NMR and mass spectrometric analysis to be etamycin—a classical depsipeptide antibiotic of the streptogramin B class. As decades have elapsed since consideration of the antibiotic properties of etamycin, we undertook an evaluation of its activity against a panel of contemporary, clinically relevant HA- and CA- MRSA strains. We find that etamycin exhibits favorable *in vitro* antibacterial activity and killing kinetics and is also protective against MRSA-induced lethality in a murine systemic infection model. These data suggest that etamycin could serve as the basis for in-depth study of related marine-derived molecules as

MRSA-targeted therapies.

3.2.2. Napyradiomycins: In 1986, a novel antibiotic class was discovered from the soil-derived organism *Chainia rubra* MG802-AF1 in Japan (Shiomi et al., 1986a; Shiomi et al., 1986b). This class of meroterpenoid dihydroquinone compounds, termed napyradiomycins, was initially characterized according to their physiochemical, spectroscopic, NMR and X-ray diffraction properties (Shiomi et al., 1987a; Shiomi et al., 1987b). In 1990, another actinomycete, *Streptomyces aculeolatus*, was found to produce structurally related napyradiomycins (Fukuda et al., 1990a; Fukuda et al., 1990b; Gomi et al., 1987; Shomura et al., 1987; Umezawa et al., 1995). Early assays revealed the napyradiomycin class to have significant activities against Gram-positive bacteria including *S. aureus*, *S. epidermidis*, *Enterococcus faecalis* and *E. faecium*, *Streptococcus pyogenes* and *S. pneumoniae*, *Haemophilus influenzae*, *Bacillus anthracis*, and *Micrococcus luteus* (Fukuda et al., 1990a; Gomi et al., 1987; Shiomi et al., 1986a; Shiomi et al., 1987b). Napyradiomycins, including A80915A (**1**) and A80915B (**2**), showed activity against *Clostridium difficile* and *C. perfringens* and other anaerobic bacteria; however, no activity was found against Gram-negative bacteria (Fukuda et al., 1990a).

Over the last decade, research has focused on the discovery and characterization of natural-products from marine-derived actinomycetes (Hopwood, 2007; Jensen et al., 2005). Fenical and colleagues recently isolated the marine-derived actinomycete strain, CNQ-525, that was found to be a member of the MAR 4 group of *Streptomyces* related bacteria (Cho et al., 2006; Jensen et al., 2005; Soria-Mercado et al., 2005b; Soria-Mercado, 2004). This strain was also found to produce

chlorine-containing meroterpenoids of the napyradiomycin class (Cho et al., 2006; Soria-Mercado et al., 2005b). Through cultivation and fractionation, numerous napyradiomycin analogs were collected and initial bioactivities of these compounds were tested. Similar to the previously discovered napyradiomycins, the majority of these marine-derived derivatives were found to have both antibacterial and cytotoxic activities (Cho et al., 2006; Soria-Mercado et al., 2005b).

3.2.3. Nosiheptide: A lipophilic thiopeptide from the actinomycete strain CNT373 was recently re-discovered by the Fenical Laboratory. This compound shares a chemical scaffold with the previously discovered terrestrial antibiotic multhiomycin. Though much knowledge and testing have already been done on this pharmaacophore, its activity against contemporary strains of MRSA make it particularly intriguing. Nosiheptide is a protein synthesis inhibitor that acts via elongation factors Tu and G. The terrestrial form was previously demonstrated to have broad Gram-positive activity but the chemical scaffold has not been tested against many multiple drug resistant pathogens causing contemporary and serious infections such as MRSA and *Enterococcus* spp.

The compound is currently used in agriculture as a feed additive but has not yet been developed as a potential antibiotic to treat MRSA infections in humans. Though the terrestrial version of this compound showed promising results, it is not clear why it was not pursued for further development. It is likely similar molecules of similar structure were pursued instead. In this study we characterize the *in vitro* activities of this compound in great detail by quantifying the time-kill kinetics, post-antibiotic effect and evaluate its activity against a panel of extremely resistant and

virulent pathogenic strains. Furthermore, we evaluate the efficacy of this compound in an in vivo survival model.

As clinical strains of MRSA become increasingly resistant to antibiotics, there is a clear need for the discovery of new antibiotics that can treat complicated infections caused by these strains. In this chapter, we evaluate these three previously described chemical scaffolds against a contemporary and clinically relevant panel of HA- and CA-associated strains of MRSA, two vancomycin-resistant (VRSA), and a panel of glycopeptide-intermediate *S. aureus* (GISA) strains. Additionally, we assess key pharmacological characteristics of these compounds using an *in vitro* time-kill kinetic assays as and probe the lasting antibiotic effects of nosiheptide. Finally we test the *in vivo* efficacy of etamycin and nosiheptide in an MRSA survival experiment. Our data illustrate that the re-characterization of these compounds is an essential process in bringing new chemicals to market. These compounds, previously discovered and not pursued, can serve as second and last-lines of therapies for patients with highly resistant bacterial infections. Further characterization is warranted.

3.3. RESULTS AND DISCUSSION

3.3.1. The depsipeptide chemical scaffold: etamycin and fijimycins: The actinomycete strain designated CNS-575 was cultured from a marine sediment collected along the coast of Fiji. The 16S rRNA gene sequence analysis places this strain within the genus Streptomyces; however, it shares ~ 98% sequence identity with any formally described species, suggesting that it may represent a new species. Solid-phase extraction and chromatographic purification yielded an 879 molecular weight peptide, which appeared as three distinct rotamers in the NMR spectrum. The presence of rotamers was not affected by changes of NMR solvent or acquisition temperature, and we ultimately performed the NMR-based structure elucidation of all three rotamers simultaneously **(TABLE 3.1.)**. The resulting planar structure was consistent with that of the previously reported terrestrially derived streptogramin, etamycin (Bateman et al., 1997; Sheehan and Ledis, 1973) **(FIGURE 3.1.)**, although a complete chemical shift assignment of etamycin has not previously been reported. Acid hydrolysis followed by analysis using advanced Marfey's method (Fujii et al., 1997) revealed the stereochemical configuration to be consistent with etamycin.

3.3.1.1. Antibiotic activities of the depsipeptide etamycin: Etamycin was originally isolated from terrestrial actinomycete *S. griseus* alongside the streptogramin-A antibiotic griseoviridin, and the two molecules together displayed synergism common for other streptogramins, including bactericidal activity primarily against some Gram-positive organisms (Garcia-Mendoza, 1965).

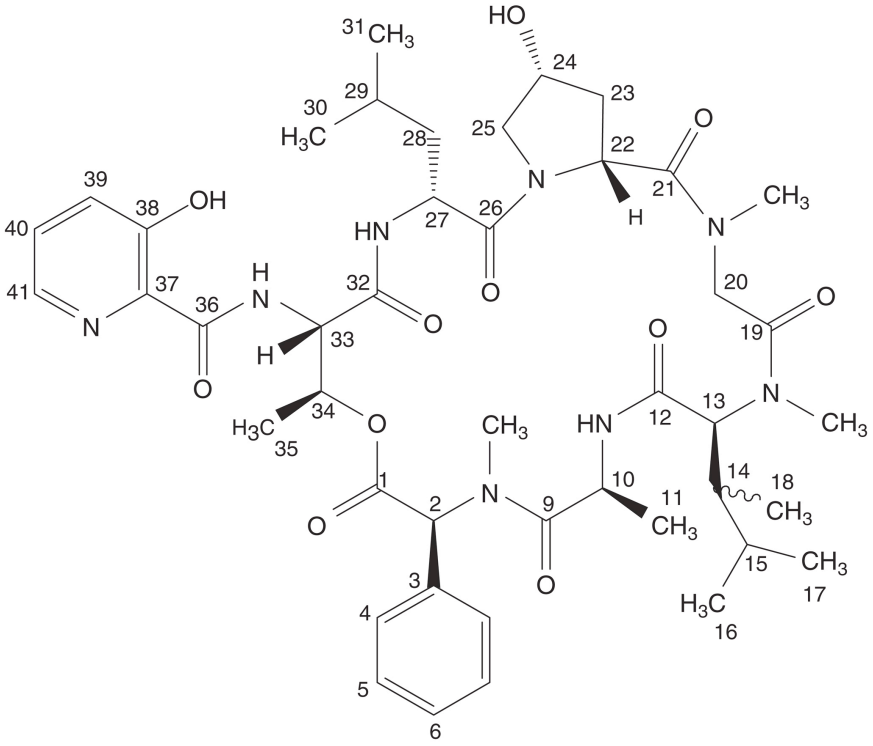

FIGURE 3.1. The chemical structure of the depsipeptide etamycin. (Numbered atoms correspond to data in **TABLE 3.1**).

TABLE 3.1. ^{1}H NMR, ^{13}C NMR and ^{15}N NMR of etamycin (each rotamer) in $CDCl_3$

		Rotamer 1 (major)				Rotamer 2		Rotamer 3	
		δ_N	δ_C[a]		δ_H (m, J (Hz))	δ_C[a]	δ_H	δ_C[a]	δ_H
Phg	1		169.6	C		169.5		169.5	
	2		62.8	CH	5.66 (s)	61.6	5.96	63.2	5.60
	3		130.3	C		130.9		130.4	
	4, 8		129.7	CH	7.41 (m)	129.4	7.46	129.4	7.36
	5, 7		129[b]	CH	7.4[b]	129[b]	7.4[b]	129[b]	7.4[b]
	6		129[b]	CH	7.4[b]	129[b]	7.4[b]	129[b]	7.4[b]
	2-NCH_3	182.5	31.8	CH_3	2.80 (s)	31.4	2.87	32.4	2.78
Ala	9		173.5	C		174.1		173.2	
	10		45.8	CH	5.05 (m)	45.3	5.10	46.2	4.98
	11		17.9	CH_3	1.39 (d, 6.6)	16.5	1.40	18.1	1.28
	10-NH	179.5			7.26		7.93		7.48
β-MeLeu	12		168.9	C		168.4		167.2	
	13		58.4	CH	5.09 (d, 10.3)	62.8	3.77	61.9	3.93
	14		35.4	CH	2.21 (m)	37.1	2.26	36.2	2.35
	15		28.3	CH	1.80 (m)	27.3	1.51	27.2	1.61
	16		15.4	CH_3	0.77 (d, 7.1)	15.8	0.79	15.3	0.81
	17		21.5	CH_3	0.94 (d, 6.2)	21.9	0.90	21.6	0.95
	18		8.5	CH_3	0.60 (d, 7.1)	8.5	0.75	8.4	0.71
	13-NCH_3	195.5	30.0	CH_3	2.82 (s)	29.3	2.93	28.6	2.91
Gly	19		167.5	C		167.8		167.7	
	20a		52.3	CH_2	3.87 (d, 16.8)	50.5	3.40	52.3	3.87
	20b				5.34 (d, 16.8)		5.39		6.03
	20-NCH_3	192.5	35.6	CH_3	2.92 (s)	33.3	3.21	36.4	3.02
Hyp	21		173.9	C		173.3		173.7	
	22		53.9	CH	5.17 (d, 6.1)	55.2	4.82	56.6	4.53
	23a		37.4	CH_2	2.05 (d, 13.7)	35.4	1.94	37.0	2.13
	23b				2.15 (m)		2.26		
	24		70.8	CH	4.52 (m)	71.3	4.44	70.5	4.38
	25a		58.1	CH_2	3.72 (dd, 5.6, 11.3)	56.0	3.81	57.9	3.73
	25b				4.42 (dd, 5.8, 11.3)				3.82
	24-OH				6.68 (d, 11.5)		5.44		6.52
	22-N	167.5							
Leu	26		172.0	C		171.5		170.9	
	27		49.0	CH	4.89 (m)	48.9	5.02	48.8	5.03
	28a		39.4	CH_2	1.48 (ddd, 4.4, 9.0, 13.4)	39.4	1.38	40.8	1.61
	28b				1.91 (m)		2.14		1.80
	29		24.2	CH	1.85 (m)	24.2	1.87	24.1	1.69
	30		21.0	CH_3	0.93 (d, 6.4)	20.6	1.01	21.5	0.95
	31		23.0	CH_3	0.98 (d, 7.0)	23.3	0.99	23.2	0.94
	27-NH	174.5			8.33 (d, 8.5)		8.15		7.84
Thr	32		165.9	C		166.1		165.9	
	33		53.0	CH	4.88 (m)	53.4	4.84	53.0	4.93
	34		70.0	CH	5.17 (m)	69.7	5.25	70.0	5.27
	35		13.4	CH_3	1.17 (d, 6.8)	13.5	1.22	13.9	1.20
	33-NH	199.0			8.93 (d, 7.5)		9.02		8.95
Hpca	36		167.7	C		167.8		168.1	
	37		130.8	C		130.8		130.6	
	38		157.3	C		157.3		157.3	
	39		125.6	CH	7.25 (m)	125.6	7.25	125.7	7.27
	40		128.5	CH	7.30 (m)	128.5	7.29	128.7	7.3[b]
	41		139.6	CH	8.07 (d, 3.9)	139.6	8.04	139.8	8.09
	38-OH				11.77 (s)		11.74		11.67
	41-N		197.5						

[a] ^{13}C shifts obtained from HMBC and HSQC spectra.
[b] Overlapping peaks.

We investigated in more detail the antibiotic properties of etamycin as a single agent against a panel of clinically relevant MRSA strains and discovered it to possess very good activity. MIC ranged from 1–2 μg/ml for CA-MRSA strains and certain HA-MRSA strains, to 8-16 μg/ml for the HA-MRSA strains ATCC 33591 and Sanger 252 **(TABLE 3.2.)**. Etamycin also showed a low level of activity against strains of the Gram-positive bacteria *S. pyogenes* and *S. agalactiae* (MIC=8 μg/ml) and minimal activity against vancomycin-resistant *E. faecalis* (MIC=16 μg/ml). The spectrum of etamycin activity extended to strains of the Gram-negative coccobacilli and respiratory tract pathogens *M. catarrhalis* (MIC=1 μg/ml) and to a lesser extent *H. influenzae* (MIC=16 μg/ml), but not to other Gram-negative pathogens tested including *E. coli*, *S. typhimurium* and *P. aeruginosa*. To assess a potential therapeutic index for etamycin against MRSA, we analyzed its effects in a mammalian HeLa cell cytotoxicity assay. We found that etamycin exhibited no cytoxicity at concentrations up to 128 μg/ml (data not shown), suggesting the potential for a favorable therapeutic index against MRSA.

3.3.1.2. Etamycin in vitro time-kill kinetics: We studied the time-kill kinetics of etamycin at different concentrations for comparison against vancomycin, the most common agent used in current MRSA therapy. Evaluation was conducted at 1X, 4X and 10X the respective MIC of each drug against the CA-MRSA (USA300) strain UAMS-1182 **(FIGURE 3.2.)**. As shown in **FIGURE 3.2.**, etamycin killed UAMS-1182 somewhat more rapidly than vancomycin at 10XMIC during the first 6 h; however, vancomycin was able to reduce the number of viable bacteria to below the threshold of detection of this assay by 24 h, whereas killing by etamycin, although

TABLE 3.2. Minimum inhibitory Concentrations of Etamycin against contemporary MRSA and drug-resistant bacterial strains

Strain	MIC (µg/ml)
MSSA UAMS-1 (USA200)	1 - 2
MRSA Sanger 252	8 - 16 (2)[a]
MRSA-ATCC33591 [a]	16
MRSA NRS22 MRSA (USA600)	1-4
MRSA USA300 (UAMS1182) [b]	1
MRSA NRS192	2
MRSA NRS386 (USA700)[b]	2
LRSA NRS119	1–2
E. faecalis (vanB)	16 (16)[a]
S. pyogenes (M1 strain 5448)	8
S. agalactiae (serotype III strain COHI)	8
M. catarrhalis (ATCC 25238)	1
H. influenzae (type b, ATCC 10211)	16
E. coli (ATCC 25922)	>256
S. typhimurium (ATCC 13311)	>256
P. aeruginosa (ATCC 27853)	>256

Abbreviations: CA, community associated; HA, hospital associated; MIC, minimum inhibitory concentrations; MSSA, methicillin-sensitive *Staphylococcus* aureus; MRSA, methicillin-resistant *Staphylococcus aureus*; LRSA, Linezolid-resistant *Staphylococcus aureus*.

[a] Values in parentheses represent MICs for Synercid against these bacterial strains tested under identical conditions as for etamycin.

[b] Strain NRS386 is associated with both community and health-care infections.

(Table adapted from Table 2; Haste, N.M., et al. *J. Antibiotics* (2010)).

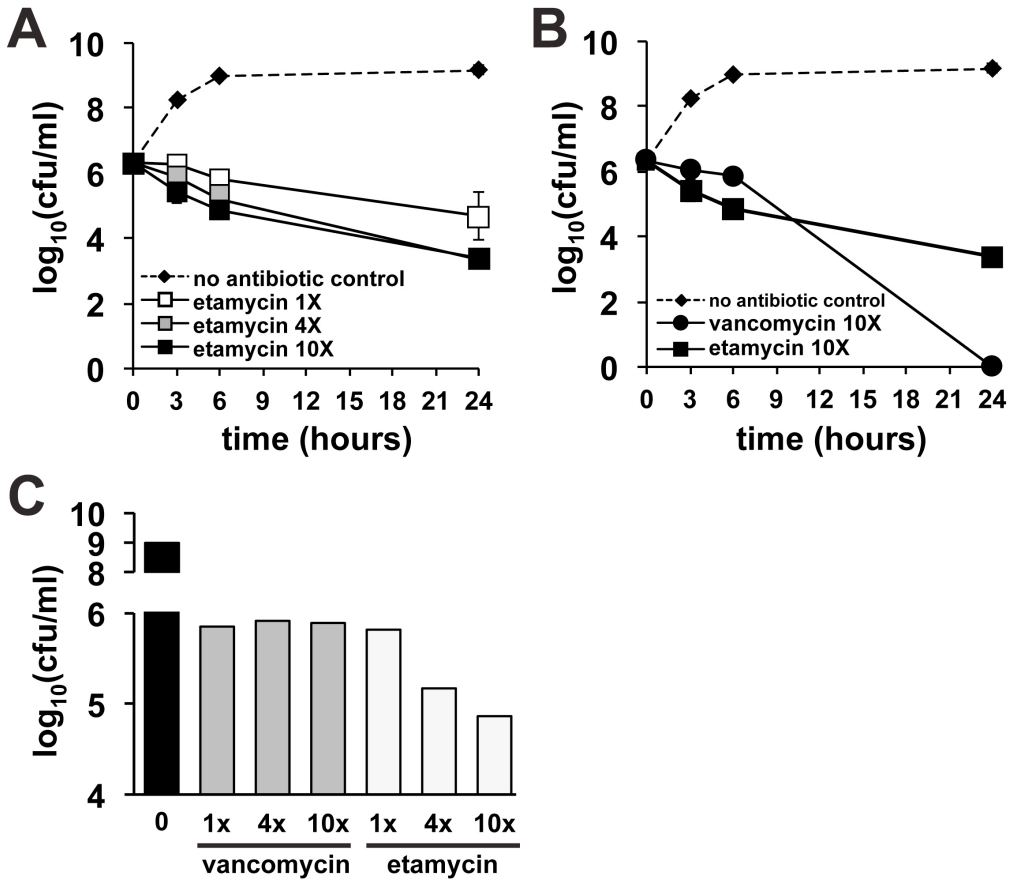

FIGURE 3.2. ***In vitro*** **time-kill kinetics of etamycin against CA-MRSA strain UAMS1182. (A)** Concentration dependence of etamycin at one, four and ten times the MIC over 24 h. MRSA was incubated with the specified concentrations of etamycin, and surviving bacteria were enumerated at the given times by quantitative culture on agar in the absence of the compound. **(B)** Comparison of killing kinetics of etamycin with vancomycin at ten times the MIC for each drug. Surviving bacteria were enumerated at the given times by quantitative culture on agar. **(C)** Quantitative cultures **six hours** post-incubation with vehicle control (0) or drug at one, four and ten times the MIC of vancomycin or etamycin. The data represent the mean of three independent experiments. The limit of detection of the assay is 1.6 $\log_{10}$ (cfu/ml).

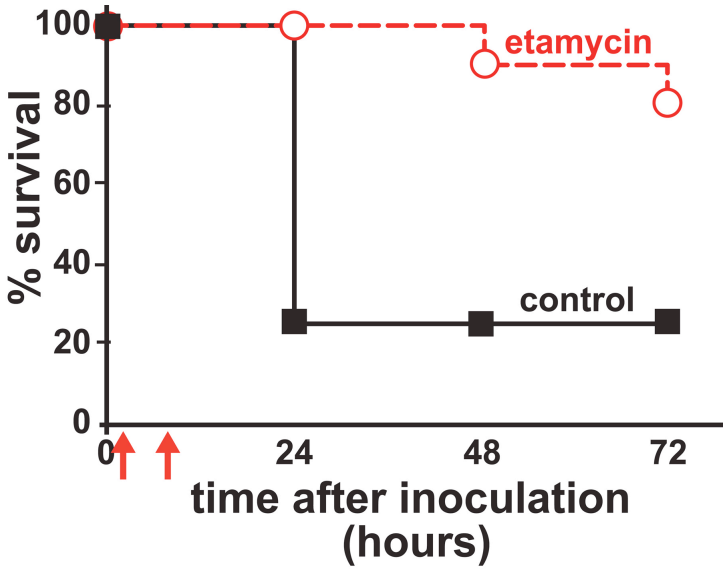

FIGURE 3.3. *In vivo* efficacy of etamycin in a murine MRSA sepsis study. Female CD1 mice (8 week old) were injected i.p. with 2 x10^9 cfu of HA- MRSA strain Sanger 252 in 1% mucin. At 1 and 8h after infection (indicated by red arrows), the mice were injected i.p. with either 20 mg/kg etamycin (*n*=10) or DMSO vehicle control (*n*=8). The mice were monitored for signs of sepsis for up to 72 h, and mice that became moribund were humanely euthanized.

substantial, remained incomplete. Collectively, these data suggest that etamycin acts in both time- and concentration-dependent mechanisms and is faster-acting but significantly less bactericidal than vancomycin.

3.3.1.3. Efficacy of etamycin in an in vivo systemic murine MRSA infection model: As a first assessment of the in vivo efficacy of etamycin, we used a murine systemic infection model, conservatively choosing as the challenge strain MRSA Sanger 252, against which etamycin exhibited a higher MIC of 8–16 μg/ml. Female CD1 mice (8 weeks old) were treated with etamycin (20 mg/kg) or vehicle control at 1 and 8 h after intraperitoneal (i.p.) MRSA infection, and general health and survival were followed up for up to 72 h. Within 6–12 h of MRSA infection, most mice in the control group exhibited signs of sepsis including lethargy, dehydration, and piloerection, whereas the severity of these symptoms was greatly reduced or absent in most of the etamycin-treated animals. As shown in **FIGURE 3.3.**, the two doses of etamycin offered significant protection to mice infected with MRSA during the 72 h monitoring period (20% mortality vs 75% morality in controls).

3.3.1.4. Anti-MRSA activities of three depsipeptide analogs of etamycin: The activities of etamycin relatives, the fijimycins A–C **(FIGURE 3.4.),** were examined *in vitro* against three MRSA strains to compare the potency of each chemical scaffold with that of etamycin. The strains tested consisted of hospital-associated (HA)-MRSA strain ATCC33591, the sequenced HA-MRSA strain Sanger 252 and the community-

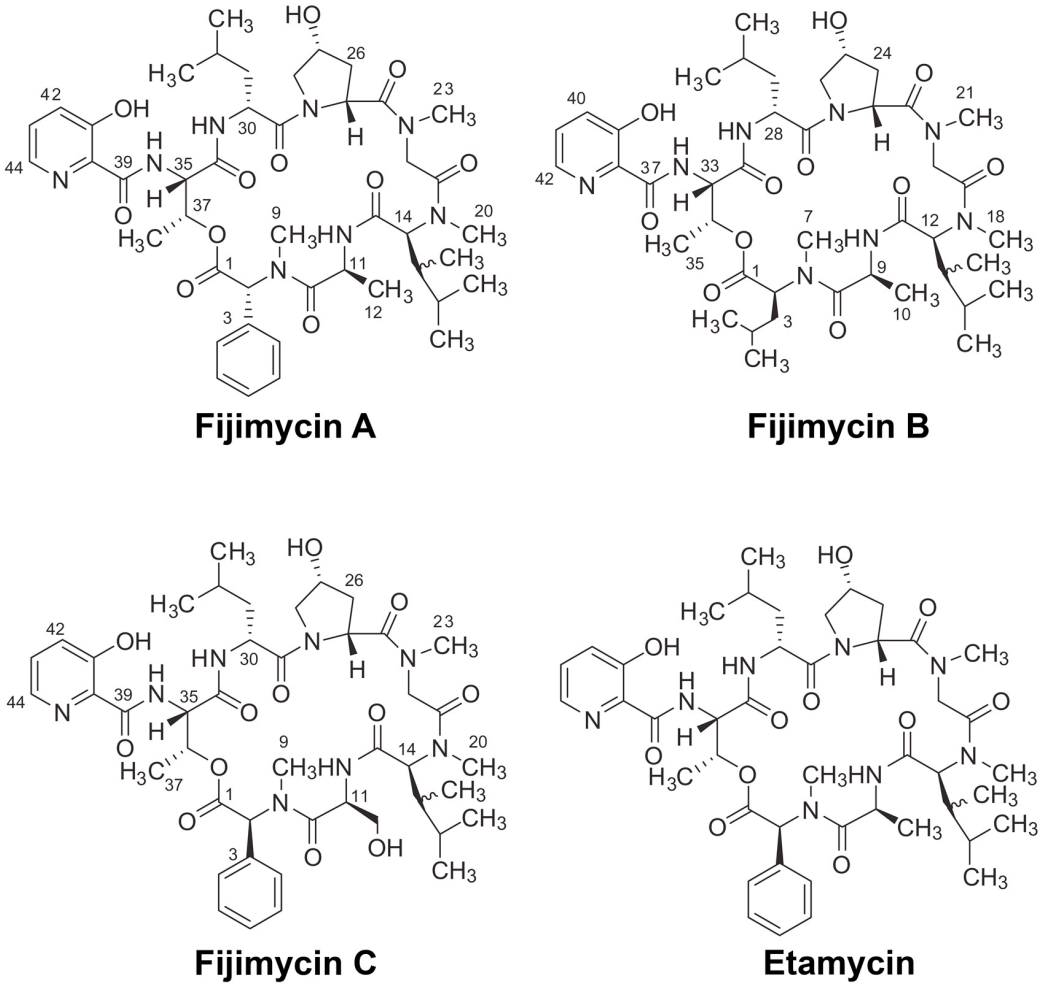

FIGURE 3.4. Structures of fijimycins A – C and etamycin A. (Adapted from Sun, P., et al. *Bioorganic & Medicinal Chemistry,* **19:**6557-62 (2011)).

TABLE 3.3. Minimum inhibitory Concentrations (MIC (μg/ml)) of Fijimycins A-C and Etamycin against contemporary MRSA

Compound	ATCC33591 (HA-MRSA)	Sanger252 (HA-MRSA)	UAMS1182 (USA300 CA-MRSA)
Fijimycin A	16	32	4
Fijimycin B	>32	n/a	>32
Fijimycin C	32	n/a	8
Etamycin A	16	16	4

Abbreviations: CA, community associated; HA, hospital associated; MRSA, methicillin-resistant *Staphylococcus aureus*.

(Table adapted from Table 4; Sun,P., et al. *Bioorg. Med. Chem.* (2010)).

associated (CA)-MRSA USA300 strain UAMS1182. Results are shown in **TABLE 3.3.** and indicate that in addition to etamycin A, fijimycin A and fijimycin C had potent MIC activities against all three tested MRSA strains. The activities of the three active compounds ranged from 4 – 32 µg/ml. Fijimycin B, on the other hand, exhibited very weak inhibition against ATCC33591 and UAMS1182. Analysis of differences between the structure of fijimycin B and the others indicated that the α-phenylsarcosine group might be critical for antibiotic enhanced activity. Closer analysis of structure-activity data indicates a close relationship between etamycin A and fijimycin A. The difference between the two is a substitution of D- for L- α-phenylsacrcosine. The MIC results indicate that this structural change has little impact on antibiotic activities against MRSA.

3.3.1.5. Summary of etamycin antibiotic effects against MRSA: For the first time from a marine-derived actinomycete we isolated the streptogramin, etamycin, and found that it had marked antibacterial activity against clinically important strains of MRSA. Although etamycin was first identified more than five decades ago, its antibiotic properties had not been characterized in detail. Those early studies also describe etamycin as a bacteriostatic compound against the *S. aureus* strain Duncan (Garcia-Mendoza, 1965). We found that etamycin alone at high concentration may exhibit limited bactericidal activity against contemporary CA-MRSA strains, as after 24 h of exposure to etamycin at 4X MIC, < 1% of the starting inoculum of CA-MRSA strain UAMS1182 remained viable **(FIGURE 3.2.)**, representing an approximate three-log kill by 24 h. Furthermore, the progressive

decrease in the number of surviving bacteria over time even at 1X MIC also supports a conclusion that etamycin exhibits some, although certainly incomplete, bactericidal activity over 24 h. However, despite this result, etamycin clearly does not kill CA-MRSA as effectively as vancomycin in the 24 h assay.

The streptogramin antibiotic, quinupristin-dalfopristin (Synercid) is currently approved for use in complicated cutaneous infections caused by multiple drug-resistant gram-positive cocci, including MRSA and vancomycin-resistant *Enterococcus faecium* (Metzger et al., 2009). In this combination, streptogramins A and B together act to inhibit protein synthesis, with quinupristin (A) preventing polypeptide elongation by binding to the 50S ribosomal subunit and dalfopristin (B) binding to another site on the 50S ribosomal subunit and inducing a conformational change enhancing quinupristin activity (Allington and Rivey, 2001). In our assays we found that etamycin, presumably through protein synthesis inhibition, exhibits significant activity against MRSA alone without the benefit of its streptogramin A partner. Etamycin also demonstrated a very low level of activity against *E. faecalis* (MIC=16 μg/ml), a frequently drug-resistant nosocomial pathogen that is associated with urinary tract and surgical wound infections (Sood et al., 2008) and this activity seemed comparable to the very low level of activity of Synercid against this pathogen in our assay. Clearly, if etamycin were ever considered for introduction into clinical use, defined breakpoints would need to be determined.

Our isolation of etamycin from a novel marine-derived actinomycete species emphasizes the utility of the marine environment as a source of antibacterials (Fenical and Jensen, 2006) in particular marine-derived actinomycetes that have been shown to naturally produce a wide variety of active parent molecules and

analogs (Demain, 2009; Demain and Sanchez, 2009; Hughes et al., 2008). Etamycin was previously isolated from the terrestrial microbe, *S. griseoviridus*, naturally occurring as multiple congeners in which a hydroxyproline residue was replaced by a proline (Chopra, 1979). In addition, limited structure–activity relationship data point to the importance of the picolinyl moiety of etamycin for its activity (Bateman et al., 1997). Future studies will further investigate the activity of etamycin analogs from marine-derived actinomycetes for characterization and optimization of activity toward further preclinical development.

3.3.2. Bactericidal kinetics of marine-derived napyradiomycins against contemporary methicillin-resistant *Staphylococcus aureus*

The actinomycte strain CNQ-525 was isolated and cultured from a marine-sediment collected at 152 m depth off the coast of La Jolla, CA, USA. This strain was subjected to 16S rRNA sequence analysis and found to be part of the MAR 4 group that is within the family *Streptomycetaceae (Cho et al., 2006; Soria-Mercado et al., 2005a)*.This strain has been identified as a prolific producer of halogenated MAR 4 derivatives. Two of these compounds, **1** and **2 (FIGURE 3.5.)**, were purified from extracts of the saline cultures of strain CNQ-525.

3.3.2.1. Potent In vitro antibacterial activities of the napyradiomycins:

More recently, we observed that napyradiomycins from the marine strain CNQ-525 showed activities against a test strain of MRSA and vancomycin-resistant *Enterococcus* (VRE) (Cho et al., 2006). We investigated in detail the antibiotic

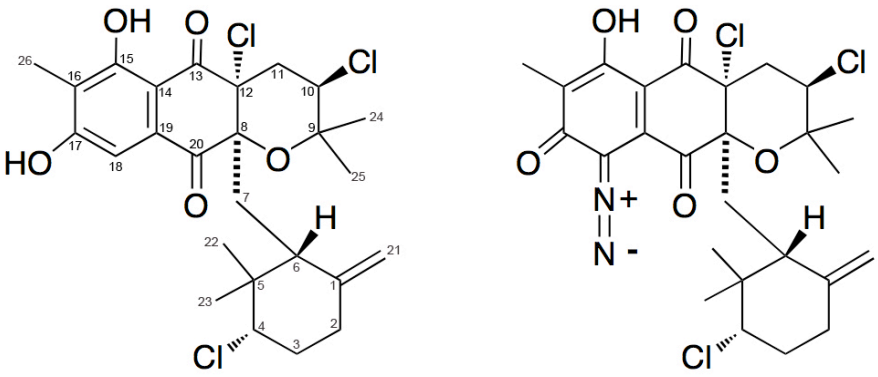

A80915A
(1)

A80915B
(2)

FIGURE 3.5. Structures of two napyradiomycins 1 and 2 isolated from the marine-derived actinomycete strain CNQ-525 and earlier from *S. aculeolatus* [10].

properties of napyradiomycins against a panel of clinically relevant MRSA strains. Minimum inhibitory concentration (MIC) assays were preformed using broth microdilution assays and our results show that both napyradiomycins **1** and **2** possess potent anti-MRSA activities against a series of HA- and CA-MRSA strains, two VRSA strains and a series of glycopeptide-intermediate (GISA) strains **(TABLE 3.4.)**. For **1**, the MIC was ~2 μg/mL against the CA-MRSA strains UAMS-1182 and TCH1516, both isolates of the USA300 clone currently epidemic in U.S. Similarly, against the same strains, the diazoketone **2** showed slightly more potent activities against the respective strains with MIC values averaging 1.5 μg/mL. Against HA-MRSA strains, both compounds exhibited MICs in the range of 1–3 μg/mL. The napyradiomycins retained their activities against the Michigan and Pennsylvania VRSA isolates as well as against GISA strains with overall MICs ranging from 0.5–4 μg/mL.

3.3.2.2. Napyradiomycins have rapid bactericidal kinetics in in vitro time-kill studies: We studied the time-kill kinetics of strain CNQ-525 derived **1** and **2** at two different concentrations, using for compared to vancomycin and gentamicin, two clinical agents used for MRSA therapy. *In vitro* time-kill analyses were conducted at 1× and 10× of derivative **1**, **2**, vancomycin or gentamicin control against CA-MRSA USA300 (TCH1516) **(FIGURE 3.6A.–C.)** and against the HA-MRSA Sanger252 **(FIGURE 3.6D.–F.)**. Over the first 4 h, the bactericidal activity for the two napyradiomycins **1** and **2** was more rapid than that observed for the vancomycin control, and more closely paralleled the kinetics seen in the gentamicin controls **(FIGURE 3.6C., 3.6F.)**.

TABLE 3.4. Minimum Inhibitory Concentrations (μg/mL) of napyradiomycins against contemporary antibiotic-resistant *Staphylococcus aureus* strains.

Strain	Compound 1 A80915A	Compound 2 A80915B
S. aureus ATCC 29213	2	4
MRSA-ATCC33591 [a]	1–2	2
NRS70 (N315) [a]	1	2
Sanger 252 [a]	1–2	1
NRS100 (COL) [a]	1	2
MRSA clinical bacteremia isolate c-44 [a]	3	1.5
MRSA clinical bacteremia isolate c-88 [a]	1.5–3	1.5
MRSA USA300 (UAMS1182) [b]	1.5–3	1–3
MRSA USA300 (TCH1516) [b]	2	1–2
VRSA (Michigan Isolate)	1–2	2–4
VRSA (Pennsylvania Isolate)	1–2	4
GISA (HIP5836) (New Jersey) [c]	0.5	1
GISA (PC-3) (New York) [c]	0.5	1
Hetero-GISA A5940 [c]	1	4

[a] HA-MRSA strains; [b] CA-MRSA strains; [c] Sakoulas *et al.*

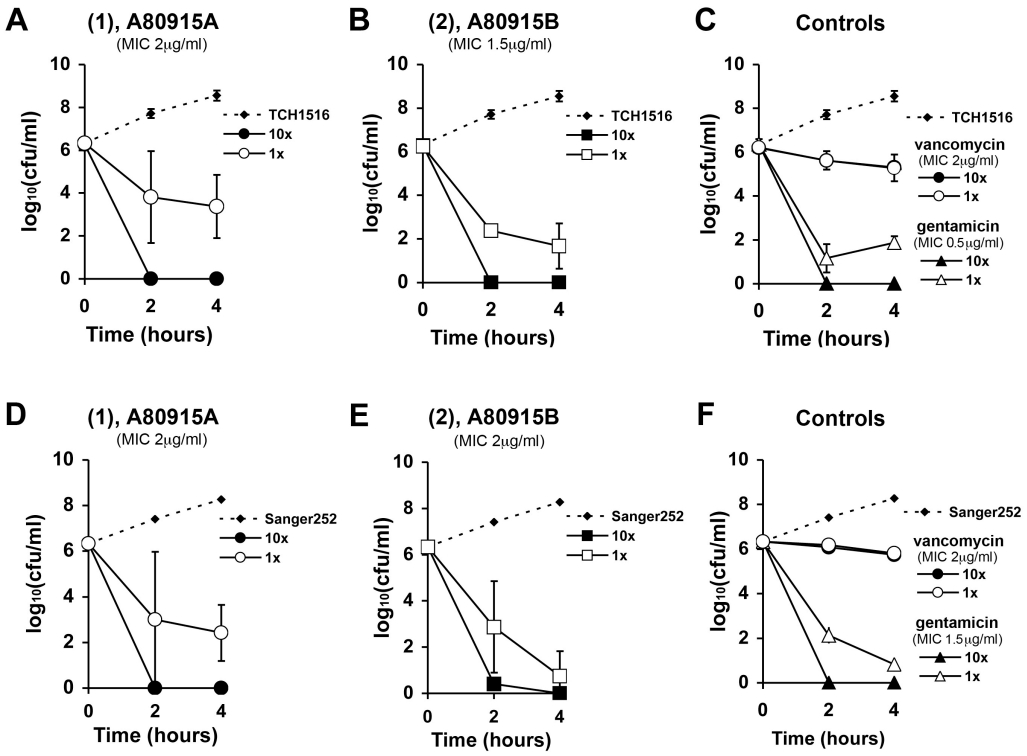

FIGURE 3.6. ***In vitro*** **time-kill studies of two napyradiomcyin analogs**. Curves of A80915A (**1A**,**D**); A80915B (**2B**,**E**); controls vancomycin and gentamicin (**C**,**F**) against CA-MRSA TCH1516 (**A**–**C**) and HA-MRSA Sanger252 (**D**–**F**).

Cultures incubated with 10× MIC of **1**, **2** or gentamicin showed complete killing at 2 h. Cultures treated with 1× MIC of **1** showed a nearly two-log reduction in bacterial counts at 4 h. The diazoketone derivative **2** showed slightly more potent and rapid killing with nearly a four-log decrease in bacterial counts at just 2 h in 1× MIC treated cultures. Vancomycin treated cultures showed time-dependent kinetics, with no difference in bacterial counts between the 10× and 1× treated cultures over the first 4 h period.

Napyradiomycins **1** and **2** (A80915A and A80915B) share similar, but not identical, structural features **(FIGURE 3.5)**. The main difference between these two derivatives is the existence of a diazoketone functionality attached to the napthoquinone core **(FIGURE 3.5B)**. Common to both of these scaffolds is the existence of a methyl group at the C16 position and the exocyclic methylene group at C1. Interestingly, the original napyradiomycins isolated by Shiomi *et al.* (Shiomi et al., 1986a; Shiomi et al., 1987a; Shiomi et al., 1986b; Shiomi et al., 1987b) lacked this C16 methyl group, however, the compounds extracted by Fukuda *et al.*, contained this methyl feature (Fukuda et al., 1990b).

3.3.2.3. The napyardiomycins are cytotoxic to mammalian cells: This structural-activity relationship (SAR) data can be of importance in designing new derivatives as antibiotic candidates. For example, the C16 methyl group of A80915A (**1)** has been found to slightly reduce the cytotoxic activity in comparison to a napyradiomycin lacking the methyl group (Farnaes, 2009). Using an antiproliferative bioassay, we quantified the cytotoxicity of napyradiomycins **1** and **2** using HCT-116 human colon adenocarcinoma cells. Our results revealed a low therapeutic index for

both compounds. IC_{50} values for compounds **1** and **2** were 3 μM and 500 nM, respectively. These results correlate with the studies of Fukuda *et al.*, which previously showed that in napyradiomycin derivative A80915B (**2**) the diazoketone group increased mammalian cell cytotoxicity (Fukuda et al., 1990a). Furthermore, our time kill analyses show that both the diazoketone derivative and **1** have effective bactericidal killing, even at 1× MIC **(FIGURE 3.6)**. Though the diazoketone **2** may appear to have more rapid kinetics, compound **1** has similar kinetics. With this structure information in hand, it is conceivable that the napyradiomycin scaffold could be modified to contain structural moieties that reduce mammalian cell cytotoxicity yet retain or enhance anti-MRSA activities we report here.

3.3.2.4. The activity of napyradiomycins in the presence of human serum: In addition to achieving reduced cytotoxicity and enhanced antibiotic activities, further development of napyradiomycins as viable anti-MRSA drug candidates would also involve optimizing compound bioavailability. A recent study on terpenoids produced by actinomycetes compared various napyradiomycin scaffolds and revealed that the antibacterial activities were greatly diminished in the presence of horse serum (Motohashi et al., 2008b). We confirmed these results against the CA-MRSA USA300 strain TCH1516 using a resazurin-based color change broth microdilution MIC assay to assess for bacterial growth in the presence of serum. Our results show that in the presence of 20% normal human serum, the activity of napyradiomcyins is abolished. These results highlight a critical obstacle in the development of napyradiomycin analogs as clinical anti-MRSA therapeutics. Focused SAR studies of the napyradiomycin scaffold could conceivably identify a

compound with activity in the presence of serum. Alternatively, the current napyradiomycin derivatives could be contemplated for topical applications.

Napyradiomycins have been described as novel terpenoids with promising broader therapeutic application (Farnaes, 2009). This novel scaffold has generated recent interest in both its biosynthetic pathway (Motohashi et al., 2008b) as well as in possible chemical syntheses (Motohashi et al., 2008a). The study of the molecular biosynthetic gene cluster associated with strain CNQ-525 has revealed that napyradiomycins are biosynthesized through a mixture of processes and genes involving polyketide pathways, halogenation, terpenoid biosynthetic pathways and chloronium ion-induced cyclization via a vanadium-dependent chloroperoxidase (Motohashi et al., 2008b). Terpenoid biosynthesis stems from a mevalonate pathway. Besides napyradiomycins, various marine-derived secondary metabolites are biosynthesized through a mevalonate pathway. For example, oxaloterpin, naphterin, terpentecin, and other terpene containing scaffolds are produced by actinomycetes with a mevalonate pathway (Farnaes, 2009; Sakoulas et al., 2002).

3.3.3. Characterization of nosiheptide activity against contemporary strains of MRSA

Nosiheptide, a lipophilic thiopeptide, has been rediscovered from the marine actinomycete strain CNT373. Previously identified in terrestrial actinomycetes, its macrocyclic core **(FIGURE 3.7)** consists of a hyroxypryridine core with dhydroaminoacids, thiazoles and an amide-terminated peptide chain (Yu et al., 2010). It belongs to a class of antibiotics, the thiopeptides, that contains over 70 structurally distinct chemical scaffolds (Bagley et al., 2005). Thiopeptides are sulfer-

containing macrocyclic peptides produced by actinomycetes. The majority of thiopeptides are protein synthesis inhibitors (Bagley et al., 2005). Nosiheptide, also called multhiomycin (Endo and Yonehara, 1978), was one of the first thiopeptides discovered. In 1977, the chemical was identified in *Streptomyces actuosus 40037* (Benazet et al., 1980; Pascard et al., 1977). In this initial discovery, nosiheptide was noted to have potent activities against gram-positive strains of bacteria. Further these early papers indicated that nosiheptide was inactive in an *in* vivo model of infection. It was in these early papers that authors suggested its potential as a feed additive in livestock food (Benazet et al., 1980). Early on, nosiheptide, under the name of Primofax®, was used as a growth-promoting antibiotic in animals (Cromwell et al., 1984).

The biosynthetic pathways of nosiheptide production have been studied extensively (Yu et al., 2009; Yu et al., 2010) and great understanding of its core structural features is known. However, it appears that more recent research on nosiheptide has concerned its biosynthetic pathway rather than its activities against contemporary, multi-drug resistant strains of MRSA. Here we evaluate the newly discovery marine-derived nosiheptide for its activity against a panel of multi-drug resistant clinical and community associated MRSA strains.

3.3.3.1. Potent antibiotic activities of nosiheptide against contemporary drug-resistant pathogens: Nosiheptide exhibited potent activity against all contemporary MRSA strains tested including multidrug-resistant clinical isolates **(TABLE 3.5)**, with MIC values $\leq$ 0.125 mg/L. Nosiheptide was also highly active against *Enterococci spp* and the contemporary virulent BI strain (also known as the

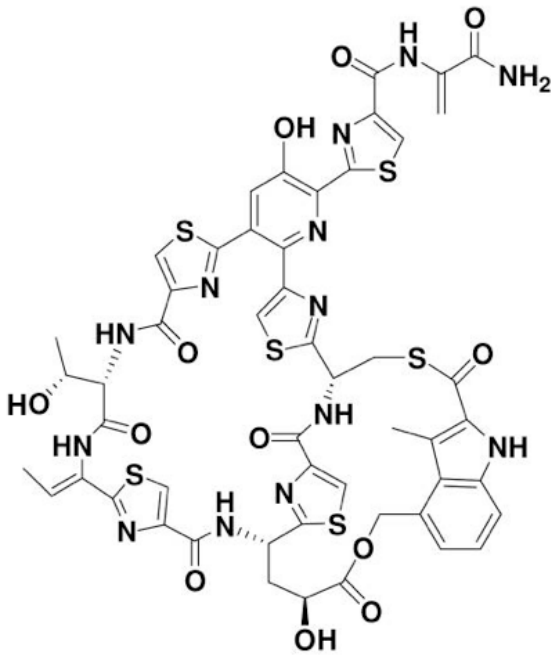

FIGURE 3.7. The structure of marine-derived nosiheptide

TABLE 3.5. Minimum Inhibitory Concentrations (MIC) of nosiheptide against contemporary multiple-drug resistant pathogens

Gram-positive bacterial strains	**MIC *broth media* (µg/ml)**	**MIC *20% serum* (µg/ml)**
***S.aureus* strains**		
TCH1516	0.06	0.06
Sanger 252	0.03	
A5937	0.125	
A5940 VISA	0.125	
A6300	0.125	
A6298 VISA	0.125	
0616 Daptomycin Sensitive	0.125	
0701 Daptomycin Resistant	0.06	
HIP5836 NJ VISA	0.125	
RN9120	0.06	
RN9120 VISA	0.25	
VRSA PA	0.06	
VRSA MI	0.125	
ATCC 33591	0.06	
ATCC 29213	0.125	
Other species		
S. epidermidis	0.5	
VRE -CUS	0.125	
VRE- WMC	0.125	
C. difficile BI	0.008	

Gram-negative bacterial strains	**MIC *broth media* (µg/ml)**
M. catarrhalis	0.5
E. coli 1008	> 4
E. coli 1035	> 4
Pseudomonas	> 4
Acinetobacter	> 4
Enterobacter	> 4

NAP1 or ribotype 027 strain) of *C. difficile* but was inactive against most Gram-negative strains tested.

3.3.3.2. Nosiheptide exhibits a favorable in vitro time kill kinetic profile: Time-kill analysis revealed nosiheptide to be rapidly bactericidal against MRSA in a concentration- and time-dependent manner **(FIGURE 3.8.)**. The activity of nosiheptide at 1, 10 and 20X MIC was tested against the USA300 TCH1516. Noteably, nosiheptide displayed a 2-log kill at 6 hours at all tested concentrations. This indicates that nosiheptide is a time-dependent antibiotic. A commonly used first-line therapy for contemporary MRSA is vancomycin, also a time-dependent antibiotic. Comparison between nosiheptide (**FIGURE 3.8A.)** and vancomycin **(FIGURE 3.8B.)** reveal that nosiheptide kills MRSA much more rapidly over the first 6 hour period than vancomycin. We see a 2-log difference in the 1, 10 and 20X MIC cultures of nosiheptide. This contrasts greatly with the 0.5-log difference in all vancomycin treated cultures at the same time point (**FIGURE 3.8C.)**.

3.3.3.3. Nosiheptide has an extremely prolonged post-antibiotic effect against both a CA-MRSA USA300 and a HA-MRSA, Sanger 252: Notably, nosiheptide exhibited a prolonged post-antibiotic effect (PAE) against both CA-MRSA (TCH1516) **(FIGURE 3.9A.)** and a HA-MRSA (Sanger252) **(FIGURE 3.9B.)** compared to the first-line MRSA antibiotic, vancomycin **(FIGURE 3.9.).** Specifically, against both CA- and HA- tested strains, the 10X MIC nosiheptide-treated cultures showed no recovery even at 6 hours. This contrasts greatly to the 10X MIC vancomycin-treated bacteria which showed 4-log bacterial recovery in the CA-MRSA culture. Furthermore, HA-MRSA was unaffected by the addition of vancomycin

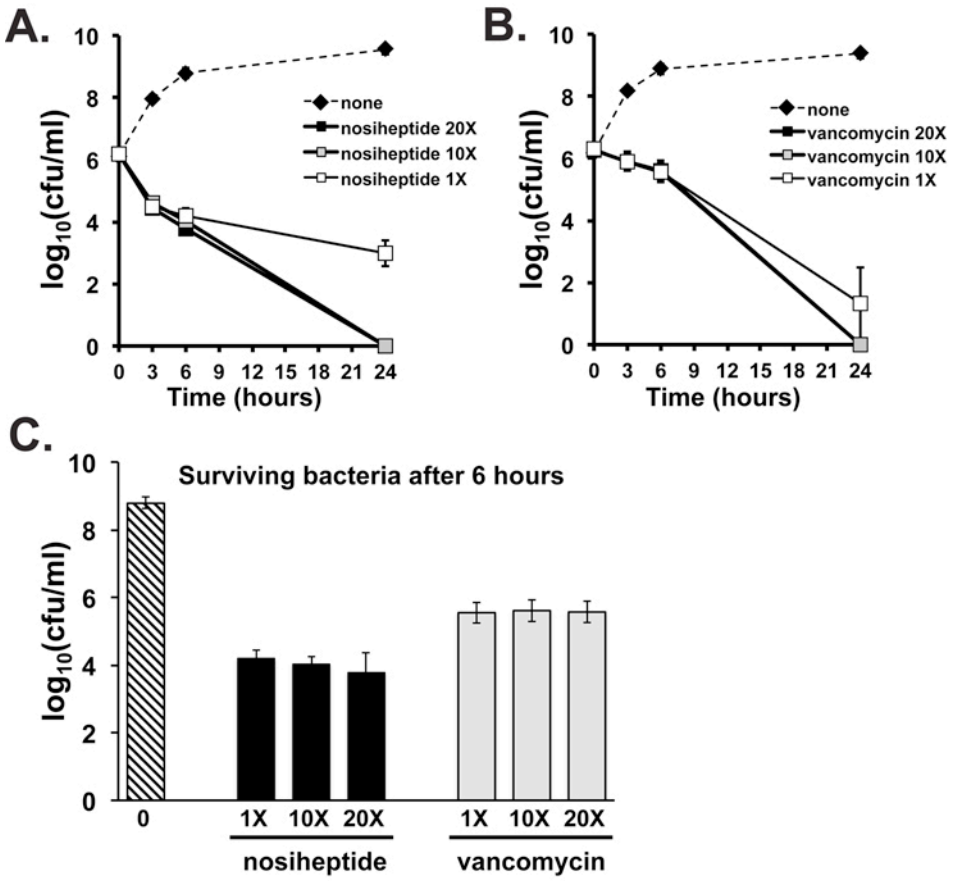

FIGURE 3.8. Time-kill analysis of nosiheptide against MRSA.

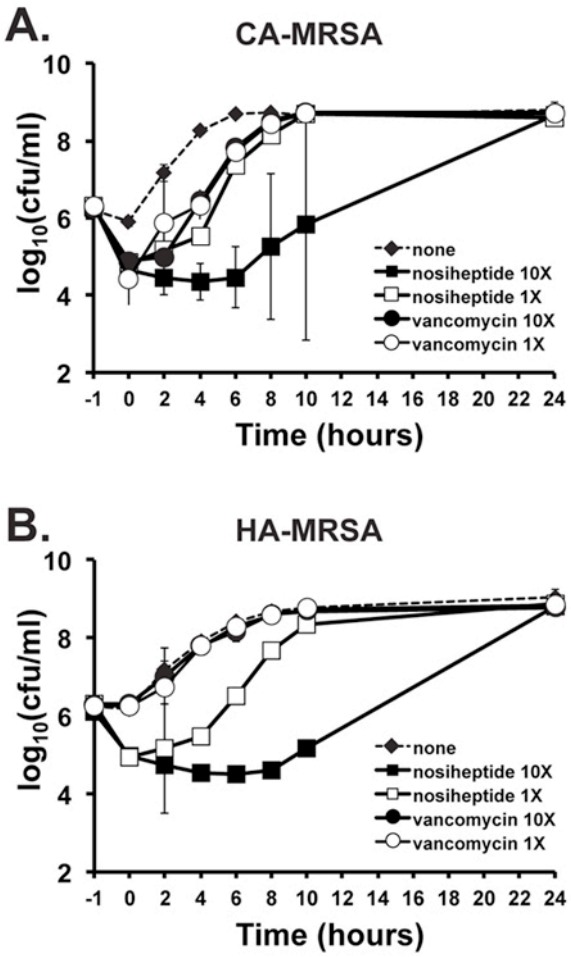

FIGURE 3.9. ***In vitro*** **post-antibiotic effect (PAE) of nosiheptide.** (A) PAE against TCH1516, a community associated (CA)- MRSA, and **(B)** PAE against Sanger252, hospital-associated (HA)- MRSA.

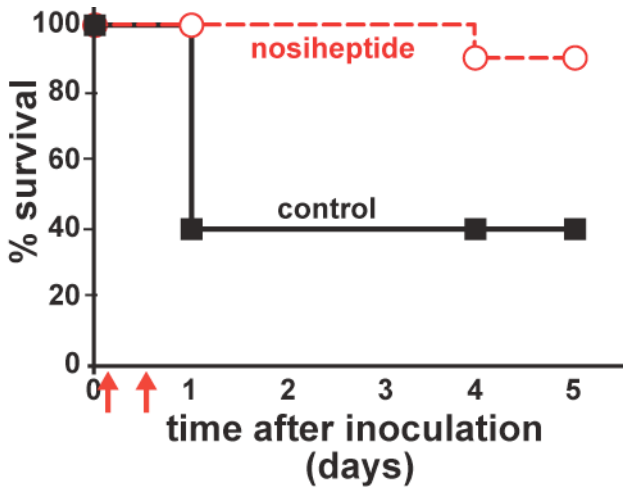

FIGURE 3.10. Effect of nosiheptide treatment on the survival of mice in a murine systemic (i.p.) infection model. Female CD1 mices (n = 10/group) were infected with 2 x 10^9 cfu HA-MRSA strain Sanger 252. At 1 and 8 hour (red arrows) post-infection, nosiheptide or vehicle control was administered i.p. to each mouse at a dose of 1mg/kg.

(FIGURE 3.9B.) yet nosiheptide showed similar activity to that seen in the CA-MRSA-treated cultures **(FIGURE 3.9A.)**.

3.3.3.4. Nosiheptide is not cytotoxic to mammalian cells: Nosiheptide was found to be noncytotoxic against mammalian cells at >> 100X MIC (data not shown), and its anti-MRSA activity was not inhibited by 20% human serum (data not shown).

3.3.3.5. The activity of nosiheptide is unaffected by human serum: The MIC of nosiheptide in the presence or the absence of serum is equal. The addition of 20% human serum to assay media did not in any way affect the potency of nosiheptide **(TABLE 3.5).**

3.3.3.6. Nosiheptide exhibits activity in an in vivo systemic challenge model. Treatment of mice with two doses of nosiheptide post inoculation with MRSA offered great protection from systemic infection. Mice treated with 1mg/kg nosiheptide at 1 and 8 h post-infection showed only a 10% mortaility on day 5. Alternately, untreated mice experienced 60% mortality by day **5 (FIGURE 3.10).** In fact, untreated 60% of untreated mice died within the first 24 hours post infection. This contrasts greatly with the 100% survival of treated mice at the same time point.

3.3.4. Chapter Summary

We have shown three chemical scaffolds, previously discovered and identified as possible antimicrobial agents, a now rediscovered as

marineactinomycete-derived compounds. All three compounds, etamycin from the depsipeptide class, napyradiomycin, a complex meroterpenoid, and nosiheptide a macrocyclic thiopepide now show potent antibiotic activities against contemporary strains of multi-drug resistant pathogens. Nosiheptide was evaluated against drug-resistant C. difficle, as well as multi-resistant VRE in addition to contemporary MRSA. All of these compounds show promising antibiotic activities that could be useful in treating contemporary infections that are resistant to commonly used therapies.

Each of these compounds faces a challenge that possibly prevents its movement to becoming a clinically used therapeutic. Etamycin, though potent, is inhibited in the presence of human serum. Napyradiomycin, though it displays superb bactericidal killing kinetics, is very cytotoxic and has potential for use as an anticancer agent rather than as an antimicrobial. Thirdly, though nosiheptide is extremely potent and it retains activity in the presence of human serum, the compound lacks solubility. Each of these three main hurdles stands in the way of potential future use of these compounds in the clinic. Perhaps these drawbacks can be engineered out using stepwise structure-activity-based design of new chemical scaffolds. With the rise of multi-drug resistant MRSA in the clinic and the community, new drugs with novel mechanisms of action and previously unused chemical scaffolds will be useful in the battle against the superbugs.

3.3. MATERIALS & METHODS

3.4.1. Depsipeptide studies

3.4.1.1. Bacterial strains tested in etamycin studies: A panel of HA- and CA-MRSA and other Gram-positive and -negative bacterial strains was used to probe the antimicrobial activity of etamycin. These included MRSA strains ATCC 33591, NRS22 (USA600), NRS71 (Sanger 252, genome strain), NRS119, USA200 (UAMS-1), NRS192, USA300 (UAMS-1182) and strain NRS386 (USA700). Isolates with the NRS designation were obtained through the Network of Antimicrobial Resistance in *Staphylococcus aureus* (NARSA) program supported under NIAID/NIH contract # HHSN272200700055C. The USA200 and USA300 isolates were kind gifts of Greg Somerville at the University of Nebraska, Lincoln, and originally obtained from Mark Smeltzer at the University of Arkansas Medical Center. Other Gram-positive strains tested were *Streptococcus pyogenes* serotype M1 strain 5448,13 *Streptococcus agalactiae* strain COH114 and vancomycin-resistant *Enterococcus faecalis* (ATCC 51299). The Gram-negative strains used were *Pseudomonas aeruginosa* (ATCC 27853), *Escherichia coli* (ATCC 25922), *Moraxella catarrhalis* (ATCC 25238) and *Haemophilus influenzae* (Type b, ATCC 10211).

The actinomycete strain CNS-575 was isolated from a sediment sample collected from the Nasese shoreline, Viti Levu, Fiji, at low tide from a depth of ≈ 0.5 m (coordinates 18.09'04.0 S and 178.27'11.4 E). The 16S ribosomal RNA gene sequence (accession number Bankit 1235828) places this strain within the genus *Streptomyces*.

3.4.1.2. Fermentation and isolation of etamycin, Culture conditions for

(CNS-575): A 2 ml frozen stock of actinomycete strain CNS-575 was used to inoculate 25 ml A1 medium (10 g starch, 4 g yeast extract, 2 g peptone in 1 l seawater) in a 125 ml Erlenmeyer flask and shaken at 27 °C. The 5-day-old seed culture was then used to inoculate a 1 l culture in A1bfe+C (A1 media described above, with the addition of 1 g $CaCO_3$, 5 ml of 2% (w/v) KBr stock solution and 5 ml of 0.8% (w/v) $Fe_2(SO_4)$·4H2O stock solution). Lastly, 25 ml aliquots of the 3-day-old 1l culture were used to inoculate each of 18 1l cultures in 2.8 l Fernbach flasks containing medium A1bfe+C. Strain CNS-575 was allowed to grow with shaking for 7 days at 27 °C before extraction.

3.4.1.3. Isolation of etamycin (CNS-575): Column chromatography was carried out on silica gel (Selecto Scientific, Suwanee, GA, USA; particle size 63–200 µm). HPLC was carried out on a Beckman System Gold liquid chromatograph (126) (Beckman-Coulter, Brea, CA, USA) equipped with a Shimadzu diode array detector (SPD- M10AVP) (Shimadzu Corporation, Kyoto, Japan) and using an Ultracarb ODS (30) column (Phenomenex, Torrance, CA, USA; 250 X 10.0 mm, 5 µm particle size). A 40 l culture of strain CNS-575 was extracted using XAD-7 resin and eluted with acetone (2X). The acetone solvent was removed by evaporation, and the remaining water was extracted three times with ethyl acetate. The obtained extract (1.83 g) was fractionated on silica gel (step gradient from 100:1 to 5:1 dichloromethane: methanol eluent). Fractions with antibacterial activity were eluted with 50:1 and 20:1 dichloromethane: methanol. The active fractions (487 mg) were pooled and subjected to HPLC separation (isocratic, 60% aqueous acetonitrile eluent, 3 ml/min flow rate) to give etamycin (108.9 mg) after 31 min.

3.4.1.4. Spectroscopic analysis of etamycin (CNS-575): All NMR spectra were measured using a Varian Oxford AS500 spectrometer (Varian Inc., Palo Alto, CA, USA) (5 mm double-resonance inverse broadband probe) at 500 and 125MHz for ^{1H} and ^{13C} NMR, respectively. Offline processing was conducted using Mestre-C NMR Software (Mestrelab Research, La Coruña, Spain; http://www.mestrec.com). ^{1H} and ^{13C} chemical shifts were referenced with the CDCl3 solvent peaks at δ 7.26 and δ 77.0, respectively (Figure 1 and Table 1). The IR spectrum was recorded in KBr on a Nicolet IR100 FTIR spectrometer (Thermo, Waltham, MA, USA). The UV spectrum was recorded in methanol on a Beckman Coulter DU800 spectrophotometer (Beckman-Coulter). The optical rotation was measured in methanol on a Jasco P-2000 polarimeter (Jasco, Inc., Easton, MD, USA). HR-MS were acquired at the UCSD Molecular Mass Spectrometry Facility.

3.4.1.5. Susceptibility testing of etamycin (CNS-575): Minimum inhibitory concentration (MIC) assays were performed by micro- broth dilution. Briefly, an overnight culture of the test strain was diluted to 1:100 in broth and grown to mid-logarithmic phase at 37°C in a shaking incubator. Todd-Hewitt broth (obtained from Hardy Diagnostics, Santa Maria, CA, USA) was used for all strains except *H. influenzae*, for which the susceptibility testing was carried out in brain–heart infusion media supplemented with hemin (10 µg/ml) and NAD (10 µg/ml). The culture was pelleted and resuspended to OD_{600}=0.4 in phosphate-buffered saline. The bacteria were then added to a 96-well test plate containing etamycin dilutions in broth; the final bacterial concentration was $5x10^5$ cfu/ml in a final volume of 100 ml. Vancomycin (Hospira, Lake Forest, IL, USA) was used as a control for all MRSA

strains. Other control antibiotics included: ampicillin (Sandoz, Princeton, NJ, USA) for *E. faecalis* and *Streptococcus spp*, cloramphenicol (Sigma Chemical, St Louis, MO, USA) for *M. catarrhalis* and *H. influenzae*, and ciprofloxacin (Bedford Laboratories, Bedford, OH, USA) for *P. aeruginosa* and *E. coli.* The test plate containing the etamycin dilutions and target bacteria was incubated at 37 °C in a shaking incubator for 18 – 20 h. MIC was determined to be the lowest concentration of etamycin that inhibited bacterial growth as determined by turbidometric assessment at OD600.

3.4.1.6. Cytotoxicity assay of etamycin (CNS-575): Analysis of mammalian cell cytotoxicity was carried out essentially as described (Jere, 2008). Briefly, etamycin dilutions were added to HeLa cells ($2x10^4$ cells per well) in a sterile 96-well plate. Cytotoxicity was assayed by MTS at 24 h using the CellTiter 96 AQueous non-radioactive cell proliferation assay according to the manufacturer's instructions (Promega, Madison, WI, USA). Plates were read at A_{490} in a Versamax microplate reader (Molecular Devices, Mountain View, CA, USA).

3.4.1.7. In vitro time-kill assays of etamycin (CNS-575): Time-kill assays were carried out as previously described (Credito et al., 2007; Tsuji et al., 2008; Ueda, 2005) but with some modifications. Briefly, MRSA strain USA300 (UAMS-1182) was cultured overnight at 37 °C in Todd-Hewitt broth. The bacteria were then grown to mid-logarithmic phase and prepared in phosphate-buffered saline as for the MIC assays. Test tubes were prepared in duplicate containing vehicle control, etamycin, or vancomycin at concentrations of 1, 4 or 10 times the MIC of 4 µg/ml and 1.5 µg/ml, respectively. Bacteria were added to each tube at a starting inoculum of

~5 x 10^5 cfu/ml in a final volume of 5 ml. The cultures were incubated in a 37 °C shaking incubator, and aliquots were removed from each test tube at 0, 3, 6 and 24 h. These aliquots were serially diluted in phosphate- buffered saline and plated on Todd-Hewitt agar plates in the absence of antibiotics. Colonies were enumerated after 24 h at 37 °C. The limit of detection of this assay equated to 40 cfu/ml.

3.4.1.8. In vivo studies of etamycin (CNS-575): Female CD-1 (ICR) mice (8 weeks old) (Charles River, Wilmington, MA, USA) were injected i.p. with 2 x 10^9 cfu of HA-MRSA strain Sanger 252 in 4% mucin. At 1 and 8 h after infection, the mice were injected intraperitoneally (i.p.) with etamycin (20 mg /kg) or an equivalent volume of vehicle control. The mice were observed for signs of sepsis, including lethargy, piloerection and dehydration. Survival was monitored for a total of 72 h, and mice that became moribund during the study were humanely euthanized, as were any surviving mice at the end of the study. These studies were reviewed and approved by the University of California San Diego Animal Subjects Committee.

3.4.2. Napyradiomcyins

3.4.2.1. Isolation and cultivation of CNQ-525 and purification of napyradiomycin derivative 1 (A80915A) and derivative 2 (A80915B): The actinomycete strain CNQ-525, identified as a member of the MAR 4 clade (related to the genus *Streptomyces*) was isolated from a marine sediment collected at a depth of 152 m near La Jolla, CA, USA. Procedures detailing the isolation and cultivation of this strain and the purification of napyradiomycin compounds were previously published [16]. Briefly, strain CNQ-525 was cultivated by shaking at 30 °C for 7 days

in liquid nutrient media (10 g starch, 4 g yeast extract, 2 g peptone, 1 g $CaCO_3$, 5 ml of 0.8% (w/v) $Fe_2SO_4 \cdot 4H_2O$ stock solution in 1 l of seawater). Cultivation was followed by extraction using an Amberlite XAD-7 resin for 6 h, filtration and extraction by acetone. The crude whole culture extract was separated by silica gel and Flash chromatography using ethyl acetate and iso-octane into ten fractions with differing polarities. Subsequently, the fractions were analyzed by LCMS, and compounds **1** and **2** were isolated by HPLC and analyzed for weight and purity prior to antibacterial assays. Compounds **1** and **2** were dissolved in DMSO, protected from light, and stored at –20 °C. Fresh samples were thawed immediately prior to each assay.

3.4.2.2. Bacterial strains tested in napyradiomcyin studies: A panel of HA- and CA-MRSA strains were used to evaluate the activity of napyradiomycins against contemporary and clinically relevant strains of MRSA. These strains included ATCC33591, NRS70 (N315), Sanger 252, NRS100 (COL), an MRSA clinical isolate designated #44 and a second clinical isolate designated #88, as well as UAMS1182 and TCH1516 (both USA 300 strains). In addition, the methicillin-sensitive (MSSA) strain ATCC 29213, a susceptible reference strain of *S. aureus*, was included in the panel. To further evaluate napyradiomycins against multiresistant *S. aureus* strains, we tested a panel of glycopeptide-intermediate (GISA) and two vancomycin-resistant (VRSA) strains, including HIP5836 (GISA, New Jersey, U.S.), A5940 (Hetero-GISA), PC-3 (GISA, New York, U.S.), and VRSA (Michigan, U.S.) and VRSA (Pennsylvania, U.S.). Isolates with the NRS designation were acquired via the Network of Antimicrobial Resistance in *Staphylococcus aureus* (NARSA) program (supported under NIAID/NIH contract HHSN272200700055C). The USA300 isolate was

obtained from Greg Somerville at the University of Nebraska, Lincoln and originally received from Mark Smeltzer at the University of Arkansas Medical Center. The second USA300 isolate, TCH1516 (ATCC BAA-1717) and the HA-MRSA strain ATCC 33591 were obtained from the American Type Culture Collection (Manassas, VA, U.S.). Michigan and Pennsylvania VRSA strains, the panel of GISA strains, and the two MRSA clinical bacteremia isolates were obtained from George Sakoulas, MD, USA (University of California San Diego).

3.4.2.3. Susceptibility testing of napyradiomcyins: Minimum inhibitory concentration (MIC) assays were performed by broth microdilution according to CLSI guidelines [24]. Vancomycin (Hospira, Lake Forest, IL, USA) or Gentamicin Sulfate (Hospira, Lake Forest, IL, USA) served as the MRSA control antibiotic. The MIC was determined to be the lowest concentration of antibiotic that inhibited bacterial growth detected at A_{600}.

3.4.2.4. Time-kill analyses of napyradiomycin derivatives: Time-kill analyses were carried out as described (Haste et al., 2010). Two strains, the CA-MRSA USA300 strain TCH1516, and the HA-MRSA Sanger252 were prepared as described above for MIC assays to an OD_{600} of 0.4 in phosphate-buffered saline in 5 mL polystyrene Falcon tubes. Tubes contained the vehicle control (DMSO), compound **1** or compound **2**, vancomycin and gentamicin at 1× or 10× MIC. The MICs against TCH1516 were 2 μg/ml, 1.5 μg/mL, 2μg/ml and 0.5 μg/ml, respectively for compound **1**, **2**, vancomycin and gentamicin. For Sanger252, MICs were 2 μg/ml for compounds **1**, **2**, and vancomycin and 1.5 μg/ml for gentamicin. Bacteria were

added to the tubes at 5×10^5 cfu/ml in 4 ml and were incubated in a shaking incubator at 37 °C. Aliquots from each tube were removed at 0, 2 and 4 h and were serially diluted in phosphate-buffered saline and plated on Todd-Hewitt agar (Hardy Diagnostics, Santa Maria, CA, USA) in the absence of antibiotics. Viable colonies were enumerated after 24 h at 37 °C with a limit of detection for the time-kill assay of 40 cfu/ml. The 0, 2, and 4 h time points were plotted to best show the early kinetics of antibiotic activities.

3.4.2.5. Effect of human serum on napyradiomcyin activity: The MIC in the presence of 20% pooled human serum was completed similar to the broth microdilution assays described above except that resazurin (Sigma-Aldrich, St. Louis, MO, USA) was added at a final testing concentration of 0.675 mg/ml to assess bacterial growth. Plates were covered with foil and incubated for 24 h with shaking at 37 °C. After incubation, plates were assessed visually for color change from blue to pink to indicate bacterial growth. The MIC in the presence of 20% serum was determined to be the lowest antibiotic concentration that did not induce a blue to pink color change.

3.4.2.6. Antiproliferative Bioassay: Test for Cytotoxicity of Napyradiomcyins against HCT-116 cells: Aliquot samples of HCT-116 human colon adenocarcinoma cells were transferred to 96-well plates and incubated overnight at 37 °C in 5% CO_2/air. Test compounds were added to the plates in DMSO and serially diluted. The plates were then further incubated for another 72 h, and at the end of this period, a CellTiter 96 Aqueous non-radioactive cell proliferation

assay (Promega) was used to assess cell viability. Inhibition concentration (IC_{50}) values were deduced from the bioreduction of MTS/PMS by living cells into a formazan product. MTS/PMS was first applied to the sample wells, followed by incubation for 3 h. Etoposide (Sigma; IC_{50} = 1.549 mM) and DMSO (solvent) were used as the positive and negative controls in this assay. The quantity of the formazan product (in proportion to the number of living cells) in each well was determined by the Molecular Devices Emax microplate reader set to 490 nm wavelength. IC_{50} values were calculated using the analysis program Prism.

3.4.2. Nosiheptide

Materials and methods used in nosiheptide studies were based off those described for marinopyrrole A, napyradiomycin and etamycin.

3.5. ACKNOWLEDGEMENTS

This chapter was reproduced with permission from co-authors and modified from three different papers, two published and one in preparation.

Work described in **Chapter 3.3.1.** is modified from: Haste NM, Perera VR, Maloney KN, Tran DN, Jensen P, Fenical W, Nizet V,Hensler ME. Activity of the streptogramin antibiotic etamycin against methicillin-resistant *Staphylococcus aureus*. J Antibiot (Tokyo). (2010)63(5):219-24, PMCID: PMC2889693, and Sun P, Maloney KN, Nam SJ, Haste NM, Raju R, Aalbersberg W, Jensen PR, Nizet V, Hensler ME, Fenical W. Fijimycins A-C, three antibacterial etamycin-class depsipeptides from a marine-derived *Streptomyces sp*. *Bioorg Med Chem.* (2011) 19:6557-62, PMCID:PMC3205191.This work was supported by the National Institutes of Health Training Program in Marine Biotechnology (T32 GM067550 to NH), by the National Institutes of Health (RO1GM084350-01 to WF and VN), by the National Institutes of Health International Cooperative Biodiversity Groups program (U01- TW007401-01 to WF and PRJ), and by the National Institutes of Health Cancer Therapeutics Training Program (T32 CA121938 to KNM). We gratefully acknowledge R Raju and B Aalbersberg for providing the actinomycete strain CNS-575. We also acknowledge George Sakoulas, MD, for many helpful discussions.

Work described in **Chapter 3.3.2.** was modified from: Haste NM, Farnaes L, Perera VR, Fenical W, Nizet V, Hensler ME. Bactericidalkinetics of marine-derived napyradiomycins against contemporary methicillin-resistant *Staphylococcus aureus*. Mar Drugs. (2011);9:680-9,PubMed Central PMCID: PMC3124980.**N**.M.H. was supported by the National Institutes of Health Training Program in Marine Biotechnology (T32 GM067550) and Ruth L. Kirschstein National Research Service

Award (NRSA) from National Institutes of Health Grants (5 F31 GM90658-02). We thank the National Institutes of Health (RO1 GM084350-02 to W.F. and V.N.) for their generous grant support.

Work described in **Chapter 3.3.3.** is a manuscript in preparation. Haste N, Thienphrapa W, Hensler ME, et al. Characterization of Nosiheptide Activity Against Contemporary Methicillin-Resistant *Staphylococcus aureus,* In preparation. N.M.H. was supported by the National Institutes of Health Training Program in Marine Biotechnology (T32 GM067550) and Ruth L. Kirschstein National Research Service Award (NRSA) from National Institutes of Health Grants (5 F31 GM90658-02). We thank the National Institutes of Health (RO1 GM084350-02 to W.F. and V.N.) for their generous grant support.

3.6. REFERENCES

Allington, D.R., and Rivey, M.P. (2001). Quinupristin/dalfopristin: a therapeutic review. Clin Ther *23*, 24-44.

Bagley, M.C., Dale, J.W., Merritt, E.A., and Xiong, X. (2005). Thiopeptide antibiotics. Chem Rev *105*, 685-714.

Bateman, K.P., Thibault, P., Yang, K., White, R.L., and Vining, L.C. (1997). Probing the substrate specificity of an enzyme catalyzing inactivation of streptogramin B antibiotics using LC-MS and LC-MS/MS. J Mass Spectrom *32*, 1057-1063.

Benazet, F., Cartier, M., Florent, J., Godard, C., Jung, G., Lunel, J., Mancy, D., Pascal, C., Renaut, J., Tarridec, P.*, et al.* (1980). Nosiheptide, a sulfur-containing peptide antibiotic isolated from Streptomyces actuosus 40037. Experientia *36*, 414-416.

Boucher, H.W. (2009). Bad bugs, no drugs: no ESKAPE! An update from the Infectious Diseases Society of America. Clin Infect Dis *48*, 1-12.

Cho, J.Y., Kwon, H.C., Williams, P.G., Jensen, P.R., and Fenical, W. (2006). Azamerone, a terpenoid phthalazinone from a marine-derived bacterium related to the genus Streptomyces (Actinomycetales). Org Lett *8*, 2471-2474.

Chopra, C. (1979). Congeners of etamycin produced by Streptomyces griseoviridus. J Antibiot (Tokyo) *32*, 392-401.

Como-Sabetti, K. (2009). Community-associated methicillin-resistant Staphylococcus aureus: trends in case and isolate characteristics from six years of prospective surveillance. Public Health Rep *124*, 427-435.

Cornaglia, G., and Rossolini, G.M. (2009). Forthcoming therapeutic perspectives for infections due to multidrug-resistant Gram-positive pathogens. Clin Microbiol Infect *15*, 218-223.

Credito, K., Lin, G., and Appelbaum, P.C. (2007). Activity of daptomycin alone and in combination with rifampin and gentamicin against Staphylococcus aureus assessed by time-kill methodology. Antimicrob Agents Chemother *51*, 1504-1507.

Cromwell, G.L., Stahly, T.S., Speer, V.C., and O'Kelly, R. (1984). Efficacy of nosiheptide as a growth promotant for growing-finishing swine--a cooperative study. J Anim Sci *59*, 1125-1128.

Demain, A.L. (2009). Antibiotics: natural products essential to human health. Med Res Rev *29*, 821-842.

Demain, A.L., and Sanchez, S. (2009). Microbial drug discovery: 80 years of progress. J Antibiot (Tokyo) *62*, 5-16.

Endo, T., and Yonehara, H. (1978). Identity of multhiomycin with nosiheptide. The Journal of antibiotics *31*, 623-625.

Farnaes, L.L.L. (2009). Novel Analogs and a Protein Target for the Napyradiomycins (University of California, San Diego).

Fenical, W., and Jensen, P.R. (2006). Developing a new resource for drug discovery: marine actinomycete bacteria. Nat Chem Biol *2*, 666-673.

Fujii, K., Ikai, Y., Oka, H., Suzuki, M., and Harada, K.A. (1997). Nonempirical method using LC/MS for determination of the absolute configuration of constituent amino acids in a peptide: combination of Marfey's method with mass spectrometry and its practical application. Anal Chem *69*, 5146-5151.

Fukuda, D.S., Mynderse, J.S., Baker, P.J., Berry, D.M., Boeck, L.D., Yao, R.C., Mertz, F.P., Nakatsukasa, W.M., Mabe, J., Ott, J.*, et al.* (1990a). A80915, a new antibiotic complex produced by Streptomyces aculeolatus. Discovery, taxonomy, fermentation, isolation, characterization, and antibacterial evaluation. J Antibiot (Tokyo) *43*, 623-633.

Fukuda, D.S., Mynderse, J.S., and Yao, R.C. (1990b). Antibiotic A80915 and process for its production (US, Eli Lilly and Company (Indianapolis, IN)).

Garcia-Mendoza, C. (1965). Studies on the mode of action of etamycin (Viridogrisein). Biochim Biophys Acta *97*, 394-396.

Gomi, S., Ohuchi, S., Sasaki, T., Itoh, J., and Sezaki, M. (1987). Studies on new antibiotics SF2415. II. The structural elucidation. J Antibiot (Tokyo) *40*, 740-749.

Haste, N.M., Perera, V.R., Maloney, K.N., Tran, D.N., Jensen, P., Fenical, W., Nizet, V., and Hensler, M.E. (2010). Activity of the streptogramin antibiotic etamycin against methicillin-resistant Staphylococcus aureus. J Antibiot (Tokyo) *63*, 219-224.

Hopwood, D.A. (2007). Therapeutic treasures from the deep. Nat Chem Biol *3*, 457-458.

Hughes, C.C., Prieto-Davo, A., Jensen, P.R., and Fenical, W. (2008). The marinopyrroles, antibiotics of an unprecedented structure class from a marine Streptomyces sp. Org Lett *10*, 629-631.

Jensen, P.R., Gontang, E., Mafnas, C., Mincer, T.J., and Fenical, W. (2005). Culturable marine actinomycete diversity from tropical Pacific Ocean sediments. Environ Microbiol *7*, 1039-1048.

Jere, D. (2008). Poly (amino ester) composed of poly (ethylene glycol) and aminosilane prepared by combinatorial chemistry as a gene carrier. Pharm Res *25*, 875-885.

Kwon, H.C., Kauffman, C.A., Jensen, P.R., and Fenical, W. (2006). Marinomycins A-D, antitumor-antibiotics of a new structure class from a marine actinomycete of the recently discovered genus /`marinispora/'. J Am Chem Soc *128*, 1622-1632.

McArthur, K.A. (2008). Lynamicins A-E, chlorinated bisindole pyrrole antibiotics from a novel marine actinomycete. J Nat Prod *71*, 1732-1737.

Metzger, R., Bonatti, H., and Sawyer, R. (2009). Future trends in the treatment of serious gram-positive infections. Drugs Today (Barc) *45*, 33-45.

Mincer, T.J., Jensen, P.R., Kauffman, C.A., and Fenical, W. (2002). Widespread and persistent populations of a major new marine actinomycete taxon in ocean sediments. Appl Environ Microbiol *68*, 5005-5011.

Motohashi, K., Irie, K., Toda, T., Matsuo, Y., Kasai, H., Sue, M., Furihata, K., and Seto, H. (2008a). Studies on terpenoids produced by actinomycetes. 5-dimethylallylindole-3-carboxylic Acid and A80915G-8"-acid produced by marine-derived Streptomyces sp. MS239. J Antibiot (Tokyo) *61*, 75-80.

Motohashi, K., Sue, M., Furihata, K., Ito, S., and Seto, H. (2008b). Terpenoids Produced by Actinomycetes: Napyradiomycins from Streptomyces antimycoticus NT17. J Nat Prod *71*, 595-601.

Pascard, C., Ducruix, A., Lunel, J., and Prange, T. (1977). Highly modified cysteine-containing antibiotics. Chemical structure and configuration of nosiheptide. J Am Chem Soc *99*, 6418-6423.

Patel, M. (2009). Community-associated meticillin-resistant Staphylococcus aureus infections: epidemiology, recognition and management. Drugs *69*, 693-716.

Sakoulas, G., Eliopoulos, G.M., Moellering, R.C., Jr., Wennersten, C., Venkataraman, L., Novick, R.P., and Gold, H.S. (2002). Accessory gene regulator (agr) locus in geographically diverse Staphylococcus aureus isolates with reduced susceptibility to vancomycin. Antimicrob Agents Chemother *46*, 1492-1502.

Sheehan, J.C., and Ledis, S.L. (1973). Total synthesis of a monocyclic peptide lactone antibiotic, etamycin. J Am Chem Soc *95*, 875-879.

Shiomi, K., Iinuma, H., Hamada, M., Naganawa, H., Manabe, M., Matsuki, C., Takeuchi, T., and Umezawa, H. (1986a). Novel antibiotics napyradiomycins. Production, isolation, physico-chemical properties and biological activity. J Antibiot (Tokyo) *39*, 487-493.

Shiomi, K., Iinuma, H., Naganawa, H., Isshiki, K., Takeuchi, T., and Umezawa, H. (1987a). Biosynthesis of napyradiomycins. J Antibiot (Tokyo) *40*, 1740-1745.

Shiomi, K., Nakamura, H., Iinuma, H., Naganawa, H., Isshiki, K., Takeuchi, T., Umezawa, H., and Iitaka, Y. (1986b). Structures of new antibiotics napyradiomycins. J Antibiot (Tokyo) *39*, 494-501.

Shiomi, K., Nakamura, H., Iinuma, H., Naganawa, H., Takeuchi, T., Umezawa, H., and Iitaka, Y. (1987b). New antibiotic napyradiomycins A2 and B4 and stereochemistry of napyradiomycins. J Antibiot (Tokyo) *40*, 1213-1219.

Shomura, T., Gomi, S., Ito, M., Yoshida, J., Tanaka, E., Amano, S., Watabe, H., Ohuchi, S., Itoh, J., Sezaki, M.*, et al.* (1987). Studies on new antibiotics SF2415. I. Taxonomy, fermentation, isolation, physico-chemical properties and biological activities. J Antibiot (Tokyo) *40*, 732-739.

Sood, S., Malhotra, M., Das, B.K., and Kapil, A. (2008). Enterococcal infections & antimicrobial resistance. Indian J Med Res *128*, 111-121.

Soria-Mercado, I.E., Prieto-Davo, A., Jensen, P.R., and Fenical, W. (2005a). Antibiotic terpenoid chloro-dihydroquinones from a new marine actinomycete. J Nat Prod *68*, 904-910.

Soria-Mercado, I.E., Prieto-Davo, A., Jensen, P.R., and Fenical, W. (2005b). Antibiotic terpenoid chloro-dihydroquinones from a new marine actinomycete. J Nat Prod *68*, 904-910.

Soria-Mercado, I.E.J., P.R.; Fenical, W.; Kassel, S.; Golen, J. (2004). 3,4a-Di chloro-10a-(3-chloro-6-hydroxy-2,2,6-tri methyl cyclo hexyl methyl)-6,8-di hydroxy-2,2,7-tri methyl-3,4,4a,10a-tetra hydro-2H-benzo [g] chromene-5,10-dione. Acta Crystallographica *E60*, o1627-o1629.

Spellberg, B. (2008). The epidemic of antibiotic-resistant infections: a call to action for the medical community from the Infectious Diseases Society of America. Clin Infect Dis *46*, 155-164.

Tsuji, B.T., Yang, J.C., Forrest, A., Kelchlin, P.A., and Smith, P.F. (2008). In vitro pharmacodynamics of novel rifamycin ABI-0043 against Staphylococcus aureus. J Antimicrob Chemother *62*, 156-160.

Ueda, Y. (2005). In vitro and in vivo antibacterial activities of SM-216601, a new broad-spectrum parenteral carbapenem. Antimicrob Agents Chemother *49*, 4185-4196.

Umezawa, K., Masuoka, S., Ohse, T., Naganawa, H., Kondo, S., Ikeda, Y., Kinoshita, N., Hamada, M., Sawa, T., and Takeuchi, T. (1995). Isolation from Streptomyces of a novel naphthoquinone compound, naphthablin, that inhibits Abl oncogene functions. J Antibiot (Tokyo) *48*, 604-607.

Yu, Y., Duan, L., Zhang, Q., Liao, R., Ding, Y., Pan, H., Wendt-Pienkowski, E., Tang, G., Shen, B., and Liu, W. (2009). Nosiheptide biosynthesis featuring a unique indole side ring formation on the characteristic thiopeptide framework. ACS Chem Biol *4*, 855-864.

Yu, Y., Guo, H., Zhang, Q., Duan, L., Ding, Y., Liao, R., Lei, C., Shen, B., and Liu, W. (2010). NosA catalyzing carboxyl-terminal amide formation in nosiheptide maturation via an enamine dealkylation on the serine-extended precursor peptide. J Am Chem Soc *132*, 16324-16326.

CHAPTER 4.

Targeting virulence factors: Novel approach to the discovery or repurposing of therapies to attenuate virulent methicillin-resistant *Staphylococcus aureus* infections

---

4.1. ABSTRACT

Infections caused by antibiotic-resistant MRSA (methicillin-resistant *Staphylococcus aureus*) have reached epidemic proportions globally, today causing more deaths in the United States than any other bacterial pathogen. Intensifying this problem, MRSA strains are increasingly multi-resistant to other traditional antibiotics. Thus new therapies are urgently needed. In the battle against superbugs such as MRSA, it is imperative to look toward alternative mechanisms in designing new drugs. One such approach is the targeted neutralization of bacterial virulence factors. In the search for new anti-MRSA therapies, the virulence factor α-toxin becomes a central focus. Expression of this pore forming cytotoxin, which is essential for *S. aureus* pathogenicity in animal infection models, is controlled by the well-studied accessory gene regulator (*agr*) locus and its encoded transcription factor, AgrA. In this study, we use *in silico* modeling to show that diflunisal, a commonly used non-steroidal anti-inflammatory drug, is predicted to be an AgrA inhibitor. Transcriptional expression, protein detection, and functional hemolysis assays demonstrated that diflunisal reduces MRSA α-toxin production. Further characterization of this effect, using

MRSA strains treated with diflunisal, indicated other phenotypic effects such as reduced pigment production, slowed growth, and induction of autolysis to are also mediated by the drug. Diflunisal is shown to sensitize MRSA to otherwise subinhibitory concentrations of the antibiotic daptomycin and the host-derived antimicrobial peptide LL-37. Therefore, diflunisal represents a candidate inhibitor of α-toxin and other MRSA virulence phenotypes that could potentially be used alone or in combination with other therapies in the battle against this leading drug-resistant pathogen.

4.2. INTRODUCTION

Each year, *Staphylococcus aureus* causes more than 10 million skin and soft tissue infections in the United States (McCaig et al., 2006). Since 1882, numerous studies have identified *S. aureus* as a leading cause of a wide variety of human infections and described the pathogen's intrinsic ability to develop antibiotic resistance. Community-associated MRSA (CA-MRSA), first described in the 1990s and now epidemic in the United States (Cookson, 2011), possesses important genetic differences compared to earlier hospital-associated (HA)-MRSA strains (Kobayashi and DeLeo, 2009). CA-MRSA produces high levels of cytolytic toxins, exhibits faster growth rates and can cause unusually virulent infections (Kobayashi and DeLeo, 2009). USA300, the predominant clone of disease-causing CA-MRSA, produces a wide spectrum of human disease ranging from uncomplicated skin infections to severe, life-threatening infections such as necrotizing fasciitis, necrotizing pneumonia or sepsis (Diep and Otto, 2008; Kobayashi and DeLeo, 2009; Udo et al., 1993).

S. aureus pathogenesis is multifaceted. While notorious for its ability to cause severe invasive disease, *S. aureus* frequently asymptomatically colonizes the skin and mucous membranes of healthy individuals (Burian et al., 2010; Otto, 2010). At any given time, approximately one-third of the population is colonized with *S. aureus.* To survive in the human host, the bacteria must adapt to changes in temperature, motility, stress, host innate immunity, as well as compete with bacteria of the normal host microflora to establish their niche in the host. Colonization in the anterior nares is recognized as a major risk factor for subsequent development of clinical *S. aureus* infection (Burian et al., 2010; von Eiff et al., 2001; Wertheim et al., 2004).

Though *S. aureus* infection often presents without minimal symptoms, e.g. an uncomplicated skin lesion, it has the ability to disseminate into the deep tissues or bloodsteam and produce a wide variety of serious infections described above. The propensity of *S. aureus* to produce systemic infections is due to its production of numerous virulence factors that act alone or in concert to evade the host immune system and/or induce pathological damage to host tissues.

4.2.1. Bacterial Virulence Factors: Virulence factors are defined as bacterial products that allow a pathogen to establish itself within a host and induce disease (Otto, 2010; Smith, 1977; Sparling, 1983; Sugarman, 1980; Ward and Kunkel, 1983). Examples include proteins, enzymes, associated sugars that allow for bacterial attachment, proliferation, invasion and dissemination and induction of tissue injury. Whether the bacteria are able to induce disease depends on the interactions between the host and the microbe (Smith, 1977). *S. aureus* produces an assortment of virulence factors that support its survival within the host and contribute to disease pathophysiology (Nizet, 2007) **(FIGURE 4.1)**.

Virulence factors can be categorized in three groups based on their overall biological functions: (a) adherence and attachment at the site of infection, (b) invasion and proliferation within the host and (c) host immune evasion and dissemination (Blickwede, 2004). The pathogenesis of an *S. aureus* infection is complex, involving interplay between virulence factors secreted by the bacteria and their effects on host. Of critical importance is the ability of *S. aureus* to target human leukocytes with factors that disrupt their function or promote accelerated cell death. *S. aureus*

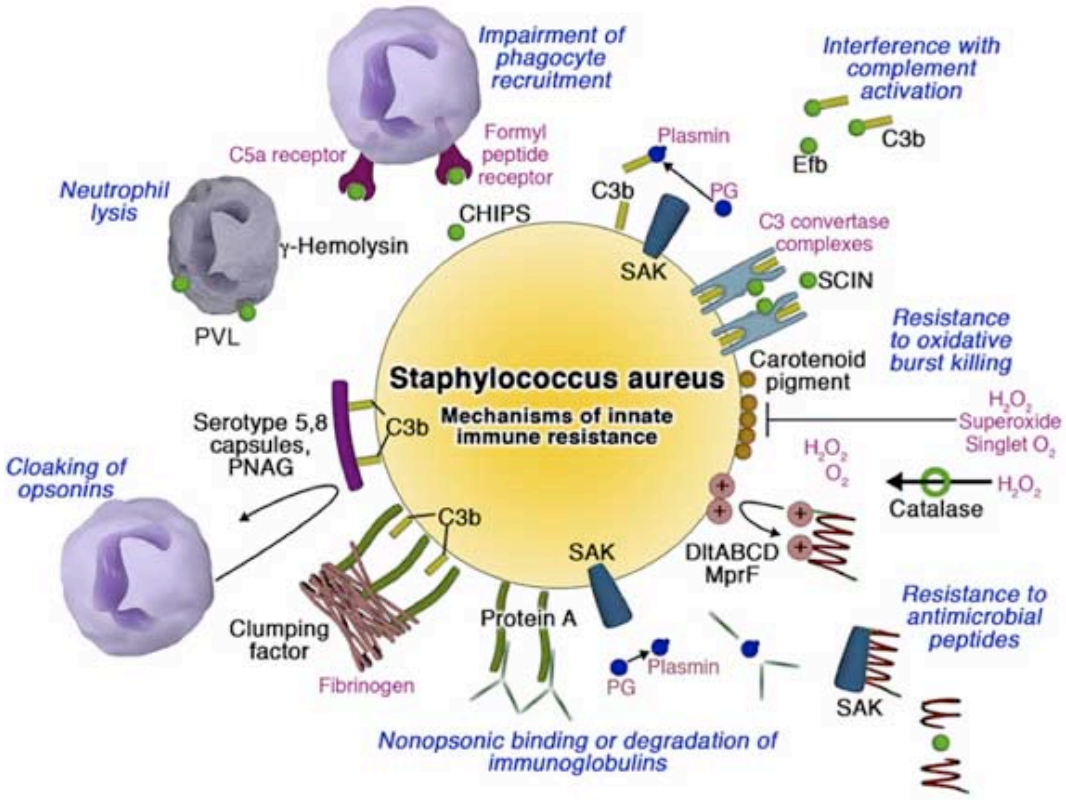

(Figure reprinted from Nizet, 2007)

FIGURE 4.1. Means by which *Staphylococcus aureus* counters host innate immune defense. (Figure reprinted from Nizet, 2007) The well-characterized golden carotenoid pigment gives Staphylococcus aureus its name as well as providing a shield from environmental stresses like oxidants. Catalase detoxifies hydrogen peroxide. Insertion of positive charge modifications on the cell wall increases resistance to antimicrobial peptides, thus subverting an innate immune defense and proteases (aureolysin) further enhance resistance by cleaving peptides. Cell wall proteins (Protein A, fibrinogen binding clumping factor, surface polysaccharide capsule, poly N-acetylglucosamine (PNAG)) coat the bacterial surface to increase adhesion, enhance binding to target tissues, block recognition from host phagocytes. Many other factors aid in the ability of *S. aureus* to resist immune activation, recognition, binding and killing through a number of well-defined processes.

produces multi-subunit toxins such as γ-hemolysin **(FIGURE 4.1., FIGURE 4.2D.)**, and the bacteriophage-encoded Panton-Valentine Leukocidin (PVL) **(FIGURE 4.1., Figure 4.2C.)**, that form pores in leukocyte membranes (Nizet, 2007). The cytotoxin α-hemolysin (encoded by the *hla* gene) **(FIGURE 4.1., FIGURE 4.2A., 4.2B.)** forms pores in erythrocytes, monocytes and lymphocytes and has been implicated as a major contributor to *S. aureus* pneumonia (Kobayashi and DeLeo, 2009).

4.2.2. Virulence factors as targets for antimicrobial therapies: *S. aureus* is able to subvert host immune response, protecting itself from phagocytes (Postma et al., 2004), antimicrobial peptides (Nizet, 2006), oxidative burst (Liu et al., 2005) and other cellular processes that target its elimination. The effective treatment *S. aureus* infections is further complicated by the development of antibiotic resistance, and the deadly pathogen has shown the ability to acquire resistance to almost all antibiotics currently used, including vancomycin (Moellering, 2011; Talbot et al., 2006). When USA300 CA-MRSA strains were first noted in the early 1990s, they were susceptible to commonly used beta-lactam antibiotics. Now, these invasive strains are becoming resistant even to last-line therapies (Moellering, 2011). New approaches are thus of critical important to combat the threat of drug-resistant *S. aureus* infections.

Therapies that act to neutralize specific virulence factors, effectively rendering a bacteria nonpathogenic to the host, are one theoretical approach that could prove effective in treating MRSA. Along with drugs that serve to generally boost innate immune system function, such interventions can help tip the balance in the battle against the superbug back in favor of the host. In addition, anti-virulence therapies

could be useful adjuncts to conventional therapy, diminishing the intrinsic resistance properties of the bacteria and rendering it more susceptible to commonly used antibiotics and innate immune defenses.

4.2.3. S. aureus alpha-hemolysin (α-toxin): The epidemic USA300 strain of CA-MRSA produces high levels of α-toxin, a key facilitator in *S. aureus* infections and pathogenesis in various infection models (Bubeck Wardenburg et al., 2007b) (Li et al., 2009).. This secreted pore-forming toxin is encoded by the gene *hla* **(FIGURE 4.2B**). Secreted water-soluble monomers of the Hla protein interact with surface receptors on host cells and oligomerize into functional membrane-bound heptameric beta-barrels. Susceptible cell types include erythrocytes, lung epithelial cells (Liang and Ji, 2007), monocytes, macrophages and other immune cells **(FIGURE 4.2A)**. The transmembrane pores generated by α-toxin allow selective movement of ions across the cell membrane, activating cell-signaling pathways, interfering with osmotic gradients, depleting nutrients and ultimately leading to cell death. α-toxin is critical for USA300 and USA400 virulence in a murine pneumonia model (Bubeck Wardenburg et al., 2007a) and is involved in *S. aureus*-induced bovine mastitis (Liang et al., 2011).

In addition to its function as a cytolytic pore-forming toxin, alpha-toxin at subcytolytic levels is also a modulator of a number of other signaling pathways in the host cell. The toxin (a) activates caspases and induce apoptosis (Bantel et al., 2001), (b) alters the activity of ADAM10, a mammalian zinc-dependent metalloprotease, to therebydisrupt epithelial barriers (Inoshima et al., 2011), (c) induces interleukin-17 (Niebuhr et al., 2011) thus up-regulating skin inflammation associated with chronic

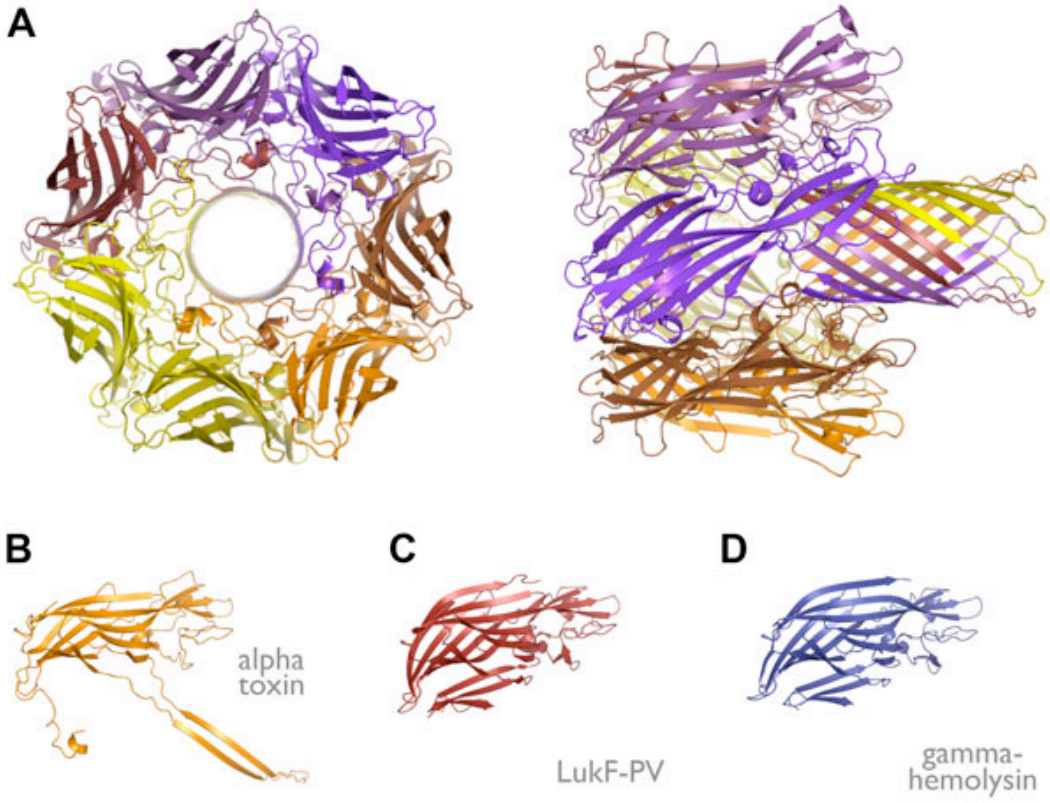

FIGURE 4.2. Alpha-toxin is a heptameric pore-forming toxin. (A) The structure of the 7 alpha-toxin monomers creating a beta barrel pore-forming toxin. A “top” view and a “side” view are shown. **(B – D)** The alpha-toxin monomer is structurally related to LukF-PV monomer and the gamma hemolysin monomer.

skin infections, and (d) stimulates the production of CXC chemokines increasing neutrophil recruitment to foci of lung infection (Bartlett et al., 2008) and aggravating inflammation.

Regulation of α-toxin expression is complex. The two-component accessory gene regulator (Agr) system and the staphylococcal accessory protein effector (SaeRS) positively regulate α-toxin expression, while toxin production is counterregulated by the staphylococcal accessory regulator (SarA).

4.2.4. Targeting alpha-toxin production: α-toxin has been the focus of therapeutic research since its identification in the 1920s (Parker, 1924). During that time, the "acute killing poison" was noted for its destructive action on erythrocytes and epithelial cells (Weld and Gunther, 1931) and for its ability to cause severe gastroenteritis in individuals that ingested milk from cows with *S.aureus* mastitis (Crabtree and Litterer, 1934). Because of its early identification as a critical factor in *S. aureus* infections, α-toxin has been considered a potential therapeutic target.

In recent years, α-toxin has been the target of vaccine-development and immunization studies in addition to the development of small molecule inhibitors. Animal vaccination studies have shown promise in providing host protection against pneumonia and skin-infection. For example, active vaccination with a mutant (H35L) α-toxin monomer or monoclonal antibodies prevented pore formation and protected against *S. aureus* pneumonia (Bubeck Wardenburg and Schneewind, 2008) (Ragle and Bubeck Wardenburg, 2009), and passive immunization with α-toxin specific antisera reduced skin lesion size in the murine models (Kennedy et al., 2010).

Another approach to block the pathogenic effects of α-toxin is to prevent pore

formation or to disrupt protein-binding partners crucial to the establishment of pores. Beta-cyclodextrin derivatives (Ragle et al., 2010) and other cationic cyclodextrins (Yannakopoulou et al., 2011) have recently been examined for their ability to inhibit assembly of the pore and thus reduce infectious mortality. Research suggests that alpha-toxin requires ADAM10, a zinc metalloprotease, as well as certain membrane lipids to form a high-affinity interaction with the host cell and initiate oligomerization of the pore (Inoshima et al., 2011; Wilke and Bubeck Wardenburg, 2010). Thus, inhibitors of zinc metalloproteases in addition to small molecules that prevent binding of alpha-toxin to ADAM10 represent valid therapeutic concepts.

Finally, a number of small molecules have been shown to inhibit various effects of α-toxin. Salicylic acid reduced transcription of α-toxin and attenuated its effect in endovascular infections (Kupferwasser et al., 2003) and endocarditis (Herrmann, 2003). Likewise, allicin, an natural organosulfer compound, reduced toxin production in a dose-dependent manner ((Leng et al., 2011). Farrerol, a traditional Chinese medicine with antioxidant, anti-inflammatory and anti-bacterial effects showed direct bactericidal activity against *S.* aureus and at sub-inhibitory concentrations reduced toxin expression (Qiu et al., 2011). Magnolol, a Chinese medicinal herb, and eugenol, an essential oil in plants also reduced toxin production (Xiang et al., 2010) (Qiu et al., 2010).

One of the most extensively characterized two-component regulator systems in *S. aureus* is the accessory gene regulator (*Agr*) quorum-sensing system **(FIGURE 4.3.)**. *Agr* consists of a histidine kinase (AgrC) that, upon activation, phosphorylates AgrA, a response regulator / transcription factor. AgrA controls the expression of α-toxin in addition to a number of other virulence factors. By targeting AgrA, a small-

molecule inhibitor would have the effect of blocking the expression of *hla.*

In this study we have identified a novel inhibitor of AgrA through homology modeling. Using the refined model, a virtual screening approach, we probed over 100,000 small molecules for AgrA binding. Over 100 were identified as possible hits and were assayed for a-toxin neutralization in hemolysis assays Diflunisal, a bi-phenyl-fluorinated non-steroidal anti-inflammatory (NSAID), as was validated in this fashion. Here we characterize the effects of diflunisal on MRSA alpha-toxin expression and other virulence phenotypes using a variety of *in vitro* assays.

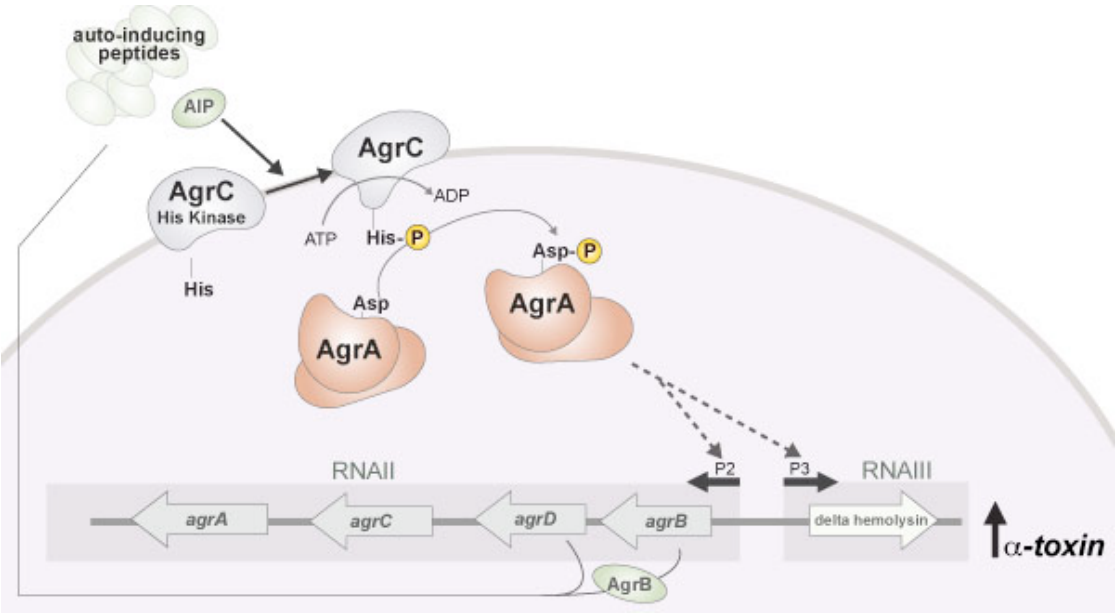

FIGURE 4.3. The Agr Pathway. Activated AgrC Histidine Kinase phosphorylates AgrA on an aspartic acid active site residue. The activated AgrA binds as a transcription factor to promotors on the *agr* regulon to increase α-toxin production.

4.3. RESULTS & DISCUSSION

4.3.1. Diflunisal, a predicted inhibitor of AgrA, is a potent inhibitor of alpha-toxin production and hemolysis.

4.3.1.1. Sequence homology and structure modeling of AgrA: The *S. aureus* genome encodes a variety of two-component regulatory systems **(TABLE 4.1.)**. AgrA is a 28kDa response regulator protein composed of two-domains: a 125-residue N-terminal receptor (REC) domain and a smaller C-terminal DNA-binding (effector) domain, which are tethered together. Response regulators are divided into three general subfamilies based on their type of C-terminal effector domain. Sequence analysis indicates AgrA is a member of the OmpR/PhoB subfamily. An extensive search was done to probe the NCBI database of sequenced *S. aureus* genomes for other OmpR/PhoB family members **(TABLE 4.1)**. Sequence analyses of the N-terminal domain of AgrA shared significant homology with N-terminal domains of other members of the OmpR/PhoB family **(FIGURE 4.4A., 4.4B.)**. The sequence variation between members of this family of response regulators lies in the C-terminal effector domain **(FIGURE 4.4C.**, sequence not shown**)**.

The N-terminus of OmpR/PhoB response regulators is critical for propagating the regulatory signal. Active AgrC, phosphorylated on a conserved histidine, binds into a binding pocket on AgrA, and transfers the phosphoryl group to a conserved aspartic acid (Asp59). Upon phosphorylation of the N-terminal receiving domain, AgrA becomes active, and undergoes a conformational change that induces dimerization and subsequent activation of the C-terminal DNA-binding domain. The C-terminal domain acts as a transcription factor for the P2 and P3 promotors of the

agr regulon, and results ultimately in the induced expression of multiple *S. aureus* toxins, including α-toxin.

By preventing the phosphorylation of N-terminal AgrA, through blocking the phosphoryl-histidine binding pocket, S. aureus toxin production could potentially be inhibited. At this point, there are no available protein structures of the N-terminal portion of AgrA, only a structure of the C-terminal DNA-binding portion (Sidote et al., 2008). Homologs to AgrA in *S. aureus* or other species have previously been described **(TABLE 4.1., 4.2.)** and provide a useful scaffold for building a homology model.

One search for N-terminal domains related to AgrA (1-125) yielded NtrC of *Aquifex aeolicus* **(FIGURE 4.4.)**. NtrC and AgrA share 24% sequence homology, and key functional residues are conserved **(FIGURE 4.4A.)**. In general, REC domains share only ~26% sequence identity (Gao and Stock, 2009) but their structural fold is significantly conserved **(FIGURE 4.5.)**. Thus, it is very likely that a homology model of the as-yet-unknown AgrA N-terminal domain (1-125) (Agr_N), based-off a known REC domain structure such as *A. aeolicus* NtrC (PDB 1NY5), could yield a relevant model for design of AgrA inhibitors. The SWISS-MODEL / Swiss-PDBViewer (Guex and Peitsch, 1997) were employed for an initial model of AgrA_N. This model was carefully inspected and subsequently subjected to energy refinement with the Crystallography and NMR System (CNS) (Brunger et al., 1998). The resulting structure was structurally similar to OmpR/PhoB subfamily members **(FIGURE 4.5.)**.

TABLE 4.1. Staphylococcal Response Regulators (OmpR/PhoB Family)

Response Regulator	Sensor Kinase	Uniprot	Name / Description	Regulation	D-site	T/S-site	(ϕ)-site	PDB ID
AgrA	AgrC	A8Z4U3	Accessory gene regulator	*Exp:* cell-wall assoc proteins (protein A, fnb) *Post-exp:* α, β - toxins, TSST-1, CP [1-2]	D59	T88	F107	3bs1[a]
ArlR	ArlS	A8Z3Z2	Adhesion autolysis	Affects secreted peptidoglycan hydrolase, extracellular proteolytic activities [3]	D52	T79	Y98	
GraR	GraS	A8Z181	Glycopeptide resistance- regulator	Glycopeptide resistance [4-5], increase capsule, reduced exoprotein production [6]	D51	S78	Y97	
HssR	HssS	A8Z552	Heme sensing regulator	Adaptive response to heme; up regulation of heme-regulated transporter efflux pump [7]	D52	T79	Y98	
KdpE[b]	KdpD	P21866[b] A8Z4Y3	K+ (potassium) dependent	Capsular polysaccharide synthesis, role in virulence [8,9]	D52[b] D53	S79[b] S80	Y98[b] Y99	1zh2[b] 1zh4[b]
LuxR[c]	LuxS	Q99UF4[c] A8YY19	Quorum sensing "LuxR" family	Reduces cell-cell adhesion, PIA (downregulate biofilm) [10]	D56[c] D54	T84[c] T82	Y103[c] Y101	3b2n[c]
LytR	LytS	A8Z0M4	Lytic regulator	Control rate of autolysis thru intrinsic murein hydrolase activity [11,12]	D53	T81	Y98	
NreC	NreB	D9RD36	Nitrogen metabolism	Expression of nitrate/nitrite reductases, transporters [13]	D53	T82	Y101	
SaeR	SaeS	A8YZX7	*S. aureus* exoprotein regulator	Invasion of host cells, transcription of DNAse, coagulase, α, β - toxins [14]	D51	T79	Y98	
SrrA	SrrB	P38684[d] A8Z2C6	System respiratory response	Responds to environmental oxygen , activates PIA production in anerobic conditions [15]	D53[d] D53	T80[d] T80	Y99[d] Y99	1zgz[d]
VraR	VraS	A8YY57	Van-resistance associated regulator	Induced transcription of cell wall genes [16] Involved in oxacillin/ glycopeptide resistance [5]	D55	T83	Y102	2rnj[e]
WalR	WalK	A8YYU1	YycG/YycF system	Glycopeptide resistance[5], autolysis, cell wall, division/aggregation, biofilm [17,18]	D53	T80	Y99	

[a] PDB ID 3bs1 refers to the AgrA LytTR (DNA binding domain). The response recognition domain is not included in this structure.
[b] PDB IDs 1zh2 and 1zh4 and UNIPROT P21866 correspond to KdpE is from *E.coli* (40% homology to *S. aureus* KdpE).
[c] PDB ID 3b2n refers to UNIPROT Q99UF4 (a different *S. aureus* strain).
[d] PDB ID 1zgz refers to the structure of TorR (E.coli) which is the homolog of SrrA *(S.aureus)* (TorR shares 33% homology to *S. aureus* SrrA)
[e] PDB IDs 2rnj is the NMR structure of only the DNA binding region of VraR *S. aureus*. The response recognition domain is not included in this structure.

[1] (Novick and Muir, 1999); [2] (Novick, 2003); [3] (Fournier and Klier, 2003); [4] (Neoh et al., 2008); [5] (Galbusera et al., 2011); [6] (Howden et al., 2010); [7] (Stauff et al., 2007); [8] (Xue et al., 2011); [9] (Zhao et al., 2010); [10] (Kong et al., 2006); [11] (Brunskill and Bayles, 1996); [12] (Martin et al., 1999); [13] (Somerville and Proctor, 2009); [14] (Voyich et al., 2009); [15] (Ulrich et al., 2007); [16] (Boyle-Vavra et al., 2006); [17] (Dubrac et al., 2007); [18] (Delaune et al., 2011)

FIGURE 4.4. AgrA alignment with similar *S. aureus* regulators. Alignment of the *S. aureus* OmpR/PhoB sub-family response regulator REC domains with NtrC. Conserved residues (indicated by red dot), conserved hydrophobicity (indicated by yellow shade), and predicted diflunisal interactions (•). Alignment generated in CLUSTALW2. UNIPROT IDs of selected sequences are: AgrA (A8Z4U3); ArlR (A8Z3Z2); GraR (A8Z181); HssR (A8Z552); KdpE (A8Z4Y3); LuxR (A8YY19); LytR (A8Z0M4); nreC (A8Z580); saeR (A8YZX7); SrrA (A8Z2C6); WalR (A8YYU1); VraR (A8YY57) and NtrC (O67198) of *A. aeolicus*.

A

```
                                    10        20        30        40        50        60
AgrA(S.a)   --------------------MKIFICEDDPKQRENMVTIIKNYIMIEEKPMEIALATDNPYEVLEQAKNMNDIGCYFLDIQLSTDIN
PrrA (M.tb) MDTGVTS-------------PRVLVVDDDSDVLASLERGLR-----LSG-FEVATAVDG-AEALRSAT-ENRPDAIVLDINMP-VLD
PhoP(M.tb)  MRKGVDLVTAGTPGENTTPEARVLVVDDEANIVELLSVSLK-----FQG-FEVYTATNG-AQALDRAR-ETRPDAVILDVMMP-GMD
PhoP(B.sub) MNK------------------KILVVDDEESIVTLLQYNLE-----RSG-YDVITASDG-EEALKKAE-TEKPDLIVLDVMLP-KLD
KdpE(E.c)   MTN------------------VLIVEDEQAIRRFLRTALE-----GDG-MRVFEAETL-QRGLLEAA-TRKPDLIILDLGLP-DGD
Pho(E.c)    --------------------MRVLVVEDNALLRHHLKVQIQ-----DAG-HQVDDAEDA-KEADYYLN-EHIPDIAIVDLGLP-DED
TorR(E.c)   ------------------MPHHIVIVEDEPVTQARLQSYFT-----QEG-YTVSVTASG-AGLREIMQ-NQSVDLILLDINLP-DEN
RR(P.p)     ---------------PVAARPLVLVVDDNAVNREALILYLK-----SRG-IDAVGADGA-EEARLYLHYQKRIGLMITDLRMQ-PES
NtrC(A.a)   --------------------MNVLVIEDDKVFRGLLEEYLS-----MKG-IKVESAERG-KEAYKLLS-EKHFNVVLLDLLLP-DVN
LuxR(S.a)   --------------------MTSLIIAEDQNMLRQAMVQLIK-----LHGDFEILADTDN-GLDAMKLIEEYNPNVVILDIEMP-GMT
Spo0A(B.st) ------------------MSIKVCIADDNRELVSLLDEYIS-----SQPDMEVIGTAYN-GQDCLQMLEEKRPDILLLDIIMP-HLD
                             : : :*:      :   :                                . . *: :

                    70        80        90        100       110       120       130       137
AgrA(S.a)   GIKLGSEIRK-HDPVGNIIFVTSHSELTYLTFVYKVAAMDFIFKD-DPAELRTRIIDCLETAHTRLQLLSKD
PrrA (M.tb) GVSVVTALRA-MDNDVPVCVLSARSSVDDRVAGLEAGADDYLVKPFVLAELVARVKALLRRRG-STATSSSE
PhoP(M.tb)  GFGVLRRLRA-DGIDAPALFLTARDSLQDKIAGLTLGGDDYVTKPFSLEEVVARLRVILRRAGKGNKEPRNV
PhoP(B.sub) GIEVCKQLRQ-QKLMFPILMLTAKDEEFDKVLGLELGADDYMTKPFSPREVNARVKAILRRSEIAAPSSEMK
KdpE(E.c)   GIEFIRDLR--QWSAVPVIVLSARSEESDKIAALDAGADDYLSKPFGIGELQARLRVALRRHSATTAPDPLV
Pho(E.c)    GLSLIRRWRS-NDVSLPILVLTARESWQDKVEVLSAGADDYVTKPFHIEEVMARMQALMRRNSGLASQ----
TorR(E.c)   GLMLTRALR--ERSTVGIILVTGRSDRIDRIVGLEMGADDYVTKPLELRELVVRVKNLLWRIDLARQAQPHT
RR(P.p)     GLDLIRTIRASERAALSIIVVSGDTDVEEAVDVMHLGVVDFLLKPVDLGKLLELVNKELKIG----------
NtrC(A.a)   GLEILKWIKE-RSPETEVIVITGHGTIKTAVEAMKMGAYDFLTKPCMLEEIELTINKAIEHRKLRKEN----
LuxR(S.a)   GLEVLAEIRK-KHLNIKVIIVTTFKRPGYFEKAVVNDVDAYVLKERSIEELVETINKVNNGEKEYSATLMTS
Spo0A(B.st) GLAVLERIRAGFEHQPNVIMLTAFGQEDVTKKAVELGASYFILKPFDMENLAHHIRQVYGKTTPVVRKAAPA
            *      ::          .::                  :: *     ::   :
```

B

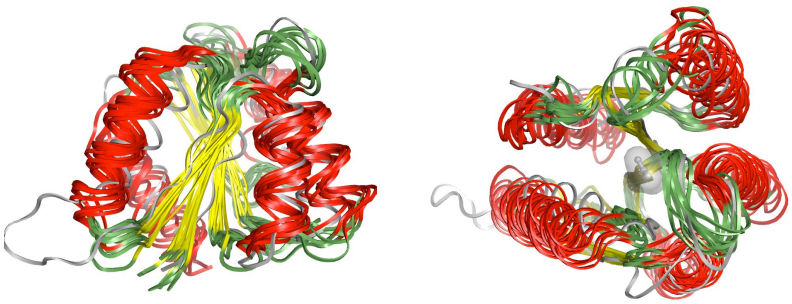

FIGURE 4.5. Known structures of response regulators can be used as templates for homology models. (A) Sequence alignment of selected response regulators. **(B)** Response regulators with known structures were analyzed for their structural homology. The homology model of AgrA, derived by the NtrC (*A. aeolicus*) template, was compared to other REC structures. The structure of N-terminal domains is conserved. α-helices are colored red, loops are green and beta strands indicated by yellow. AgrA model is in grey and shows an extended loop in the region of residues 22-29 and Asp59 is highlighted (surface rendering).

TABLE 4.2. Select structures of response-regulator domains

Response Regulator	PDB ID	Species	Uniprot	Name / Description	Sensor Kinase	PMID Ref
LuxR	3b2n	*S.aureus Mu50*	Q99UF4	Quorum sensing "LuxR" family	LuxS	
PhoP	1mvo	*B. subtilis*	P13792	Alk phosphatase synthesis reg protein	PhoR	12486062
PhoP	2pkx	*E.coli*	P23836	Alk phosphatase synthesis reg protein	PhoR	17545283
PhoP	3r0j	*M. tuberculosis*	P71814	Alk phosphatase synthesis reg protein	PhoR	21634789
PrrA	1ys6 1ys7	*M. tuberculosis*	P0A5Z6	early intracellular multiplication	PrrB	To be published
Spo0A	1dz3	*B. stearo-thermophilus*	P52934	Stage 0 sporulation protein A	KinD	10731426
TorR	1zgz	*E.coli*	P38684	Response to anaerobic cond. and tri-methylamine N-oxide	TorS	16322582
KdpE	1zh2	*E.coli*	P21866	Osmoregulation and K+ sensing	KdpD	16322582
NtrC	1zy2	*A.aeolicus*	O67198	nitrogen-regulatory protein C of enteric bacteria	NtrB	1619010
Resp Reg	3hdv	*P. putida*	Q88QX9	*Not identified*	*Not identified*	To be published

Not included in list: DosR- *M.tuberculosis* (3c3w, Wisedchaisri et al, J.Mol.Biol 2008), DrrB- *T. maritima* (1p2f, 3nns, Robinson et al, J. Bacteriology 2003), NarL- *M.tuberculosis* (1rnl, Baikalov, et al, Biochem. 1996); StyR- *P. fluorescens* (1yio, 1zn2, Milani et al, Structure 2005); DctD- S. Meliloti (1l5z, 1qkk, Park et al, FASEB J 2002); Rcp1-cyanobacteria *Synechocystis sp.* (1i3c, 1jlk, Im et al Prot Sci 2002), PleD (Wassmann et al Structure 2007); WspR- *P.aeurginosa* (3bre, De et al PLoS Biol 2008) and many others not listed here.

TABLE 4.3. Optimization of four virtual screening hits using two *in vitro* assays

(A) % Inhibition of USA300 α-toxin production

Compound #	1 μg/ml	10 μg/ml
1	0.0 ± 7.0	68.8 ± 11.3
2	31.3 ± 9.0	61.0±14.8
3	49.4 ± 4.6	53.0 ± 5.9
4	33.0 ± 3.6	62.3 ± 1.8

(B) % Inhibition of Hemolysis in rabbit blood

Compound #	1 μg/ml	10 μg/ml
1	49.0 ± 2.2	76.6 ± 8.1
2	38.6 ± 6.4	55.6 ± 9.3
3	34.3 ± 6.9	84.7 ± 6.7
4	71.1 ± 5.9	83.7 ± 8.5

Data obtained by Professor Menachem Shoham, PhD and colleagues at Case Western University and was provided as part of a joint collaborative project.

4.3.1.2. Virtual screening of the NCI library for small-molecule inhibitors of the AgrA N-terminal phosphoryl-binding pocket: With the homology model of AgrA in hand, over 100,000 compounds from the National Cancer Institute Compound Library (NCI) and ZINC database (Irwin and Shoichet, 2005) were subjected to rigorous virtual screening using GLIDE, a Linux-based Schrödinger Suite program (Friesner et al., 2004; Friesner et al., 2006; Halgren et al., 2004). Over 100 compounds resulted as hits from this screen. These were subjected to further analysis and refinement.

4.3.1.3. Refinement of top-scoring hits using in vitro testing: *In vitro* analyses testing α-toxin production were used to process top-scorers. An ELISA assay was used to determine relative α-toxin levels of USA300 after incubation with candidate compounds. There were a few potent inhibitors of α-toxin production **(TABLE 4.3A.)** and rabbit blood hemolysis **(TABLE 4.3B.)** at concentrations that did not inhibit or slow bacterial growth (data not shown).

4.3.1.4. Identification of diflunisal as an AgrA and α-toxin inhibitor: Each of the four compounds that were tested for inhibition of α-toxin production **(TABLE 4.3A.)** and rabbit blood hemolysis **(TABLE 4.3B.),** and showed positive results in both assays. Diflunisal (compound 4) showed exceptional inhibitory activities and was carried on for further analysis. At 50 µg/ml, diflunisal reduced *hla* expression by roughly 3,000-fold **(FIGURE 4.6A.)** and expression of the gene encoding the toxin phenol soluble modulin-alpha (*psm-*α)by 2,000-fold **(FIGURE 4.6A.)**. Interestingly, only treatment of *S. aureus* with diflunisal, and not with any of the other tested

compounds, caused a significant reduction in *RNAIII* expression **(FIGURE 4.6A.)**. The ability of diflunisal to impede *RNAIII* expression suggests that diflunisal may target other regulatory pathways such as those outlilned in **TABLE 4.1**.

4.3.1.5. Diflunisal reduces the overall production of α-toxin in USA300 MRSA: Four separate assays confirm that quantities of α-toxin are significantly reduced in the presence of diflunisal. ELISA assays which measured toxin production following incubation with three concentrations of diflunisal, indicated that α-toxin production was lowered in a concentration-dependent manner (**FIGURE 4.6B.).** Cultures treated with 50 μg/ml of diflunisal exhibited a clear reduction, producing 30% of toxin compared to controls. Bacteria exposed to 10 μg/ml of the produced only slightly more toxin **(TABLE 4.3A. and Figure 4.6B.)**. These data demonstrate the potency of diflunisal in attenuating α-toxin production. These results were validated in the rabbit hemolysis assays described above, as diflunisal treatment reduced the ability of MRSA to lyse red blood cells **(TABLE 4.3B.).**

To further validate the effect of diflunisal on *S. aureus* production of α-toxin, supernatants from 48 h cultures of USA300 TCH1516, incubated with diflunisal at 0, 5, 10, 20, 30, 40 and 50 μg/ml, were examined for alpha-toxin production via western immunoblot analysis **(FIGURE 4.6D.).** The result is even more striking, indicating the absence of α-toxin in all treated supernatants.

4.3.1.6. Diflunisal-treated S. aureus shows less hemolysis on blood plates: To directly assay whether diflunisal would decrease *S. aureus* hemolysis

typically seen on a blood agar, we tested two different strains for their ability to cause hemolysis after 24 h pre-incubation with diflunisal at varying concentrations. WR69 (kindly provided by Dr. George Sakoulas) is an MSSA blood isolate from a patient with an epidural abscess, and produces only α-toxin, and no δ-toxin. Twenty-four h WR-69 cultures exposed to diflunisal at 50, 40, 30, 20, 10, 5 and 0 μg/ml were spotted on blood agar. A large difference in hemolysis was observed between cultures treated with high concentrations of diflunisal vs. those treated with lower concentrations **(FIGURE 4.6D)**. We conclude that this effect can mainly be attributed to the marked reduction in α-toxin expression.

Sequence-type (ST)-59 MRSAis an extremely virulent strain from Taiwan that produces Panton-Valentine Leucocidin (PVL and displays unique genetic characteristics and multi-drug resistance (Takano et al., 2008) To test whether diflunisal reduces hemolysis of ST-59, cultures exposed to different doses of diflunisal were prepared in an identical manner as above and spotted on blood agar to qualify hemolysis. The results once again show reduced hemolysis in high concentrations of diflunisal **(FIGURE 4.6E.)**.

Salicylic acid, an NSAID sharing similar structural features with diflunisal, is the active metabolite of aspirin. Prior studies have shown that salicylic acid has the ablility to attenuate bacterial virulence by increasing extracellular adhesion protein expression (Kupferwasser et al., 2003; Palma et al., 2006) or decreasing capsule production (Alvarez et al., 2010) in *S. aureus* (Alvarez et al., 2011), , reducing *Pseudomonas aeruginosa* virulence factors (Bandara et al., 2006), and altering stress response pathways in *Bacillus subtilis* (Duy et al., 2007). To test the ability of

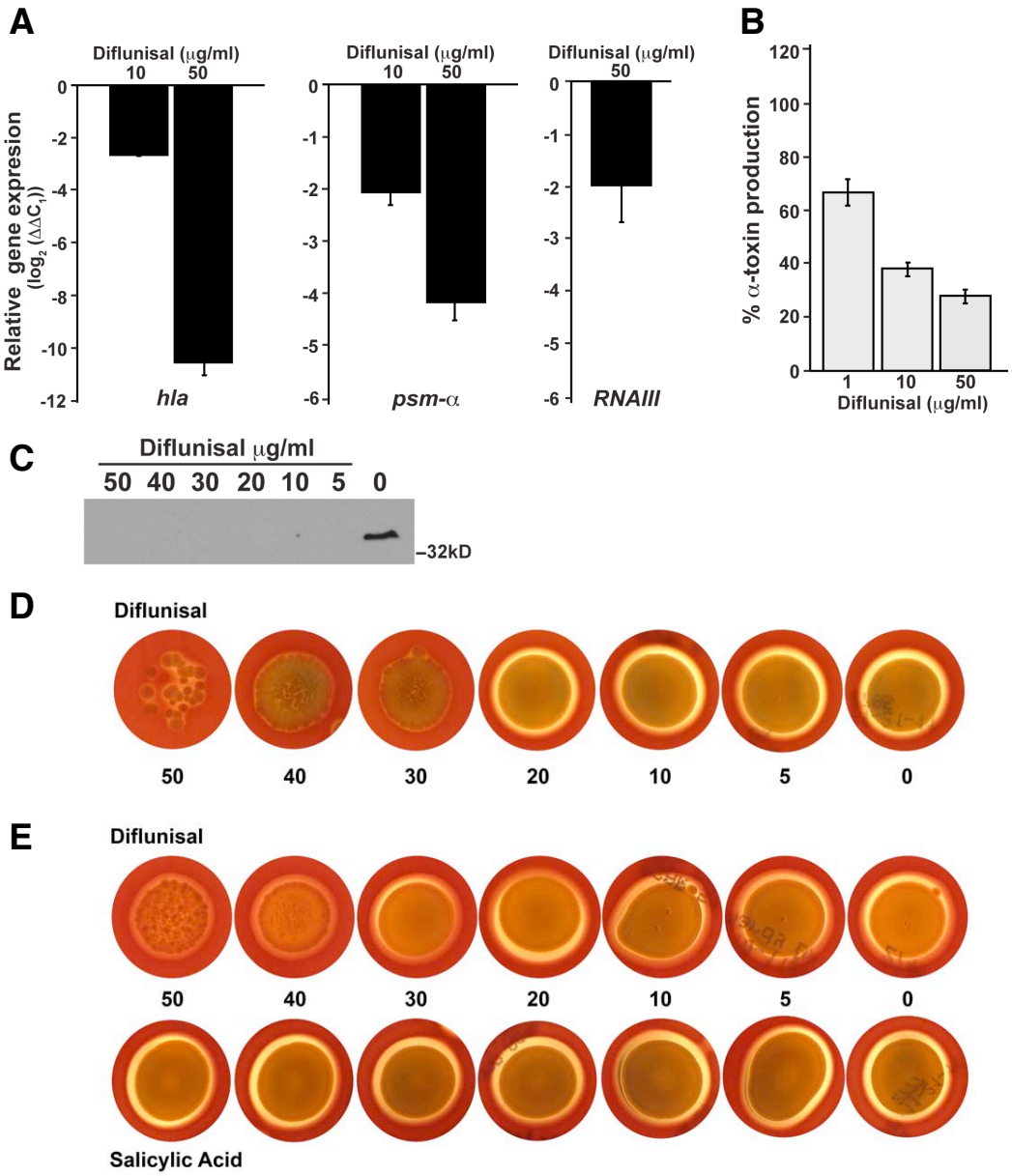

FIGURE 4.6. The effects of diflunisal on products downstream of AgrA. (A) Diflunisal inhibits *hla, psm-α* and *RNAIII* expression; **(B)** USA300 MRSA of α-toxin production is significantly reduced in a concentration-dependent manner; **(C)** 48-hour supernatants show no α-toxin production in a Western blot. **(D/E)** Strains incubated for 24h with diflunisal or salicylic acid at different concentrations were spotted on sheep-blood agar **(D)** WR-69 (an α-toxin-only producer (no β or δ-toxins)) and **(E)** the very virulent ST-59 showed concentration-dependent decreased hemolysis on blood agar. This effect is not exhibited in ST-59 treated with salicylic acid.

***[Panels A and B:** Data obtained by Professor Menachem Shoham, PhD and colleagues at Case Western University and was provided as part of a joint collaborative project. **Panel C:** assay was done by N. Haste and Morgan Pence (acknowledged). **Panel D and E:** assay was done by N. Haste.]*

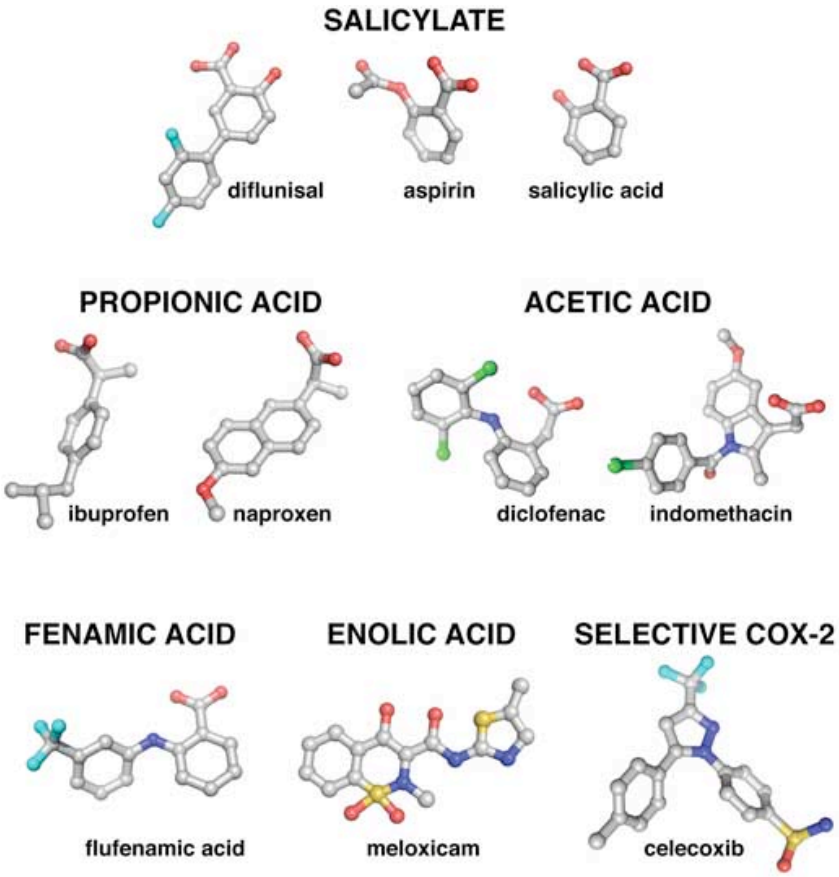

FIGURE 4.7. The chemical scaffolds of various non-steroidal anti-inflammatory agents (NSAIDs).

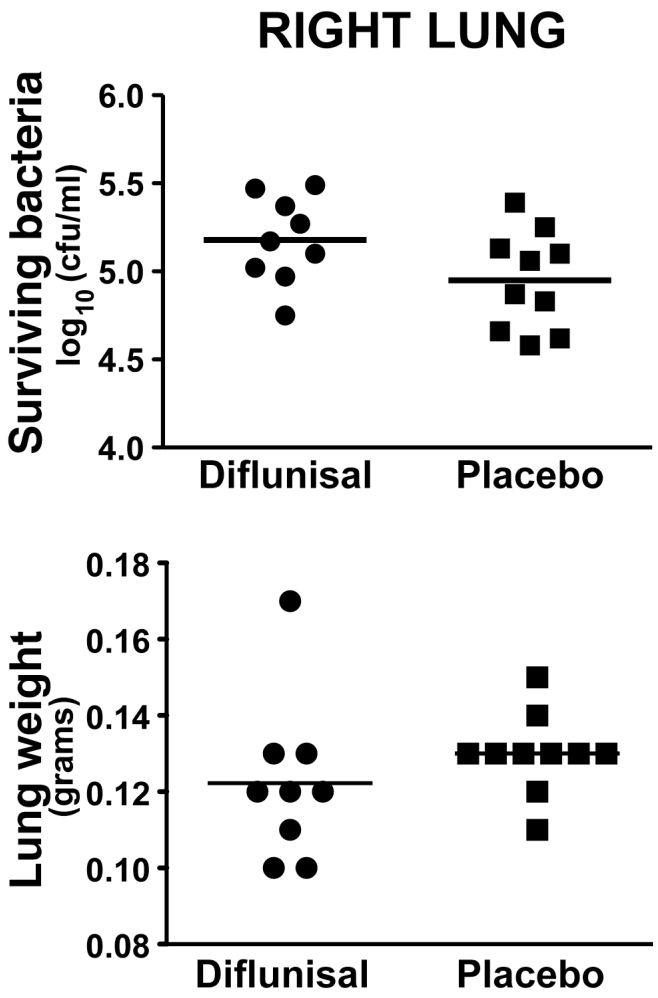

FIGURE 4.8. Systemic pre-treatment of mice with diflunisal did not provide protection from USA300 MRSA pneumonia. C57BL6 mice were pre-treated with diflunisal (0.625 mg/mouse) at 0, 6 and every 12 hours for a total of 7 doses prior to nasal inoculation with TCH1516 USA300 MRSA (2 x 10^8 cfu/mouse). The right lung was harvested from treated and placebo mice, weighed and assayed for surviving bacteria. Pretreatment of mice with diflunisal did not provide significant protection against or impairment from recovery of the infection as shown by surviving cultures (top) and lung weight (bottom).

salicyclic acid to prevent overall hemolysis, ST-59 cultures were incubated with decreasing concentrations of salicylic acid in an assay that mirrored that of diflunisal. The result **(FIGURE 4.6E.)** indicates that at these concentrations, salicylic acid does not inhibit ST-59 hemolysis, incontrast to what we observed with diflunisal.

4.3.1.7. Pre-treatment with diflunisal did not alter infectious outcome in a murine pneumonia model: Diflunisal is one of many commonly used NSAIDs, prescribed for their analgesic, antipyretic and anti inflammatory effects **(FIGURE 4.7.)**. It is conceivable that a patient who develops a *S. aureus* infection may already be taking a steady dose of diflunisal or other NSAID, either to treat pain associated with infection or to treat a separate underlying condition. A current debate exists in the literature regarding the effects of NSAIDs on the outcome of concurrent infection. Several studies have presented arguments against the use of NSAIDs, citing that their analgesic or anti-inflammatory effect, could impair proper diagnosis of worsening infection, for example in the case of group A *Streptococcus* necrotizing fasciitis (Aronoff and Bloch, 2003). Other studies have suggested that NSAIS is associated with an increased frequency of bacterial infections in children (Leroy et al., 2010) or can worsen soft-tissue infections in mice (Weng et al., 2011). However, an equal number of studies have suggested that NSAID use during infections can improve outcomes. For example, NSAID use was found to significantly reduce the risk for *S. aureus* bacteremia in hemodialysis patients using tunneled catheters (Sedlacek et al., 2007; Yang and Lin, 2007) and to promote antibacterial effects and synergy with antibiotics in treating urinary tract infection and diabetic foot ulcers (Akhter et al.,

2010).

We performed a pilot study using an *in vivo* model of *S. aureus* pneumonia to test whether pre-treatment of mice with diflunisal could reduce the severity of an infection. Eleven-week old C57BL6 mice were pre-treated with seven doses of diflunisal (0.624 mg/mouse/dose) or placebo control. Mice were later infected with a sub-lethal dose of USA300 MRSA strain TCH1516 in the left naris. The dose of diflunisal was selected to be well below cytotoxic levels -- the 50% systemic Lethal Dose (LD_{50}) in mice is known to be 124 mg/kg. At the time of infection, diflunisal was expected to have achieved steady state with an *in vivo* half-life of 8-12 h. The right lung was harvested 24 h after infection and results **(FIGURE 5.8.)** showed no significant difference between the control and treatment groups. We plan further inspection of the influence of diflunisal treatment on *S. aureus* in vivo using different dosing regimens and infectious challenge conditions, including concurrent antibiotic treatment.

4.3.1.8. Allelic replacement mutagenesis of MRSA TCH1516 USA300 hla:

To study the role of alpha toxin in tissue culture and small animal models of infection, we sought to delete the encoding *hla* gene from USA 300 MRSA strain TCH1516 by allelic exchange mutagenesis

The *hla* gene shows strong conservation between all sequenced *S. aureus* strains. Among these bacteria, the differences in the effects of α-toxin may derive from the regulation of *hla* gene expression**.** Precise deletion of *hla* was confirmed by PCR and did not affect growth rate of the bacterium in liquid culture **(FIGURE 4.9A.)**.

4.3.1.9. Alpha-toxin contributes to TCH1516 skin infection: To evaluate the virulence of the isogenic *hla* mutant, an *in vivo* skin infection was used in which 10 week old C57BL6 mice were infected ~10^8 cfu/mouse of wild-type MRSA strain TCH1516, the isogenic Δhla mutant, and media control. Skin lesion sizes were monitored and measured on days 3, 6 and 12. By day 12, all mice that received the mutant Δhla strain had resolved the infection and no longer had visible lesions. On the other hand, mice that were challenged with the wild-type TCH1516 still had large lesions **(FIGURE 4.9B.)**. The results from this study are striking and indicate that the isogenic *hla* mutant can serve as a useful experimental tool for comparing and contrasting the effects of putative α-toxin virulence factor inhibitors.

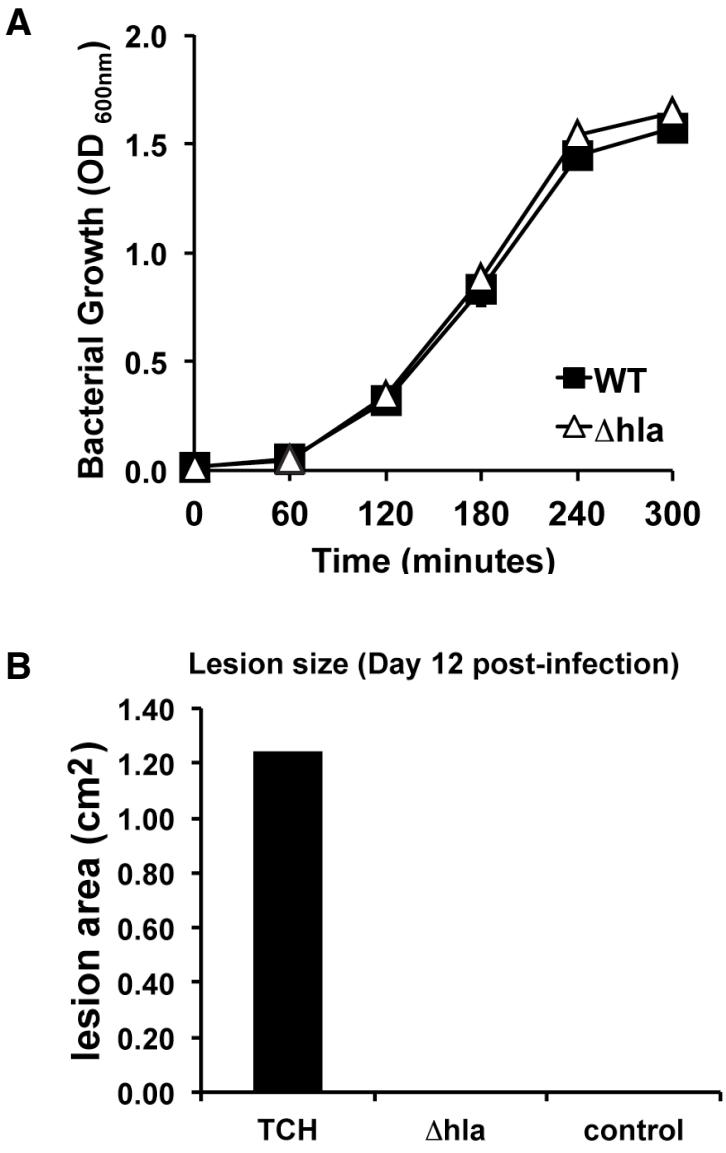

FIGURE 4.9. The isogenic alpha-toxin (*hla)* mutant. (A) The mutant strain exhibits an identical growth rate compared to the wildtype parent strain. **(B)** Skin lesion areas twelve days post infection highlight a significant difference between the virulence of the wildtype and the Δhla mutant strains.

4.3.2. Additional phenotypic changes induced by diflunisal in MRSA

On close observation of the droplets prepared on blood agar **(FIGURE 4.6.)**, we repeatedly noticed the appearance of small colony variants and reduced colony forming units (cfu) in the spots where MRSA has been treated with 50 μg/ml of diflunisal. Traditional MIC assays were performed to assess potential direct antibiotic effects of diflunisal on MRSA. The MIC of diflunisal against CA-MRSA strain TCH1516 was calculated to be 800 μg/ml, 16-fold higher than the maximal doses used in our hemolysis inhibition studies. To further determine the extent to which diflunisal influenced phenotypic changes to *S. aureus,* a panel of assays tested alterations in growth, viability, pigment and susceptibility to co-administered antibiotics.

4.3.2.1. High concentrations of diflunisal prevent S. aureus growth: ***Traditional*** growth curves were set up to test sublethal, growth inhibitory effect of diflunisal on the MRSA growth at concentrations higher than tested in initial α-toxin inhibitor assays **(FIGURE 4.10A.)**. Optical density was measured every 30 min for 6 h and shows that 50, 10 and 0 μg/ml treated cultures share similar growth kinetics **(FIGURE 4.10A.)**. However, at higher concentrations MRSA cultures are unable to achieve the same bacterial density and show slowed growth **(FIGURE 4.10B.)**. This there is concentration dependent effect of higher concentrations of diflunisal to slow MRSA growth and induce stationary phase at reduced bacterial densities.

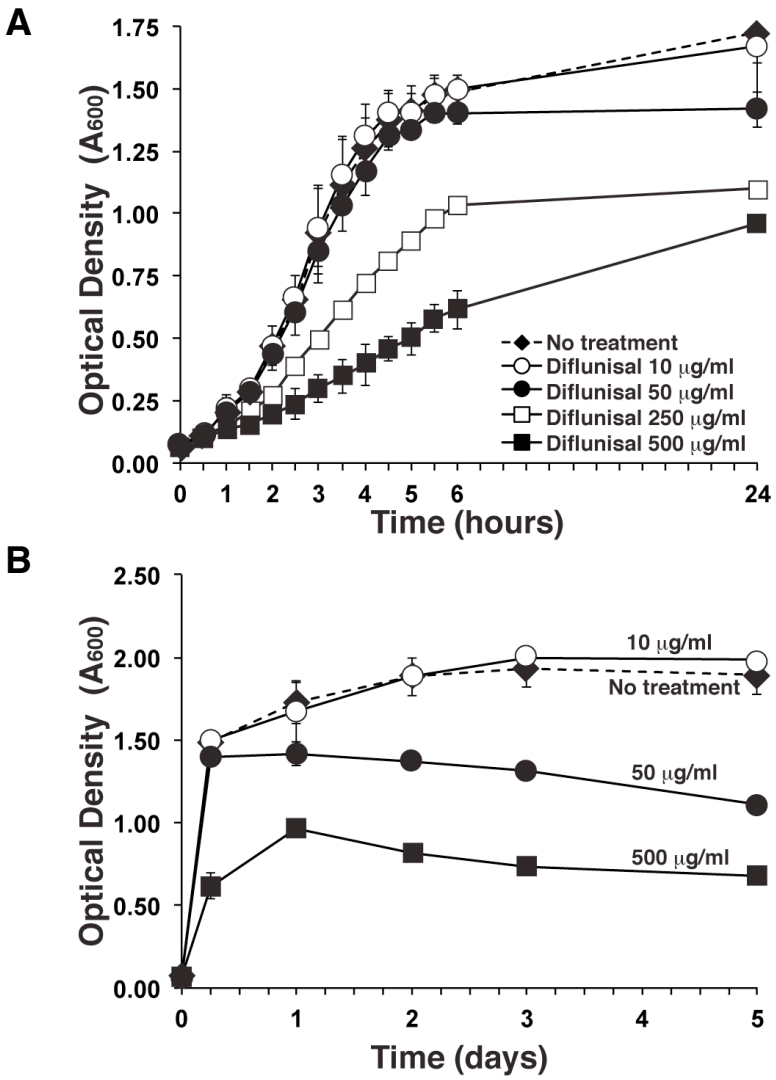

FIGURE 4.10. MRSA growth curves in the presence of diflunisal. (A) Cultures treated with diflunisal at 0, 10 or 50 μg/ml have similar rates of growth over the first six hours. There is a concentration dependent reduction in growth-rate for the cultures treated with higher concentrations of diflunisal. Interestingly, 50 μg/ml cultures do not increase in density after 6 h. **(B)** TCH1516 cultures treated with 500 or 50 μg/ml never reach the same density as the placebo control and 10 μg/ml treated cultures. In addition, they showed a slow reduction in turbidity over a 5-day period of incubation.

4.3.2.2. Diflunisal-treated S. aureus undergoes autolysis in late-stationary phase: Initial assessment of growth curves showed that the 50 μg/ml treated culture allowed normal growth kinetics during the first 6 h of treatment exposure. However, inspection of the later time points reveals that 50 μg/ml cultures do not achieve equal bacterial densities during late-stationary phase when compared to the 10 μg/ml and un-treated bacteria.

To determine whether the bacteria treated with diflunisal 50 μg/ml would slowly increase in density over a longer time period to achieve equality with untreated cultures, optical densities of MRSA exposed to diflunisal at 500, 50, 10 and 0 μg/ml were measured at 6 h, 24 h and every day for five days. Our results revealed instead a gradual reduction in bacterial turbidity in the 500 and 50 μg/ml treated cultures over time **(FIGURE 5.10B.)**, a finding that was confirmed through quantitative cfu assessment

The delayed bactericidal effect was determined to be *agr*-independent, as similar results were obtained when the assay was repeated using an *agr+* MSSA strain (RN6607 in comparison to is agr- derivative (RN9120)) **(FIGURE 5.11A.)**. In contrast to diflunisal, salicylic aciddid not reduce bacterial densities or quantities even over 11-days of exposure **(FIGURE 5.11B.)**. When MRSA strain TCH1516 was exposed to higher concentrations of diflunisal (200 μg/ml), bacteria never reach the same turbidity or equal quantities as the placebo control. These cultures also undergo similar cfu reduction, suffering 1 – 3 $\log_{10}$ decreases in viable bacteria at 48 h (data not shown), suggesting an autolytic phenomenon.

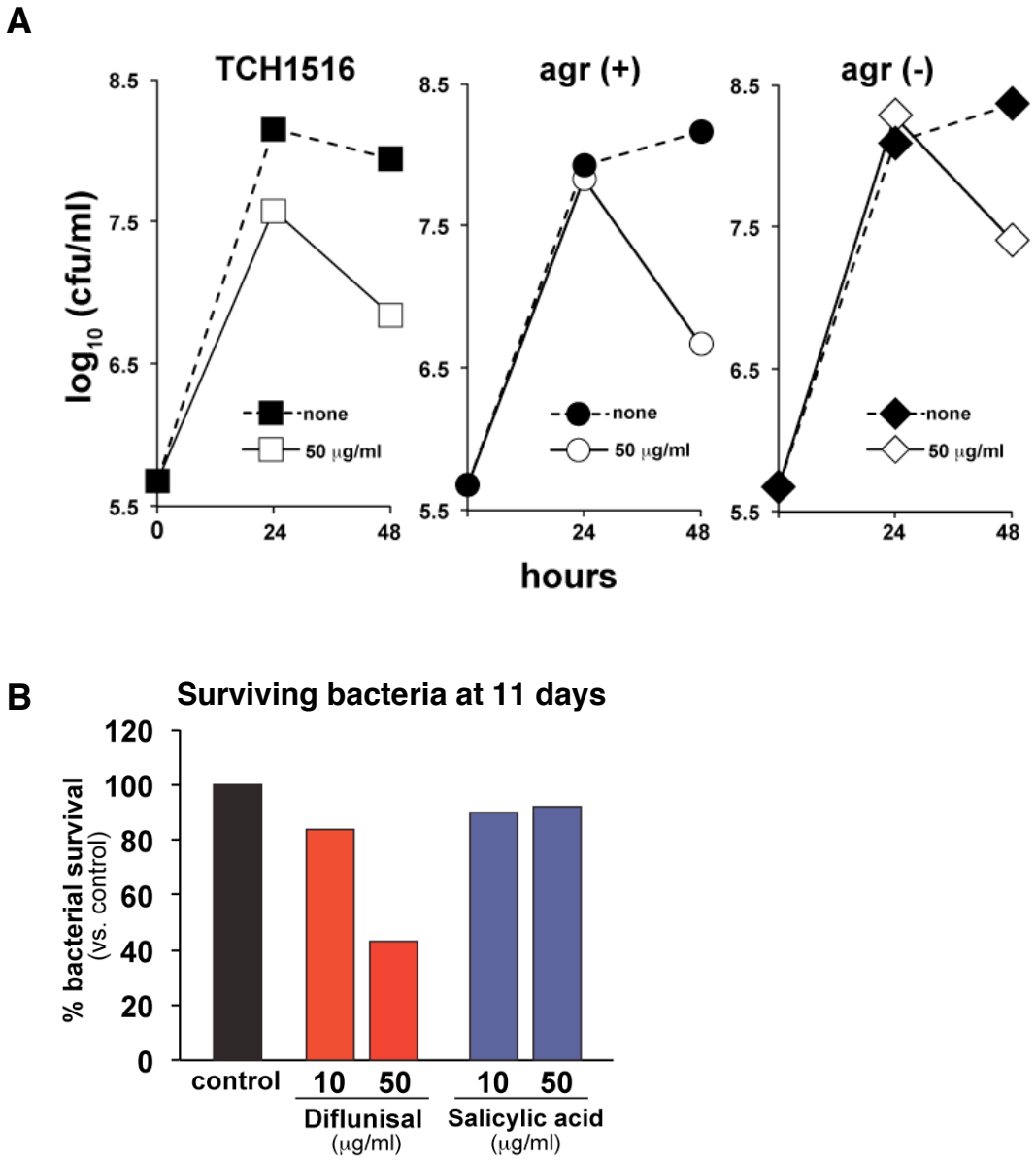

FIGURE 4.11. Diflunisal-treated *S. aureus* undergoes autolysis in late-stationary phase. **(A)** The trend is agr-independent. Three strains of *S. aureus,* wild-type USA300 TCH1516 MRSA, an agr(+) RN6607 and and agr(-) RN9120 (both MSSA) all show similar profiles over a 24 and 48 h period. At 24 hours, bacteria counts are relatively equal, with TCH1516 have slightly less in the treatment group. At 48 h, the counts of all three strains have reduced by at least one $\log_{10}$. (B) Bacterial cultures (ST-59 MRSA for diflunisal treatment, TCH1516 for salicylic acid treatment) were incubated for 11 days in the presence or absence of compounds. At 11 days, cultures treated with diflunisal 50 μg/ml showed a 60% reduction in bacterial survival and distinct loss of culture turbidity (data not shown).

4.3.2.3. Pigment inhibition by diflunisal: Following incubation of MRSA strain TCH1516 with diflunisal, we observed a significant decrease in the pigmentation of treated vs. non-treated bacteria **(FIGURE 4.12A.)**. *S. aureus* yellow-golden pigmentation is caused by the carotenoid-like pigment staphyloxanthin. Staphyloxanthin production of MRSA was analyzed following exposure to 0, 10, 20, 30, 40 and 50 μg/ml of diflunisal at different time points (12, 24, 36 and 48 h). A significant reduction in MRSA pigment production was observed beginning at diflunisal concentrations greater than 10 μg/ml **(FIGURE 4.12B.)**. The dramatic reduction in pigmentation can be seen as early as 12 h, a time point when there are roughly equal viable bacteria in each of the treated cultures. At time points beyond 12 h, bacteria treated with 20 – 50 μg/ml diflunisal show nearly a 4-fold reduction in pigment. Diflunisal–dependent reduction of pigment is agr-independent **(FIGURE 4.13.)**, since similar loss of pigmentation is seen in the isogenic agr(+) RN6607 and agr(-) S. aureus RN9120 strains.

It should be noted that carotenoid quantification will be dependent upon on the total quantity of bacteria, dead or alive, in a given pellet used for pigment extraction. **FIGURE 4.12C.** displays the number of viable bacteria were quantified from each treatment group.

Staphyloxanthin, is produced by a specific biosynthetic pathway. Deletion of critical enzymes in this pathway renders S. aureus nonpigmented. Without the golden pigment, *S. aureus* is weakened in its virulence and resistance to host immune clearance. Staphyloxanthin protects the bacterium from reactive oxygen species

such as hydrogen peroxide, superoxide and singlet oxygen generated by neutrophils and macrophages during phagocytic killing (Liu et al 2005; Clauditz et al 2006). Future studies are planned to test the specific effect of individual reactive oxygen species on diflunisal treated bacteria.

Interestingly, we have identified similarities between the structure of diflunisal and known inhibitors of pigment production. *S. aureus* dehydrosqualene synthase (CrtM) is required for staphyloxanthin production (Liu et al 2005). Various cholesterol-biosynthesis inhibitors block the active site of CrtM (Liu et al 2008) and prevent staphyloxanthin biosynthesis. Some active site inhibitors contain a core biphenyl structure. In addition, these and others carry a key carboxylic acid that coordinates in the active site. It is possible that diflunisal binds in the CrtM active site and prevents pigment biosynthesis. Specific enzyme inhibition assays with purified S. aureus CrtM are currently planned to test this hypothesis.

4.3.2.4. Diflunisal acts synergistically with cell wall antibiotics: In addition to promoting resistance to reactive oxygen species, *S. aureus* pigment is known to contribute to cell wall rigidity and the resistance of the bacterium to killing by cationic antimicrobial peptides (PMID: 21115796). We tested the effects of diflunisal treatment in combination with the cationic antibiotic daptomycin and the host-derived cationic antimicrobial peptide, cathelicidin LL-37. Using a checkerboard format, aliquots were removed after 18-24 h quantify viable bacteria in the placebo, diflunisal alone, antibiotic alone, diflunisal + antibiotic treated cultures. Diflunisal was shown to have additive antibiotic effects with both agents **(FIGURE 4.14.)**.

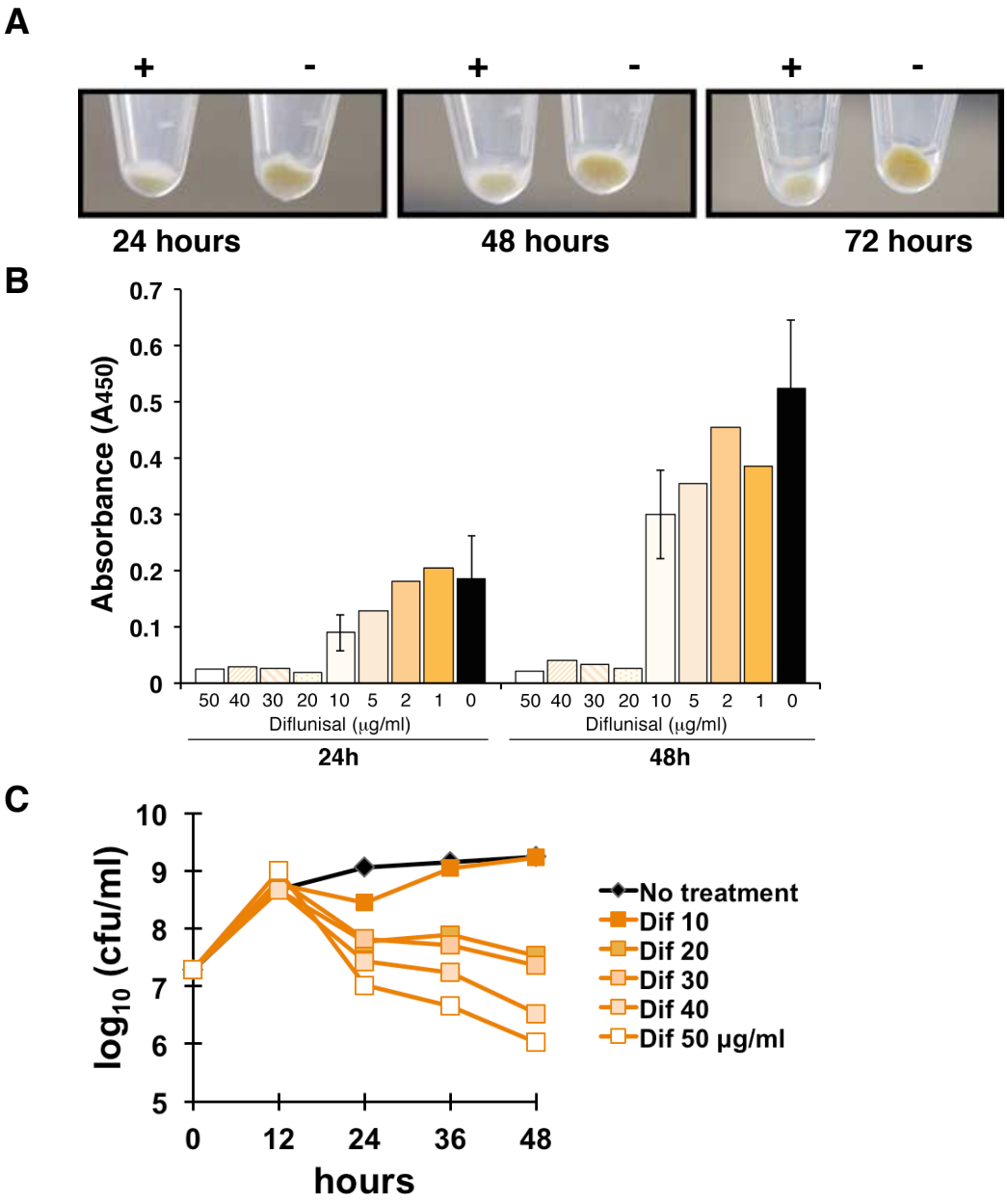

FIGURE 4.12. Diflunisal reduces pigment production in TCH1516. (A) Photographs of three different time points of treated (50 μg/ml) and non-treated USA300 cultures indicate lack of pigment in treated groups. **(B)** An array of decreasing diflunisal concentrations was analyzed for its effect on TCH1516 pigment production. A slight concentration-dependent effect is seen and the loss of pigment is drastic. **(C)** Quantitative cultures to assay for viable bacteria in each of the treatment groups at four different time points. The effect of autolysis is apparent.

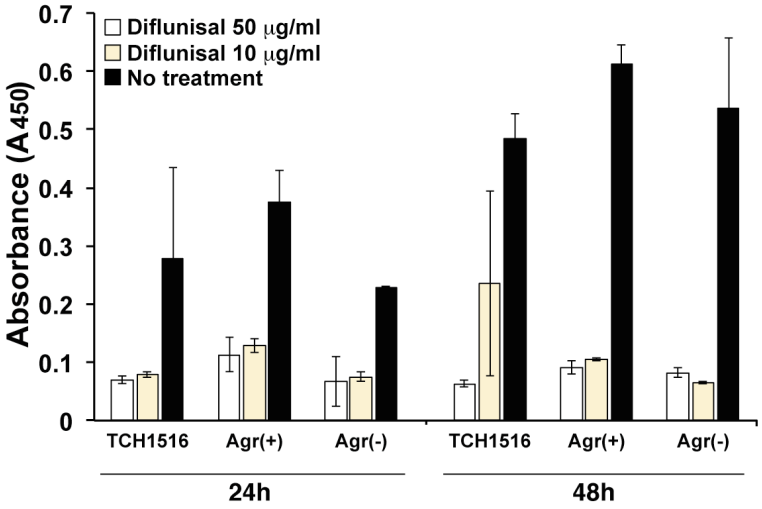

FIGURE 4.13. The effect of diflunisal on pigment production is agr-independent.

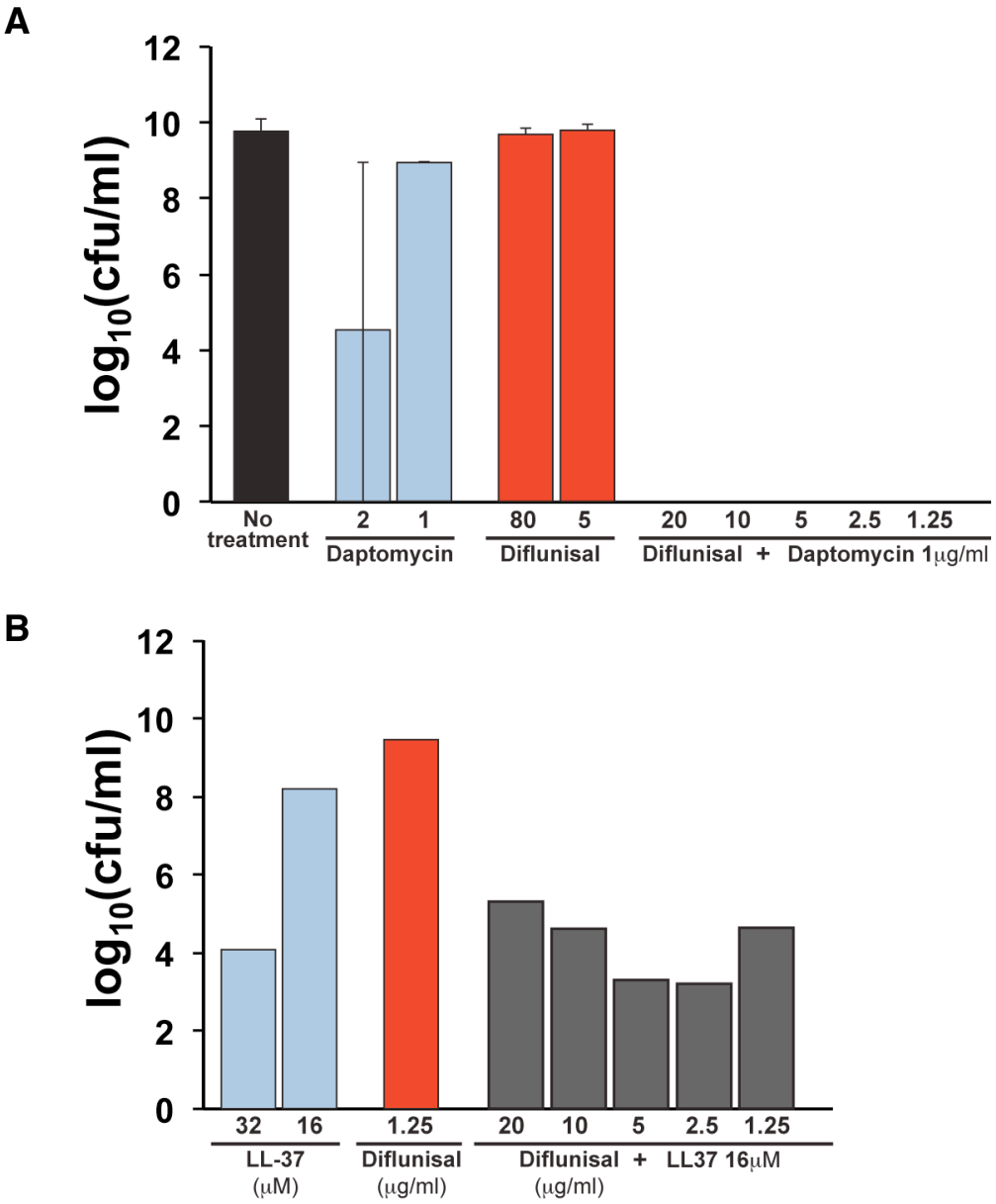

Figure 4.14. Diflunisal acts in synergy with daptomycin (A) and LL-37 (B). Quantitative cultures from checkerboard assays indicate significant reduction in viable bacteria when diflunisal is added to sub-concentrations of both antibiotics.

The MIC of daptomycin in this assay was 2 – 2.5 μg/ml and we observed no activity of daptomycin at 1 μg/ml. When diflunisal at any concentration above 1.25 μg/ml was added to daptomycin 1 μg/ml, no viable bacteria were recoveredlimit of detection (1.2 $\log_{10}$ cfu/ml) **(FIGURE 4.14A.)**.

Similarly, when diflunisal is added in the same way to sub-MIC (16 μM) LL-37, there is a subsequent multi-log reduction in viable bacteria **(FIGURE 4.14B.).** Synergistic effects are of major importance in the battle against drug-resistant pathogens. These finding warrants future *in vivo* studies to test combination therapies in a mouse model of infection.

In addition, future studies should include daptomycin-intermediate glycopeptide-resistant *S. aureus* to see if this effect can help overcuome resistance in these highly resistant strains. We are also extending our work the mouse cathelicidin antimicrobial peptide CRAMP, a homolog of human LL-37, to determine whether studies of sensitization to host innate immunity can be carried out in WT and CRAMP-deficient mouse infection models

4.3.3. Diflunisal appears to directly affect immune cells

4.3.3.1. Diflunisal induces neutrophil oxidative burst but not extracellular traps: To test whether diflunisal could directly influence influence aspects of the innate immune response important in host defense against MRSA, human neutrophils were assayed for oxidative burst following diflunisal treatment. Results from the Nitroblue Tetrazolium (NBT) assay indicate a small increase in oxidative burst in PMNs treated with 50 μg/ml, but not 10 μg/ml **(FIGURE 4.15A)**.

Increases in oxidative burst were still less than treatment with a postive control neutrophil activator, (phorbol myristate acetate), PMA.

Though diflunisal induced neutrophil oxidative burst, results of Picogreen spectrofluorometric assays indicate that it does not stimulate neutrophil extracellular traps **(FIGURE 4.15B.).** These results were confirmed in preliminary microscopy studies (data not shown).

4.3.3.2. Treatment with diflunisal is not toxic to neutrophils: A lactate dehydrogenase (LDH) assay was used to ensure the effect of oxidative burst was due to stimulation of NADPH-oxidase and not through toxicity to PMNs. Results of treated and non-treated PMNs show equal levels of LDH release over the course of a 3 h incubation. These results indicate that concentrations up to 50 μg/ml diflunisal are not toxic to neutrophils.

4.3.4. Summary of diflunisal as an inhibitor of AgrA and alpha-toxin production

Results of the above studies indicate that diflunisal is a potent inhibitor of α-toxin expression and production. Reduced expression of the toxin was confirmed in a variety of hemolysis assays and via immunoblots. Further *in* vivo studies are warranted to determine the potential benefits of diflunisal treatment in *S. aureus* infection. Other studies NSAIDs have provided mixed results, concluding their are both positive and negative implications when administered prior to or during the course of infections. However, there does not currently exist enough well controlled on this topic. It is clearly important to further probe whether diflunisal provides an advantage in the battle against *S. aureus* infection, since the application of an existing

approved medication for adjunctive therapy of difficult infections could follow an accelerated clinical evaluation pathway

During the course of these experiments, additional observations were made that suggests diflunisal may have additional desirable pharmacological effects on *S. aureus* beyond a-toxin inhibition. Diflunisal showed direct inhibitor effects on bacterial growth in later growth phases cultures from reaching the same densities as their untreated counterparts. Importantly, during late stationary phase, diflunisal-exposed *S. aureus* underwent an autolysis-like event where both turbidity and viable bacteria were drastically reduced compared to placebo control. Diflunisal-treated bacteria experienced drastic reductions in the staphyloxanthin pigment virulence factor in an *agr*-independent manner. Consequently, these bacteria were also more susceptible to killing when exposed to the pharmaceutical *S. aureus* therapeutic daptomycin or the endogenous host defense peptide LL-37.

From our *in silico* analysis, it is possible that diflunisal not only binds within the AgrA active site but also within the active site of other two-component systems (TCS) **(Table 5.1)** in *S. aureus.* The downstream effects of inhibiting each of these TCS is likely complex and wide-ranging. TCS are the predominant signal transduction system in prokaryotes, and bacterial genomes often encode for dozens of TCS (Rao G and Stock AM, 2009). Some of these TCS are specifically involved in activating antibiotic resistance genes or up regulating cell-wall components to increase the thickness of the cell wall and thus impede the activities of commonly used cell-wall antibiotics. Other TCS are involved in activating or inhibiting autolysis pathways, regulating proteases and metabolic pathways. It is conceivable that diflunisal may

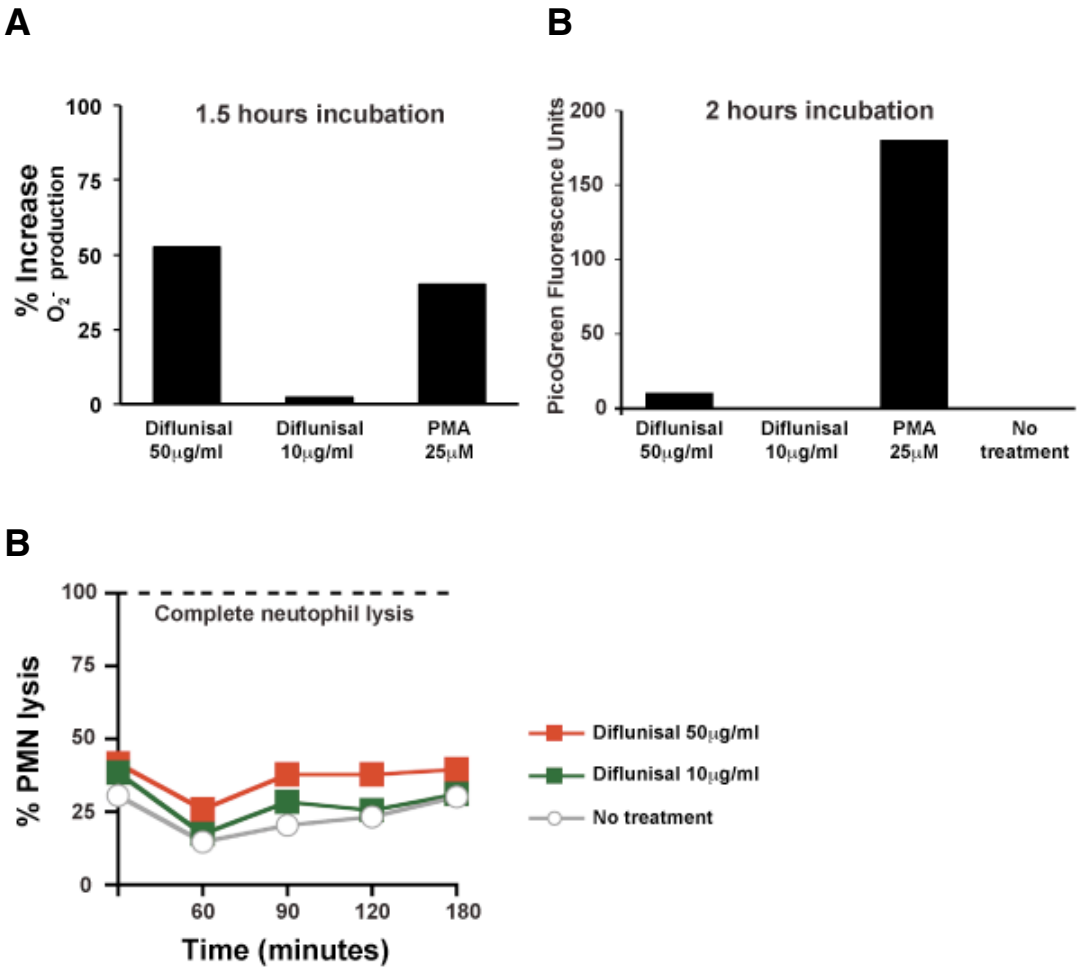

FIGURE 4.15. The effects of diflunisal on neutrophils. (A) Diflunisal increases oxidative burst in an NMT assay, **(B)** Diflunisal does not induce NETs and **(C)** difunisal does not induce neutrophil lysis.

bind within the active sites of multiple regulators and thus prevent transcription of several downstream genes involved in S. aureus adaptation to the human host and virulence. Preliminary results utilizing real-time PCR indicate that ClpB and ClpC, genes indicative of a *S. aureus* stress response, may be greatly up regulated in diflunisal-treated cultures. These results suggest a broader assessment of the effects of diflunisal on *S. aureus* can be pursued by techniques such as RNA-seq or microarray to allow a more global understanding of these affects.

4.4. MATERIALS & METHODS

4.4.1. Homology modeling of AgrA: Extensive BLAST (Altschul et al., 1990) *(http://blast.ncbi.nlm.nih.gov/Blast.cgi)* searches and protein analysis through UniProt *(http://www.uniprot.org/)* provided a list of related sequences and structural domains related to AgrA. The N-terminal 125 amino acids of AgrA were subjected to searches and then relatives were aligned in CLUSTALW (Larkin et al., 2007). The N-terminus of *Aquifex aeolicus* NtrC and AgrA shared 24% sequence homology. The available *A. aeolicus* NtrC structure, PDBID 1NY5, provided a useful template for homology modeling of AgrA. Homology modeling of the N-terminal 125 amino acids was done using the SWISS-MODEL / Swiss-PDBViewer (Guex and Peitsch, 1997). Following modeling, careful inspection and energy refinement was completed with the Crystallography and NMR System (CNS) (Brunger et al., 1998).

4.4.2. Virtual Screening of the NCI library for small-molecule inhibitors: Over 100,000 compounds from the National Cancer Institute Compound Library (NCI) and ZINC database (Irwin and Shoichet, 2005) were subjected to rigorous virtual screening using GLIDE, a Linux-based Schrödinger Suite program (Friesner et al., 2004; Friesner et al., 2006; Halgren et al., 2004). Thousands of compounds were screened daily through the most rigorous of methods. GLIDE uses a docking “funnel” to approximate the orientation, position and conformation of a potential ligand. Initial scores are further refined using the Monte Carlo sampling within GLIDE to determine the most probable ligands. Over 100 compounds resulted as hits from this screen. These were subjected to further analysis and refinement.

***4.4.3. Rabbit blood hemolysis*:** USA300 MRSA incubated with various concentrations (1, 10 or 50 μg/ml) of the most promising hits was then incubated with rabbit blood. Lysis of rabbit erythrocytes was measured through the release of hemoglobin using a spectrophotometer at an absorbance of 540nm.

4.4.4. Expression of toxin genes by qRT-PCR: The expression of *hla, phenol soluble modulin-alpha (psm-α), RNAIII* and other genes was measured using quantitative real time-PCR. Briefly, USA300 MRSA cultures were incubated for 6 h at 37 °C in the presence of 0, 10, or 50 μg/ml of the most promising hits. Following incubation, cultures were harvested, RNA was extracted (RiboPure bacterial RNA Isolation Kit (Ambion ®), and further purified via DNAse I treatment. The UV 260/ 280 ratio was evaluated to determine RNA yield. *hup*, a gene encoding for a histone-like protein, served as the housekeeping control. SYBR-green (BioRad®) served as the read-out reagent. Data were analyzed using the $\Delta\Delta C_t$ and are presented in graphical form as the $\log_2$ (treated sample/control (DMSO only) sample).

4.4.5. Western immunoblot analysis: Bacterial supernatants from 48 h cultures were collected after centrifugation at 3,200 x g for 10 min. Supernatants were filter sterilized and subsequently concentrated 20-fold using a Vacufuge (Eppendorf). Samples were mixed with 4X sample buffer and 10X reducing agent (Invitrogen), boiled for 10 min, loaded onto a 10% Bis-Tris gel (Invitrogen) and run in MOPS running buffer at 120V. The gel was then transferred onto a nitrocellulose membrane using a semi-dry apparatus (Bio-Rad) at 12V for 45 min. After transfer, the membrane was blocked for 1 h at RT in 0.05% PBS-Tween + 5% non-fat milk + 2% plasma (to

block protein A binding). The membrane was incubated overnight at 4˚C with anti-alpha hemolysin antibody conjugated to horseradish peroxidase (Abcam®) at a 1:1,000 dilution in PBS-Tween. The next day, the membrane was washed 3X with PBS-Tween and developed using chemiluminescence.

4.4.6. MRSA hemolysis on blood agar: To test the ability of diflunisal to inhibit hemolysis on blood agar, 10 ml cultures were prepared containing diflunisal, salicyclic acid or the vehicle control (0.1M NaHCO3 pH 8 + 25% ETOH) in THB. Briefly, 200 ul of overnight cultures of a virulent ST-59 MRSA or WR-69, an MSSA blood isolate that produces only alpha-toxin, were added to 10 ml of media with or without drug or vehicle in 15 ml round-bottom falcon tubes (BD®). Diflunisal or salicylic acid was added to each tube at 50, 40, 30, 20, 10, 5 or 0 μg/ml to test for the effect of various concentrations on hemolysis. Each culture contained the same volume of buffer control as both diflunisal and salicylic acid stocks were at 6.25 mg/ml in the same buffer. Tubes were incubated, at 37 °C in a shaking incubator for 24 hours. Subsequently, cultures were removed, mixed thoroughly, and 10 μl droplets were placed on sheep blood agar plates (5% Sheep Blood in Tryptic Soy Agar (TSA) (Hardy Diagnostics). The pre-incubated cultures were assayed for their ability to form zones of hemolysis on sheep blood agar after incubation at 37 °C for 18 – 24 h. Following incubation, photos of each plate were taken immediately to document the qualitative assessment of hemolysis.

4.4.7. In vivo lung infection: All animal experiments were approved by the

UC San Diego Institutional Animal Care and Use Committee. For a preliminary lung infection model, a protocol was designed based on lung infection models used by other groups (Liang et al., 2009). For this assay, 7-week-old C57BL/6J outbred mice (Charles River) were used and were . housed for a minimum of 3 days prior to the start of the experiment. Mice were pretreated for 3 days prior to bacterial infection with 7 intraperitoneal (i.p.) doses of diflunisal or an equal volume of vehicle control (0.1M $NaHCO_3$ pH 8 + 25% ETOH). Briefly, mice were anesthetized and then 0.625 mg/mouse/dose, or equal volume of placebo, was administered twice on Day 1 at two doses separated by 6 h, and subsequently every 12 h on Day 2, Day 3 and a final dose injected 6 h prior to bacterial infection on Day 4. An overnight culture of TCH1516 was used on Day 4 prepare a late log-phase (OD_{600} 0.7 -0.85) culture, which was washed, concentrated and adjusted to an OD_{600} 0.4. At OD_{600} 0.4, TCH1516 is roughly 10^8 colony forming units (cfu)/ml. Each mouse received a sub-lethal dose of 2 x 10^8 cfu, applied into the left naris in a 50 μl dose. Prior to infection, mice were anesthetized. For the infection, the concentrated TCH1516 suspension was slowly pipetted into the left naris of anesthetized mice so that they could inhale the suspension. Following infection, mice were held in supine posture to ensure that the suspension was completely inhaled and distributed equally within the lungs. Further observation immediately following inoculation was done to check for mice for recovery. One mouse died (treatment group) immediately after inoculation and was not included in the data analysis. Mice were observed 6 h post-inoculation for morbidity. For determination of bacterial load, the lungs were removed at 24 h after infection, weighed and homogenized in PBS for 2 x 1min using ziroconia beads

(1mm, Biospec) in a Mini-Beadbeater (BioSpec Products). Serial dilutions in sterile PBS were plated on THA for enumeration of viable bactera.

4.4.8. Targeted mutagenesis of hla: Precise, markerless allelic replacement of USA300 TCH1516 *hla* (Locus tag USA300HOU_1099, NC_010079.1 (1170314..1171273, complement)) was performed using PCR-based methods. A schematic is shown in **FIGURE 4.16A**. The sequence immediately upstream of *hla* was amplified with the primers **D and E (FIGURE 4.16B.)** and immediately downstream of *hla* with the primers **B and F (FIGURE 4.16B.)**. **Primers B and D** were constructed with ~25bp 5' overhangs for the opposite flanking region. The upstream and downstream PCR products were fused using **primers E and F** in a second round of PCR. These were then subcloned into the temperature-sensitive vector pKOR1 using BP clonase reaction (Invitrogen). The resulting plasmid pKOR1-*hla* was passaged through *S. aureus* RN4220. Purified plasmid was electroporated into strain TCH1516. Precise in-frame allelic replacement of *hla* was established by a two-step process of temperature shifting and antisense counterselection and confirmed by PCR. Complementation of the mutant strain was done using the pDC123 vector and **primers X and Y (FIGURE 4.16)**. Other listed primers **(FIGURE 4.16)** were used for PCR confirmations and for screening potential mutants and clones.

4.4.9. TCH1516 growth curves measuring optical density: Duplicate 10 ml cultures, prepared in large glass test tubes, were inoculated with 200 μl of

overnight TCH1516 USA300 bacteria in the presence of different concentrations of diflunisal (500, 250, 50, 10 or 0 μg/ml). Each tube contained the same amount of buffer solution (placebo) (0.1M $NaHCO_3$ pH 8 + 25% ETOH). Cultures were mixed well and incubated, shaking at 37 °C. The optical densities (OD) at an absorbance of 600 nm were measured using a spectrophotometer every half hour for six hours. Following these measurements, the optical density was measured every 24 hours for five days. Averages were assessed and plotted according to time.

4.4.10. Quantification of pigment production: All cultures were treated with the same concentration of placebo buffer (0.1M $NaHCO_3$ pH8 + 25% ETOH). Bacterial cultures were incubated at 37 °C with shaking for set time points. At 12, 24, 36 and 48 hours of incubation, 5 ml of culture was removed and quantified using methanol extraction. For multiple assays, quantitative samples were removed from each culture at time points. The data allowed for comparison between the number of viable bacteria within a culture and the amount of pigment extracted from the 5 ml sample. For methanol extraction of pigment, 5 ml of each bacterial culture was pelleted at 4,000 rpm x 10 m. Supernatant was removed and resuspended in 1ml of PBS and transferred to a sterile eppendorf tube. Bacteria were pelleted at 10,000 rpm x 10 m and the resulting supernatant was carefully aspirated. 100% methanol (0.5 ml) was added to each washed pellet, which was then placed in a 42 °C water bath for 1h. Tubes were mixed periodically during incubation. After 1 h, resulting mixtures were pelleted at 10,000 x 10 m. The supernatant was assayed for pigment by spectrophotometric reading at an absorbance of 450 nm.

A

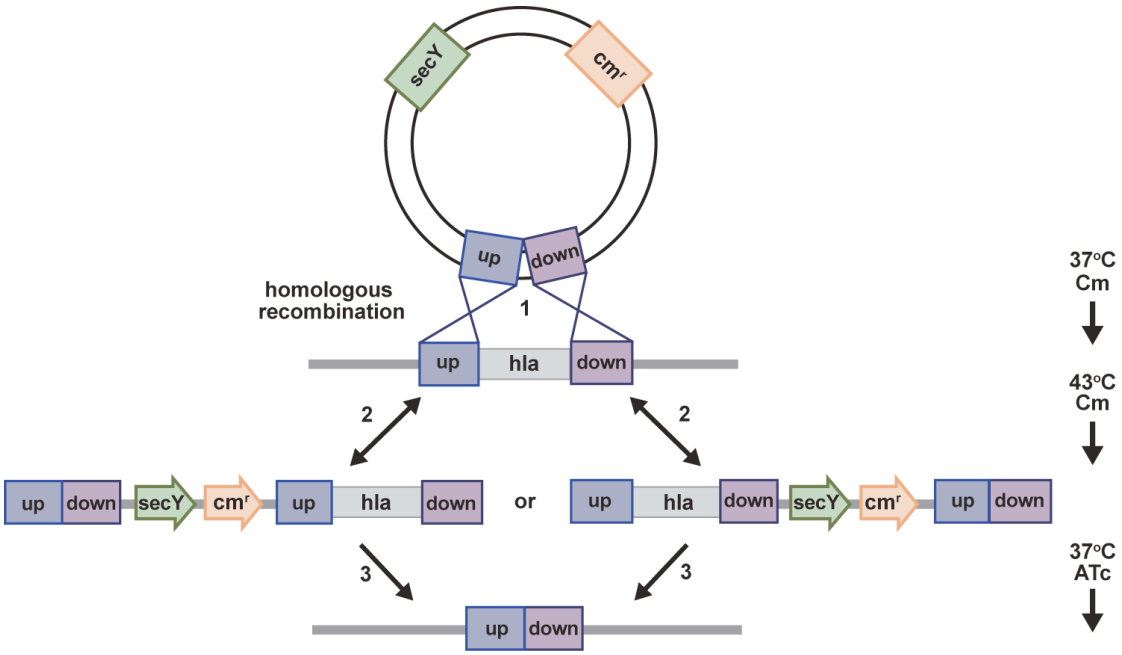

B

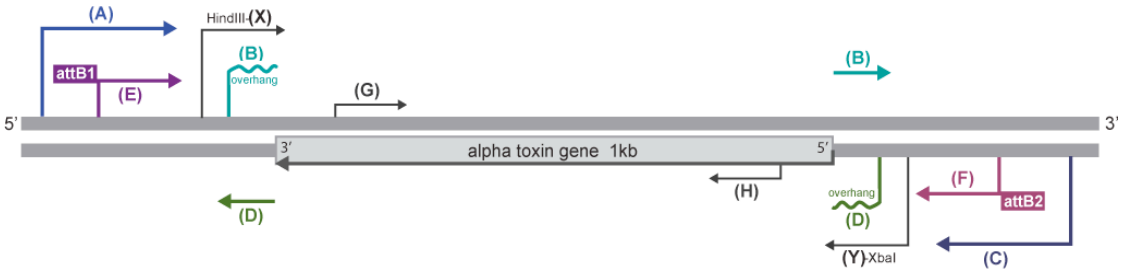

Primers

A	UpConstructUp	5'-gatgaagaagtccatacaaaatccgcatcatttg-3'
B	DownConstructUp	5'-catgaacaaataatttacatttcatcatccttctatttttttaaaac-3'
C	DownConstructDwn	5'-catgggcattttcattcggtcaactactaccaatataatattgtagagcctaag-3'
D	UpConstructDown	5'-aatagaaggatgatgaaatgtaaattatttgttcatgtca-3'
E	attB1 + Up	5'-GGGGACAAGTTTGTACAAAAAAGCAGGCTgaaattaatcatgcatg-3'
F	Down + attB2	5'-GGGGACCACTTTGTACAAGAAAGCTGGGTtattccttcatttaatg-3'
G	Confirm F	5'-ccaatttgttgaagtccagtgcaattgg-3'
H	Confirm R	5'-cctgtcgtcaatgccgcagattct-3'
X	HLYcut-3'/HindIII:	5'-gcgaagcttgtcaggaaagcaaatcaagtacat-3'
Y	HLYcut-5'/Xba1:	5'-gcgtctagaatgaaaacacgtatagtcagctca-'3'

Figure 4.16. Alpha-toxin deletion mutant. Primer location and design of the *hla* mutant.

4.4.11. Diflunisal synergy with daptomycin and LL-37: Diflunisal was tested in combination with daptomycin (Cubist) and the antimicrobial peptide LL-37. Checkerboard assays were prepared on 96-well round bottom polystyrene plates. Cation-adjusted Mueller Hinton Broth (CA-MHB) was used as the assay media for daptomycin containing assays. LL-37 assays were completed in RPMI + 5% LB. Compounds were serially diluted in combination and alone on the plate for accurate comparison with the MICs of compounds alone. TCH1516 bacteria were added to the plate in log phase (OD 0.4) at a concentration of 5×10^5 cfu/ml. Plates were covered in parafilm and incubated with shaking at 37 °C overnight. At 18 – 24 hours, aliquots were removed from the checkerboard plates for analysis of viable bacteria in the placebo control, diflunisal alone, antibiotic alone, diflunisal + antibiotic treated cultures. The optical density of each plate was determined via a microplate-reader spectrophotometer. Aliquots were diluted in PBS for serial dilutions on Todd Hewitt Agar (THA). Plates were incubated at 37 °C overnight and colonies were enumerated the next day.

4.4.12. Induction of neutrophil oxidative burst by diflunisal: The ability of diflunisal to cause neutrophil oxidative burst was assessed using a Nitroblue Tetrazolium (NBT) assay, similar to that previously described (Choi et al., 2006). The tetrazolium salt is metabolically reduced to formazans. Powder NBT (Sigma) was measured immediately before use in the assay by resuspending the powder in 1X DPBS to 2 mg/ml. Human neutrophils were isolated from healthy donors by using the PolymorphPrep system (Axis-Shield). The neutrophils were resuspended in HBSS

(with Ca^{2+} and Mg^{2+}) and plated in 96-well tissue-culture treated plates at a concentration of 5 x 10^6 PMN / well. 25 nM of phorbol 12-myristate 13-acetate (PMA) or diflunisal at 50 or 10 μg/ml were added to a final volume of 0.2 ml. Plates were covered in foil to protect from light, and incubated in a shaking incubator at 37 °C for 1.5 h. Following incubation, precipitate was noted on the bottom of the wells. Plats were spun at 1800 rpm x 5 min and media was removed from the wells. PMNs were washed with 0.1 ml of 1X PBS, spun at 1800rpm x 5 min. Following the wash, 0.04 ml of methanol was added to each well and allowed to evaporate. Upon evaporation 0.12 ml of 2 M Potassium hydroxide (KOH) was added to each well followed by 0.13 ml of DMSO. The mixture incubated at room temperature for 10 min and then the release of free radical oxygen was measured on a SoftMax Pro microplate spectrophotometer at 620 nm.

4.4.13. Neutrophil extracellular trap (NET) quantification: Neutrophils were prepared as described above. The NET quantification assay was based off (von Köckritz-Blickwede et al., 2010). Cells were seeded in RPMI (without phenol red (Mediatech #17105-CV) at 2 x 10^5 PMNs / well in a 96 –well tissue culture plate (BD Bioscience #35072). A set of PMNs were stimulated with 25 nM of phorbol 12-myristate 13-acetate (PMA), an ET inducer that served as a positive control. Placebo buffer (0.1M $NaHCO_3$ pH 8 + 25% ETOH) was added to otherwise untreated PMNs and served as the background control. Diflunisal was added to PMNs at 50 or 10 μg/ml to PMNs in test wells. Cells were incubated at 37 °C in 5% CO_2 for 2 h. Following incubation 500 mU/ml of micrococcal nuclease (Worthington #NFCP) was

added to each well in a volume of 0.05 ml and incubated for 10 m at 37 °C. To stop the reaction, 5 mM of 0.33M EDTA (pH 8) was added to each well. The assay plate was centrifuged at 1800 rpm x 8 min, after which the supernatant (0.1 ml / well) was transferred to fresh 96-well flat bottom plates (BD Bioscience). The Quant- iT Picogreen (Invitrogen, #P11496) assay was used to quantify the amount of extracellular DNA. First, fresh Picogreen was diluted 1:200 in TE buffer and 0.1 ml were added to the 0.1 ml of supernatant in each well. The mixture was incubated for 2 – 5 m in the dark and immediately spectrofluorometrically measured with an excitation wavelength of 480 nm and emission at 520 nm.

4.4.14. Measuring neutrophil toxicity using lactate-dehydrogenase release assay: To measure the effect of diflunisal on the neutrophils, the CytoTox 96® Non-Radioactive Cytotoxicity Assay (Product G1780) Promega® (www.promega.com) was used. The cell-mediated cytotoxicity assay was set up in a 96-well tissue-culture treated plate. Effector cells (neutrophils) were added at $2x10^6$ PMN/ml in a volume of 0.1 ml per well (10^5 PMN/well). Diflunisal was first diluted to 100 μg/ml in HBSS (with $Ca^{2+}$and Mg^{2+}) from a 25 mg/ml stock in 100% ethanol. The effect of diflunisal on PMN lysis was tested at 4 different concentrations (50, 10, 1 and 0 μg/ml prepared from the 100 μg/ml stock). PMNs and diflunisal or vehicle (for 0 μg/ml treatments) were added in HBSS (with $Ca^{2+}$and Mg^{2+}) buffer. All conditions were prepared in duplicate, including a 100% PMN lysis positive control. Wells were prepared for each set of time points at 0, 60, 90, 120, 180 min incubation. A blank well containing culture media served as a background control. The assay plate was

incubated at 37 °C and 5% CO_2 . At each time point, 5 μl of 0.25% Triton-X100, prepared in 1X PBS was added to the two 100% lysis controls, and cells were lysed vigorously for 30 seconds by pipetting. Following lysis, 30 μl of media from each assay condition was pipetted into a flat bottom 96-well plate, 30 μl of freshly resuspended LDH reagent was added to each well. Plates were incubated in the dark for 20 minutes at 37 °C and subsequently read at an absorbance of 490nm.

4.5. ACKNOWLDEGEMENTS

Menachem Shoham, PhD from Case Western University, Ohio contributed initial insight in the project. M.S. and colleagues determined AgrA to be a valid therapeutic target and subsequently modeled the structure based off NtrC. M.S and colleagues used the homology model to screen for inhibitors. M.S. and colleagues did initial RT-PCR and hemolysis studies. N.M.H. designed and conducted and analyzed the remainder of the cited experiments with the help of Mary Hensler, PhD (pigment quantification), Morgan Pence (immunoblot), Cheryl Okumura, PhD (*in vivo* pneumonia model), Josh Olson (pneumonia model), Jason Cole, PhD (multiple *in vivo* studies and contributed to design of animal experiments), Kathryn Akong MD/PhD (critiques and suggestions for neutrophil assays) and David Gonzalez, PhD (imaging-mass spectrometry analyses). Mary Hensler and Wdee Thienphrapa will continue future work on much of this project. N.M.H wrote this chapter. M. Hensler and V. Nizet provided invaluable input and insight into this work. Permission from M.S. was obtained to include key data and insight in this chapter.

4.6. REFERENCES

Akhter, T., Baqai, R., and Aziz, M. (2010). Antibacterial effect of NSAIDS on clinical isolates of urinary tract infection and diabetic foot infection. Pak J Pharm Sci *23*, 108-113.

Altschul, S.F., Gish, W., Miller, W., Myers, E.W., and Lipman, D.J. (1990). Basic local alignment search tool. J Mol Biol *215*, 403-410.

Alvarez, L.P., Barbagelata, M.S., Cheung, A.L., Sordelli, D.O., and Buzzola, F.R. (2011). Salicylic acid enhances Staphylococcus aureus extracellular adhesin protein expression. Microbes Infect *13*, 1073-1080.

Alvarez, L.P., Barbagelata, M.S., Gordiola, M., Cheung, A.L., Sordelli, D.O., and Buzzola, F.R. (2010). Salicylic acid diminishes Staphylococcus aureus capsular polysaccharide type 5 expression. Infect Immun *78*, 1339-1344.

Aronoff, D.M., and Bloch, K.C. (2003). Assessing the relationship between the use of nonsteroidal antiinflammatory drugs and necrotizing fasciitis caused by group A streptococcus. Medicine (Baltimore) *82*, 225-235.

Balzan, R., Sapienza, K., Galea, D.R., Vassallo, N., Frey, H., and Bannister, W.H. (2004). Aspirin commits yeast cells to apoptosis depending on carbon source. Microbiology *150*, 109-115.

Bandara, M.B., Zhu, H., Sankaridurg, P.R., and Willcox, M.D. (2006). Salicylic acid reduces the production of several potential virulence factors of Pseudomonas aeruginosa associated with microbial keratitis. Invest Ophthalmol Vis Sci *47*, 4453-4460.

Bantel, H., Sinha, B., Domschke, W., Peters, G., Schulze-Osthoff, K., and Janicke, R.U. (2001). alpha-Toxin is a mediator of Staphylococcus aureus-induced cell death and activates caspases via the intrinsic death pathway independently of death receptor signaling. J Cell Biol *155*, 637-648.

Bartlett, A.H., Foster, T.J., Hayashida, A., and Park, P.W. (2008). Alpha-toxin facilitates the generation of CXC chemokine gradients and stimulates neutrophil homing in Staphylococcus aureus pneumonia. J Infect Dis *198*, 1529-1535.

Blickwede, M. (2004). Florfenicol-dependent modulation of staphylococcal virulence properties (Hannover, Institut fur Tierzucht, Bundesforschungsanstalt fur Landwirtschaft, Neudstadt-Mariensee, Germany and Institut fur Mikrobiologie, Zentrum fur Infektionsmedizin, Tierarztliche Hochschule Hannover, Germany), pp. 119.

Boyle-Vavra, S., Yin, S., and Daum, R.S. (2006). The VraS/VraR two-component regulatory system required for oxacillin resistance in community-acquired methicillin-resistant Staphylococcus aureus. FEMS Microbiol Lett *262*, 163-171.

Brunger, A.T., Adams, P.D., Clore, G.M., DeLano, W.L., Gros, P., Grosse-Kunstleve, R.W., Jiang, J.S., Kuszewski, J., Nilges, M., Pannu, N.S., *et al.* (1998). Crystallography & NMR system: A new software suite for macromolecular structure determination. Acta Crystallogr D Biol Crystallogr *54*, 905-921.

Brunskill, E.W., and Bayles, K.W. (1996). Identification and molecular characterization of a putative regulatory locus that affects autolysis in Staphylococcus aureus. J Bacteriol *178*, 611-618.

Bubeck Wardenburg, J., Bae, T., Otto, M., Deleo, F.R., and Schneewind, O. (2007a). Poring over pores: alpha-hemolysin and Panton-Valentine leukocidin in Staphylococcus aureus pneumonia. Nat Med *13*, 1405-1406.

Bubeck Wardenburg, J., Patel, R.J., and Schneewind, O. (2007b). Surface proteins and exotoxins are required for the pathogenesis of Staphylococcus aureus pneumonia. Infect Immun *75*, 1040-1044.

Bubeck Wardenburg, J., and Schneewind, O. (2008). Vaccine protection against Staphylococcus aureus pneumonia. J Exp Med *205*, 287-294.

Burian, M., Wolz, C., and Goerke, C. (2010). Regulatory adaptation of Staphylococcus aureus during nasal colonization of humans. PLoS One *5*, e10040.

Choi, H.S., Kim, J.W., Cha, Y.N., and Kim, C. (2006). A quantitative nitroblue tetrazolium assay for determining intracellular superoxide anion production in phagocytic cells. J Immunoassay Immunochem *27*, 31-44.

Cookson, B. (2011). Five decades of MRSA: controversy and uncertainty continues. Lancet *378*, 1291-1292.

Crabtree, J.A., and Litterer, W. (1934). Outbreak of Milk Poisoning Due to a Toxin-Producing Staphylococcus Found in the Udders of Two Cows. Am J Public Health Nations Health *24*, 1116-1122.

Crowther, J.R. (2000). The ELISA guidebook. Methods Mol Biol *149*, III-IV, 1-413.

Delaune, A., Poupel, O., Mallet, A., Coic, Y.M., Msadek, T., and Dubrac, S. (2011). Peptidoglycan crosslinking relaxation plays an important role in Staphylococcus aureus WalKR-dependent cell viability. PLoS One *6*, e17054.

Diep, B.A., and Otto, M. (2008). The role of virulence determinants in community-associated MRSA pathogenesis. Trends Microbiol *16*, 361-369.

Dubrac, S., Boneca, I.G., Poupel, O., and Msadek, T. (2007). New insights into the WalK/WalR (YycG/YycF) essential signal transduction pathway reveal a major role in controlling cell wall metabolism and biofilm formation in Staphylococcus aureus. J Bacteriol *189*, 8257-8269.

Duy, N.V., Mader, U., Tran, N.P., Cavin, J.F., Tam le, T., Albrecht, D., Hecker, M., and Antelmann, H. (2007). The proteome and transcriptome analysis of Bacillus subtilis in response to salicylic acid. Proteomics *7*, 698-710.

Fournier, B., and Klier, A. (2003). Response to the criticisms of Richard P. Novick in his review 'Autoinduction and signal transduction in the regulation of staphylococcal virulence' (Novick, 2003, Mol Microbiol 48: 1429-1449). Mol Microbiol *50*, 1085-1086.

Friesner, R.A., Banks, J.L., Murphy, R.B., Halgren, T.A., Klicic, J.J., Mainz, D.T., Repasky, M.P., Knoll, E.H., Shelley, M., Perry, J.K.*, et al.* (2004). Glide: a new approach for rapid, accurate docking and scoring. 1. Method and assessment of docking accuracy. J Med Chem *47*, 1739-1749.

Friesner, R.A., Murphy, R.B., Repasky, M.P., Frye, L.L., Greenwood, J.R., Halgren, T.A., Sanschagrin, P.C., and Mainz, D.T. (2006). Extra precision glide: docking and scoring incorporating a model of hydrophobic enclosure for protein-ligand complexes. J Med Chem *49*, 6177-6196.

Galbusera, E., Renzoni, A., Andrey, D.O., Monod, A., Barras, C., Tortora, P., Polissi, A., and Kelley, W.L. (2011). Site-specific mutation of Staphylococcus aureus VraS reveals a crucial role for the VraR-VraS sensor in the emergence of glycopeptide resistance. Antimicrob Agents Chemother *55*, 1008-1020.

Gao, R., and Stock, A.M. (2009). Biological insights from structures of two-component proteins. Annu Rev Microbiol *63*, 133-154.

Guex, N., and Peitsch, M.C. (1997). SWISS-MODEL and the Swiss-PdbViewer: an environment for comparative protein modeling. Electrophoresis *18*, 2714-2723.

Halgren, T.A., Murphy, R.B., Friesner, R.A., Beard, H.S., Frye, L.L., Pollard, W.T., and Banks, J.L. (2004). Glide: a new approach for rapid, accurate docking and scoring. 2. Enrichment factors in database screening. J Med Chem *47*, 1750-1759.

Herrmann, M. (2003). Salicylic acid: an old dog, new tricks, and staphylococcal disease. J Clin Invest *112*, 149-151.

Howden, B.P., Davies, J.K., Johnson, P.D., Stinear, T.P., and Grayson, M.L. (2010). Reduced vancomycin susceptibility in Staphylococcus aureus, including vancomycin-intermediate and heterogeneous vancomycin-intermediate strains: resistance mechanisms, laboratory detection, and clinical implications. Clin Microbiol Rev *23*, 99-139.

Inoshima, I., Inoshima, N., Wilke, G.A., Powers, M.E., Frank, K.M., Wang, Y., and Bubeck Wardenburg, J. (2011). A Staphylococcus aureus pore-forming toxin subverts the activity of ADAM10 to cause lethal infection in mice. Nat Med *17*, 1310-1314.

Irwin, J.J., and Shoichet, B.K. (2005). ZINC--a free database of commercially available compounds for virtual screening. J Chem Inf Model *45*, 177-182.

Kennedy, A.D., Bubeck Wardenburg, J., Gardner, D.J., Long, D., Whitney, A.R., Braughton, K.R., Schneewind, O., and DeLeo, F.R. (2010). Targeting of alpha-hemolysin by active or passive immunization decreases severity of USA300 skin infection in a mouse model. J Infect Dis *202*, 1050-1058.

Kobayashi, S.D., and DeLeo, F.R. (2009). An update on community-associated MRSA virulence. Curr Opin Pharmacol *9*, 545-551.

Kong, K.F., Vuong, C., and Otto, M. (2006). Staphylococcus quorum sensing in biofilm formation and infection. Int J Med Microbiol *296*, 133-139.

Kupferwasser, L.I., Yeaman, M.R., Nast, C.C., Kupferwasser, D., Xiong, Y.Q., Palma, M., Cheung, A.L., and Bayer, A.S. (2003). Salicylic acid attenuates virulence in endovascular infections by targeting global regulatory pathways in Staphylococcus aureus. J Clin Invest *112*, 222-233.

Larkin, M.A., Blackshields, G., Brown, N.P., Chenna, R., McGettigan, P.A., McWilliam, H., Valentin, F., Wallace, I.M., Wilm, A., Lopez, R.*, et al.* (2007). Clustal W and Clustal X version 2.0. Bioinformatics *23*, 2947-2948.

Leng, B.F., Qiu, J.Z., Dai, X.H., Dong, J., Wang, J.F., Luo, M.J., Li, H.E., Niu, X.D., Zhang, Y., Ai, Y.X.*, et al.* (2011). Allicin reduces the production of alpha-toxin by Staphylococcus aureus. Molecules *16*, 7958-7968.

Leroy, S., Marc, E., Bavoux, F., Treluyer, J.M., Gendrel, D., Breart, G., Pons, G., and Chalumeau, M. (2010). Hospitalization for severe bacterial infections in children after exposure to NSAIDs: a prospective adverse drug reaction reporting study. Clin Drug Investig *30*, 179-185.

Li, M., Diep, B.A., Villaruz, A.E., Braughton, K.R., Jiang, X., DeLeo, F.R., Chambers, H.F., Lu, Y., and Otto, M. (2009). Evolution of virulence in epidemic community-associated methicillin-resistant Staphylococcus aureus. Proc Natl Acad Sci U S A *106*, 5883-5888.

Liang, X., Hall, J.W., Yang, J., Yan, M., Doll, K., Bey, R., and Ji, Y. (2011). Identification of single nucleotide polymorphisms associated with hyperproduction of alpha-toxin in Staphylococcus aureus. PLoS One *6*, e18428.

Liang, X., and Ji, Y. (2007). Involvement of alpha5beta1-integrin and TNF-alpha in Staphylococcus aureus alpha-toxin-induced death of epithelial cells. Cell Microbiol *9*, 1809-1821.

Liang, X., Yan, M., and Ji, Y. (2009). The H35A mutated alpha-toxin interferes with cytotoxicity of staphylococcal alpha-toxin. Infect Immun *77*, 977-983.

Liu, G.Y., Essex, A., Buchanan, J.T., Datta, V., Hoffman, H.M., Bastian, J.F., Fierer, J., and Nizet, V. (2005). Staphylococcus aureus golden pigment impairs neutrophil killing and promotes virulence through its antioxidant activity. J Exp Med *202*, 209-215.

Martin, P.K., Li, T., Sun, D., Biek, D.P., and Schmid, M.B. (1999). Role in cell permeability of an essential two-component system in Staphylococcus aureus. J Bacteriol *181*, 3666-3673.

McCaig, L.F., McDonald, L.C., Mandal, S., and Jernigan, D.B. (2006). Staphylococcus aureus-associated skin and soft tissue infections in ambulatory care. Emerg Infect Dis *12*, 1715-1723.

Moellering, R.C., Jr. (2011). MRSA: the first half century. J Antimicrob Chemother.

Neoh, H.M., Cui, L., Yuzawa, H., Takeuchi, F., Matsuo, M., and Hiramatsu, K. (2008). Mutated response regulator graR is responsible for phenotypic conversion of Staphylococcus aureus from heterogeneous vancomycin-intermediate resistance to vancomycin-intermediate resistance. Antimicrob Agents Chemother *52*, 45-53.

Niebuhr, M., Gathmann, M., Scharonow, H., Mamerow, D., Mommert, S., Balaji, H., and Werfel, T. (2011). Staphylococcal alpha-toxin is a strong inducer of interleukin-17 in humans. Infect Immun *79*, 1615-1622.

Nizet, V. (2006). Antimicrobial peptide resistance mechanisms of human bacterial pathogens. Curr Issues Mol Biol *8*, 11-26.

Nizet, V. (2007). Understanding how leading bacterial pathogens subvert innate immunity to reveal novel therapeutic targets. J Allergy Clin Immunol *120*, 13-22.

Novick, R.P. (2003). Autoinduction and signal transduction in the regulation of staphylococcal virulence. Mol Microbiol *48*, 1429-1449.

Novick, R.P., and Muir, T.W. (1999). Virulence gene regulation by peptides in staphylococci and other Gram-positive bacteria. Curr Opin Microbiol *2*, 40-45.

Otto, M. (2010). Looking toward basic science for potential drug discovery targets against community-associated MRSA. Med Res Rev *30*, 1-22.

Palma, M., Bayer, A., Kupferwasser, L.I., Joska, T., Yeaman, M.R., and Cheung, A. (2006). Salicylic acid activates sigma factor B by rsbU-dependent and -independent mechanisms. J Bacteriol *188*, 5896-5903.

Parker, J.T. (1924). The Production of an Exotoxin by Certain Strains of Staphylococcus Aureus. J Exp Med *40*, 761-772.

Postma, B., Poppelier, M.J., van Galen, J.C., Prossnitz, E.R., van Strijp, J.A., de Haas, C.J., and van Kessel, K.P. (2004). Chemotaxis inhibitory protein of Staphylococcus aureus binds specifically to the C5a and formylated peptide receptor. J Immunol *172*, 6994-7001.

Prithiviraj, B., Bais, H.P., Weir, T., Suresh, B., Najarro, E.H., Dayakar, B.V., Schweizer, H.P., and Vivanco, J.M. (2005). Down regulation of virulence factors of Pseudomonas aeruginosa by salicylic acid attenuates its virulence on Arabidopsis thaliana and Caenorhabditis elegans. Infect Immun *73*, 5319-5328.

Qiu, J., Feng, H., Lu, J., Xiang, H., Wang, D., Dong, J., Wang, J., Wang, X., Liu, J., and Deng, X. (2010). Eugenol reduces the expression of virulence-related exoproteins in Staphylococcus aureus. Appl Environ Microbiol *76*, 5846-5851.

Qiu, J., Xiang, H., Hu, C., Wang, Q., Dong, J., Li, H., Luo, M., Wang, J., and Deng, X. (2011). Subinhibitory concentrations of farrerol reduce alpha-toxin expression in Staphylococcus aureus. FEMS Microbiol Lett *315*, 129-133.

Ragle, B.E., and Bubeck Wardenburg, J. (2009). Anti-alpha-hemolysin monoclonal antibodies mediate protection against Staphylococcus aureus pneumonia. Infect Immun *77*, 2712-2718.

Ragle, B.E., Karginov, V.A., and Bubeck Wardenburg, J. (2010). Prevention and treatment of Staphylococcus aureus pneumonia with a beta-cyclodextrin derivative. Antimicrob Agents Chemother *54*, 298-304.

Sedlacek, M., Gemery, J.M., Cheung, A.L., Bayer, A.S., and Remillard, B.D. (2007). Aspirin treatment is associated with a significantly decreased risk of Staphylococcus aureus bacteremia in hemodialysis patients with tunneled catheters. Am J Kidney Dis *49*, 401-408.

Sidote, D.J., Barbieri, C.M., Wu, T., and Stock, A.M. (2008). Structure of the Staphylococcus aureus AgrA LytTR domain bound to DNA reveals a beta fold with an unusual mode of binding. Structure *16*, 727-735.

Smith, H. (1977). Microbial surfaces in relation to pathogenicity. Bacteriol Rev *41*, 475-500.

Somerville, G.A., and Proctor, R.A. (2009). At the crossroads of bacterial metabolism and virulence factor synthesis in Staphylococci. Microbiol Mol Biol Rev *73*, 233-248.

Sparling, P.F. (1983). Bacterial virulence and pathogenesis: an overview. Rev Infect Dis *5 Suppl 4*, S637-646.

Stauff, D.L., Torres, V.J., and Skaar, E.P. (2007). Signaling and DNA-binding activities of the Staphylococcus aureus HssR-HssS two-component system required for heme sensing. J Biol Chem *282*, 26111-26121.

Sugarman, B. (1980). Attachment of bacteria to mammalian surfaces. Infection *8*, 132-141.

Takano, T., Higuchi, W., Otsuka, T., Baranovich, T., Enany, S., Saito, K., Isobe, H., Dohmae, S., Ozaki, K., Takano, M*., et al.* (2008). Novel characteristics of community-acquired methicillin-resistant Staphylococcus aureus strains belonging to multilocus sequence type 59 in Taiwan. Antimicrob Agents Chemother *52*, 837-845.

Talbot, G.H., Bradley, J., Edwards, J.E., Jr., Gilbert, D., Scheld, M., and Bartlett, J.G. (2006). Bad bugs need drugs: an update on the development pipeline from the Antimicrobial Availability Task Force of the Infectious Diseases Society of America. Clin Infect Dis *42*, 657-668.

Udo, E.E., Pearman, J.W., and Grubb, W.B. (1993). Genetic analysis of community isolates of methicillin-resistant Staphylococcus aureus in Western Australia. J Hosp Infect *25*, 97-108.

Ulrich, M., Bastian, M., Cramton, S.E., Ziegler, K., Pragman, A.A., Bragonzi, A., Memmi, G., Wolz, C., Schlievert, P.M., Cheung, A.*, et al.* (2007). The staphylococcal respiratory response regulator SrrAB induces ica gene transcription and polysaccharide intercellular adhesin expression, protecting Staphylococcus aureus from neutrophil killing under anaerobic growth conditions. Mol Microbiol *65*, 1276-1287.

von Eiff, C., Becker, K., Machka, K., Stammer, H., and Peters, G. (2001). Nasal carriage as a source of Staphylococcus aureus bacteremia. Study Group. N Engl J Med *344*, 11-16.

von Köckritz-Blickwede, M., Chow, O.C., Ghochani, M., and Nizet, V. (2010). Visualization and Functional Evaluation of Phagocyte Extracellular Traps. In Methods in Microbiology: Immunology of Infection, D. Kabelitz, and S.H.E. Kaufmann, eds., pp. 139- 160.

Voyich, J.M., Vuong, C., DeWald, M., Nygaard, T.K., Kocianova, S., Griffith, S., Jones, J., Iverson, C., Sturdevant, D.E., Braughton, K.R.*, et al.* (2009). The SaeR/S gene regulatory system is essential for innate immune evasion by Staphylococcus aureus. J Infect Dis *199*, 1698-1706.

Ward, P.A., and Kunkel, S.L. (1983). Bacterial virulence and the inflammatory system. Rev Infect Dis *5 Suppl 4*, S793-796.

Weld, J.T., and Gunther, A. (1931). Differentiation between Certain Toxic Properties of Filtrates of Hemolytic Staphylococcus Aureus. J Exp Med *54*, 315-322.

Weng, T.C., Chen, C.C., Toh, H.S., and Tang, H.J. (2011). Ibuprofen worsens Streptococcus pyogenes soft tissue infections in mice. J Microbiol Immunol Infect.

Wertheim, H.F., Vos, M.C., Ott, A., van Belkum, A., Voss, A., Kluytmans, J.A., van Keulen, P.H., Vandenbroucke-Grauls, C.M., Meester, M.H., and Verbrugh, H.A. (2004). Risk and outcome of nosocomial Staphylococcus aureus bacteraemia in nasal carriers versus non-carriers. Lancet *364*, 703-705.

Wilke, G.A., and Bubeck Wardenburg, J. (2010). Role of a disintegrin and metalloprotease 10 in Staphylococcus aureus alpha-hemolysin-mediated cellular injury. Proc Natl Acad Sci U S A *107*, 13473-13478.

Xiang, H., Qiu, J.Z., Wang, D.C., Jiang, Y.S., Xia, L.J., and Deng, X.M. (2010). Influence of magnolol on the secretion of alpha-toxin by Staphylococcus aureus. Molecules *15*, 1679-1689.

Xue, T., You, Y., Hong, D., Sun, H., and Sun, B. (2011). The Staphylococcus aureus KdpDE two-component system couples extracellular K+ sensing and Agr signaling to infection programming. Infect Immun *79*, 2154-2167.

Yang, C.Y., and Lin, Y.P. (2007). Direct antistaphylococcal effects of high-dose aspirin in hemodialysis patients? Am J Kidney Dis *50*, 342; author reply 342-343.

Yannakopoulou, K., Jicsinszky, L., Aggelidou, C., Mourtzis, N., Robinson, T.M., Yohannes, A., Nestorovich, E.M., Bezrukov, S.M., and Karginov, V.A. (2011). Symmetry requirements for effective blocking of pore-forming toxins: comparative study with alpha-, beta-, and gamma-cyclodextrin derivatives. Antimicrob Agents Chemother *55*, 3594-3597.

Zhao, L., Xue, T., Shang, F., Sun, H., and Sun, B. (2010). Staphylococcus aureus AI-2 quorum sensing associates with the KdpDE two-component system to regulate capsular polysaccharide synthesis and virulence. Infect Immun *78*, 3506-3515.

CHAPTER 5.

Exploring the *Plasmodium falciparum* cyclic-adenosine monophosphate (cAMP)-dependent Protein kinase (PKA) Regulatory Subunit (PfPKA-R) as a therapeutic target

---

5.1. ABSTRACT

Plasmodium falciparum is an abundant pathogen throughout the third-world. It causes malaria, a disease that nearly 1 million people die from each year. As with bacterial pathogens, these parasites are becoming increasingly resistant to commonly used therapies. There is a great need for new therapeutics to target this treatable and curable pathogen. The recent genome sequencing of *P. falciparum* introduced a great volume of data for basic research and identification of new *Plasmodia* targets. Protein kinases are critical signaling molecules in cells. Intracellular parasites like *Plasmodia* encode for a great number of protein kinases. One of the prototype mammalian kinases, PKA, is conserved in the parasite yet has a number of distinct differences in sequence and scaffold that indicate it as a potential and valid therapeutic target.

Various roles have been defined for PKA in malaria pathogenesis. Here, we summarize specific similarities and differences between mammalian and *Plasmodia* isoforms and streamline the expression and purification of the *P. falciparum* (Pf)PKA-R subunit. In addition, we identify a putative myristylation and palmitylation site at the R-subunit N-terminus that appears to play a role in membrane localization.

Further, understanding of the interactions between the pathogen and the host is undoubtedly necessary for the development of new therapies and therapeutic targets to treat malaria.

5.2. INTRODUCTION

Malaria poses a significant public health threat, infecting over 200 million new people each year and causing nearly 1 million deaths (Bowman and Horrocks, 2000; Guerra et al., 2010; Wells, 2010; Winzeler, 2008). Malaria is caused by the apicomplexa parasite *Plasmodium* and transmitted by a mosquito vector (Bray and Garnham, 1982). Five *Plasmodia* species can cause disease in humans. The most prevalent, *Plasmodium falciparum*, is endemic in 87 countries and associated with the highest mortality and morbidity (Bowman and Horrocks, 2000; Snow et al., 2008). Malaria caused by *P. falciparum* is characterized by characterized by symptoms that arise during parasite development in the red blood cell and consist of anemia, fever, metabolic acidosis, neurological symptoms (Winzeler, 2008).

5.2.1. Increasing resistance to traditional anti-malarial therapies: The emergence and dissemination of drug-resistant *Plasmodium* further intensifies the public health threat. Despite recent scientific advances and improvement of contemporary therapies, malaria is still a major cause of illness and mortality throughout the world. Further understanding of the interactions between the pathogen and the host is undoubtedly necessary for the development of new therapies and therapeutic targets to treat malaria. Of the nearly 2000 new drugs brought to market in the twenty-year period between the mid 1970s and 1990s, only 3 of these were anti-malarial therapies (Greenwood and Mutabingwa, 2002). This strikingly low number is made further noteworthy when compared to millions of people affected by malaria worldwide each year. Nearly 50% of the world's

population is at risk for malaria (WHO, 2011), however, much of the populations at risk are in locations without the resources and infrastructure to conduct research and bring new therapies to market.

The emergence of drug-resistant malaria has further intensified the need for novel therapies. Commonly used treatments such as chloroquine and sulphapoxine / pyrimethamine are now less useful (Wells, 2010). Today, the most effective treatment is artemisinin combination therapy (ACT) (Lin et al., 2010), combining arteminisin, a natural-product peroxide-containing compound, with a second anti-malarial therapy of a different class. Although ACTs have been shown to be effective (Lin et al., 2010), resistance has been recently observed (Wongsrichanalai and Meshnick, 2008).

Recent advances such as the *Plasmodium* genome project (Hoffman et al., 2002) and advances in systems biology have improved understanding of the proteins and cellular processes involved in the malaria life-cycle and disease pathogenesis. This abundant data has allowed for the identification of new drug targets and vaccine candidates. With *Plasmodia* genomic data in hand vaccines could potentially be tailored to act on stage-specific targets to enhance the host immune response against the pathogen. There are novel opportunities for identifying unique drug targets such as those involved in parasite development, parasite signaling in different life-cycle stages and parasite survival and persistence within the red blood cell.

5.2.2. Malaria lifecycle, pathogenesis and symptoms: *P. falciparum* is an obligate intracellular parasite of the apicomplexa phylum (Morrissette and Sibley, 2002). Members of this phylum have evolved mechanisms to rapidly invade and

extensively modify their hosts (Matthews, 2011) and can cause widespread global health issues in humans and animals. For example, *Toxoplasma gondii (T. gondii)* is an opportunistic pathogen that causes flu-like swelling of lymph nodes, muscle aches and, in severe cases, brain encephalitis or blindness (Montoya and Liesenfeld, 2004). *Babesia bovis (B. bovis)* a tick-transmitted cattle parasite (Brayton et al., 2007) and *Eimeria tenella (E. tenella),* a parasite that causes cecal coccidiosis in chickens (Visco, 1975), pose great risks to life stock.

One can generalize the lifecycle of apicomplexa intracellular parasites into three basic stages: the infective stage (sporogony), the asexual stage (merogony), and the sexual stage (sometimes called gametogony). The lifecycle of *P. falciparum* is extremely complicated, with stages occurring in both humans and mosquitos **(FIGURE 5.1.)**. Briefly, the female *Anopheles* mosquito ingests *Plasmodium* gametocytes when they feed on infected human blood. Once in the mosquito stomach, the male and female gametes produce a zygote (Tilley et al., 2011), which then transforms readily into an ookinete that migrates within the mosquito and matures into an oocyst (Baton and Ranford-Cartwright, 2005). Sporozoites develop and multiply within the oocysts until they burst out and migrate into mosquito salivary glands (Baton and Ranford-Cartwright, 2005). It is there that the sporozoites are positioned to infect a human through a mosquito bite.

The mosquito spreads infective sporozoites to the host via the saliva. These migrate to the liver, invade hepatocytes, reproduce and proliferate to merozoites (Tilley et al., 2011) over a period of days before they are released from vesicles and red blood cells (RBC). It is within RBCs that the majority of symptoms attributed to malarial pathogenesis arise. In RBCs the merozoites progress through asexual

replication, reproduce and multiply to repeatedly infect naïve RBCs and continually multiply to great numbers within blood (NIAID, 2010). The malarial lifecycle becomes circular when some of these merozoites develop into specialized gametocytes that can again be taken up by feeding *Anopheles* mosquito to begin the lifecycle over again.

Malaria symptoms arise from the interaction of *P. falciparum* with host cells, primarily RBCs. *P. falciparum* has evolved specialized processes to invade, live in and exit host cells. This obligate intracellular pathogen relies on host cells for nutrients and survival (Tilley et al., 2011). To do this, it damages the infected cell by secreting numerous proteins that challenge the framework of the cell and act to circumvent the host immune response.

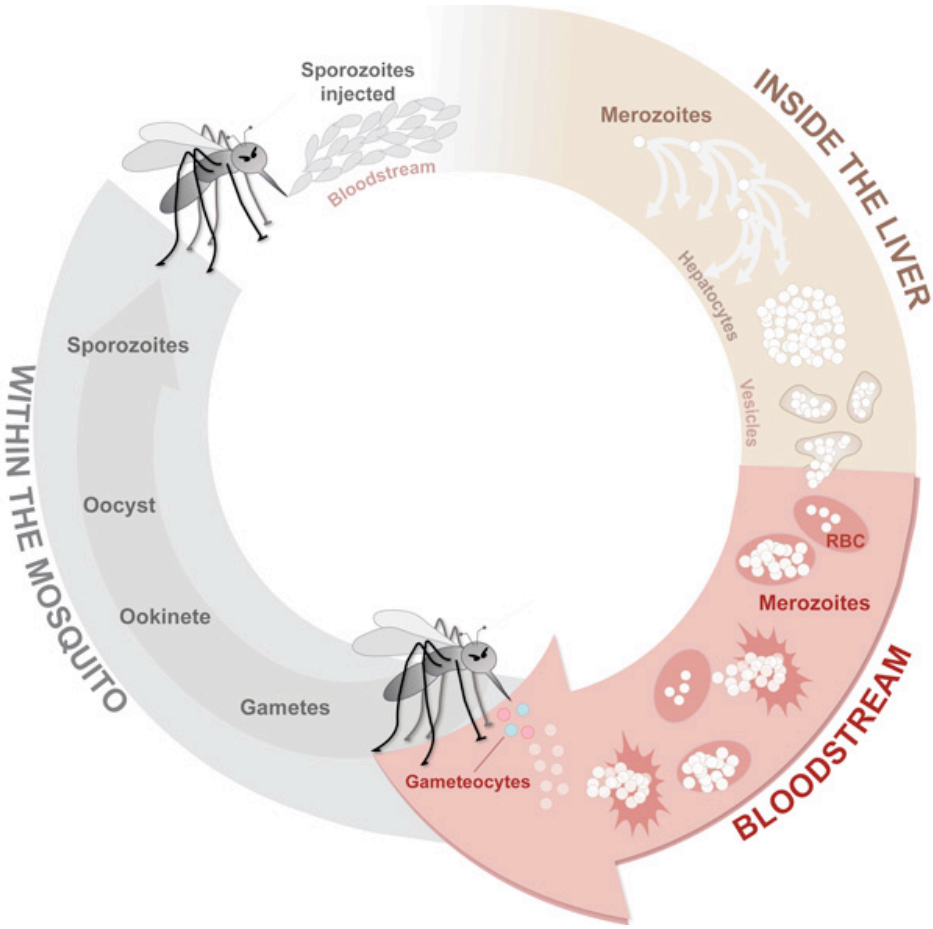

FIGURE 5.1. Lifecycle of *P. falciparum.* The lifecycle can be divided in three phases, (1) sexual reproduction and development in the mosquito, (2) infection and multiplication within human liver hepatocytes and (3) development and proliferation within human RBCs. The majority of malaria symptoms arise from *P. falciparum* infection of RBCs.

Credits: *This image was created by N.H but was based off three resources (MVI, 2011; NIAID, 2010; Tilley et al., 2011).*

Secreted adhesins make the infected RBC surface sticky and thus prevent circulation to the spleen and immune recognition (Buffet et al., 2011), lipases degrade membranes, proteases degrade proteins, kinases and other signaling molecules play crucial roles in regulating parasite invasion, development and the establishment of anion channels (Glenister et al., 2002). These channels, called New Permeation Pathways (NPPs), are anion conductance channels that play a key function in acquiring nutrients, exporting waste and increasing the permeability of the membrane to small molecules (Goldberg and Cowman, 2010). By changing the architecture and physiology of the RBC, the parasite obstructs normal tissue perfusion and drastically disturbs the delivery of oxygen to tissues. The symptoms of malaria arise primarily from parasite invasion and persistence in RBCs.

Symptoms of malaria usually present with viral-like fever and flu-like malaise, chills, headaches and sometimes dizziness, nausea, abdominal pain and myalgia (Trampuz et al., 2003). *P. falciparum* can also induce severe symptoms of acidosis, pulmonary edema, sever anemia, cerebral malarial and other metabolic complications such as hypoglycemia (Trampuz et al., 2003).

5.2.3. Importance of phosphorylation and cAMP signaling in P. falciparum pathogenesis: A mechanism for the ability of *P. falciparum* to invade, adapt to and significantly modify host cells is through controlling protein phosphorylation. Strict regulation of cellular events during various life cycle stages relies heavily on phosphorylation (Billker et al., 2009; Dvorin et al., 2010; Treeck et al., 2011). With a great deal of genomic information (Gardner et al., 2002; Hoffman et al., 2002) and sequence databases for *P. falciparum* the malarial protein kinome

has been previously described (Doerig, 2004; Doerig et al., 2010; Doerig et al., 2008; Doerig et al., 2005; Doerig and Meijer, 2007; Leroy and Doerig, 2008). Similarly, several bioinformatic analyses by other groups have identified > 60 putative protein kinases in the *P. falciparum* genome (Anamika et al., 2005; Anamika and Srinivasan, 2007; Ward et al., 2004).

5.2.4. The mammalian cAMP-dependent protein kinase: Communication within and between cells involves highly complex processes of signal transduction. Signaling pathways communicate information gathered from the extracellular and intracellular environment to influence gene transcription and modify molecular machinery for various tasks. Reversible protein phosphorylation plays a prominent role in cellular signaling and communication. This important cellular regulatory system occurs in both eukaryotic and prokaryotic organisms. At the core of this system are numerous protein kinases, sophisticated and highly regulated enzymes that add a phosphate group to a target protein, and protein phosphatases, that remove the phosphate. Depending on target protein function, the action of adding a phosphate can activate or inactivate enzymatic properties, change structural conformation and thus affect cellular localization and impact downstream cellular processes. Reversible protein phosphorylation is a highly complex and tightly regulated system.

Protein kinases are critical members of the signal transduction cascade. The human genome encodes for over 500 protein kinases (2% of the genome) (Manning et al., 2002). The structural fold of this protein family is highly conserved, consisting of a catalytic domain that is roughly 300 amino acids long, containing a small and

highly dynamic ATP binding lobe and a large C-terminal lobe. The primary and secondary structures of protein kinases can be divided into a number of conserved families that share similar functions or targets. Hanks and Hunter defined 12 distinct subdomains **(Figure 5.2 (top), 5.3)** that are shared within kinase secondary structures (Hanks and Hunter, 1995). These subdomains, illustrated by color-coding, contain highly conserved residues that are critical to the dynamics, kinetics and function of the kinase fold **(FIGURE 5.3.)**. This remarkable conservation can be seen in the structural fold of four examples of the protein kinase family, PKA, cSrc, CDK1 and Phosphorylase Kinase **(FIGURE 5.2.)**. On closer examination, the electrostatic surface these four enzymes show unique differences and display unique chemical diversity **(FIGURE 4.2.)**. The unique surface features of these proteins contribute to the highly specific protein:protein interactions that constitute the dynamic properties of cell signaling networks.

The cyclic-adenosine monophosphate (cAMP)-dependent protein kinase (PKA) catalytic subunit (C-subunit) is a prototype for the protein kinase superfamily. A member of the AGC kinase family, the PKA C-subunit is involved in numerous cellular processes. The first structural determination of a kinase was in the fully active form of PKA and helped define the conserved structural fold **(FIGURES 5.2., 5.4.)** of the kinase family (Knighton et al., 1991a; Knighton et al., 1991b). PKA regulation is mediated by both phosphorylation and by cAMP. It exists as a tetrameric enzyme in the mammalian cell, consisting of two C-subunits that bind a dimer of two identical regulatory subunits (R-subunits) in an R_2C_2 conformation **(FIGURE 5.4A.)**. In this tetrameric conformation, the C-subunits are considered inactive, as the R-subunit acts as an inhibitor by binding into the active site of the C-subunit (Johnson et al., 2001; Taylor et al., 2005).

Regulatory subunits in most eukaryotes consist of an N-terminal dimerization and docking (D/D) domain, a flexible linker and two cAMP-binding domains at the C-terminus. The N-termini of each R-subunit monomer form a stable X-type four-helix bundle motif that modulates binding interactions with cellular proteins, such as anchoring domains and membranes (Banky et al., 1998; Banky et al., 2000; Banky et al., 2003; Leon et al., 1997). The D/D domain is joined to the cAMP-binding domains through a long disordered linker region containing an auto-inhibitory sequence that binds in the C-subunit active site cleft (Herberg et al., 1994). Two cAMP-binding domains modulate the activity of PKA. Upon binding of cAMP to the two cAMP-binding domains of each dimer, the R-subunits undergo a conformational change that releases active C-subunit into the cellular environment.

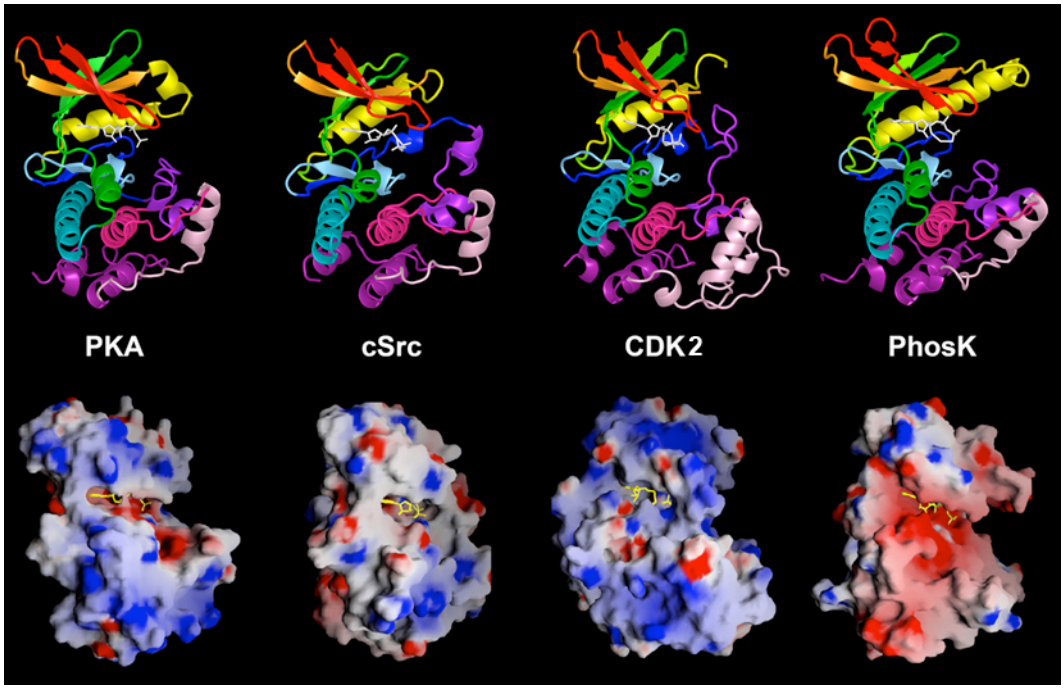

FIGURE 5.2. Select members of the protein kinase superfamily. On the top are four representative crystal structures colored according to subdomains (initially defined by (Hanks and Hunter, 1995) and re-aligned according to sequential and sequential features). The highly divergent surface electrostatics and landscapes of these four kinases can be noted on in the surface renderings (prepared in GRASS (Nayal et al., 1999). Structures were prepared from PDB files: PKA (PDB 1atp); cSrc (PDB 2src); cdk2 (PDB 1hck); PhosK (PDB 1phk).

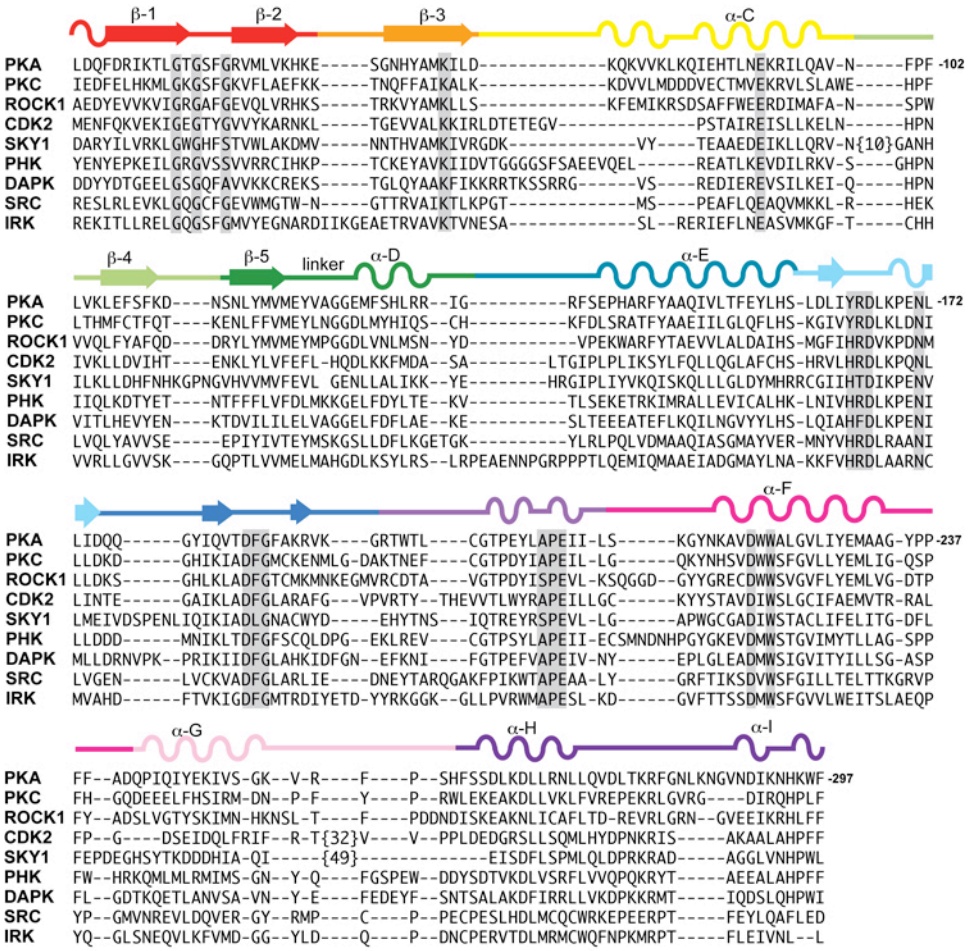

FIGURE 5.3. Alignment of protein kinase core sequences. The catalytic subunits of each kinase are shown, subdomain are numbered accordingly (Hanks and Hunter, 1995) and identified by color. Sequences were aligned by CLUSTALW and optimized by structural alignment and analysis using PYMOL®. Sequence identifications refer to the following UniProtKB numbers: **PKA**, cAMP-dependent protein kinase (UniProt P05132 KAPCA_MOUSE); **PKC**, protein kinase C alpha type (Uniprot Q04759 KPCT_HUMAN); **ROCK1,** Rho-associated protein kinase-1 (UniProt Q13464 ROCK1_HUMAN); **CKD2**, cyclin-dependent protein kinase 2 (UniProt P24941CDK2_HUMAN); **SKY1**, serine/threonine protein kinase of *Saccharomyces cerevisiae* (UniProt Q03656 SKY1_YEAST); **PHK**, phosphorylase kinase gamma-1 (UniProt Q16816 PHKG1_HUMAN); **DAPK**, death-associated protein (DAP) kinase-1 (UniProt P53355 DAPK1_HUMAN); **SRC**, proto-oncogene tyrosine-protein kinase Src (UniProt P12931 SRC_HUMAN); and **IRK**, insulin-receptor tyrosine kinase (Uniprot P06213 INSR_HUMAN).

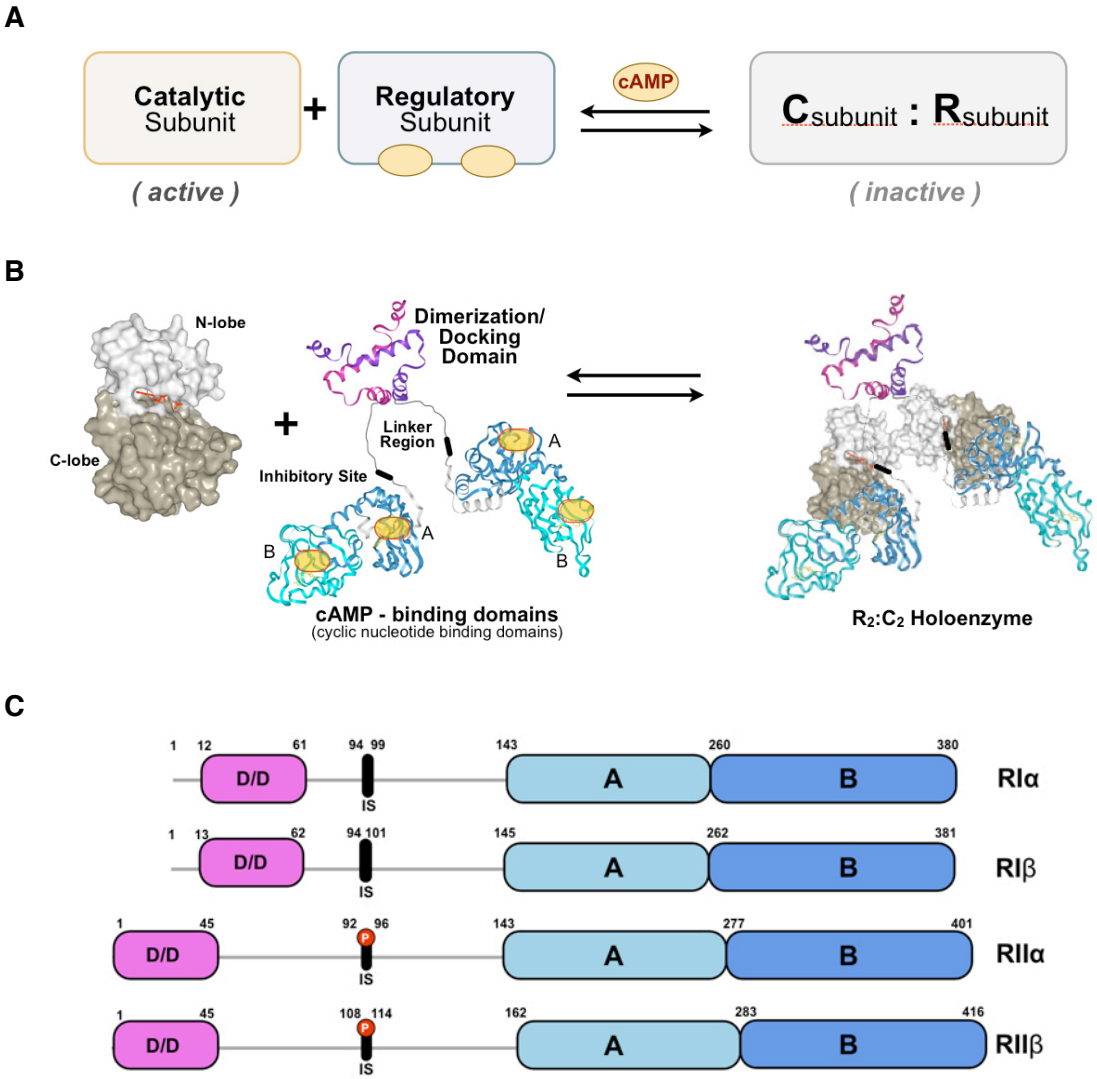

FIGURE 5.4. cAMP-dependent protein kinase (PKA). **(A, B)** Activation of PKA by cAMP. (**B, left)** Core structure of the active PKA enzyme showing the small (N-lobe) in white and the large (C-lobe) in tan with a free cAMP-bound R2 dimer consisting of a Dimerization / Docking Domain (D/D) connected to the two cAMP-binding domains by a flexible dimer containing an inhibitory sequence. **(B, right)** a schematic view of a holoenzyme formation consisting of two inactive C-subunits bound to two cyclic-nucleotide free R-subunits. **(C)** Four PKA R-subunit isoforms. RI α and RIIβ consist of slightly shorter sequences and an inhibitor site that does not have a phosphorylation motif. In contrast, the Type-II isoforms have a phosphorylated serine in their inhibitor sites.

5.2.5. Parasitic protein kinases: valid targets for drug discovery*:* With the genome of *P. falciparum* sequenced, we are now able to study the large genomic databases and compare and contrast the genomes and proteins of *Plasmodium* to mammals. Evidence and rationale show that there are large phylogenetic differences between protein kinases in *P. falciparum* and the protein kinases found in their hosts (Doerig et al., 2005). Due to these vast phylogenetic distances, *P. falciparum* protein kinases are considered valid targets for antimalarial chemotherapies (Doerig et al., 2005; Doerig and Meijer, 2007). With increasing focus on mammalian protein kinases as drug targets for cancer and neurodegenerative disorders, the scientific community has created large databases of possible small molecule kinase inhibitors and probed the structures of mammalian kinomes for crucial insights into key structural features that would aid in drug-design. By utilizing these resources and targeting kinases that are crucial to malaria survival and pathogenesis we are in a unique position to identify new targets and candidates for anti-malarial therapies.

5.2.5.1. The importance of cyclic-nucleotide signaling in malarial pathogenesis: Cyclic nucleotides like cyclic-adenosine monophosphate (cAMP) are intracellular signaling molecules that allow for cellular communication. These molecules are commonly referred to as “ancient signaling molecules.” In fact, cAMP is a signal for stress in most organisms, ranging from humans to bacteria (Berman et al., 2005). In *Plasmodium* the cyclic nucleotides like cAMP and cGMP can carry a variety of functions, inducing functions like chemotaxis and sexual commitment

(Baker, 2011). *P. falciparum* produces cAMP through a genome-encoded adenylate cyclase (Read and Mikkelsen, 1991). In regards to malarial pathogenesis, it seems that PKA may play a large role. *P. falciparum* is understood to modify the movement of nutrients, waste and ions across the red blood cell membrane for its survival in the host. The intracellular parasite establishes anion channels and "new permeation pathways" (NPPs) **(FIGURE 5.5)** in the RBC membrane to pass nutrients like sugars, peptides, amino acids, nucleotides and anions/ cations into the RBC (Martin et al., 2009; Merckx et al., 2009; Merckx et al., 2008). Malarial symptoms are further induced by parasitic degradation of RBC hemoglobin for nutrient extraction. Malarial pathogenesis depends largely on intracellular molecular signaling pathways, specifically mediated by phosphoinositide, Ca^{2+} -dependent mechanisms and cyclic-adenosine monophosphate (cAMP).

5.2.5.2. P. falciparum PKA R-subunit (PfPKA-R) in malaria disease: Recently, experimental evidence that PfPKA-R could be involved in the activation of the anion conductance channels (Merckx et al., 2008) suggests that PfPKA-R may play a crucial role in malarial pathogenesis. Merckx and colleagues found PfPKA-R played a role in the activation of red blood cell membrane conductance. In addition, they found that tight regulation of cAMP signaling appeared to be critical for normal life-cycle development and parasite growth (Merckx et al., 2008).

Other key processes appear to be controlled and regulated by PfPKA-C and PfPKA-R. Studies showing that the kinase inhibitor staurosorine inhibited *P. falciparum* merozoite invasion into red blood cells (Dluzewski and Garcia, 1996) and similar evidence that the compound prevented *P. knowlesi* invasion into monkey

RBCs (Ward et al., 1994) indicate the role for PKA in parasite invasion. A recent study evaluated the importance of apical membrane antigen-1 (AMA-1) in parasite invasion (Leykauf et al., 2010). The function of AMA-1 depends on phosphorylation by PKA. For the parasite to invade a host red blood cell, a tight junction must form at the apical membrane. The process of forming a tight junction is highly dependent on the signaling events via phosphorylation. Specifically, the authors demonstrate that Ser610 on the C-terminal cytoplasmic tail of AMA-1 is phosphorylated by PfPKA-C and mutation of Ser610Ala or pharmacological inhibition of PKA phosphorylation (using H89 inhibition) elicits a dramatic reduction in the parasite's ability to invade the RBC (Leykauf et al., 2010).

These data highlight the importance of the PfPKA-regulatory subunit in the study of malarial pathogenesis. The defined role for PKA in *plasmodia* signaling and development establish a key platform for investigating PfPKA-R specific features and considering it a valid therapeutic target.

Together these studies highlight the importance of *Pf*PKA, in malarial pathogenesis. The defined role for PKA in *P. falciparum* signaling and development establish a key platform for investigating PfPKA-R specific features and considering it a valid therapeutic target. To investigate this, Susan Taylor (UCSD) and Gordon Langsley (INSERM, Paris FR) established a collaboration with the goal of studying the sequence, structure and function of PfPKA in malaria pathogenesis. Using bacterial expressed PfPKA-R (Merckx et al., 2008), this collaboration is in a unique position to probe these unique sequence and structural features with hopes to gain insight for the discovery of novel therapeutics to treat malaria.

In the following study, we outline specific features that distinguish PfPKA-R

from its mammalian counterparts, uncover novel sequence characteristics that provide further knowledge on the role of the protein in malarial pathogenesis. In addition, we have optimized the expression and purification, genetically modify the PfPKA-R in a recombinant *E. coli* system with the hopes to crystallize the structure and gain critical insight into drug-able features of this protein.

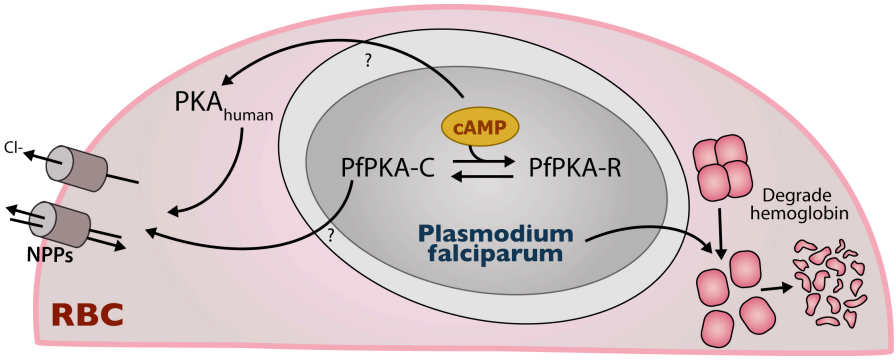

FIGURE 5.5. A possible role of PKA in malarial pathogenesis in the RBC. The intracellular parasite, situated within a parasitophorous vacuole, establishes anion channels and "new permeation pathways" (NPPs) in the RBC membrane to pass nutrients like sugars, peptides, amino acids, nucleotides and anions/ cations (Martin et al., 2009; Merckx et al., 2008). Malarial symptoms are further induced by parasitic degradation of RBC hemoglobin for nutrient extraction. Malarial pathogenesis depends largely on intracellular molecular signaling pathways, specifically mediated by phosphoinositide, Ca^{2+} -dependent mechanisms and cyclic-adenosine monophosphate (cAMP).

Abbrev: NPPs ("New Permeation Pathways"), Cl- (chloride/anions), PfPKA (Plasmodium falciparum PKA) C (catalytic subunit), R (regulatory subunit). Figure drawn based off a similar (Merckx et al., 2009) schematic.

5.3. RESULTS AND DISCUSSION

5.3.1. Sequence Analysis of PfPKA C-subunit: Because of the essential role eukaryotic kinases play in important cellular functions, they are promising drug target candidates. To probe the similarities and differences between the sequences of PfPKA-C compared to mammalian C-subunits, types alpha and beta as well as other *Plasmodium spp.* This analysis examines in detail specificities of the sequence that may prove to alter its localization and function.

The mammalian PKA-C subunit is a member of the AGC kinase family. The members of this family, including Protein kinase C, Akt (Protein Kinase B), cGMP-dependent protein kinase and others share similar structural and sequential motifs (Kannan et al., 2007). As in most of the other kinase families, the kinase core, residues 40 – 300 in PKA, is particularly conserved (described above). The tails provide key differences. AGC kinases are known for having a C-terminus (residues 327 – 336 in mammalian C-subunit) that is highly dynamic and plays a role in binding and recognizing protein and peptide substrates. The PxxP motif on the C-terminal tail provides a unique consensus for binding proteins. A hydrophobic capping motif at the protein C-terminus (PKA residues 347 – 350) interacts with residues in the small lobe of the C-subunit, a motif also conserved in the AGC family. At the N-terminal end of the protein, PKA has unique structural features that impact its interaction with proteins as well as its localization within cells. At the very N-terminus a glycine serves as a myristylation site. This moiety anchors within a hydrophobic pocket, but may also be dynamic and allow for interaction with lipid membranes. A conserved Trp30 is seen in all mammalian PKA N-termini and functions to stabilize the small

and large lobes of the C-subunit. In addition, a conserved Ser10 is a conserved phosphorylation site.

In comparing mammalian C-subunits to the *Plasmodium* counterparts **(FIGURE 5.6.)** a high degree of conservation is noted. On further assessment, specific differences can be noted that may specifically impact the activity of the parasite C-subunit. At the N-terminus, various differences can be noted: the myristylation site conserved in mammalian forms is absent, the A-helix Trp30, noted above for its important interaction in the hinge region, is also missing. One closer examination of residues in the hinge region, specifically Phe100 and Phe102 in PfPKA-C, we notice an interesting alteration in Phe100. In mammals and other species such as worms and flies, a conserved phenylalanine is seen in this position. In Akt, PKC and RSK, a conserved histidine occupies this position (Kannan et al., 2007). In fact, it is generally noted that other eukaryotic protein kinases carry a conserved histidine in this site. *P. falciparum* PKA-C differs from its mammalian counterparts and carries a histidine, as seen in other AGC kinases and most other eukaryotic kinases. Phe108, conserved in mammalian C-subunits, is glycine in *Plasmodium spp,* an observation also seen in PKN. Much of the core sequence is highly conserved. Though there are definite similarities in the C-terminal tail between *Plasmodium* and mammalian isoforms such as the conserved PxxP motif (residues 213 – 216 in mammalian C), there are also specific differences from mammalian isoforms. For example, a hydrophobic Val in all *Plasmodium spp.* replaces Tyr330, a crucial residue due to its interaction with ATP through hydrogen bonding interactions. Interestingly, the PKA C-subunit of *T. gondii* **(FIGURE 5.6)** does not share this feature with *Plasmodium*. Adjacent to Tyr330 is an Asp329 in mammalian isoforms

and is replaced by a basic Arg or Lys in *Plasmodium spp.* The phosphorylated Ser338 in PKA is mutated to an acidic Asp in *Plasmodium*.

The sequence differences between C-subunits of mammalian and *Plasmodium spp.* are relatively minimal compared to that of the regulatory subunits. In targeting kinases to treat infectious diseases, the goal would be to find a target that would differ greatly from its mammalian host counterpart, or not exist in the human host to bypass possible co-interactions, and unwanted side-effects of acting both host and organism proteins. With this insight one might suggest that the therapeutic target of interest in this signaling system of *P. falciparum* is not the C-subunit, but rather the highly divergent regulatory subunit and the holoenzyme complex that forms between the C and R-subunits.

5.3.2. The unique N-terminus of PfPKA-R: The N-terminus of PfPKA-R is highly divergent from mammalian isoforms. Mammalian R-subunit isoforms have an N-terminal segment of approximately 50 residues forming an anti-parallel X-type helical bundle. This interaction forms a dimer composed of two R-subunits **(FIGURE 5.7A.)**. The hydrophobic surface formed by the X-type bundle forms a docking motif for binding to scaffolding proteins known as A-Kinase Anchoring Proteins (AKAPs) **(FIGURE 5.7C.).** As shown in **FIGURE 5.4C** (above), there are four mammalian isoforms. These isoforms have tissue-specific expression and interact with different substrates and cellular components. On the other hand, the N-terminal portion of *Plasmodium* R-subunits differs greatly from that of all mammalian forms. It is much longer and does not share the prototypical sequence for forming a helical bundle **(FIGURE 5.7B., 5.7D.)**. Instead, we hypothesize that the primary structure indicates

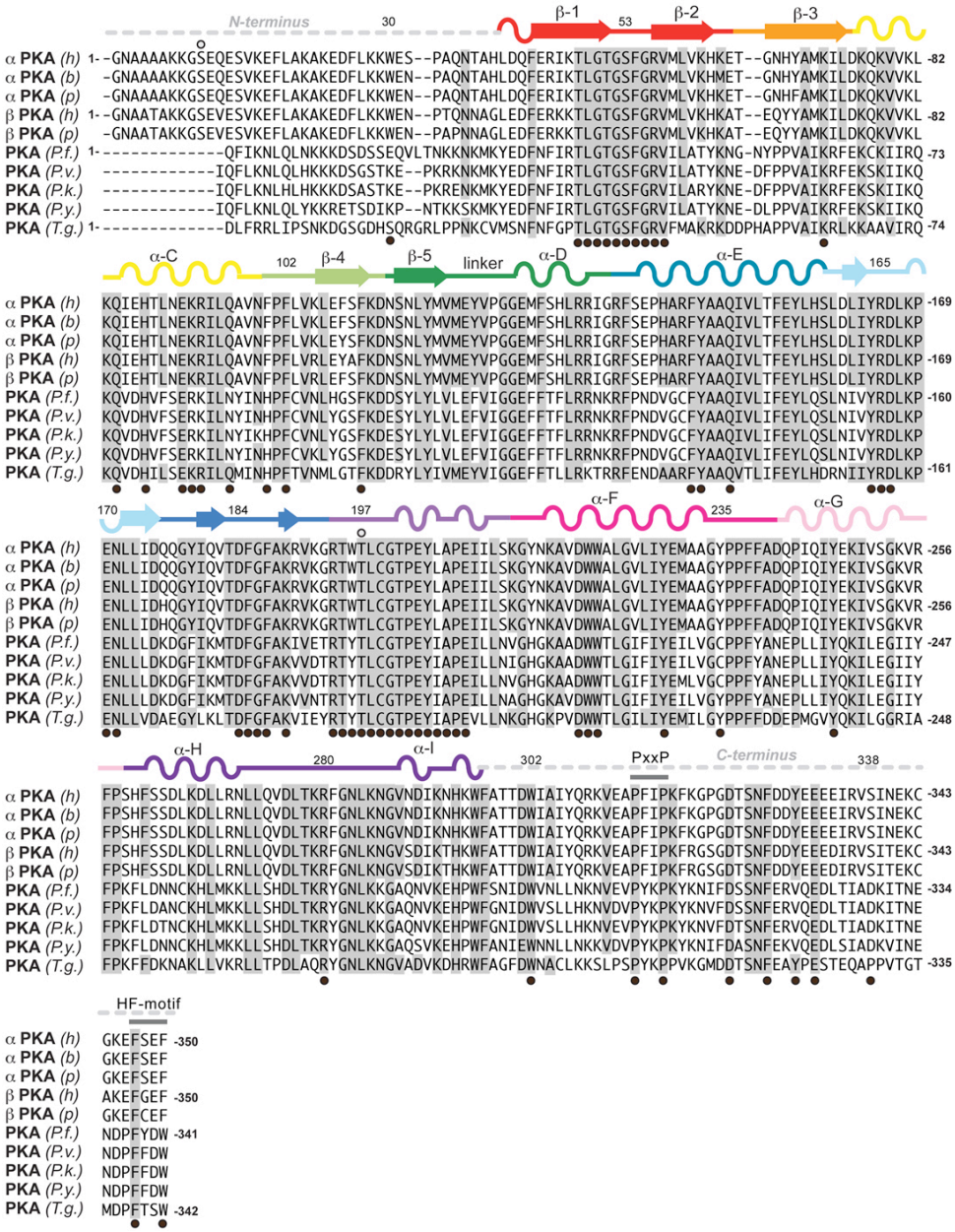

FIGURE 5.6. Sequence alignment of C*α* and C*β* mammalian cAMP-dependent Protein Kinase C-subunits (PKA) with *Plasmodium* and *Toxoplasma gondii* isoforms. Sequences are labeled according to species and isoform: (h), *homo sapiens*, *α*PKA (P17612 KAPCA_HUMAN), *β*PKA (P22694 KAPCB_HUMAN); (b) = bovine, (*Bos taurus*) *α*PKA (P00517 KAPCA_BOVIN); (p), pig (*Sus scrofa*) *α*PKA (P36887 KAPCA_PIG), *β*PKA (P05383 KAPCB_PIG); *(P.f), Plasmodium falciparum* isolate 3D7 (gene *Pf*PKAc, uniprot Q7K6A0_PLAF7); *(P.v.), Plasmodium vivax* (gene PVX_086975, uniprot A5KE97_PLAVI); *(P.k.), Plasmodium knowlesi* strain H (gene PKH_073290, uniprot B3L322_PLAKH); *(P.y.), Plasmodium yoelii yoelli* (gene PY052325, uniprot Q7RE33_PLAYO); *(T.g.) Toxoplasma gondii* VEG (gene TGVEG_066990, uniprot B9Q7X8_TOXGO).

the *P. falciparum* R-subunit to be a monomer.

Even within just the *Plasmodium spp.* one can observe great variability in the length and sequence characteristics of the N-terminal regions **(FIGURE 5.7D)**. Interestingly, the N-terminus of PfPKA-R is at least 10 or more residues longer than any of the compared forms. PfPKA-R appear to share homology with *P. berghei* specifically in the N-terminal region and with the other *Plasmodium spp.* in residues 20 – 60 **(FIGURE 5.7D.)**.

According to a recent phosphoproteomic analysis, Ser19 in *P. falciparum* was identified as a phosphorylated residue (Treeck et al., 2011). PfPKA-R has several additional residues phosphorylated in vivo. In comparing the given R-subunit alignment, Ser19 of *P. falciparum* aligns with a threonine residue in *P. berghei* (Thr12). This suggests that *P. berghei* may also be phosphorylated at the same position. Sequence homology between the two proteins further supports this hypothesis with homology at $Arg8^{PfR}/Arg1^{PbR}$, $Gly10^{PfR}/Gly3^{PbR}$, $Lys11^{PfR}/Lys4^{PbR}$, $Asp16^{PfR}/Asp9^{PbR}$ and $Asn18^{PfR}/Asn11^{PbR}$.

5.3.2.1. Identification of a putative N-terminal myristylation and palmitylation motif in PfPKA-R: Sequence analyses yielded a key observation regarding the N-terminus of PfPKA-R that may impact its localization and function within the cell. We discovered N-terminal motif containing the sequence MGxxC as a putative myristylation (Gly) site and palmitylation (Cys) site **(FIGURE 5.8)**. It is interesting to note that this motif is only present in *P. falciparum*. Exhaustive BLAST and genomic searches showed that no other *Plasmodium* species possessed this N-

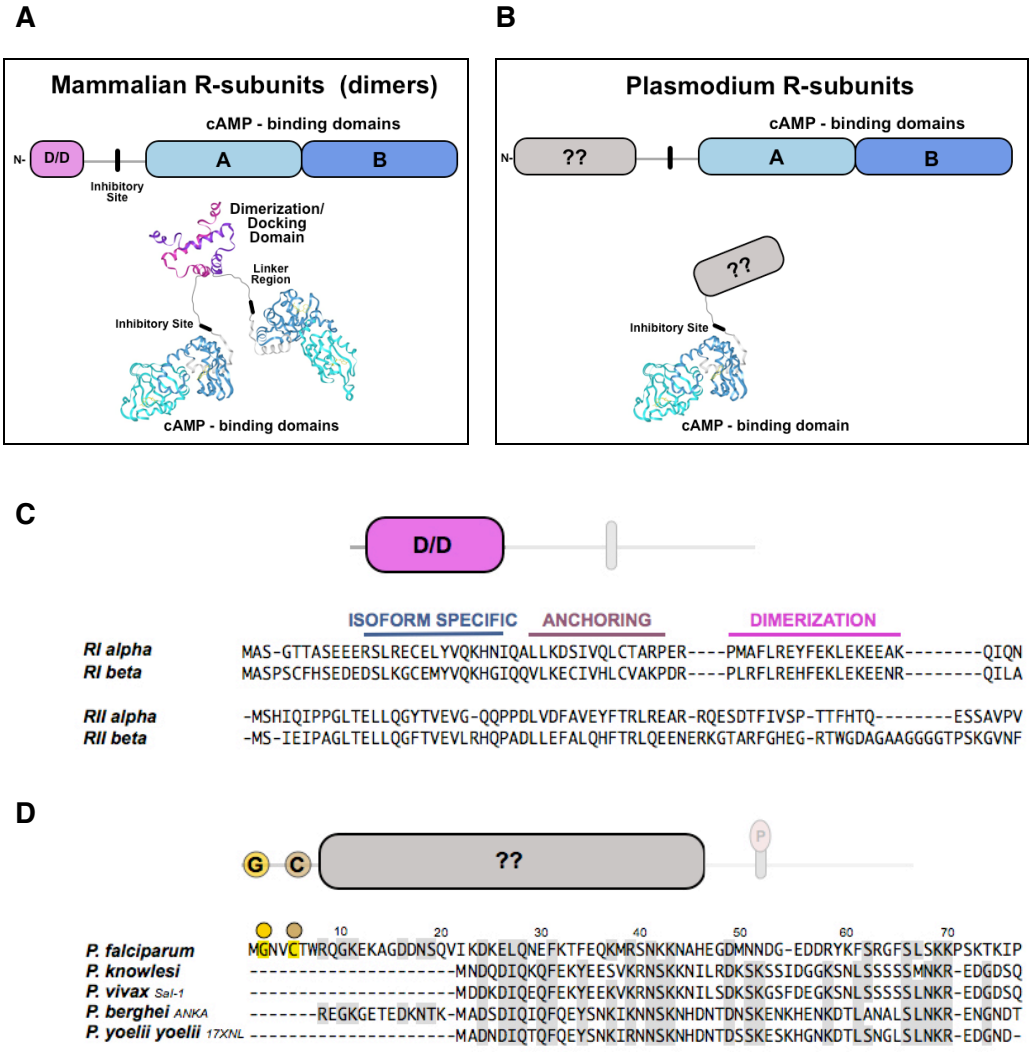

FIGURE 5.7. Domain organization of Mammalian (Panel A, C) and *Plasmodium* (Panel B, D) Regulatory Subunits.

terminal MGxxC motif. BLAST searches with other apicomplexa, however, yielded interesting results. The PKA regulatory subunit of *T. gondii* also contained a similar N-terminal putative myristylation and palmitylation motif **(FIGURE 5.8B.)**. A similar motif has been noted previously in the N-terminus of *Eimeria tenella* and *T. gondii* cGMP-dependent protein kinases (TgPKG). A recent study identified a membrane-associated TgPKG isoform with a motif that was myristylated and palmitoylated at Gly2 and Cys4 respectively and that localized to the parasite plasma membrane (Donald and Liberator, 2002; Gurnett et al., 2002). Mutagenesis of Gly2Ala and Cys4Ala abolished localization and revealed the importance of this sequence motif. In addition to this finding, the *N*-myristoyltransferase in *P. falciparum* is expressed in asexual blood-stage forms (Gunaratne et al., 2000) and sequence alignments with the human counterpart indicate high sequence identity **(FIGURE 5.8C.)**. Further, the *P. falciparum* genome encodes for 13 distinct proteins with a conserved DHHC-motif **(FIGURE 5.8D.)**, indicative of an active palmitoylation system (Seydel et al., 2005). We hypothesize that the similar sequence found in *P. falciparum* and *T. gondii* PKA R-subunits **(FIGURE 5.8B.)** also provides a mechanism for R-subunit localization.

5.3.2.2. The inhibitory sequence of PfPKA-R is "Type II –like": The mammalian regulatory subunits of PKA are multifunctional and highly dynamic modular domains. They exist in two general forms, RI and RII that are distinct in their sequence, capacity to be autophosphorylated, sensitivity to activation by cAMP and localization within the cell. RI and RII each have an α and a β isoforms and each of these have different expression profiles throughout cells and tissues. R-

A

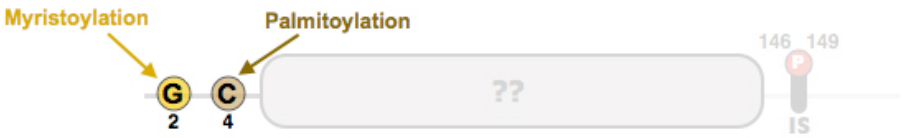

B

C

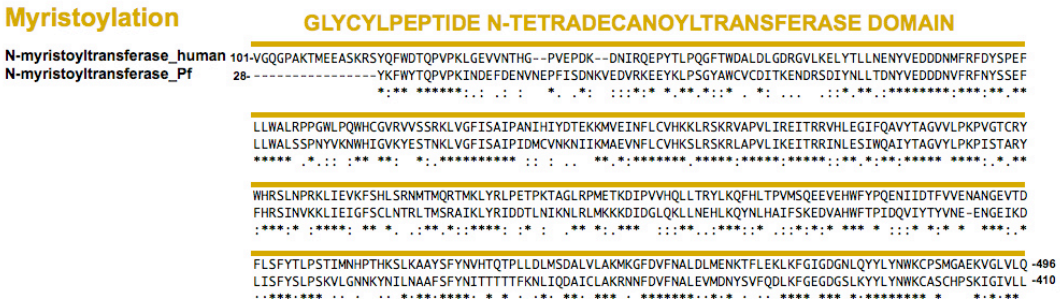

D

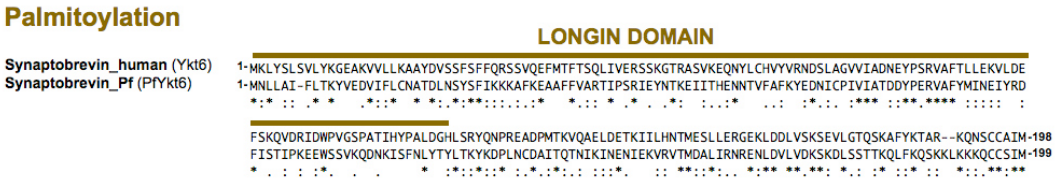

FIGURE 5.8. Predicted myristylation and palmitylation sites in the *P. falciparum* R-subunit and *P. falciparum* encoded acyltransferases.

subunits act as competitive inhibitors to PKA. The inhibitor site is located on the linker region between the N-terminus and the two cAMP binding domains. RI and RII isoforms have distinct inhibitor sites. RII has a serine residue in the phosphorylation site (P-site) that is autophosphorylated by the C-subunit. RI isoforms, however, are distinct in that they contain a pseudosubstrate inhibitor site, with an alanine or glycine in the P-site **(FIGURE 5.9A)**.

Sequence comparisons of the *P. falciparum* R-subunit indicate that the P-site is a probable PKA substrate inhibitor **(FIGURE 5.9A)**. It has a serine in the P-site and thus appears to be more RII-like. Despite conservation within the P-site, PfPKA-R otherwise contains a mixture of RI or RII like features. Small differences exist that could potentially alter the affinity to mammalian or *Plasmodium* C-subunit. The Arg94$^{RI_\alpha}$ and Ar95 $^{RI_\alpha}$ in the autoinhibitor site are conserved in all mammalian R-subunits (Buechler et al., 1993). In the mammalian holoenzyme, these arginine side-chains for ion-pairs with specific glutamic acid residues. PfPKA-R maintains two basic residues in the P-2 and P-3 positions, arginine and lysine respectably. We hypothesize that the P-3 lysine residue would no effect the interactions within this site.

5.3.2.3. Features of the PfPKA-R cAMP binding domains: The cAMP-binding domain is an ancient signaling motif. It is conserved in throughout all genomes (Canaves and Taylor, 2002). In mammalian PKA, cAMP binding to the holoenzyme causes R-subunit release and consequent activation of the C-subunit. Each cAMP-binding domain is comprised of an A-helix followed by an eight-stranded beta-barrel and two helices. Between beta strands 6 and 7 is the conserved cAMP-

binding motif, the phosphate-binding cassette (PBC). The PBC is the docking site for cAMP. The three-dimensional structure of the PBC is quite conserved and serves to dock cAMP and protect the phosphate molecule from break down by cellular phosphodiesterases.

Sequence comparisons between the *Plasmodium* and Mammalian R-subunit isoforms indicate that the PBCs are highly conserved. Within the mammalian PBC are two residues essential for binding cAMP. The arginine **(Arg230, FIGURE 5.9B.)** and glutamic acid **(Glu221, FIGURE 5.9B.)** serve as crucial residues for binding to cAMP. These residues are conserved in the *P. falciparum* R-subunit. Further, the tyrosine residue that is known to interact with the C-subunit in holoenzyme formations of RIα (Tyr205) is also conserved. The main species-specific differences lie within the A-domain.

A conserved proline that provides a kink in the PBC is mutated to a lysine residue. A BLAST search in the NCBI database indicates that there are numerous species and cyclic-nucleotide binding domains that contain a similar basic residue in this position. For example, the cGMP protein kinases of *Campunotus floridanus* (EFN635501.1), *Apis cerana* (AEQ57337.1), *Apis mellifera* (AF469010-1), *Pheidole pallidula* (ABW22624.1), *Nasonia vitripennis* (XP_003424431.1), *Bombus terrestris* (ACS36224.1), *Acromyrmex echinatior* (EG170107.1), *Bombyx mori* (AF465600-1), *Danio rerio* (XP684200.4) contain lysine in place of proline just as *Plasmodia* show.

In general, the cAMP-binding domains of *P. falciparum* show sequence homology with their mammalian counterparts **(FIGURE 5.10.)**. Cyclic-nucleotide binding domains (CNB) are highly conserved throughout evolution. Catabolite gene activator protein (CAP) **(FIGURE 5.10.)** is linked to a DNA binding protein, which acts

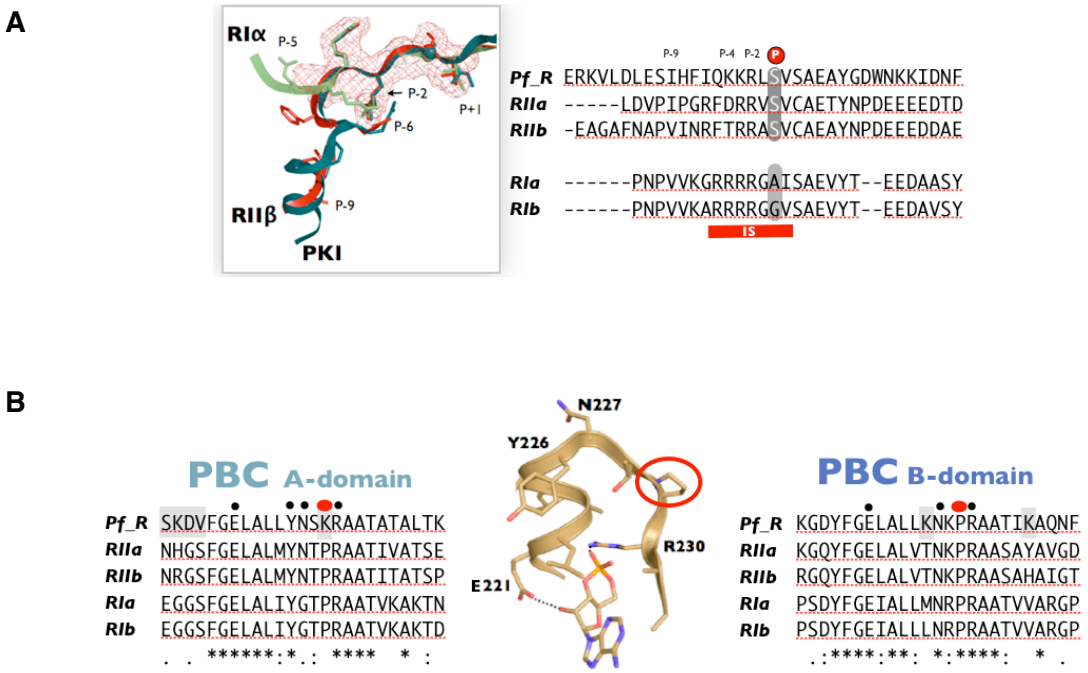

FIGURE 5.9. The inhibitor-site and cyclic-nucleotide binding domains of the *P. falciparum* R-subunit. (A) Comparison of mammalian and PfPKA-R inhibitor site. **(B)** Alignment of isoform-specific phosphate-binding cassettes.

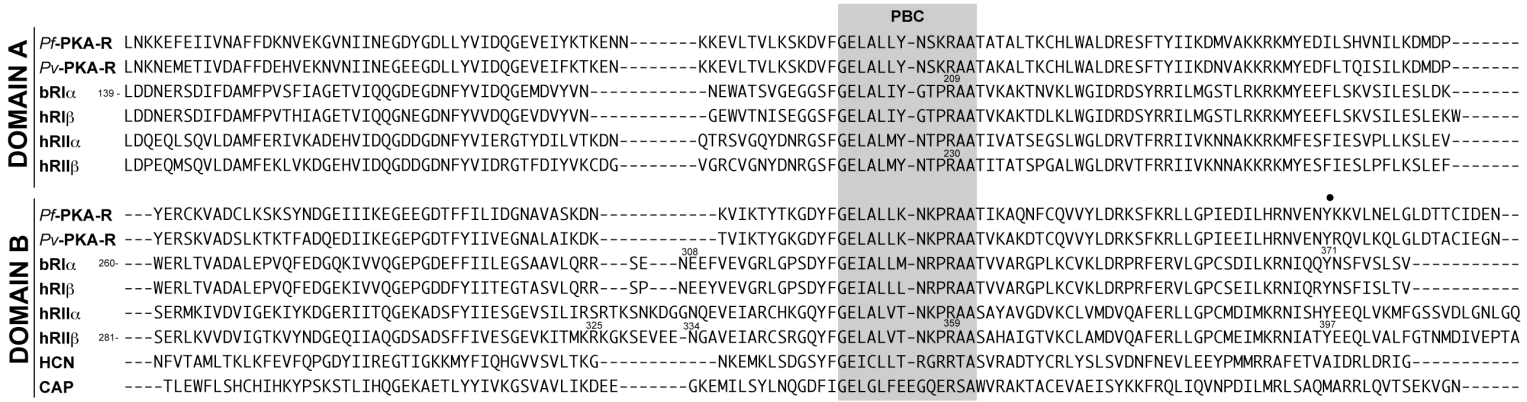

FIGURE 5.10. Alignment of cAMP-binding domains A and B. Aligned sequences include *Pf*PKA-R, *P. vivax* regulatory subunit, mammalian RI and RII isoforms, Hyperpolarization-activated cyclic nucleotide-gated (HCN), and cataboite gene activator protein.

as a transcription factor. The activation of hyperpolarization-activated cyclic nucleotide gated channel (HCN) relies on cAMP signaling. All of these domains contain a conserved hydrophobic shield that surrounds the cyclic nucleotide. These residues also appear to be highly conserved in the *Plasmodium* isoforms. For example, the capping Trp260 of RIα is conserved in *Plasmodia,* as is the domain B capping residue, Tyr371 of RIα. Two other residues crucial to the molecular dynamics of the R-subunit helix are also conserved in *Plasmodia.* Arg239 (RIα) is important for holoenzyme formation. The basic residue forms ionic bonds with an aspartic residue of the A-helix that in turn interfaces with the C-subunit. A second arginine, Arg 241 (RIα), is important for C-subunit activation. It forms ionic bonds with the PBC Glu200 residue that coordinates cAMP binding. In *P. falciparum*, Arg239 is a basic lysine, thus probably conserving the dynamics of the C-helix. Secondly, the 241-position (RIα) is a conserved arginine, thus conserving the electrostatic switch with Glu200.

In general, the core cAMP-binding domains of PfPKA-R are highly conserved among mammalian isoforms. The differences observed between the R-subunits lie mainly in the N-terminus and linker region of PfPKA-R.

5.3.3. Expression, Purification, Crystallization of PfPKA-R: PfPKA-R encoded with a maltose-binding protein (MBP) fusion protein was obtained from Gordon Langsley and colleagues at INSERM (Paris, France) (Merckx et al., 2008). The 441-residue protein (PlasmoDB identifier PFL1110c / GenBank AJ441326) was initially characterized by Langsley and colleagues to determine if the regulatory subunit was able to modulate cAMP-dependent kinase activity.

Initial work with the MBP-tagged protein yielded little pure protein. Subsequently, PfPKA-R was cloned into a pET28a-modified plasmid, which encodes for six histidine residues at the protein N-terminus. Though initial nickel-resin purification yielded protein, this protein was unstable. It degraded into a 35 – 40 kD fragment and a 9 – 12 kD piece. Western blot indicated the small piece was the N-terminus (data not shown). Analysis of the N-terminus highlighted a domain much different than seen in mammalian isoforms. Because of this, N-terminal truncations were engineered with hopes to express a highly stable cAMP-binding domain core. Four N-terminal deletion mutants were engineered into pET28a. These consisted of (Δ1-80), (Δ1-122), (Δ1-133) and (Δ1-148) **(FIGURE 5.11A.)**. Small-scale expressions showed (Δ1-148) to express extremely well **(FIGURE 5.11B.)**. This construct was used for the majority of expression, purification and crystallization studies.

Expression of PfPKA-R(149-441) yielded significant amounts of pure protein **(FIGURE 4.11C.)**. Following size-exclusion purification, protein was pooled and set up for crystallization **(FIGURE 5.11D.)**. The initial crystallization studies yielded a number of potential hits. Subsequent studies could not repeat the exact conditions. To test formed crystals, cryo-protectants were added and crystals were mounted on cryo-pins, flash-frozen in liquid nitrogen. Initial screening was done at 100K in the UCSD Home Source. Collected data revealed the tested crystals as salt.

5.3.4. Complex formation with mammalian C-subunit (mC) and/or PfPKA-C and PfPKA-R subunits: From a drug discovery perspective, forming a holoenzyme complex of C and R is crucial in screening for inhibitors of holoenzyme

formation or dissociation. With large databases and resources of potential kinase inhibitors available for screening, it would be extremely advantageous to form a holoenzyme complex, either a hetero-holoenzyme such as with mammalian C-subunit and *Plasmodium* R-subunit or a traditional PfPKA-C complexed with PfPKA-R. Specifically, finding inhibitors at allosteric sites to the conventional sites (ATP binding site, cAMP binding site) would be beneficial in screening selectively for Pf-holoenzyme inhibitors.

It is unknown if endogenously, during the course of infection, PfPKA-R interacts with the host mammalian C-subunit (as depicted in **FIGURE 5.5.**). If this interaction indeed occurs, finding inhibitors of this interaction would be of critical value. Thus, one of the goals of this project is to form a holoenzyme complex of PfPKA-R with a C-subunit.

In addition to the original PfPKA-R plasmid, we have also worked with a plasmid expressing PfPKA-C from the Gordon Langsley Lab in France. This plasmid has been optimized for expression in *E. coli*. Though the protein expressed well, it was insoluble. The Taylor and Langsley lab continue to troubleshoot the expression in different vectors and conditions. Thus, we have focused thus far on the mammalian C-subunit and its potential interactions with *Plasmodium* R-subunit. We used three purified PfPKA-R proteins (the full-length, Δ1-133 and Δ1-148). After removing residual endogenous cAMP, and purifying the R-subunit we attempted to form holoenzyme complex in a 2C:1PfPKA-R ratio and in the presence of 0.1 mM AMP-PNP and 5mM $MgCl_2$. We ran these mixtures through analytical size exclusion. To allow for a detailed analysis as to whether these proteins were forming a complex, we also ran each individual protein separately yet under the exact

conditions as was done in the combined C-subunit + R-subunit run to compare elution volumes. Trials with native gels proved inconclusive and coomassie stains on previous combination runs had shown possible complex formation **(FIGURE 5.12.)**. However, after further analyses of elution volumes of the proteins together and alone, one can conclude that all proteins are eluting at the same volume **(FIGURE 5.12.)**. Mammalian C-subunit, PfPKA-R and the C+PfPKA-R eluted in the same fractions. If a complex was formed, one would expect it to run at a much earlier elution volume rather than at the same volume as the individual components alone. Though these results indicate that the formation of a complex is unlikely, one should note that it is possible these two proteins form a weak affinity complex that is either unstable or highly dynamic and may not sustain as a holoenzyme during elution on the size-exclusion column. Further tests are required in order to support this hypothesis.

5.3.5. Mutations in the N-terminal Gly2 and Cys5 abolish localization of* PfPKA-*R to the plasma membrane of mammalian cells: We hypothesized that PfPKA-R and TgPKA-R utilize N-terminal myristoylation and palmitoylation motifs (MGxxC) at the N-terminus for localization similar to motifs in the related PKG N-termini of *T. gondii* and *E. tenella* (Donald and Liberator 2002; Gurnett et al 2002). In order to test this hypothesis, we mutated the N-terminal residues of PfPKA-R in a systematic manner to probe the N-terminal motif more thoroughly. Using QuickChange mutagenesis and cell-culture techniques, we tested the role of the N-terminus in localization. A primary goal was to engineer constructs that could be

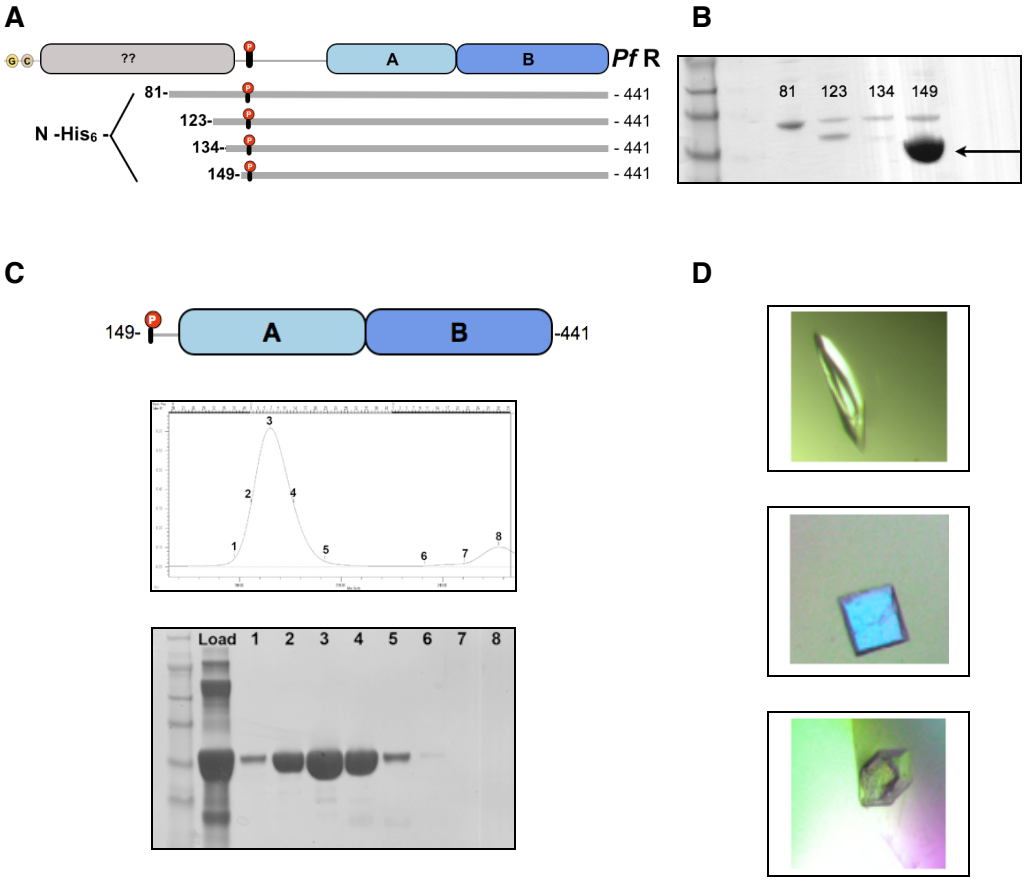

FIGURE 5.11. PfPKA-R deletion mutants. (A) Shows a schematic representation of the N-terminal deletions for 4 different constructs. In **(B**) a small-scale expression (~10 ml) check on each of the four-deletion mutants was performed using a nickel-resin purification system. The (Δ1-148) construct showed the most optimal expression (indicated in B, arrow). Further studies focused on the (Δ1-148) construct. **(C)** Purification of the His6-(Δ1-148)PfPKA-R construct in *E. coli* system. Protein was purified via a nickel-based (IMAC) purification system and then was further purified over a sepharose S200 size-exclusion chromatography column**. (D)** Following purification, protein was set up for initial crystallization trials. Shown are the most promising hits.

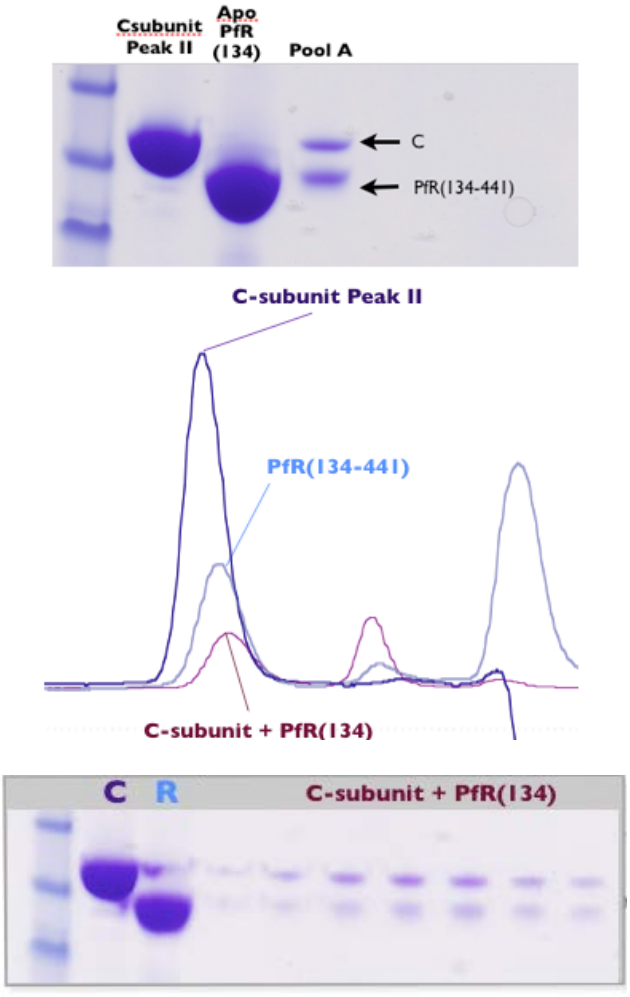

FIGURE 5.12. Size-exclusion chromatography of mammalian C-subunit and PfPKA-R. The mammalian C-subunit and *P. falciparum* R-subunit do not appear to form a holoenzyme complex. Coomassie stains of column elutions on first glance indicate a possible complex formation, however, Further analysis via size-exclusion indicates that these proteins are eluting at the same volume rather than as a complex.

tested in cell culture for their ability to localize to membranes. A stepwise approach was used to investigate the role of Gly2 and Cys5 in PfPKA-R.

To test localization, we engineered a short N-terminal fragment (residues 1 – 20). To this fragment we accomplished the following protein constructs: 1) wild-type (Δ21 – 441)PfPKA-R GFP-tagged; 2) Gly2Ala (Δ21 – 441)PfPKA-R GFP-tagged; 3) Cys5Ala (Δ21 – 441)PfPKA-R GFP-tagged; and 4) Gly2Ala-Cys5Ala ("MACVA") (Δ21 – 441)PfPKA-R GFP-tagged. PfPKA-R N-terminal disorder was accomplished using Regional Order Neural Network (RONN: http://www.strubi.ox.ac.uk/RONN) (Thomson et al 2003; Yang et al 2005). This analysis was done to design a short N-terminal peptide for localization studies. *Pf*PKA-R was analyzed using RONN and the sizes of breakdown products seen on previous SDS-PAGE gels of the full-length protein to engineer a construct that would be stable for expression. Results yielded an N-terminal segment of 109 residues (approximately 12.6 kDa) for our analysis.

These constructs were transfected on the pEGFP-N1 vector into HeLA cells. After allowing cells to grow and express the constructs, the cells were fixed for visualization **(FIGURE 4.13.)**.

***5.3.6. Chapter conclusions*:** PKA plays a crucial role in a variety of *Plasmodia* cellular events. Form its involvement in parasite development, merozoite invasion of and survival within RBCs. This work summarizes some of the species-specific differences between mammalian and *P. falciparum* PKA isoforms. The C-subunit shares high sequence conservation between species, except it does not contain a putative myristylation site at the N-terminus. *P. falciparum* encode for only one R-subunit isoform. This isoform shares both similarities and contrasting

differences between the four mammalian isoforms. Specifically, the N-terminus is longer than any mammalian form and does not share the similar dimerization / docking X-type helix bundle motif that is common to mammalian subunits. Therefore, it is hypothesized that PfPKA-R exists as a monomer rather than a dimer. The N-terminal sequence is further unique from mammalian isoforms in that it contains an N-terminal glycine and cysteine, which are putative myristoylation and palmitoylation sites. Results show that mutating these residues in PfPKA-R abolishes localization within a tissue-culture cell. Interestingly, these sites are conserved in the *T. gondii* PKA R-subunit as wells in *T. gondii* and *E. tenella* PKG and within these proteins it has previously been determined to be necessary for membrane localization. Finally, the core cAMP-binding domains of PfPKA-R share features of all isoforms with the exception of a lysine residue in place of the conserved Pro208 (RIα) in the phosphate-binding cassette.

Like its mammalian counterparts, the linker region tethering the N-terminus to the cAMP-binding domains appears to be highly flexible and disordered. Due to this flexibility, truncations of the N-terminus appear to stabilize and enhance protein expression. An N-terminal deletion mutant Δ1-148 showed to express extremely well when expressed in the His-tag vector pET28a. Initial crystallization trials were unsuccessful, but proved promising.

With great need for new therapies to treat drug-resistant malaria, PfPKA-R poses a valid therapeutic target. By targeting the R-subunit, therapies could possibly have multi-fold effects including preventing invasion, parasite development, and inhibiting the effect of the destructive NPPs.

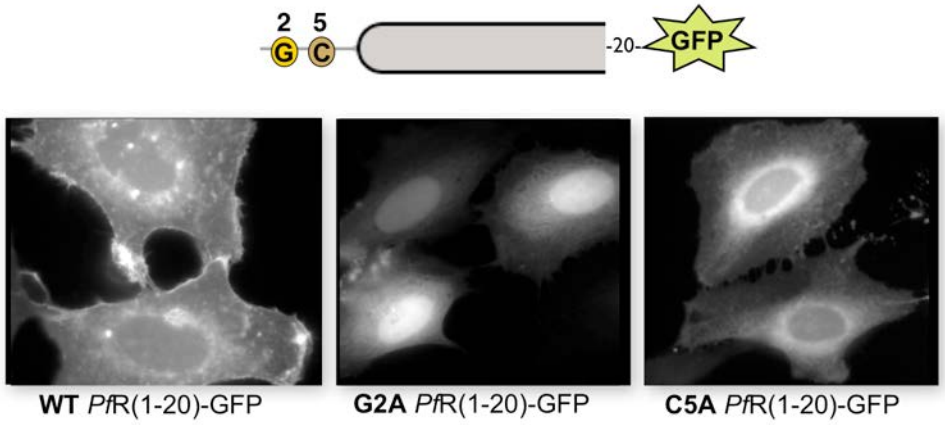

FIGURE 5.13. Examining the role of Gly2 and Cys5 in localization to the cell membrane.

5.4. MATERIALS AND METHODS

5.4.1. Bioinformatic analyses*:* Sequence analyses and alignments were completed using the CLUSTALX program. The highly divergent surface electrostatics and landscapes of these kinase catalytic subunits were analyzed using surface renderings prepared in GRASS (Nayal et al., 1999). C-subunit structural renderings were prepared from PDB files: PKA (PDB 1atp); cSrc (PDB 2src); cdk2 (PDB 1hck); PhosK (PDB 1phk). Further characterization of sequential similarities and differences were analyzed using a variety of GenBank available sequences. These included *homo sapiens*, αPKA (P17612 KAPCA_HUMAN), βPKA (P22694 KAPCB_HUMAN); bovine, (*Bos taurus*) αPKA (P00517 KAPCA_BOVIN); (p), pig (*Sus scrofa*) αPKA (P36887 KAPCA_PIG), βPKA (P05383 KAPCB_PIG); *(P.f), Plasmodium falciparum* isolate 3D7 (gene *Pf*PKAc, uniprot Q7K6A0_PLAF7); *(P.v.), Plasmodium vivax* (gene PVX_086975, uniprot A5KE97_PLAVI); *(P.k.), Plasmodium knowlesi* strain H (gene PKH_073290, uniprot B3L322_PLAKH); *(P.y.), Plasmodium yoelii yoelli* (gene PY052325, uniprot Q7RE33_PLAYO); *(T.g.) Toxoplasma gondii* VEG (gene TGVEG_066990, uniprot B9Q7X8_TOXGO).

5.4.2. Design of constructs to probe localization of the N-terminus: Short N-terminal fragments (residues 1 – 20) were engineered: 1) wild-type (Δ21 – 441)*Pf*PKA-R GFP-tagged; 2) Gly2Ala (Δ21 – 441)*Pf*PKA-R GFP-tagged; 3) Cys5Ala (Δ21 – 441)*Pf*PKA-R GFP-tagged; and 4) Gly2Ala-Cys5Ala (“MACVA”) (Δ21 – 441)*Pf*PKA-R GFP-tagged. To help design these constructs, an analysis on the N-terminus protein disorder characteristics of *Pf*PKA- was accomplished using Regional Order Neural Network (RONN: http://www.strubi.ox.ac.uk/RONN)

(Thomson et al 2003; Yang et al 2005). This analysis was done to design a short N-terminal peptide for localization studies. *Pf*PKA-R was analyzed using RONN and the sizes of breakdown products seen on previous SDS-PAGE gels of the full-length protein to engineer a construct that would be stable for expression. The stable (Δ21 – 441)*Pf*PKA-R GFP-tagged; 2) Gly2Ala (Δ21 – 441)*Pf*PKA-R GFP-tagged; 3) Cys5Ala (Δ21 – 441)*Pf*PKA-R GFP-tagged constructs were engineered using the Stratagene Quickchange mutagenesis. Finally, mutated gene constructs were transformed on the pEGFP-N1 vector into XL-1 supercompetent cells and mutations were confirmed via nucleotide sequencing.

On the other hand, we had difficulty in obtaining a full-length GFP-tagged construct. After troubleshooting, we used a lower (55°C) annealing temperature based on the gene-specific part of the primer as well as the use of a Cold Fusion reaction and yielded transformed colonies. Sequencing results indicated successful transformation and the products were subjected to Quickchange mutagenesis for G2A and C5A mutants. Resulting constructs were transformed into XL-1 supercompetent cells. The full-length constructs proved to be extremely toxic to HeLA cells and this procedure is still being optimized.

After constructs were confirmed, DNA was transfected into HeLA cells. Tissue culture media (DMEM + 10% FBS + 1% Glutamax for starting culture). Transfection was done in FUGENE6 containing OptiMEM media without serum. The reaction was incubated at 25 °C for 5 minutes and then diluted transfection reagent was added to DNA, incubated at room temp for 15 – 45 min and then applied in drop-wise fashion and swirling in a tissue culture dish. The transfected cells were placed back at 37 °C + 5% CO_2 until fixing. Fixing media (4% paraformaldehyde in

DPBS) was prepared at 37 C, fixed for 20 minutes at room temperature, removed and fixed cells were washed five times with DPBS. Fixed cells were stored at 4 °C in DPBS until imaging.

5.4.3. Expression and Purification of* Pf*PKA-R: *Pf*PKA-R encoded with a maltose-binding protein (MBP) fusion protein was obtained from Gordon Langsley and colleagues at INSERM (Paris, France) (Merckx et al., 2008). The 441-residue protein (PlasmoDB identifier PFL1110c / GenBank AJ441326) was initially characterized by Langsley and colleagues to determine if the regulatory subunit was able to modulate cAMP-dependent kinase activity. This protein was utilized for further mutagenesis, deletion mutants, and engineering of studied constructs.

The genomic sequence **(FIGURE 5.14.)** was then cloned from the maltose-binding protein vector to a modified pET28a plasmid. This plasmid encoded for six histidine residues at the protein N-terminus and carries a kanamycin resistance plasmid. pET28a-PfPKA-R vectors were cloned into XL1 blue competent *E. coli* cells and then into competent BL21 *E. coli* cells (DE3, Novagen) for expression.

Cultures of BL21 E.coli were prepared in one – liter autoclaved flasks. On average, 6 liters to 12 liters of bacteria were grown for protein expression. Overnight cultures in kanamycin were prepared. Small starter cultures were prepared from overnight cultures and allowed to grow to late-log phase (OD600 0.6 – 0.8), shaking at 37 °C in kanamycin and 2X YT *E.coli* broth media. Subsequently, one-liter flasks of YT media containing kanamycin were inoculated with late-log phase cultures and incubated, shaking at 37 °C until cultures reached late-log phase (roughly 3 – 5 h). Following growth, plasmid expression was induced with the addition of Isopropyl β-

D-1-thiogalactopyranoside (IPTG) and the cultures were incubated at 16 °C for 16 – 20 h for optimal expression.

Following expression, bacterial cultures were centrifuged and pelleted in Beckman centrifuge at 5000 rpm for 20 min. Pellets were isolated, pooled and lysed on ice. To lyse the bacteria a buffer containing 20 mM Tris pH 7.5, 150 mM NaCl, 5 mM BME and a protease inhibitor cocktail containing Benzamidine (10 mM), 4-(2-Aminoethyl) benzenesulfonyl fluoride hydrochloride (AEBSF) (0.4 mM), Pepstatin (1 μM), Leupeptin (1 μM) and Tosyl phenylalanyl chloromethyl ketone (TPCK) and Tosyllysine Chloromethyl Ketone Hydrochloride (TLCK) (28 μM each).

Lysate was pelleted at 15 krpm for 40 m at 4 °C to separate the supernatant and pellets. Supernatants were combined for further purification over a nickel resin and then size-exclusion chromatography using a s200 gel filtration column (BioRad). Peak fractions were pooled and confirmed by size through SDS-PAGE.

Though initial nickel-resin purification yielded protein, this protein was unstable. It degraded into a 35 – 40 kD fragment and a 9 – 12 kD piece. Analysis of the N-terminus highlighted a domain much different than seen in mammalian isoforms. Because of this, N-terminal truncations were engineered with hopes to express a highly stable cAMP-binding domain core. Four N-terminal deletion mutants were engineered into pET28a. These consisted of (Δ1-80), (Δ1-122), (Δ1-133) and (Δ1-148) using primers listed in **TABLE 5.1**. Small-scale expressions showed (Δ1-148) to express extremely well. This construct was used for the majority of expression, purification and crystallization studies.

```
1       atgggcaatgtgtgcacatggagacaagggaaagaaaaagcaggtgacgataattcacaa
         M  G  N  V  C  T  W  R  Q  G  K  E  K  A  G  D  D  N  S  Q
61      gtaataaaagataaagaattacaaaacgagtttaaaacattcgaacaaaaaatgagaagt
         V  I  K  D  K  E  L  Q  N  E  F  K  T  F  E  Q  K  M  R  S
121     aataaaaaaaatgctcatgaaggagatatgaataatgatggtgaagatgatagatataaa
         N  K  K  N  A  H  E  G  D  M  N  N  D  G  E  D  D  R  Y  K
181     ttttccagaggtttttcattaagtaaaaaaccaagtaaaactaaaatatccgattaccaaa
         F  S  R  G  F  S  L  S  K  K  P  S  K  T  K  I  P  I  T  K
241     acggatagtgaaatattagatggattggattattctgaaatgagtaaacaagttcttatg
         T  D  S  E  I  L  D  G  L  D  Y  S  E  M  S  K  Q  V  L  M
301     actttaaataaaaaaaatatacttaatgacgacggttcaagcgacggtaacgacacagat
         T  L  N  K  K  N  I  L  N  D  D  G  S  S  D  G  N  D  T  D
361     gttcacagcatgttcgataggaaagaaatagagagaaaggtattggatttagaaagtata
         V  H  S  M  F  D  R  K  E  I  E  R  K  V  L  D  L  E  S  I
421     catttcatacagaagaaaagattatctctgtgagtgccgaagcatatggtgactggaataaa
         H  F  I  Q  K  K  R  L  S  V  S  A  E  A  Y  G  D  W  N  K
481     aagattgataatttattcctaaagtttataagaaagatgaaaaagaaaaggccaagata
         K  I  D  N  F  I  P  K  V  Y  K  K  D  E  K  E  K  A  K  I
541     agagaagcattgaatgaatccttttgtttaatcatttaaataagaaagaatttgaaatt
         R  E  A  L  N  E  S  F  L  F  N  H  L  N  K  K  E  F  E  I
601     attgtaaatgcatttttgataaaaatgtagaaaaaggggttaatattataaatgaagga
         I  V  N  A  F  F  D  K  N  V  E  K  G  V  N  I  I  N  E  G
661     gattatggagatttattatatgttatagatcaaggtgaagttgaaatatataaaacaaaa
         D  Y  G  D  L  L  Y  V  I  D  Q  G  E  V  E  I  Y  K  T  K
721     gaaaataataaaaaagaagtattaacagtattaaaatctaaagatgtttttggagaatta
         E  N  N  K  K  E  V  L  T  V  L  K  S  K  D  V  F  G  E  L
781     gccttattatataattctaaaagagctgcaacagctacagccttaaccaaatgccattta
         A  L  L  Y  N  S  K  R  A  A  T  A  T  A  L  T  K  C  H  L
841     tgggccttagatagagaatcttttacatatataataaaagatatggttgctaagaaaaga
         W  A  L  D  R  E  S  F  T  Y  I  I  K  D  M  V  A  K  K  R
901     aaaatgtatgaagatattcttagtcatgtaaatattttaaaagacatggatccatatgaa
         K  M  Y  E  D  I  L  S  H  V  N  I  L  K  D  M  D  P  Y  E
961     agatgtaaagttgctgattgcttaaaatctaaaagttataatgatggagaaattattatt
         R  C  K  V  A  D  C  L  K  S  K  S  Y  N  D  G  E  I  I  I
1021    aaagaaggagaagaaggagatacatttttttatccttatagatggaaatgctgtagcttct
         K  E  G  E  E  G  D  T  F  F  I  L  I  D  G  N  A  V  A  S
1081    aaagataataaagtcatcaaaacttatacaaagggagattactttggagaattagctctt
         K  D  N  K  V  I  K  T  Y  T  K  G  D  Y  F  G  E  L  A  L
1141    ctcaaaaataaaccaagagctgctaccataaaagcacaaaatttttgtcaagtcgtctat
         L  K  N  K  P  R  A  A  T  I  K  A  Q  N  F  C  Q  V  V  Y
1201    ttagatagaaaaagtttcaaaagattattaggacctattgaggatatattacatagaaat
         L  D  R  K  S  F  K  R  L  L  G  P  I  E  D  I  L  H  R  N
1261    gttgaaaattacaaaaaagttctgaacgaattaggtttggatacaacttgtattgatgaa
         V  E  N  Y  K  K  V  L  N  E  L  G  L  D  T  T  C  I  D  E
1321    aattaa  1326
         N  -
```

FIGURE 5.14. Encoding sequence of the *P. falciparum* -cAMP-dependent protein kinase (PKA) Regulatory Subunit. The 441 amino acid protein refers to Uniprot ID Q8T323 and GenBank ID AJ441326.1 (1-1326).

Table 5.1. Primer sequences

A. N-terminal localization Primers for pEGFP-N1 vector

ID	RE		Sequence
N-terminus	**EcoRI**	**F**	5'- GGGGAATTCATGGGCAATGTGTGCACATGG -3'
20 aa	**BamHI**	**R**	5'- GGGGGATCCTTGTGAATTATCGTCACCTGC -3'
109 aa	**BamHI**	**R**	5'- GGGGGATCCATTAAGTATATTTTTTTTATT -3'
≤ 441 aa C-term	**BamHI**	**R**	5'- GGGGGATCCATTTTCATCAATACAAGTTGT -3'
≤ 441 aa C-term	**SalI**	**R**	5'- GGGGTCGACATTTTCATCAATACAAGTTGT -3'

pEGFP-N1 vector GenBank Accession # U55762) RE = Restriction Enzyme; primers based of UNIPROT Q8T323 (Genbank AJ441326.1) encoded on the complementing strand.

B. N-terminal Deletion Mutants for Expression in pET28a+ His6 vector

ID	RE		Sequence
N-terminus	**EcoRI**	**F**	5'- GGGGAATTCATGGGCAATGTGTGCACATGG -3
(Δ1 – 80)	**EcoRI**	**F**	5'- GGGGAATTCACGGATAGTGAAATATTAGATGGATTGGAT -3'
(Δ1 – 122)	**EcoRI**	**F**	5'- GGGGAATTCGTATTGGATTTAGAAAGTATACAT -3'
(Δ1 – 133)	**EcoRI**	**F**	5'- GGGGAATTCAGCATGTTCGATAGGAAAGAA -3'
(Δ1 – 148)	**EcoRI**	**F**	5'- GGGGAATTCTCTGTGAGTGCCGAAGCATATGGT -3'
(Full-length)	**HindIII**	**R**	5'- GGGAAGCTTTTAATTTTCATCAATACAAGTTGTATC -3'

C. QuickChange Mutagenesis Primers

Name	Direction	Sequence
Gly2Ala	**F**	5'- ATGG**C**CAATGTGTGCACATGGAGACAAGGG -3'
	R	5'- CCCTTGTCTCCATGTGCACACATTGG**C**CAT -3'
Cys5Ala	**F**	5'- ATAGGCAATGTG**GC**CACATGGAGACAAGGG -3'
	R	5'- CCCTTGTCTCCATGTG**GC**CACATTGCCCAT -3'
G2A + C5A (double)	**F**	5'- ATGG**C**CAATGTG**GC**CACATGGAGACAAGGG -3'
	R	5'- CCCTTGTCTCCATGTG**GC**CACATTG**G**CCAT -3'

5.5. ACKNOWLEDGEMENTS

We thank Gordon Langsley at INSERM in Paris for providing the *E. coli* optimized *PfPKA-C* fused to GST and with PfPKA-C fused with maltose binding tag. We also thank Gordon and colleagues for many useful discussions regarding results, future directions and planned collaborations. N.M.H designed and conducted and analyzed most of the experiments. Alex Doo contributed equally and was involved in the design and analysis of many experiments. Ganapathy Sarma, PhD served as a very helpful advisor early on in this project. Mira Sastri, PhD, Manjula Darshi, PhD, Michael Deal, PhD, Jessica Bruystens helped out immensely on technical advise, experimental design and trouble-shooting. Jian Wu, PhD has contributed substantial work in crystallization trials. N.M.H wrote the paper. Some of this work will appear in modified form in a Special Issue of Microbes & Infection. Permission was obtained from Dr. Gordon Langsley, Dr. Susan Taylor and Alex Doo before presenting this work in this chapter. N.M.H was supported by the Ruth L. Kirschstein National Research Service Award (NRSA) from National Institutes of Health Grants (5F31 GM090658-02).

5.6. REFERENCES

Anamika, Srinivasan, N., and Krupa, A. (2005). A genomic perspective of protein kinases in Plasmodium falciparum. Proteins *58*, 180-189.

Anamika, K., and Srinivasan, N. (2007). Comparative kinomics of Plasmodium organisms: unity in diversity. Protein Pept Lett *14*, 509-517.

Baker, D.A. (2011). Cyclic nucleotide signalling in malaria parasites. Cell Microbiol *13*, 331-339.

Banky, P., Huang, L.J., and Taylor, S.S. (1998). Dimerization/docking domain of the type Ialpha regulatory subunit of cAMP-dependent protein kinase. Requirements for dimerization and docking are distinct but overlapping. J Biol Chem *273*, 35048-35055.

Banky, P., Newlon, M.G., Roy, M., Garrod, S., Taylor, S.S., and Jennings, P.A. (2000). Isoform-specific differences between the type Ialpha and IIalpha cyclic AMP-dependent protein kinase anchoring domains revealed by solution NMR. J Biol Chem *275*, 35146-35152.

Banky, P., Roy, M., Newlon, M.G., Morikis, D., Haste, N.M., Taylor, S.S., and Jennings, P.A. (2003). Related protein-protein interaction modules present drastically different surface topographies despite a conserved helical platform. J Mol Biol *330*, 1117-1129.

Baton, L.A., and Ranford-Cartwright, L.C. (2005). Spreading the seeds of million-murdering death: metamorphoses of malaria in the mosquito. Trends Parasitol *21*, 573-580.

Berman, H.M., Ten Eyck, L.F., Goodsell, D.S., Haste, N.M., Kornev, A., and Taylor, S.S. (2005). The cAMP binding domain: an ancient signaling module. Proc Natl Acad Sci U S A *102*, 45-50.

Billker, O., Lourido, S., and Sibley, L.D. (2009). Calcium-dependent signaling and kinases in apicomplexan parasites. Cell Host Microbe *5*, 612-622.

Bowman, S., and Horrocks, P. (2000). Assessing the impact of Plasmodium falciparum genome sequencing. Microbes Infect *2*, 1479-1487.

Bray, R.S., and Garnham, P.C. (1982). The life-cycle of primate malaria parasites. Br Med Bull *38*, 117-122.

Brayton, K.A., Lau, A.O., Herndon, D.R., Hannick, L., Kappmeyer, L.S., Berens, S.J., Bidwell, S.L., Brown, W.C., Crabtree, J., Fadrosh, D.*, et al.* (2007). Genome sequence of Babesia bovis and comparative analysis of apicomplexan hemoprotozoa. PLoS Pathog *3*, 1401-1413.

Buechler, Y.J., Herberg, F.W., and Taylor, S.S. (1993). Regulation-defective mutants of type I cAMP-dependent protein kinase. Consequences of replacing arginine 94 and arginine 95. J Biol Chem *268*, 16495-16503.

Buffet, P.A., Safeukui, I., Deplaine, G., Brousse, V., Prendki, V., Thellier, M., Turner, G.D., and Mercereau-Puijalon, O. (2011). The pathogenesis of Plasmodium falciparum malaria in humans: insights from splenic physiology. Blood *117*, 381-392.

Canaves, J.M., and Taylor, S.S. (2002). Classification and phylogenetic analysis of the cAMP-dependent protein kinase regulatory subunit family. J Mol Evol *54*, 17-29.

Dluzewski, A.R., and Garcia, C.R. (1996). Inhibition of invasion and intraerythrocytic development of Plasmodium falciparum by kinase inhibitors. Experientia *52*, 621-623.

Doerig, C. (2004). Protein kinases as targets for anti-parasitic chemotherapy. Biochim Biophys Acta *1697*, 155-168.

Doerig, C., Abdi, A., Bland, N., Eschenlauer, S., Dorin-Semblat, D., Fennell, C., Halbert, J., Holland, Z., Nivez, M.P., Semblat, J.P.*, et al.* (2010). Malaria: targeting parasite and host cell kinomes. Biochim Biophys Acta *1804*, 604-612.

Doerig, C., Billker, O., Haystead, T., Sharma, P., Tobin, A.B., and Waters, N.C. (2008). Protein kinases of malaria parasites: an update. Trends Parasitol *24*, 570-577.

Doerig, C., Billker, O., Pratt, D., and Endicott, J. (2005). Protein kinases as targets for antimalarial intervention: Kinomics, structure-based design, transmission-blockade, and targeting host cell enzymes. Biochim Biophys Acta *1754*, 132-150.

Doerig, C., and Meijer, L. (2007). Antimalarial drug discovery: targeting protein kinases. Expert Opin Ther Targets *11*, 279-290.

Donald, R.G., and Liberator, P.A. (2002). Molecular characterization of a coccidian parasite cGMP dependent protein kinase. Mol Biochem Parasitol *120*, 165-175.

Dvorin, J.D., Martyn, D.C., Patel, S.D., Grimley, J.S., Collins, C.R., Hopp, C.S., Bright, A.T., Westenberger, S., Winzeler, E., Blackman, M.J.*, et al.* (2010). A plant-like kinase in Plasmodium falciparum regulates parasite egress from erythrocytes. Science *328*, 910-912.

Gardner, M.J., Hall, N., Fung, E., White, O., Berriman, M., Hyman, R.W., Carlton, J.M., Pain, A., Nelson, K.E., Bowman, S.*, et al.* (2002). Genome sequence of the human malaria parasite Plasmodium falciparum. Nature *419*, 498-511.

Glenister, F.K., Coppel, R.L., Cowman, A.F., Mohandas, N., and Cooke, B.M. (2002). Contribution of parasite proteins to altered mechanical properties of malaria-infected red blood cells. Blood *99*, 1060-1063.

Goldberg, D.E., and Cowman, A.F. (2010). Moving in and renovating: exporting proteins from Plasmodium into host erythrocytes. Nat Rev Microbiol *8*, 617-621.

Greenwood, B., and Mutabingwa, T. (2002). Malaria in 2002. Nature *415*, 670-672.

Guerra, C.A., Howes, R.E., Patil, A.P., Gething, P.W., Van Boeckel, T.P., Temperley, W.H., Kabaria, C.W., Tatem, A.J., Manh, B.H., Elyazar, I.R.*, et al.* (2010). The

international limits and population at risk of Plasmodium vivax transmission in 2009. PLoS Negl Trop Dis *4*, e774.

Gunaratne, R.S., Sajid, M., Ling, I.T., Tripathi, R., Pachebat, J.A., and Holder, A.A. (2000). Characterization of N-myristoyltransferase from Plasmodium falciparum. Biochem J *348 Pt 2*, 459-463.

Gurnett, A.M., Liberator, P.A., Dulski, P.M., Salowe, S.P., Donald, R.G., Anderson, J.W., Wiltsie, J., Diaz, C.A., Harris, G., Chang, B.*, et al.* (2002). Purification and molecular characterization of cGMP-dependent protein kinase from Apicomplexan parasites. A novel chemotherapeutic target. J Biol Chem *277*, 15913-15922.

Hanks, S.K., and Hunter, T. (1995). Protein kinases 6. The eukaryotic protein kinase superfamily: kinase (catalytic) domain structure and classification. Faseb J *9*, 576-596.

Herberg, F.W., Dostmann, W.R., Zorn, M., Davis, S.J., and Taylor, S.S. (1994). Crosstalk between domains in the regulatory subunit of cAMP-dependent protein kinase: influence of amino terminus on cAMP binding and holoenzyme formation. Biochemistry *33*, 7485-7494.

Hoffman, S.L., Subramanian, G.M., Collins, F.H., and Venter, J.C. (2002). Plasmodium, human and Anopheles genomics and malaria. Nature *415*, 702-709.

Johnson, D.A., Akamine, P., Radzio-Andzelm, E., Madhusudan, M., and Taylor, S.S. (2001). Dynamics of cAMP-dependent protein kinase. Chem Rev *101*, 2243-2270.

Kannan, N., Haste, N., Taylor, S.S., and Neuwald, A.F. (2007). The hallmark of AGC kinase functional divergence is its C-terminal tail, a cis-acting regulatory module. Proc Natl Acad Sci U S A *104*, 1272-1277.

Knighton, D.R., Zheng, J.H., Ten Eyck, L.F., Ashford, V.A., Xuong, N.H., Taylor, S.S., and Sowadski, J.M. (1991a). Crystal structure of the catalytic subunit of cyclic adenosine monophosphate-dependent protein kinase. Science *253*, 407-414.

Knighton, D.R., Zheng, J.H., Ten Eyck, L.F., Xuong, N.H., Taylor, S.S., and Sowadski, J.M. (1991b). Structure of a peptide inhibitor bound to the catalytic subunit of cyclic adenosine monophosphate-dependent protein kinase. Science *253*, 414-420.

Leon, D.A., Herberg, F.W., Banky, P., and Taylor, S.S. (1997). A stable alpha-helical domain at the N terminus of the RIalpha subunits of cAMP-dependent protein kinase is a novel dimerization/docking motif. J Biol Chem *272*, 28431-28437.

Leroy, D., and Doerig, C. (2008). Drugging the Plasmodium kinome: the benefits of academia-industry synergy. Trends Pharmacol Sci *29*, 241-249.

Leykauf, K., Treeck, M., Gilson, P.R., Nebl, T., Braulke, T., Cowman, A.F., Gilberger, T.W., and Crabb, B.S. (2010). Protein kinase a dependent phosphorylation of apical membrane antigen 1 plays an important role in erythrocyte invasion by the malaria parasite. PLoS Pathog *6*, e1000941.

Lin, J.T., Juliano, J.J., and Wongsrichanalai, C. (2010). Drug-Resistant Malaria: The Era of ACT. Curr Infect Dis Rep *12*, 165-173.

Manning, G., Whyte, D.B., Martinez, R., Hunter, T., and Sudarsanam, S. (2002). The protein kinase complement of the human genome. Science *298*, 1912-1934.

Martin, R.E., Ginsburg, H., and Kirk, K. (2009). Membrane transport proteins of the malaria parasite. Mol Microbiol *74*, 519-528.

Matthews, K.R. (2011). Controlling and coordinating development in vector-transmitted parasites. Science *331*, 1149-1153.

Merckx, A., Bouyer, G., Thomas, S.L., Langsley, G., and Egee, S. (2009). Anion channels in Plasmodium-falciparum-infected erythrocytes and protein kinase A. Trends Parasitol *25*, 139-144.

Merckx, A., Nivez, M.P., Bouyer, G., Alano, P., Langsley, G., Deitsch, K., Thomas, S., Doerig, C., and Egee, S. (2008). Plasmodium falciparum regulatory subunit of cAMP-dependent PKA and anion channel conductance. PLoS Pathog *4*, e19.

Montoya, J.G., and Liesenfeld, O. (2004). Toxoplasmosis. Lancet *363*, 1965-1976.

Morrissette, N.S., and Sibley, L.D. (2002). Cytoskeleton of apicomplexan parasites. Microbiol Mol Biol Rev *66*, 21-38; table of contents.

MVI, M.V.I. (2011). Life cycle of the malaria parasite: Many factors make malaria vacine development challenging.

Nayal, M., Hitz, B.C., and Honig, B. (1999). GRASS: a server for the graphical representation and analysis of structures. Protein Sci *8*, 676-679.

NIAID, N.I.o.A.a.I.D. (2010). Life Cycle of the Malaria Parasite.

Read, L.K., and Mikkelsen, R.B. (1991). Plasmodium falciparum-infected erythrocytes contain an adenylate cyclase with properties which differ from those of the host enzyme. Mol Biochem Parasitol *45*, 109-119.

Seydel, K.B., Gaur, D., Aravind, L., Subramanian, G., and Miller, L.H. (2005). Plasmodium falciparum: characterization of a late asexual stage golgi protein containing both ankyrin and DHHC domains. Exp Parasitol *110*, 389-393.

Snow, R.W., Guerra, C.A., Mutheu, J.J., and Hay, S.I. (2008). International funding for malaria control in relation to populations at risk of stable Plasmodium falciparum transmission. PLoS Med *5*, e142.

Taylor, S.S., Kim, C., Vigil, D., Haste, N.M., Yang, J., Wu, J., and Anand, G.S. (2005). Dynamics of signaling by PKA. Biochim Biophys Acta *1754*, 25-37.

Tilley, L., Dixon, M.W., and Kirk, K. (2011). The Plasmodium falciparum-infected red blood cell. Int J Biochem Cell Biol *43*, 839-842.

Trampuz, A., Jereb, M., Muzlovic, I., and Prabhu, R.M. (2003). Clinical review: Severe malaria. Crit Care *7*, 315-323.

Treeck, M., Sanders, J.L., Elias, J.E., and Boothroyd, J.C. (2011). The phosphoproteomes of Plasmodium falciparum and Toxoplasma gondii reveal unusual adaptations within and beyond the parasites' boundaries. Cell Host Microbe *10*, 410-419.

Visco, R.J. (1975). Eimeria tenella in gnotobiotic chickens: hematocrit, weight change, cecal pathology, and mortality. J Parasitol *61*, 194-198.

Ward, G.E., Fujioka, H., Aikawa, M., and Miller, L.H. (1994). Staurosporine inhibits invasion of erythrocytes by malarial merozoites. Exp Parasitol *79*, 480-487.

Ward, P., Equinet, L., Packer, J., and Doerig, C. (2004). Protein kinases of the human malaria parasite Plasmodium falciparum: the kinome of a divergent eukaryote. BMC Genomics *5*, 79.

Wells, T.N. (2010). Microbiology. Is the tide turning for new malaria medicines? Science *329*, 1153-1154.

WHO, W.H.O. (2011). Malaria.

Winzeler, E.A. (2008). Malaria research in the post-genomic era. Nature *455*, 751-756.

Wongsrichanalai, C., and Meshnick, S.R. (2008). Declining artesunate-mefloquine efficacy against falciparum malaria on the Cambodia-Thailand border. Emerg Infect Dis *14*, 716-719.

CHAPTER 6.

Conclusions and Perspectives

6.1. CONCLUSIONS

We are currently experiencing a global emergence of drug-resistant pathogens. There is an urgent need for new therapies to treat these infections. When Alexander Flemming discovered Penicillin in the 1920s, it was hailed as a magic bullet to cure all people of devastating bacterial infections. It is interesting to note that over the course of the last century, societies have developed in numerous ways. We have made movements towards equal rights, seen many wars, walked on the moon, and made advances in medicine and science. However, an important battle still remains. In the 1920s and today, we are still embattled in a fierce war against human pathogens.

Gram-positive and Gram-negative bacteria, parasitic organisms and viruses all pose significant threats to human and public health. Over the course of the last century hundreds of therapies have been brought to market with hopes to eradicate pathogenic diseases. Though some of these have been useful, the majority are useful for a short time until the pathogen develops inevitable resistance. Because of this new approaches and novel therapies are warranted in the battle against superbugs.

In this thesis, I highlight three theoretical methods for anti-pathogen drug discovery. These include the discovery of classical-type antibiotics such as those widely used today, and in addition bring attention to two theoretical approaches. Virulence factor inhibitors and immune-boosting agents have the potential to tip the balance in favor of the host. Further, many of the proposed therapies from these

approaches do not target the bacteria to kill it directly, but instead act to reduce its virulence and allow for the host to clear residual bacteria. With these approaches it is conceivable that microbes would not develop the same levels of resistance seen to classical antibiotics. Many virulence factor inhibitors act to render the bacteria more susceptible to antibiotics or host immunity, effectively removing the bacterial shield, taking away its weapons and reducing its strength. The work outlined in this thesis outlines two ways to target the pathogen, through novel discovery of new classical antibiotics and through targeting specific virulence factors to render a bacterium more susceptible to killing.

During the course of this dissertation work we discovered four new potent marine-derived natural products with potent anti-MRSA activities. These were discovered from marine sediments from around the world. As mentioned previously, the marine environment is a substantial and vast resource of novel chemically diverse and structurally rich chemicals. For the most part, the ocean remains a relatively untapped resource. This warrants further discovery of marine actinomycete derived natural products.

The characterization of the four studied compounds, marinopyrrole A, etamycin, napyradiomycin and nosiheptide yielded potent anti-MRSA activities. These compounds all possess exciting potential in their antibiotic activities. Each compound, however, has a drawback that currently prevents its movement toward therapeutic use. The activity of marinopyrrole A is completely abolished by serum, as is the activity of etamycin. Napyradiomycins are extremely cytotoxic and thus are poised to be better anti-cancer agents than antibiotics. Nosiheptide is extremely effective in an in vivo model but its use is limited by its low solubility. Each of these drawbacks presents a

major hurdle in advancing these novel compounds.

Work has been done on the marinopyrrole, and is presented in **Chapter 2**, describing the semi-synthetic derivatization and the total synthesis of marinopyrrole and derivatives. These resources prove useful in discovering structure activity relationships and beginning to engineer out serum inhibition. A few synthetic derivatives show partial activity in the presence of serum (64X increase in MIC compared to over 250X increase in MIC of marinopyrrole A. These results highlight the possible therapeutic potential of future engineered scaffolds.

Similarly, on first glance a second drawback of marinopyrrole A is its affinity for plastic. We found it adsorbs to plastic and quantified this effect. This could be perceived as a drawback; however, this could have beneficial clinical implications. It is possible that marinopyrrole A or a derivative of the parent could be used to coat cathethers, coat plastic surfaces to prevent bacteria adhesion and survival on equipment within the hospital. This brings attention to the unseen utility of much of this research.

In moving forward with this project, I suggest alternative methods are used to discover marine-derived and other bacterial-derived natural products. For example, by changing the media in which an actinomycete grows, one can drastically change its production of natural products. Post-translational modifications and changes in gene expression induced by an environmental change can induce large scale or small scale changes in a chemical scaffold.

Secondly, with the great utility of mass spectrometry, there is huge potential in identifying previously unseen bacteria: bacteria interactions. By placing a natural

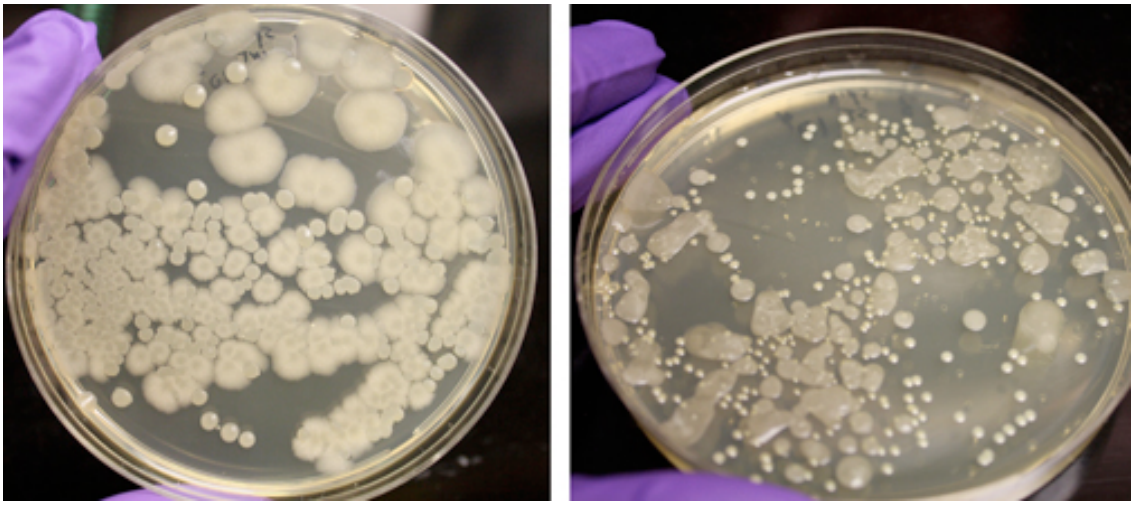

MRSA (ST-59) co-cultured with WT *Bacillus subtilis*

MRSA (ST-59) co-cultured with mutant *B. subtilis* unable to produce sporulation delaying protein (SDP)

FIGURE 6.1 Co-cultures of MRSA with wildtype *Bacillus subtilis* (A) wildtype, and **(B)** the *B. subtilis* SDP mutant indicate that SDP is active in killing *S. aureus*.

product producing bacterium on agar next to a pathogenic strain of MRSA, one can assay the interface and determine whether the bacterial species are competing and identify the elicited molecules.

Two recent examples of this type of research highlight the utility of this resource. A recent PNAS study described the activities of cannibalistic factors produced by *Bacillus subt*ilis against contemporary MRSA strains (Liu et al., 2010). Using imaging mass spectrometry, active metabolites of the cannibalism system in *B. subtilis* were identified. From this resource, two molecules, sporulation killing factor (SKF) and sportulation delaying protein (SDP) were identified. Through further *in vitro* analyses, it was found that SDP delayed growth of MRSA in a concentration-dependent manner, likely through inducing cell lysis. These results were confirmed in a preliminary result seen below in which ST59 MRSA, a highly virulent, multi-toxin producing strain of MRSA was co-incubated with wild-type *B. subtilis* or a mutant that was unable to produce the sporulation delaying protein SDP. The results are striking even though qualitative, showing that in the wild-type co-incubation there was significant reduction in ST-59 colonies. Conversely, with the mutant SDP *B. subtilis*, significantly more ST-59 colonies are seen to survive. These results further confirmed the results of the PNAS paper (Liu et al., 2010).

Similar methods have shown useful in determining molecules excreted in competition with other bacteria in a given niche. Diverse niches exist within the environment, whether in the marine environment, in soil or on the human skin. Our skin is colonized with great numbers of bacteria. These bacteria must obtain adequate nutrients to survive in this niche. In addition, they must compete with other flora residents as well as intruding pathogens. It has been proposed that bacteria that

reside in the normal flora and in the niches described above can secrete molecules to protect the niche from outside pathogenic or intruding bacteria (Gonzalez et al., 2011). The interaction between competing bacteria can be profiled using imagine mass spectrometry (IMS). Gonzalez and colleagues recently showed examples of this, thus presenting a new way to discover natural products.

Alternately, one can imagine this utility used in an opposite direction, by looking at interspecies or intercellular communications and competition at the level of an immune cell and a pathogen. There are future hopes to utilize this resource to look at exchange between pathogenic bacteria and neutrophils, macrophages and other immune cells.

This tool is useful in pursuing other directions in anti-pathogen drug discovery. Our results from **Chapter 4** indicate that diflunisal has widespread effects on the bacteria. We observed MRSA death in stationary phase culture, loss of pigment, and synergy with antimicrobial agents that suggest that the effect of diflunisal on *S. aureus* is much more complex than just as an AgrA inhibitor. To test this qualitatively, we spotted MRSA on agar containing diflunisal at different concentrations. After 48 h, these spots were cut out and assayed through imaging mass spectrometry. The results are striking and show a substantially different metabolic profile in the treated (Diflunisal 50 μg/ml) versus the untreated. This also contrasts to the mutant alpha-toxin strain which showed a similar profile to its isogenic counterpart, TCH1516.

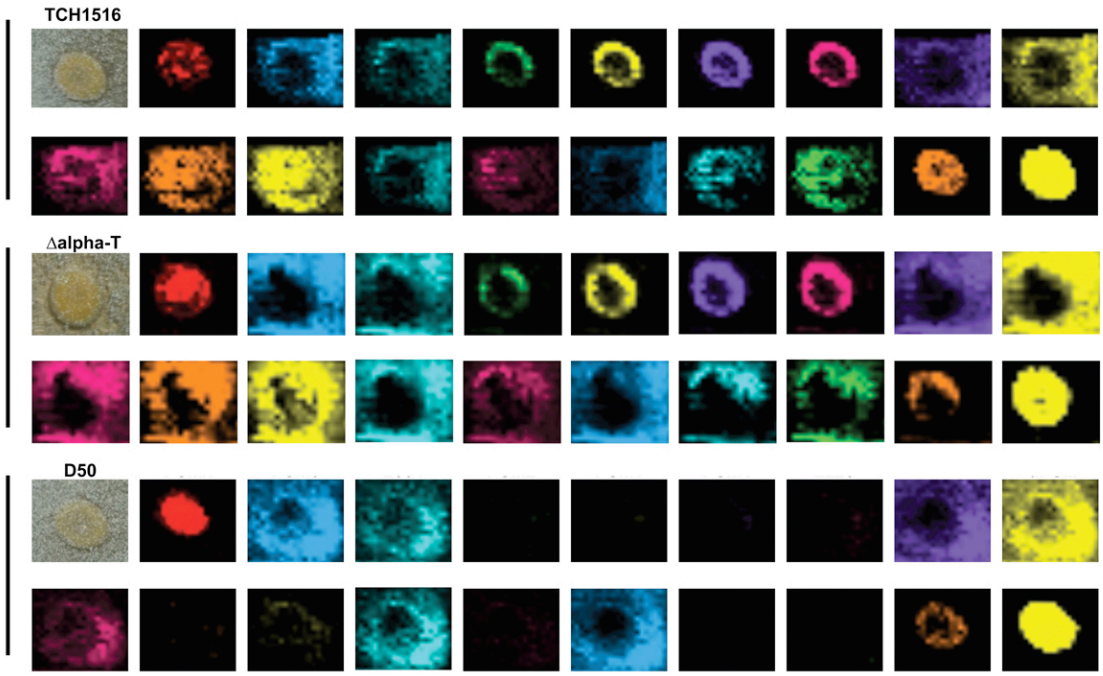

FIGURE 6.2 Imaging mass spectrometry of MRSA (strain TCH1516), an alpha-toxin mutant (TCH1516 –dhla) and MRSA treated for 48 hours with diflunisal 50 μg/ml.

6.2. SUMMARY

The three-pronged approach to anti-pathogen drug discovery provides numerous targets for further research and study. Because only one of these approaches has yielded currently-marketed therapeutics, the other two, virulence factor inhibitors and immune-boosting agents, could potentially impact the global battle against superbugs. Theoretically, with these therapies, we can help tip the balance in the battle against multi-drug resistant pathogens back in favor of the host. In the future, we hope to advance the discovery of new antimicrobials using innovative utilities such as imaging mass spectrometry and further probing virulence factor targets.

6.3. ACKNOWLEDGEMENTS

I would like to thank David Gonzalez, PhD for running the imaging mass spectrometry on the alpha-toxin WT, null and diflunisal treated cultures and Mary Hensler, PhD for help with setting up the imaging mass spectrometry experiment.

6.4. REFERENCES

Gonzalez, D.J., Haste, N.M., Hollands, A., Fleming, T.C., Hamby, M., Pogliano, K., Nizet, V., and Dorrestein, P.C. (2011). Microbial competition between Bacillus subtilis and Staphylococcus aureus monitored by imaging mass spectrometry. Microbiology *157*, 2485-2492.

Liu, W.T., Yang, Y.L., Xu, Y., Lamsa, A., Haste, N.M., Yang, J.Y., Ng, J., Gonzalez, D., Ellermeier, C.D., Straight, P.D.*, et al.* (2010). Imaging mass spectrometry of intraspecies metabolic exchange revealed the cannibalistic factors of Bacillus subtilis. Proc Natl Acad Sci U S A *107*, 16286-16290.